EFFECTS OF EXTRAPOLATION BOUNDARY CONDITIONS ON SUBSONIC MEMS FLOWS OVER A FLAT PLATE

A THESIS SUBMITTED TO
THE GRADUATE SCHOOL OF NATURAL AND APPLIED SCIENCES
OF
MIDDLE EAST TECHNICAL UNIVERSITY

BY

ÖZHAN HULUSİ TURGUT

IN PARTIAL FULFILLMENT OF THE REQUIREMENTS

FOR

THE DEGREE OF MASTER OF SCIENCE

IN

AEROSPACE ENGINEERING

JANUARY 2006

Approval of the Graduate School of Natural and Applied Sciences.

Prof. Dr. Canan Özgen
Director

I certify that this thesis satisfies all the requirements as a thesis for the degree of Master of Science.

Prof. Dr. Nafiz Alemdaroğlu
Head of Department

This is to certify that we have read this thesis and that in our opinion it is fully adequate, in scope and quality, as a thesis for the degree of Master of Science.

Prof. Dr. M. Cevdet Çelenligil
Supervisor

Examining Committee Members

Prof. Dr. İ. Sinan Akmandor (METU, AEE) _____

Prof. Dr. M. Cevdet Çelenligil (METU, AEE) _____

Emeritus Prof. Dr. Cahit Çıray (METU, AEE) _____

Prof. Dr. M. Haluk Aksel (METU, ME) _____

Assoc. Prof. Dr. Sinan Eyi (METU, AEE) _____

I hereby declare that all information in this document has been obtained and presented in accordance with academic rules and ethical conduct. I also declare that, as required by these rules and conduct, I have fully cited and referenced all material and results that are not original to this work.

Özhan Hulusi TURGUT

ABSTRACT

EFFECTS OF EXTRAPOLATION BOUNDARY CONDITIONS ON

SUBSONIC MEMS FLOWS OVER A FLAT PLATE

Turgut, Özhan Hulusi

M.S., Department of Aerospace Engineering

Supervisor: Prof. Dr. M. Cevdet Çelenligil

January 2006, 104 pages

In this research, subsonic rarefied flows over a flat-plate at constant pressure are investigated using the direct simulation Monte Carlo (DSMC) technique. An infinitely thin plate (either finite or semi-infinite) with zero angle of attack is considered. Flows with a Mach number of 0.102 and 0.4 and a Reynolds number varying between 0.063 and 246 are considered covering most of the transitional regime between the free-molecule and the continuum limits. A two-dimensional DSMC code of G.A. Bird is used to simulate these flows, and the code is modified to examine the effects of various inflow and outflow boundary conditions. It is observed that simulations of the subsonic rarefied flows are sensitive to the applied boundary conditions. Several extrapolation techniques are considered for the evaluation of the flow properties at the inflow and outflow boundaries. Among various alternatives, four techniques are considered in which the solutions are found to be relatively less sensitive. In addition to the commonly used extrapolation techniques, in which the flow properties are taken from the neighboring boundary cells of the domain, a newly developed extrapolation scheme, based on tracking

streamlines, is applied to the outflow boundaries, and the best results are obtained using the new extrapolation technique together with the Neumann boundary conditions. With the new technique, the flow is not distorted even when the computational domain is small. Simulations are performed for various freestream conditions and computational domain configurations, and excellent agreement is obtained with the available experimental data.

Keywords: Streamline Extrapolation Technique, Boundary Conditions, Rarefied Flow, Subsonic Flow, Flat Plate, Direct Simulation Monte Carlo.

ÖZ

DÜZ BİR PLAKA ÜZERİNDE SESALTI HIZLARDAKİ MEMS AKIŞLARINA DEĞİŞİK DIŞDEĞERBİÇİMLİ SINIR KOŞULLARININ ETKİLERİ

Turgut, Özhan Hulusi

Yüksek Lisans, Havacılık ve Uzay Mühendisliği Bölümü

Tez Yöneticisi: Prof. Dr. M. Cevdet Çelenligil

Ocak 2006, 104 sayfa

Bu araştırmada, düz bir plaka üzerinde sesaltı hızlardaki sabit basınçlı seyreltilmiş akışlar, doğrudan benzetim Monte Carlo (DSMC) yöntemiyle incelenmiştir. Sonsuz incelikte, sıfır hücum açılı (sonlu veya yarı sonsuz) bir plaka göz önüne alınmıştır. Serbest molekül sınırı ile sürekli akış sınırı arasındaki geçiş rejiminin tamamına yakınını kapsayan, Mach sayısı 0.102 ile 0.4 arasında olan ve Reynolds sayısı 0.063 ile 246 arasında değişen akışlar dikkate alınmıştır. Benzetimde G. A. Bird'ün iki boyutlu bir DSMC kodu kullanılmıştır, ve bu kodda içeri ve dışarı akışlarda dışdeğerbiçim kullanan farklı sınır koşullarının etkilerini sınamak için değişiklikler yapılmıştır. Benzetimlerde, sesaltı hızlardaki seyreltilmiş akışların, uygulanan sınır koşullarına duyarlı olduğu gözlemlenmiţir. İçeri ve dışarı akış sınırlarındaki akış özelliklerinin değerlendirilmesi için çeşitli dışdeğerbiçim yöntemleri dikkate alınmıştır. Birçok farklı alternatif arasından, çözümlerin daha az hassasiyet gösterdiği dört yöntem göz önünde tutulmuştur. Akış özelliklerinin hesaplama alanındaki komşu sınır hücrelerinden alındığı sık kullanılan dışdeğerbiçim yöntemlerine ek olarak, akış çizgilerini izleyen, yeni geliştirilmiş bir dışdeğerbiçim yöntemi dışarıya akışlarda

uygulanmıştır, ve en iyi sonuçlar yeni dışdeğerbiçim yöntemiyle Neumann sınır koşullarının aynı anda kullanılmasıyla elde edilmiştir. Yeni yöntem ile, hesaplama alanı küçük olduğunda bile akış biçimi bozulmamaktadır. Benzetimler, birçok değişik serbest akış koşulları ile çeşitli hesaplama alanları için gerçekleştirilmiş ve ulaşılabilir deneysel verilerle kusursuz uyum elde edilmiştir.

Anahtar Kelimeler: Akış Çizgisi Dışdeğerbiçim Tekniği, Sınır Koşulları, Seyreltilmiş Akış, Sesaltı Hızlardaki Akışlar, Düz Plaka, Doğrudan Benzetim Monte Carlo.

ACKNOWLEDGMENTS

I would like to express my sincere gratitude to Prof.Dr. Cevdet Çelenligil for his valuable efforts in every step of this thesis. His encouragement, support and patience always guided me throughout this period. I give my warmest thanks to him.

I owe a special thank to Assoc.Prof.Dr. Sinan Eyi for his precious recommendations related with the boundary conditions. They were very helpful in guiding us to achieve our goal.

I would also like to thank Prof.Dr. Sinan Akmandor who advised us to use streamline extrapolation technique for the boundary conditions.

I appreciate the useful discussions we had with Ali Aktürk, Monier El-Farra and Mustafa Kaya during this thesis.

The continuous LaTeX assistance of Tahir Turgut and Mustafa Kaya contributed to the writing process.

I also thank Evrim Dizemen, Ebru Sarıgöl, Özgür Demir, Gönül Uluer and Cengiz Özdemir for their most noteworthy support.

I am grateful to my beloved Sinem, for her patient and spiritual support which kept me going on.

Finally, I want to express me feelings of love for my mother and sister, who were always encouraging and affectionate.

Dedicating to my father ...

TABLE OF CONTENTS

LIST OF TABLES

TABLE

LIST OF FIGURES

FIGURES

LIST OF SYMBOLS

ROMAN SYMBOLS

a	Speed of sound
$\mathbf{c}$	Field molecules that have velocity between $\mathbf{c}+\Delta\mathbf{c}$
c_r	Relative velocity with respect to class $\mathbf{c}$ molecules
C_D	Drag coefficient
d	Molecule diameter
J^-, J^0, J^+	Characteristic variables
k	Boltzmann constant
Kn	Knudsen number
L	Plate length
m	Molecular mass
$\mathrm{m}_{mixture}$	Molecular mass for gas mixture
$\mathbb{M}_{mixture}$	Molar mass for gas mixture
M	Mach number
n	Number density
N_c	Total number of collisions per unit time per unit volume
p	Pressure
q	Heat flux
$\vec{\mathbf{r}}$	Position vector
$\Re$	Universal gas constant
R	Gas constant
Re	Reynolds number
s	Entropy
S	Shortest distance between a line and a point
t	Time
T	Temperature
U	Velocity component in x-direction (Streamwise direction)
V	Velocity component in y-direction (Transverse direction)
$\vec{\mathbf{V}}$	Velocity vector
x	Cartesian, spatial coordinate for streamwise direction
X_j	Mole fraction of species j
y	Cartesian, spatial coordinate for transverse direction

GREEK SYMBOLS

α	Weighting factor
ϕ	Macroscopic quantity
γ	Specific heat ratio
Γ	Gamma function
λ	Local mean free path
ν	Collision rate per molecule per unit time
ρ	Density
σ_T	Total collision cross-section

SUBSCRIPTS

∞	Freestream values
e	Exterior values
i	Interior values
ref	Reference values
w	Surface values

CHAPTER 1

INTRODUCTION

The flow of a gas may be analyzed by essentially two different general approaches. In the conventional methods (macroscopic approaches), the gas is treated as a continuous media; and in the more recent techniques (microscopic approaches), the gas is considered as being composed of molecules and atoms.

The description of the continuum model (macroscopic approach) is in terms of the spatial and temporal variations of the velocity, density, pressure and temperature. The dependent variables in these equations are the macroscopic properties whereas the independent variables are the spatial coordinates and time. In many practical applications, the Navier-Stokes equations are used as the mathematical model for the continuum gas flows.

The molecular model (microscopic approach) recognizes the gas as a huge number of discrete molecules. Under idealized conditions, if the position, velocity and state of each molecule is known at all times, the gas motion can be determined exactly. However, this is not practical and mathematical models (using statistical quantities) are used, instead. The Boltzmann equation is the mathematical model for the calculation of the gas flows at the microscopic level. In this case, the only dependent variable is the velocity distribution function (fraction of molecules

with certain speeds at a given location and time), but the independent variables are increased to seven (3 velocity components, 3 spatial coordinates and time) which make the Boltzmann equation very difficult to solve. So, the Boltzmann equation is not conformable to analytical solutions for non-trivial problems, and presents difficulties in using conventional numerical solution methods. On the other hand, the discrete structure of the gas at the microscopic level overcomes these difficulties through direct physical, rather than mathematical, modeling methods. The physical or direct simulation approach has some computational advantages over the mathematical modeling. For example, in the physical approaches there are no numerical instabilities which are commonly encountered in the conventional continuum calculations. Today, both mathematical and physical models have their own domains of applications. For the dense flows, mathematical approaches are preferred because molecular models use more computer resources. On the other hand, the continuum models are not valid under rarefied conditions and for these cases physical models are adapted.

The transport terms in the Navier-Stokes equations, namely the mass, momentum and energy equations, lose their validity when gradients of the macroscopic variables become so steep that their scale length is of the same order as the average distance traveled by the molecules between collisions, called *mean free path*, λ [1]. An important dimensionless parameter, Knudsen Number (Kn), expresses up to which extent the continuum equations are not valid and molecular approach is to be used. Knudsen number is defined as the ratio of the mean free path, to the characteristic dimension, L, i.e.

$$Kn = \frac{\lambda}{L} \quad . \tag{1.1}$$

The Kn domain ($0 < Kn < \infty$) is often divided into four regimes. For $Kn < 0.01$, *continuum* regime, the Navier-Stokes equations are applied. For $0.01 < Kn < 0.1$, *slip flow* regime, Navier-Stokes equations are applied with a slip-flow boundary condition. For $0.1 < Kn < 10$, *transition* regime, full Boltzmann equation is used. For $Kn > 10$, *free molecular* regime, collisionless Boltzmann equation is applied.

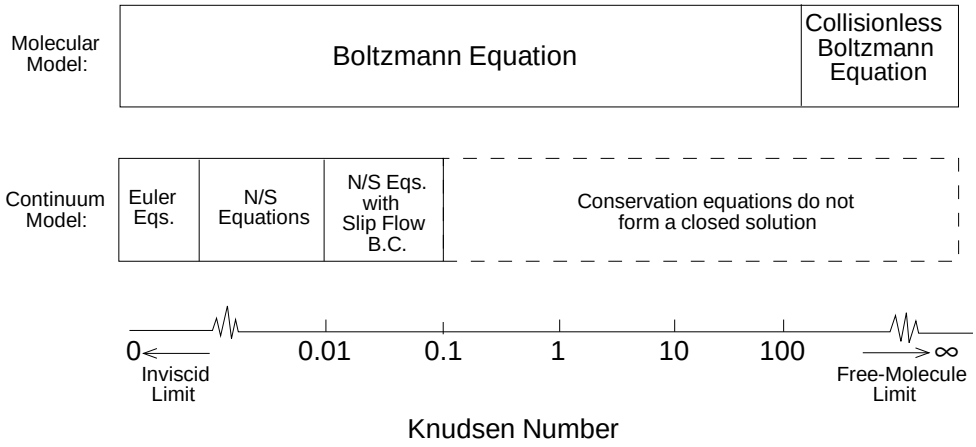

Figure 1.1: Flow regimes

It should be pointed out that for the transition regime the Boltzmann equation is not practical to use because of its mathematical difficulties. Additionally, it is not easy to implement thermal radiation and chemical reaction effects to the formulation of the Boltzmann equation. So, a lot of indirect methods are applied. One type of these methods can be classified as "moment methods". The Chapman-Enskog solution of the Boltzmann equation is an example to this. Another method is called as the "model equation" approach which involves an approximation to the form of the Boltzmann equation itself. The best known example is the BGK equation after Bhatnagar, Gross and Krook [2].

Note that, a limited number of "analytical" methods for the Boltzmann equation lead to closed form solutions, but most of them depend on numerical procedures for the final results. Solution of the Boltzmann equation by numerical techniques such as the conventional methods of computational fluid dynamics (CFD) is also possible. But this approach necessitates specifying a bounded grid in velocity space and is restricted to simple flow geometries, monatomic gases and low to moderate Mach numbers with today's computers.

Presence of discrete particles in a gas is the main reason for the mathematical difficulties associated with the Boltzmann equation. But, physically based simulation methods allow the particulate nature to avoid these problems. Direct simulation methods model the real gas by a huge number of simulated molecules in a computer. The position coordinates, velocity components, and internal state of each simulated molecules are stored in the computer and are modified with time as the molecules are simultaneously followed through representative collisions and boundary interactions in physical space.

Direct simulation methods may be classified as:

- deterministic simulation methods,
- probabilistic simulation methods.

The Molecular Dynamics (MD) method [3] was the first physical simulation method. The calculation of the succeeding molecular motion, including the collisions and boundary interactions, is deterministic whereas the initial configuration of the molecules is set in a probabilistic way. Intermolecular collisions occur when the cross-sections of molecules overlap. In the early MD applications the computational time needed for the application of the method was related to the square of the number of simulated molecules. This was a major handicap for the use of the MD method in the past, but in the recent MD applications the computational times are directly proportional to the number of simulated molecules [4]. A significant problem with MD method is that, the number of simulated molecules is not a free parameter for a specified molecular size, flow geometry and gas density. Also, many two-dimensional MD calculations use cylindrical molecules rather than spherical molecules which causes non-physical macroscopic properties. The MD method is proved to be applicable for the simulation of the dense gases and liquids [5].

In the transition regime, in addition to the molecule-surface interactions (in free-molecule flow this is the only interaction), the computation of intermolecular collisions is needed. In the *direct simulation Monte Carlo (DSMC)* method, the molecular motion and the intermolecular collisions are uncoupled over a small time interval. All the molecules are moved over distances

and then the intermolecular collisions are calculated in this time interval.

The DSMC method has been widely applied to hypersonic rarefied flows about space vehicles [6]. However, in recent years it has also been used for flows about small bodies near atmospheric conditions. For example, nowadays, micro-electromechanical systems (MEMS) is drawing attention in many disciplines. These are very small (micron-scale) sensors and actuators and their applications range from consumer products (airbag triggers, micro-mirror displays), industrial and medical tools (micro-valves, micro-motors), to instrumentation (micro-pressure sensors, micro shear-stress sensors) [7]. Although the mechanical and electrical properties of MEMS are well studied in the past, the fluid motion around them is not thoroughly investigated. Obviously these effects should be understood in order to design these micro-scale structures properly. Note that, the dimensions of these devices are at micron-levels, and the mean free path of the gas molecules around them is comparable to the characteristic length of the body. For this reason the flow can not be considered as continuum flow, and it is quite suitable to apply the DSMC method in the analysis of the gas flows around them.

The flow over a flat plate is one of the basic problems in fluid mechanics. This problem has been studied thoroughly for low Reynolds number cases and incompressible flows [8]. Solutions are also available with continuum equations using a slip velocity boundary condition [9], [10], [11].

Research on subsonic rarefied flows at the Middle East Technical University started with Murat Ilgaz [12]. In that study, flow in a parallel plate channel is investigated. In the present research, investigation on subsonic rarefied flows is continued and flow over an infinitely thin flat plate is studied at zero angle of attack with constant pressure. The main objective of the present study is to examine the effects of different inflow and outflow boundary conditions on the subsonic rarefied flows.

Similar studies have been performed in the past by other researchers for channel flows. For example, Nance, Hash and Hassan [13] specify pressure, temperature and transverse velocity at the inflow boundary and the streamwise velocity is determined from the fluxes across cell's boundary. At the outflow boundaries, theory of characteristics is appealed by using Whitfield's characteristic formulation [14] which sets constant exit pressure. Piekos and Breuer [15] suggest to specify temperature, transverse speed at the inflow; and pressure at both inflow and outflow boundaries.

Simulation of subsonic rarefied flows over a flat plate is more difficult in comparison with that in channel flows. This is due to the fact that inlet and exit sections are fixed for the channel flows, but in flat plate flows the top domain boundary has to be taken into account, as well. Naturally, an error in the outflow boundary conditions in channel flows affects the solution near the exit, whereas in the flat plate problem the whole solution is affected. Moreover, although calculations have been performed for flows about flat plates at hypersonic speeds [16], very few simulations are reported in the literature on the subsonic rarefied flat plate flows. It is clear that for subsonic flows, there are some extra difficulties involved, for example, the freestream and vacuum boundary conditions used in the supersonic flows are not applicable and proper extrapolation inflow and outflow conditions must be utilized. Additionally, in low speed flows, the sampling size must be increased considerably to isolate the statistical scatter from the mean quantities. Recently, Sun and Boyd [17] studied MEMS flows using Information Preservation (a modified DSMC) technique. They suggest to use characteristic boundary conditions. In their simulations, stagnation pressure and temperature are given for the inflow; and exit pressure is specified for the outflow.

In the present study, several different outflow boundary conditions are tested and a new extrapolation technique is developed. In the following chapter, the details of this new boundary condition treatment are explained. This technique is based on following the streamline trajectories and carrying the macroscopic properties along the streamlines. The method is successfully

applied with the Neumann boundary condition at the outflow boundaries. For the inflow boundaries, Riemann inflow boundary condition is used. The computed results are found to be in excellent agreement with the available experimental data of Schaaf and Sherman [18].

CHAPTER 2

THE DSMC METHOD

AND BOUNDARY CONDITIONS

2.1 The Direct Simulation Monte Carlo Method

The DSMC method is developed by Bird [1] starting in the 1960's. It has evolved since then and has become the most widely accepted numerical technique in the simulation of rarefied gas flows today. As the word "simulation" implies the DSMC is a numerical procedure rather than an analytical solution of a mathematical model.

The DSMC method models dilute gases and is based on the kinetic theory [19]. In this technique, gas flows are simulated by keeping track of a set of representative molecules. These representative molecules have the correct physical size and dynamical behavior, and each simulated molecule represents a large number of real molecules. Using a number of representative molecules enables simulation of larger number of real molecules, and meanwhile, decreases the computational time of the simulation. In the present study *"Variable Hard Sphere"* (VHS) model [20] is used in which the diameter of a molecule is a function of the relative speed of the colliding molecules. Also, to decrease the computational time, domain is divided into cells and sub-cells for the selection of collision pairs and sampling of flow properties efficiently. The cell

sizes are selected to be smaller than the local mean free paths.

The major assumption of the DSMC method is the uncoupling of molecular motion from the intermolecular collisions over a small time interval, Δt, which should be small compared to mean collision time. In the simulations, first, all the molecules are moved deterministically in Δt and the calculations are done for the boundary interactions. Secondly, intermolecular collisions are computed in this time interval statistically. This leads the computational time to be directly proportional to the number of simulated molecules. Note that the time step Δt and the cell sizes are chosen such that a molecule does not travel more than the local mean free path during this time interval.

In the simulations, first, the computational cell network is set up. The computational domain is initialized either as vacuum or uniform equilibrium flow. After arranging the positions and velocities of the initially loaded particles, solution procedure begins. Basically the following steps are followed until reaching steady-state flow:

- Motion of particles in the specified time interval Δt and the calculation of the interactions with the domain boundaries.

- Arrangement of the particles' new positions, and indexing of the molecules according to the cells/subcells they are in. (Note that after the movement process, the number of molecules in each cell has to be determined. This is necessary for the calculation of the number of collisions occurring in that time interval. Also, the identification of subcell and cell number of each molecule is necessary in choosing collision pairs because they are chosen between nearest neighbors.)

- Determination of the new particles entering the domain from the boundaries during the time interval Δt. (The number of entering molecules and their properties depend on the fluid properties at the domain boundaries. In the present simulations, the fluid properties are updated by extrapolation from the interior domain (see Section 3.3).)

- Selection of collision pairs and calculation of intermolecular collisions for this time interval Δt.

- Sampling over the particles in order to calculate average flow properties in each cell. (The average properties are assigned to the cells at their geometric centers. Note that the scatter on these averaged quantities are reduced as the total number of representative molecules are increased. Also, considering that for healthy statistical results, each molecule should be sampled only once in a given cell, and hence, samples are taken every other time step.)

The interaction of gas molecules with a solid surface is usually modeled in two simple ways [21]. In the *specular reflection*, perfectly elastic collision is considered and the velocity component parallel to surface is kept constant and the normal velocity component is reversed (assuming the surface is smooth and clean). On the other hand, in the *diffuse reflection*, molecule can bounce back from the surface in all directions independent of its initial velocity (assuming the surface is "dirty" with many irregularities). In the present study, diffuse reflection model is used with full thermal accommodation to the surface temperature.

2.2 Boundary Conditions

In the numerical simulation of fluid flows, one has to use boundary conditions due to the finiteness of the computational domains. There are several options in the specification of boundary conditions for the inflows and outflows. One option may be to use all properties from the freestream conditions directly. However, this is suitable only if the computational domain is very large both in the upstream and downstream directions, and it assumes that the solution near the domain boundaries is not influenced by the existence of the body. In the present study, small domains are considered for computational efficiency, and consequently, it becomes necessary to take the body effects into account.

In the DSMC method, if all the flow properties are known at the boundaries, they can be used as "Dirichlet" boundary conditions, and the flow can be computed without any difficulty. Unfortunately, these properties are not known in the present flows, and one needs to find some

of these properties by suitable extrapolation techniques. Once the properties along the inflow and outflow boundaries are determined, they are used to calculate the number of molecules and their internal energies entering the domain at each time step.

2.2.1 Subsonic Inflow Boundary Conditions

In this thesis, far-field subsonic inflow boundary conditions are utilized. This assumes that the inflow boundary is sufficiently away from the body but not far enough for the application of the freestream conditions. Figure 2.1 shows the inflow configuration.

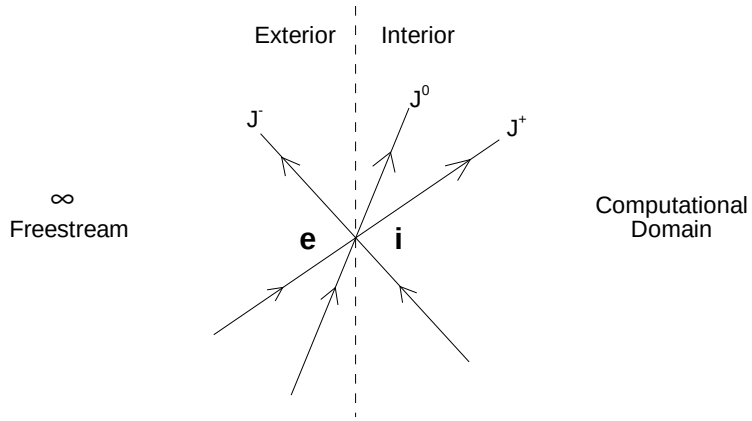

Figure 2.1: Subsonic inflow boundary.

Properties at the exterior, e, are to be determined by the freestream conditions, ∞, and interior, i. Since the flow is subsonic, according to one-dimensional inviscid characteristic formulation, there are two characteristics coming into the domain and one characteristic is leaving. Hence, one property at e needs to be extrapolated from the interior domain and the rest of the properties are taken from the freestream conditions. Two types of boundary conditions are examined in this study:

(i) In the first approach, one of the primitive variables, V (transverse velocity component), is extrapolated from the interior domain and the rest of the variables are taken from the freestream. (Note that in [13] U (streamwise velocity component) is extrapolated instead

of V). For the present study, the following exterior properties need to be determined, U_e, V_e, n_e, T_e and $X_{j,e}$. These properties are taken as $U_e = U_\infty$, $n_e = n_\infty$, $T_e = T_\infty$, $X_{j,e} = X_{j,\infty}$ and $V_e = V_i$ where n, T, X_j represent number density, temperature and mole fraction of species j, respectively.

(ii) In the second approach, one-dimensional inviscid flow is assumed locally, and Riemann invariants are used. One property is taken from interior (J_i^-) and the rest of the properties are taken from the freestream (J_∞^+, V_∞, s_∞, $X_{j,\infty}$), i.e. $J_e^- = J_i^-$, $J_e^+ = J_\infty^+$, $V_e = V_\infty$, $s_e = s_\infty$, $X_{j,e} = X_{j,\infty}$ where

$$J_\infty^+ = U_\infty + \frac{2\,a_\infty}{\gamma - 1} \quad , \quad J_i^- = U_i - \frac{2\,a_i}{\gamma - 1}$$

are the Riemann invariants, s is the entropy, a is the speed of sound and γ is the specific heat ratio. Once J_e^+ and J_e^- are determined from $J_e^+ = J_\infty^+$, $J_e^- = J_i^-$, then U_e and a_e can be found from:

$$J_e^+ = U_e + \frac{2\,a_e}{\gamma - 1} \quad , \quad J_e^- = U_e - \frac{2\,a_e}{\gamma - 1} \quad ,$$

and the results are:

$$U_e = \frac{J_e^+ + J_e^-}{2} \quad , \tag{2.1}$$

$$a_e = (J_e^+ - J_e^-)\frac{\gamma - 1}{4} \quad . \tag{2.2}$$

Temperature T_e can be evaluated as:

$$T_e = \frac{a_e^2}{\gamma R} \tag{2.3}$$

where R is the gas constant. For the transverse velocity component at exterior, $V_e = V_\infty$ is taken. Also, along the J^0 characteristic line $s_e = s_\infty$, and for isentropic flows of ideal gases (with constant specific heats)

$$\frac{p_e}{\rho_e^\gamma} = \frac{p_\infty}{\rho_\infty^\gamma} = \text{constant},$$

where ρ is the density. Knowing that

$$p = \frac{\rho a^2}{\gamma} \quad \Rightarrow \quad \frac{\rho_e a_e^2}{\gamma \rho_e^\gamma} = \frac{p_\infty}{\rho_\infty^\gamma} \quad ,$$

one can find

$$\rho_e = \left[\frac{\rho_\infty^\gamma}{p_\infty}\frac{a_e^2}{\gamma}\right]^{\frac{1}{(\gamma-1)}}.$$

After manipulating the above equation using ideal gas relation, ρ_e can be found as:

$$\rho_e = \rho_\infty \left[\frac{a_e}{a_\infty}\right]^{\frac{2}{(\gamma-1)}},$$

and number density at the exterior is

$$n_e = \frac{\rho_e}{\sum_j X_{j,\infty} m_j} \tag{2.4}$$

where m_j represents the molecular mass of species j.

2.2.2 Subsonic Outflow Boundary Conditions

For small domains, freestream boundary conditions can not be used at the outflow boundaries. For the determination of variables at the outflow boundaries, the interior solution has to be taken into account. Figure 2.2 shows the outflow configuration.

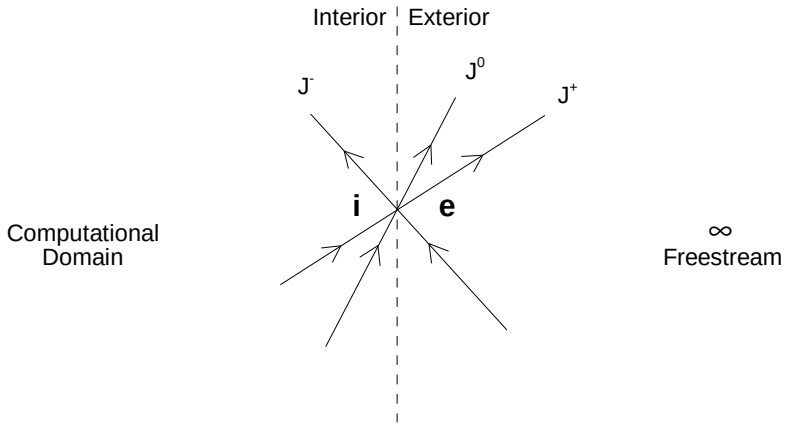

Figure 2.2: Subsonic outflow boundary.

Properties at the exterior, e, are to be determined by the freestream conditions, ∞, and interior, i. Since the flow is subsonic, there are two characteristics leaving the domain and one characteristic coming into the domain. Hence, one property at e needs to be specified from the

freestream conditions. The variables to be determined are the same as the inflow variables (U_e, V_e, n_e, T_e and $X_{j,e}$). In the present research, the exterior property which is taken from the freestream is chosen as p_∞ (i.e. $p_e = p_\infty$) because this research concentrates on the flow over a flat plate at constant pressure. Various conditions can be imposed at the outflow boundaries:

(i) The Neumann boundary condition: The normal gradient of a dependent variable, ϕ, is prescribed at the boundary as $\frac{\partial \phi}{\partial \xi} = 0$, where ξ is in the direction of extrapolation. This gives rise to extrapolation of properties from the interior domain as $U_e = U_i$, $V_e = V_i$, $n_e = n_i$ and $X_{j,e} = X_{j,i}$. Only pressure is specified as the freestream pressure ($p_e = p_\infty$). Then, the exterior temperature is calculated from the ideal gas relation ($T_e = \frac{p_e}{n_e\, k}$) where k is the Boltzmann constant.

(ii) Whitfield's characteristic formulation: The characteristic variables (J^-, J^0, J^+) shown in Figure 2.2, and the primitive variables (ρ, U, p) are related by the following equations [22]:

$$dJ^0 = d\rho - \frac{dp}{a^2} = 0 \quad , \tag{2.5}$$

$$dJ^+ = dU + \frac{dp}{\rho a} = 0 \quad , \tag{2.6}$$

$$dJ^- = dU - \frac{dp}{\rho a} = 0 \quad . \tag{2.7}$$

Using the Whitfield's characteristic formulation [14], which allows the specification of constant exit pressure,

$$\rho_e = \rho_i + \frac{p_e - p_i}{a_i^2} \quad , \tag{2.8}$$

$$U_e = U_i + \frac{p_i - p_e}{\rho_i a_i} \quad , \tag{2.9}$$

$$V_e = V_i \quad , \tag{2.10}$$

$$X_{j,e} = X_{j,i} \quad . \tag{2.11}$$

Using the ideal gas relation and the definition of the speed of sound, one can find that

$$\rho_e = \rho_i \left(1 - \frac{1}{\gamma}\right) + \frac{p_e}{\gamma R T_i} \quad , \tag{2.12}$$

$$U_e = U_i + \frac{(\rho_i R T_i - p_e)}{\rho_i \sqrt{\gamma R T_i}} \quad . \tag{2.13}$$

Also,

$$\rho_e = n_e \sum_j X_{j,e}\, m_j \quad ,$$

$$\rho_i = n_i \underbrace{\sum_j X_{j,i}\, m_j}_{call\ \mathbb{m}_{mixture}} \quad .$$

The definition of the gas constant, R, is as follows:

$$R = \frac{\Re}{\mathbb{M}_{mixture}} = \frac{k\, N_a}{\sum_j X_{j,e}\, N_a\, m_j} = \frac{k}{\sum_j X_{j,e}\, m_j} = \frac{k}{\mathbb{m}_{mixture}},$$

where $\Re$ is the universal gas constant, N_a is the Avogadro's number, $\mathbb{M}_{mixture}$ represents molar mass for mixture and $\mathbb{m}_{mixture}$ represents (average) molecular mass for mixture. Rewriting the Eqn.(2.12) with the above relations gives,

$$n_e = n_i \left(1 - \frac{1}{\gamma}\right) + \frac{p_e}{\gamma k T_i} \quad . \tag{2.14}$$

Once exit pressure is known, exterior temperature can be calculated from the ideal gas relation:

$$T_e = \frac{p_e}{n_e\, k} \quad . \tag{2.15}$$

(iii) The characteristic boundary condition at outflows can also be applied using the Riemann invariants as in the inflow boundaries described previously in Section 2.2.1. For this case $J_e^- = J_\infty^-$, $J_e^+ = J_i^-$, $V_e = V_i$, $X_{j,e} = X_{j,i}$ and $s_e = s_i$. Also, U_e, a_e and ρ_e can be determined in a similar way. In the present research, this boundary condition is also considered, however, satisfactory results are not obtained, and it is concluded that, this boundary condition needs much larger computational domains than the ones considered in the present study to give acceptable results.

Also, it should be noted that, although at the top and right boundaries the flow is expected to move outwards, sometimes during the computations, it may direct inwards. This may occur at the top edge because the normal velocity component V is much smaller than the streamwise velocity component U there. In situations like this, either the outflow boundary condition

may be replaced by inflow boundary condition at those cells, or the properties of the outflow boundaries may not be updated for that time step. Both approaches are considered in this study, and it is concluded that the former approach is preferable.

2.2.3 The Streamline Extrapolation Technique

In this study, a new type of extrapolation technique is developed for the application of outflow boundary conditions. In most applications, the extrapolation is done using the nearest neighboring cells, but in this new technique this is accomplished using the streamline trajectories.

In the present computations, a rectangular domain is used and the top and right edges of this domain correspond to outflow boundaries (as will be discussed in the next chapter in Figure 3.1). A "ghost cell" is introduced adjacent to the each cell in order to determine the flow properties at the outflow boundaries, and the following algorithm is used.

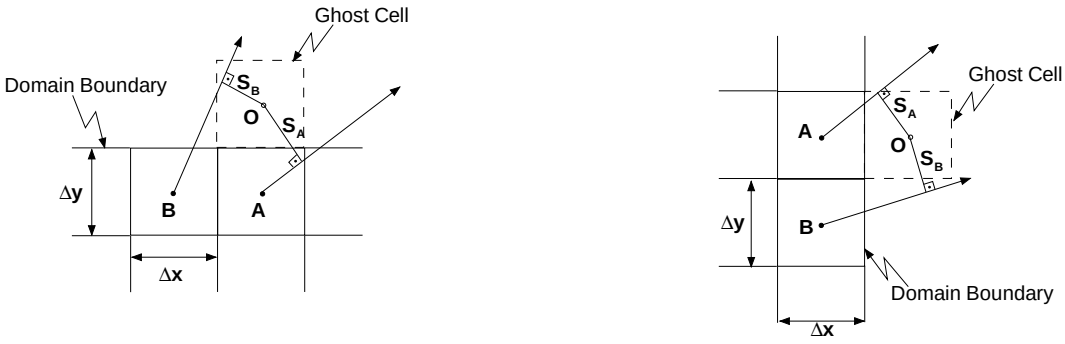

(a) Top Boundary

(b) Right Boundary

Figure 2.3: Streamline extrapolation technique.

Consider the top boundary as shown in Figure 2.3.a. Assuming that the streamlines are linear at the domain boundaries, one can draw the streamlines passing through the cell centers A and B. The fundamental assumption of this method is that the center of ghost cell lies in between these two streamlines for extrapolation of properties between A and B. If this condition is not

met, a searching process is started considering other two adjacent boundary cells until it is satisfied. Supposing the ghost cell O lies in between the streamlines passing through points A and B (as shown in Figure 2.3.a), the macroscopic properties at O are calculated by weighted interpolation (based on the shortest distances between point O and these streamlines, i.e. S_A and S_B) of the properties at cells A and B.

The shortest distance, S, between point O and a line passing through a point P is shown in Figure 2.4. Let $\vec{\mathbf{V_P}}$ denote the velocity vector at point P, and $\vec{\mathbf{r_O}}$, $\vec{\mathbf{r_P}}$ are the position vectors.

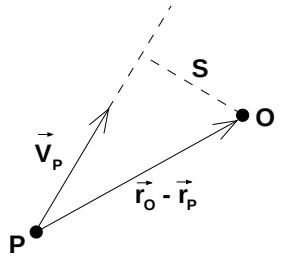

Figure 2.4: Distance between a point and a line.

S is calculated as:

$$S = \frac{|(\vec{\mathbf{r_O}} - \vec{\mathbf{r_P}}) \times \vec{\mathbf{V_P}}|}{|\vec{\mathbf{V_P}}|} \quad . \tag{2.16}$$

(i) Consider the top boundary cells in which cell O is N cells away from the point P. Then,

$$x_O = x_P + N\,\Delta x \quad ,$$

$$y_O = y_P + \Delta y \quad ,$$

$$\vec{\mathbf{V_P}} = U_P\,\vec{\mathbf{i}} + V_P\,\vec{\mathbf{j}} \quad ,$$

$$\vec{\mathbf{r_O}} - \vec{\mathbf{r_P}} = (N\,\Delta x)\,\vec{\mathbf{i}} + \Delta y\,\vec{\mathbf{j}} \quad ,$$

$$(\vec{\mathbf{r_O}} - \vec{\mathbf{r_P}}) \times \vec{\mathbf{V_P}} = (V_P\, N\, \Delta x)\, \vec{\mathbf{k}} - (U_P\, \Delta y)\, \vec{\mathbf{k}} \quad ,$$

$$S = \frac{V_P\, N\, \Delta x - U_P\, \Delta y}{\sqrt{U_P^2 + V_P^2}} \tag{2.17}$$

where Δx, Δy give the cell dimensions, and $\vec{\mathbf{i}}$, $\vec{\mathbf{j}}$, $\vec{\mathbf{k}}$ are the unit Cartesian vectors. Note that N can be $N = 0, \mp 1, \mp 2, \ldots$ and for positive N, point P is on the left of point O; for negative N, point P is on the right of point O.

(ii) If the same procedure is followed for the right boundary cells in which cell O is N cells away from the point P. Then,

$$x_O = x_P + \Delta x \quad ,$$

$$y_O = y_P + N\, \Delta y \quad ,$$

$$\vec{\mathbf{r_O}} - \vec{\mathbf{r_P}} = \Delta x\, \vec{\mathbf{i}} + (N\, \Delta y)\, \vec{\mathbf{j}} \quad ,$$

$$(\vec{\mathbf{r_O}} - \vec{\mathbf{r_P}}) \times \vec{\mathbf{V_P}} = (V_P\, \Delta x)\vec{\mathbf{k}} - (U_P\, N\, \Delta y)\, \vec{\mathbf{k}} \quad ,$$

$$S = \frac{V_P\, \Delta x - U_P\, N\, \Delta y}{\sqrt{U_P^2 + V_P^2}} \quad . \tag{2.18}$$

Again, N can be $N = 0, \mp 1, \mp 2, \ldots$ and for positive N, point P is below of point O; for negative N, point P is above point O.

Then a weighting factor, α, is calculated from

$$\alpha = \frac{S_A}{S_A + S_B} \tag{2.19}$$

and is used to determine the macroscopic quantities (ϕ), which are assigned to the ghost cell, according to the relation:

$$\phi_O = (1 - \alpha)\, \phi_A + \alpha\, \phi_B \quad . \tag{2.20}$$

It is clear that, if the streamline of A goes through point O ($S_A = 0$), then α becomes zero and the properties of cell A are assigned to cell O. On the other hand, if the streamline of B passes through point O ($S_B = 0$), then α becomes 1 and the properties of cell B are extrapolated to cell O. Also, if point O is equidistant from the streamlines passing through A and B ($S_A = S_B$), then $\alpha = 0.5$ and $\phi_O = \frac{\phi_A + \phi_B}{2}$.

CHAPTER 3

RESULTS AND DISCUSSIONS

3.1 Numerical Calculation Procedures

The aim of this study is to simulate two-dimensional rarefied subsonic gas flows over a flat plate using the DSMC method. In the simulations, air with two species (O_2 and N_2) with molar compositions of 21.2% and 78.8%, respectively, is used for the freestream. Variable-hard-sphere (VHS) model [20] is applied for the molecular collisions. In the present computations, the mean free path for the VHS molecules is calculated from

$$\lambda = \frac{(\frac{T}{T_{ref}})^{\omega}}{(2-\omega)^{\omega}\,\Gamma(2-\omega)\,\sqrt{2}\,n\,\pi\,(d_{ref})^2} \tag{3.1}$$

where ω is the temperature exponent of the coefficient of viscosity (0.74), T_{ref} is the reference temperature (298.15 K), Γ is the gamma function, n is the number density and d_{ref} is the reference diameter ($4.02 \times 10^{-10} m$). Larsen-Borgnakke model is employed to control the energy exchange between translational and internal modes. The rotational and vibrational relaxation collision numbers are 5 and 50, respectively.

3.2 Domain Configuration and Freestream Conditions

In this research, both semi-infinite plate and finite plate configurations are considered as illustrated in Figure 3.1. The temperature of the plate, T_w, is $299.4\,K$ and length of the plate is

equal to $L\,(5.584 \times 10^{-6}\,m)$ or multiples of L.

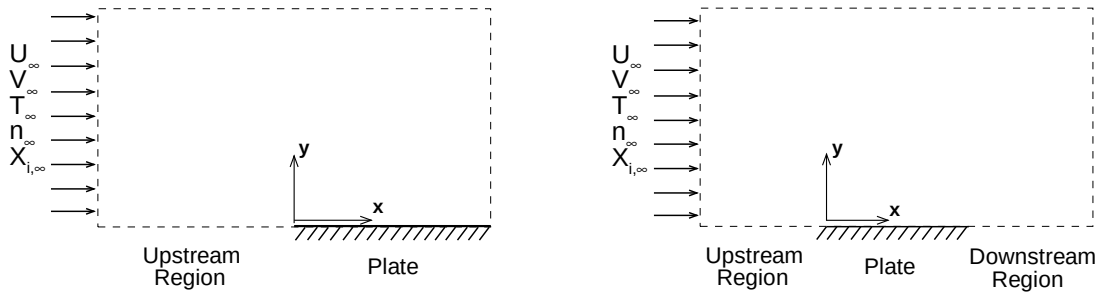

(a) Semi-infinite plate

(b) Finite plate

Figure 3.1: Schematic of the domains.

In order to get satisfactory results using the DSMC technique, the cell sizes should be of the order of local mean free path. For most of the cases investigated in the present study, Δx and Δy are taken approximately equal to λ. For a few calculations, $\Delta x > \lambda$ (in the streamwise direction of the flow) is considered, but in all computations Δy (in the transverse direction of the flow) is taken equal to λ. In all the calculations, approximately 10 representative molecules are used in each cell.

Throughout this work, various freestream conditions are considered for the subsonic rarefied flows over an infinitely thin flat plate with zero angle of attack at constant pressure. These flow conditions are tabulated in Table 3.1.

Table 3.1: Freestream conditions

U_∞ $[\frac{m}{s}]$	V_∞ $[\frac{m}{s}]$	M	T_∞ $[K]$	p_∞ $[\frac{N}{m^2}]$	n_∞ $[\frac{molecule}{m^3}]$	λ_∞ $[m]$	$X_{O_2,\infty}$ %	$X_{N_2,\infty}$ %
35.26	0	0.102	299.4	97589.09	2.36×10^{25}	5.584×10^{-8}	21.2	78.8
35.26	0	0.102	299.4	9758.909	2.36×10^{24}	5.584×10^{-7}	21.2	78.8
35.26	0	0.102	299.4	975.8909	2.36×10^{23}	5.584×10^{-6}	21.2	78.8
138.74	0	0.4	299.4	975890.9	2.36×10^{26}	5.584×10^{-9}	21.2	78.8
138.74	0	0.4	299.4	97589.09	2.36×10^{25}	5.584×10^{-8}	21.2	78.8
138.74	0	0.4	299.4	9758.909	2.36×10^{24}	5.584×10^{-7}	21.2	78.8
138.74	0	0.4	299.4	975.8909	2.36×10^{23}	5.584×10^{-6}	21.2	78.8

3.3 Boundary Conditions Used in the Simulations

In the present simulations, the following boundary conditions are used:

- **Inflow Boundary Conditions:**

Two different subsonic inflow boundary conditions are considered. For the first case, one of the variables (in this case V) is extrapolated from the interior domain (numerical boundary condition) and the other variables are specified (physical boundary condition) at the inflow boundary. For the second case, Riemann inflow boundary condition is applied [See Section 2.2.1, page 11, for both cases].

- **Outflow Boundary Conditions:**

For the domain sketched in Figure 3.1, both the top and right boundaries are outflow boundaries. Several outflow boundary conditions are considered at these boundaries. In this analysis, either Neumann boundary conditions are used or Whitfield's characteristic formulation with constant exit pressure [14] is applied [See Section 2.2.2, page 14, for these cases]. For these boundary conditions, the extrapolated properties outside the computational domain are calculated either from the closest neighboring cell or by using the streamline extrapolation technique explained in Section 2.2.3. Different case letters are assigned for different outflow boundary

conditions as listed in Table 3.2, and these case letters are used in the rest of the thesis.

Table 3.2: Different outflow boundary conditions

Case	**Outflow Boundary Condition**
A	Streamline Extrapolation & Neumann Boundary Condition
B	Streamline Extrapolation & Whitfield's Characteristic Formulation
C	Adjacent Cell & Neumann Boundary Condition
D	Adjacent Cell & Whitfield's Characteristic Formulation

The fluid properties at the domain boundaries are updated during the calculations by the use of the above-mentioned inflow and outflow extrapolation boundary conditions for subsonic flows.

3.4 Simulation Results

In this thesis, several test run results are presented for different boundary conditions, domain configurations and freestream conditions. Table 3.3 summarizes these test runs. Note that Kn and Re of each run in this table are evaluated using the corresponding plate length. In these simulations, after steady state is reached, computations are continued for about 2×10^6 time steps and samples are taken every other time step to calculate the time-averaged results. These results are presented in Figures 3.2 - 3.133. Four figures and two pages are allocated for each test run. Note that in these figures, plate's leading edge is at $x = 0$. Also, for these flows, experimental measurement is available for the drag coefficients [18].

In the present study, the density is nearly constant in the whole domain and comparison may also be made with the incompressible Blasius solution [23]. For a given x and y

$$\eta = y\sqrt{\frac{\rho_\infty U_\infty}{\mu_\infty x}} \quad ,$$

$$U = f'(\eta)\, U_\infty \quad ,$$

$$V = \frac{1}{2}\sqrt{\frac{\mu_\infty U_\infty}{\rho_\infty x}}(\eta f' - f)$$

where μ is the viscosity and $f(\eta)$ and $f'(\eta)$ are listed in [23]. The transverse velocity distribution at the top boundary is:

$$V_\infty = 0.8604\, U_\infty \sqrt{\frac{\mu_\infty}{\rho_\infty\, U_\infty\, x}} \quad .$$

Shear stress, τ, distribution is calculated from the following equation:

$$\tau(x) = 0.332 \sqrt{\frac{\rho_\infty\, \mu_\infty\, U_\infty^3}{x}} \quad .$$

The drag coefficient is calculated based on half of the wetted area:

$$C_D = \frac{2.656}{\sqrt{Re}} \quad .$$

It should be kept in mind that Blasius solution is valid for the continuum flows and underpredicts the experimental data of the drag coefficient under rarefied conditions [18]. Also, one has to remember that Blasius solution is applicable for the flows over a semi-infinite flat plate. So, comparisons with Blasius solution are only done in semi-infinite plate calculations. Also, Blasius velocity profiles are plotted only at the midpoint and end of the plate. Note that for the Blasius solution, uniform freestream velocity is assumed at the leading edge (i.e. $U = U_\infty = \text{constant}$). However, the present results indicate that when the upstream portion of the domain is taken into account, there is a velocity profile at the leading edge. Still, due to the lack of extensive experimental data, making comparisons with the incompressible Blasius solution may be useful.

Table 3.3: Different test runs

Case	M	Kn	Re	ℓ_{up} [1]	Plate Length	ℓ_{down} [2]	Domain Height	Δx	Inflow B.C.	See Page
$A.1$	0.102	0.01	12.525	L	L	–	$1.5\,L$	λ	*Riemann* [3]	25
$A.2$	0.102	0.02	6.2625	L	$0.5\,L$	–	$1.5\,L$	λ	*Riemann*	27
$A.3$	0.102	0.02	6.2625	$0.5\,L$	$0.5\,L$	$0.5\,L$	$1.5\,L$	λ	*Riemann*	29
$A.4$	0.102	0.02	6.2625	L	$0.5\,L$	L	$1.5\,L$	λ	*Riemann*	31
$A.5$	0.102	0.02	6.2625	L	$0.5\,L$	L	$1.5\,L$	$5\,\lambda$	*Riemann*	33
$A.6$	0.102	0.01	12.525	L	L	–	$1.5\,L$	λ	*V extrapolation* [3]	35
$A.7$	0.102	0.2	0.62625	$2\,L$	$0.5\,L$	$2\,L$	$2\,L$	λ	*Riemann*	37
$A.8$	0.102	2	0.062625	$2\,L$	$0.5\,L$	$2\,L$	$2\,L$	λ	*Riemann*	39
$A.9$ [4]	0.102	∞	–	$2\,L$	$0.5\,L$	$2\,L$	$2\,L$	λ	*Riemann*	41
$A.10$	0.4	0.01	49.253	L	L	–	$0.75\,L$	λ	*Riemann*	43
$A.11$	0.4	0.02	24.627	L	$0.5\,L$	–	$0.75\,L$	λ	*Riemann*	45
$A.12$	0.4	0.02	24.627	$0.5\,L$	$0.5\,L$	$0.5\,L$	$0.75\,L$	λ	*Riemann*	47
$A.13$	0.4	0.02	24.627	L	$0.5\,L$	L	$0.75\,L$	λ	*Riemann*	49
$A.14$	0.4	0.02	24.627	$0.5\,L$	$0.5\,L$	$0.5\,L$	$0.75\,L$	$5\,\lambda$	*Riemann*	51
$A.15$	0.4	0.002	246.27	$0.5\,L$	$0.5\,L$	$0.5\,L$	$0.25\,L$	$5\,\lambda$	*Riemann*	53
$A.16$	0.4	0.02	24.627	$2\,L$	$0.5\,L$	$2\,L$	$2\,L$	$2.5\,\lambda$	*Riemann*	55
$A.17$	0.4	0.02	24.627	$2\,L$	$0.5\,L$	$2\,L$	$2\,L$	λ	*Riemann*	57
$A.18$	0.4	0.2	2.4627	$2\,L$	$0.5\,L$	$2\,L$	$2\,L$	λ	*Riemann*	59
$A.19$	0.4	2	0.24627	$2\,L$	$0.5\,L$	$2\,L$	$2\,L$	λ	*Riemann*	61
$A.20$ [4]	0.4	∞	–	$2\,L$	$0.5\,L$	$2\,L$	$2\,L$	λ	*Riemann*	63
$B.1$	0.102	0.01	12.525	L	L	–	$1.5\,L$	λ	*Riemann*	65
$B.2$	0.102	0.02	6.263	L	$0.5\,L$	–	$1.5\,L$	λ	*Riemann*	67
$B.3$	0.102	0.02	6.263	$0.5\,L$	$0.5\,L$	$0.5\,L$	$1.5\,L$	λ	*Riemann*	69
$B.4$	0.102	0.02	6.263	L	$0.5\,L$	L	$2.25\,L$	λ	*Riemann*	71
$B.5$	0.102	0.01	12.525	L	L	–	$1.5\,L$	λ	*V extrapolation*	73
$B.6$	0.102	0.005	25.05	L	$2\,L$	–	$3\,L$	λ	*Riemann*	75
$B.7$	0.102	0.02	6.263	L	$0.5\,L$	–	L	λ	*Riemann*	77
$C.1$	0.102	0.01	12.525	L	L	–	$1.5\,L$	λ	*Riemann*	79
$C.2$	0.102	0.02	6.263	$0.5\,L$	$0.5\,L$	$0.5\,L$	$1.5\,L$	λ	*Riemann*	81
$C.3$	0.102	0.01	12.525	L	L	–	$1.5\,L$	λ	*V extrapolation*	83
$D.1$	0.102	0.01	12.525	L	L	–	$1.5\,L$	λ	*Riemann*	85
$D.2$	0.102	0.02	6.263	$0.5\,L$	$0.5\,L$	$0.5\,L$	$1.5\,L$	λ	*Riemann*	87
$D.3$	0.102	0.01	12.525	L	L	–	$1.5\,L$	λ	*V extrapolation*	89

[1] Domain length in the upstream direction.

[2] Domain length in the downstream direction.

[3] See Section 2.2.1, page 11.

[4] Collisionless flow.

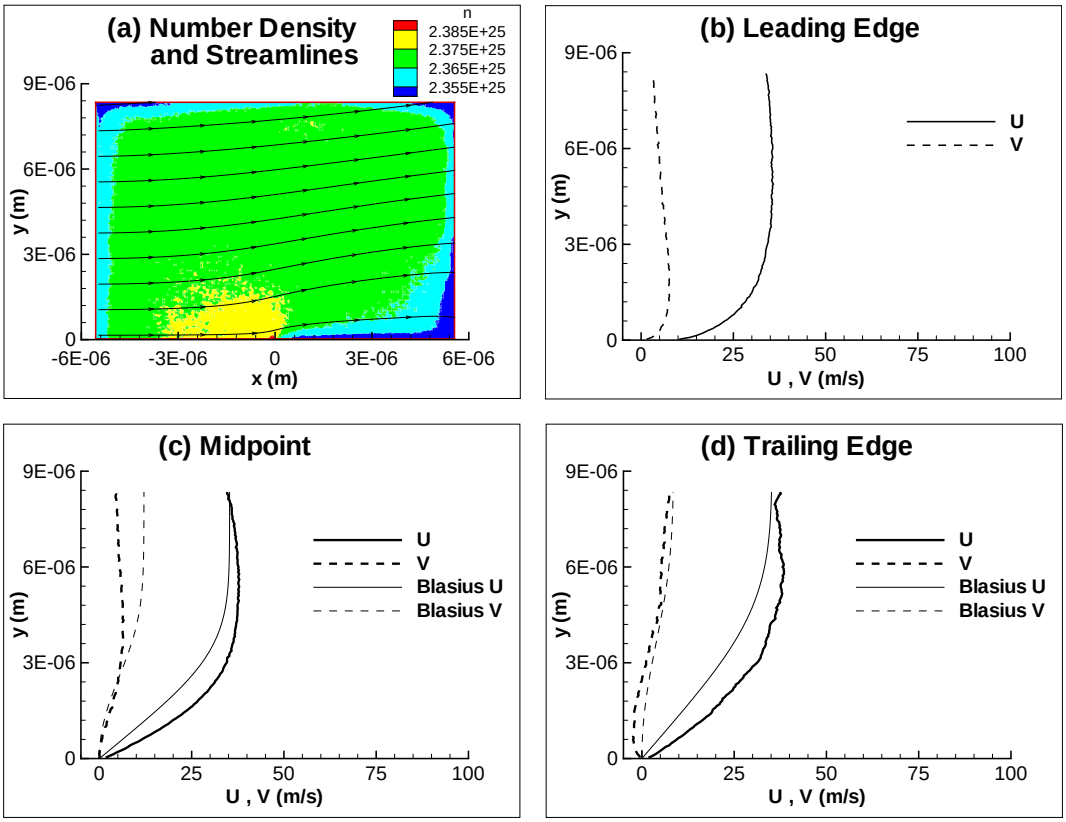

Figure 3.2: Case A.1 ; Number density contours, streamlines and velocity profiles.

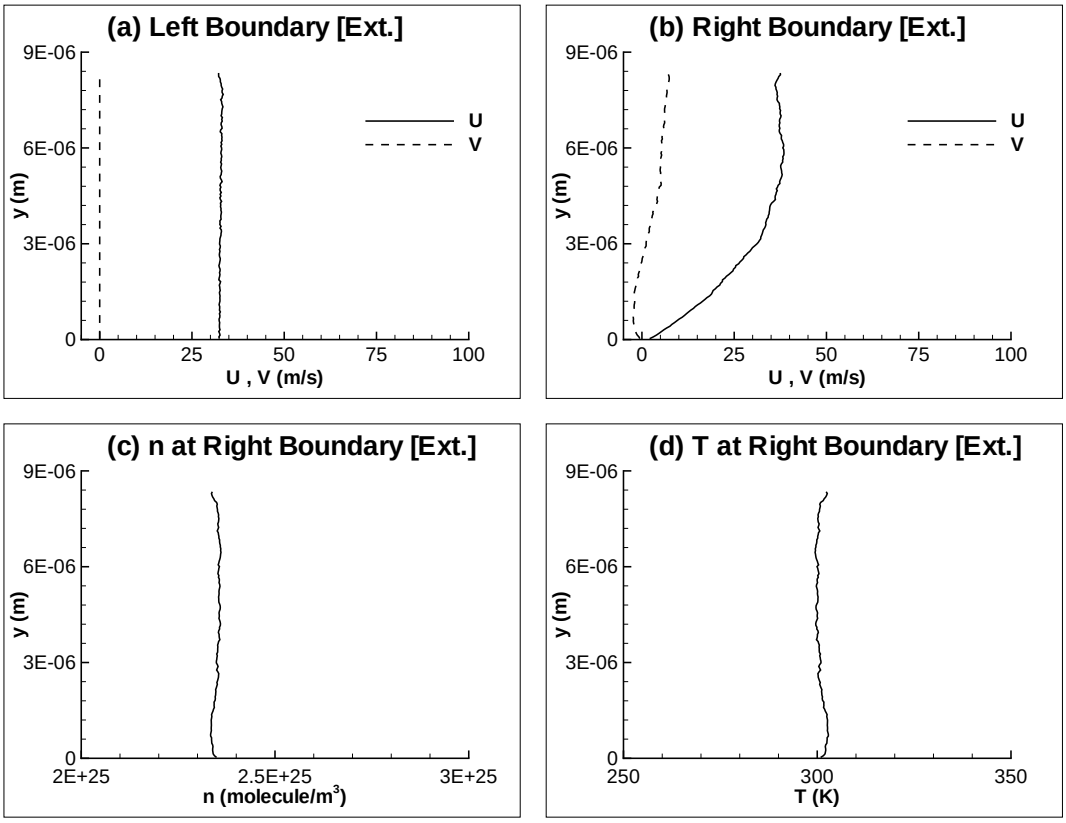

Figure 3.3: Case A.1 ; Extrapolated flowfield variables at left and right boundaries.

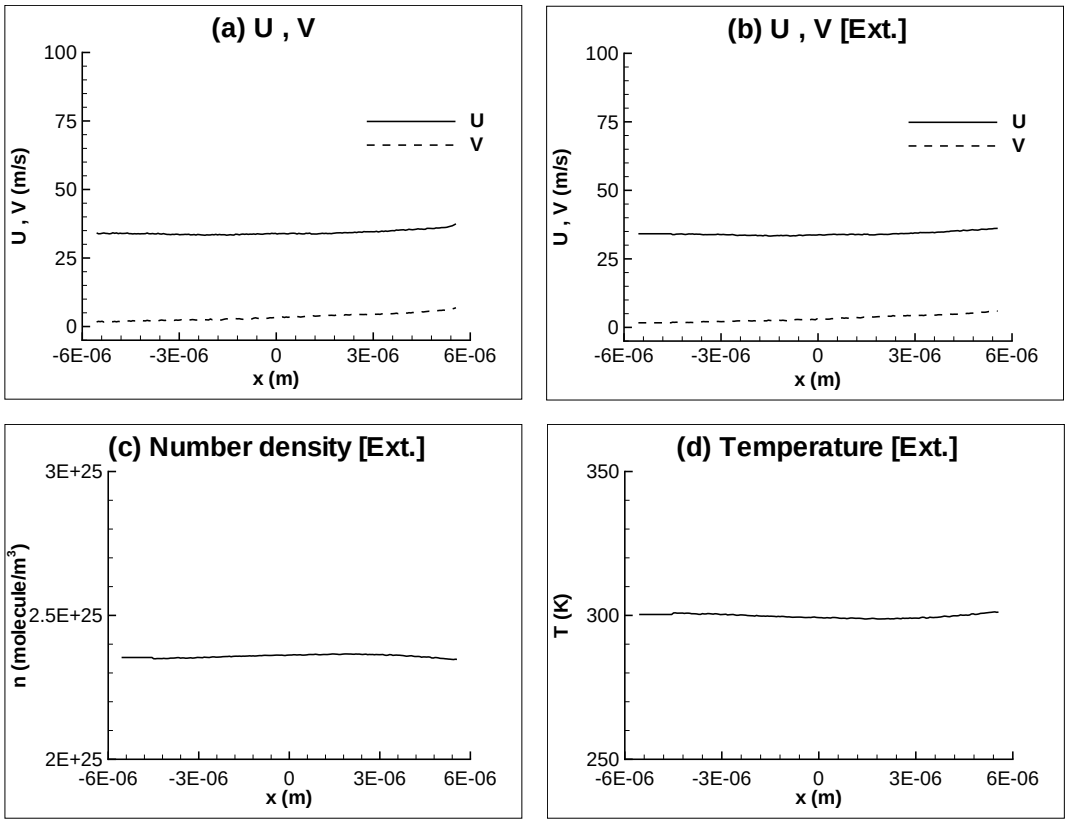

Figure 3.4: Case A.1 ; Velocities and extrapolated flowfield variables at top boundary.

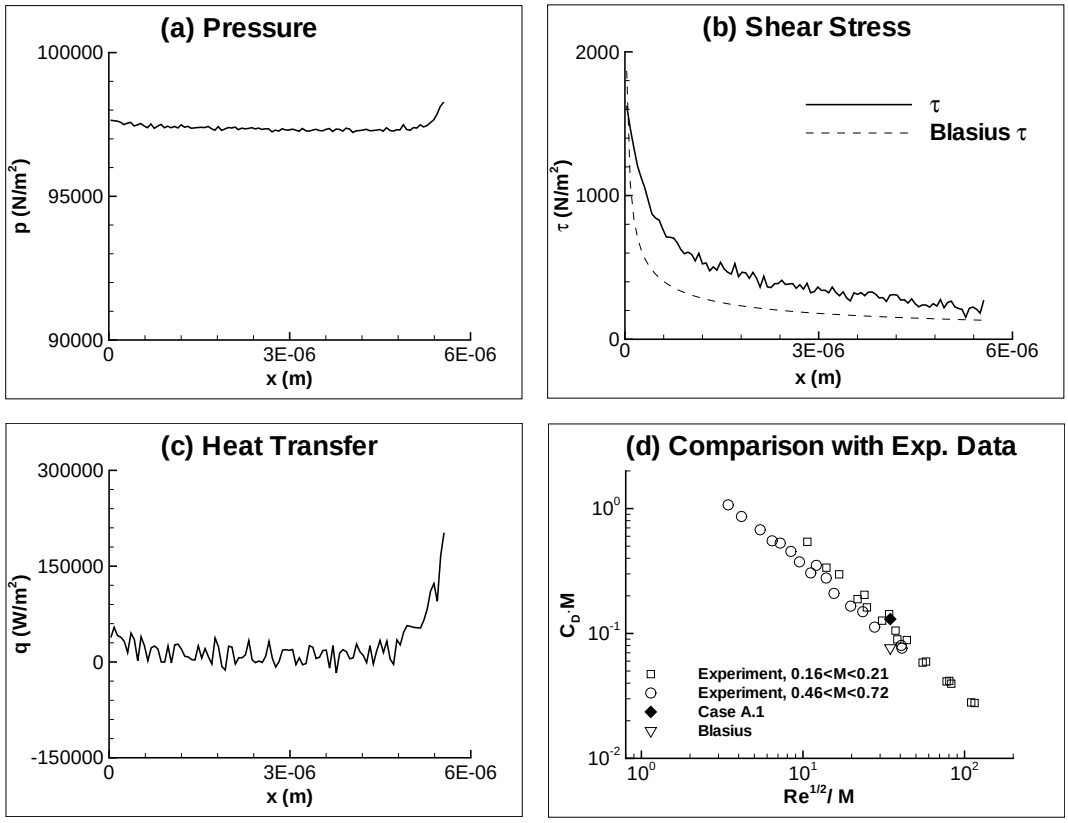

Figure 3.5: Case A.1 ; Surface properties and comparison with experimental data.

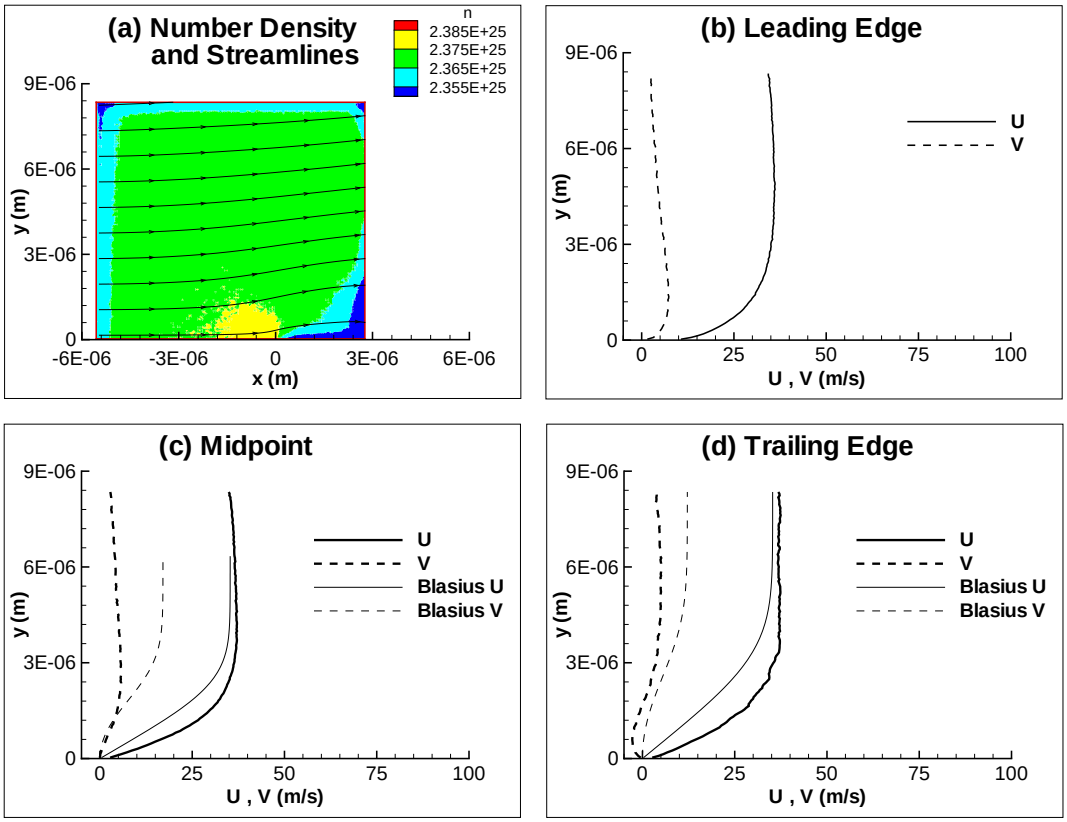

Figure 3.6: Case A.2 ; Number density contours, streamlines and velocity profiles.

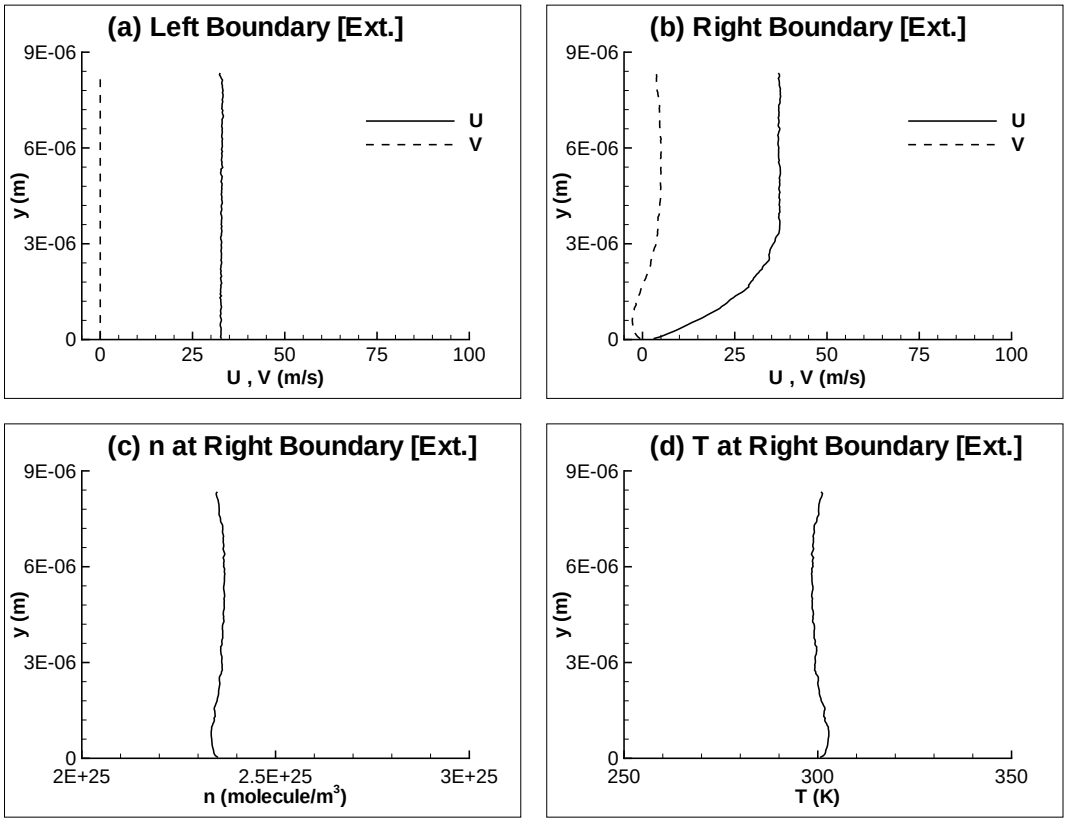

Figure 3.7: Case A.2 ; Extrapolated flowfield variables at left and right boundaries.

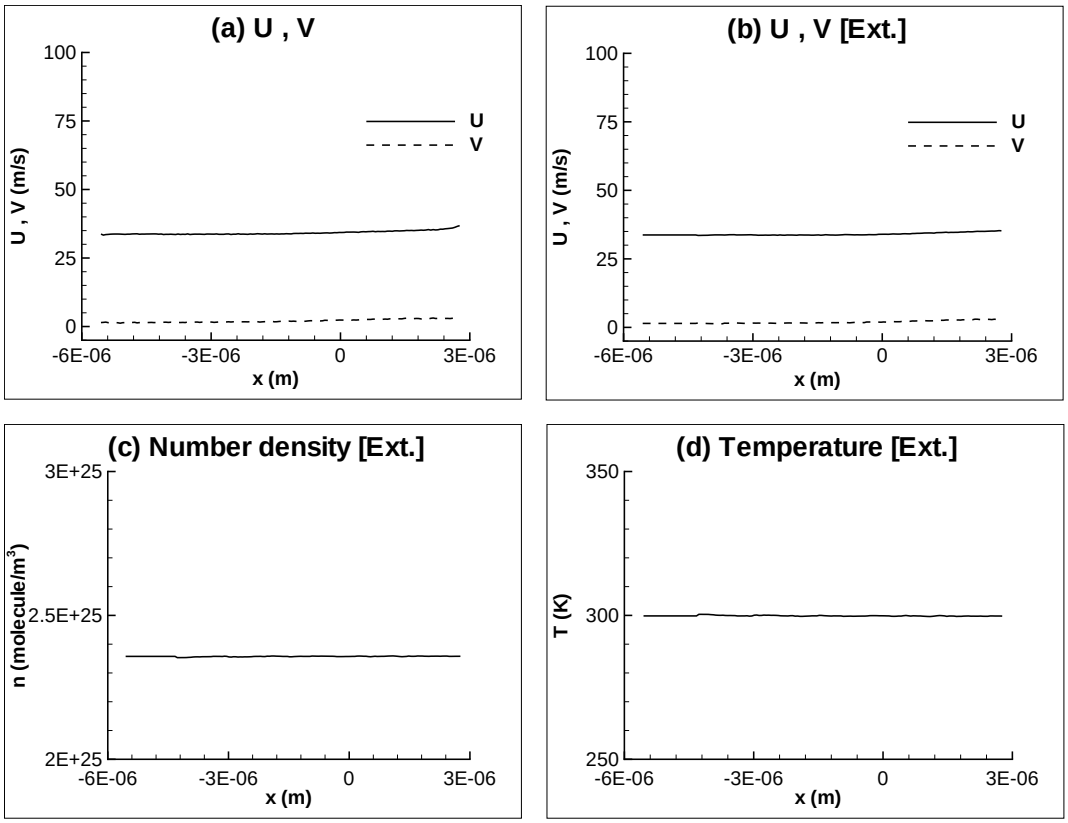

Figure 3.8: Case A.2 ; Velocities and extrapolated flowfield variables at top boundary.

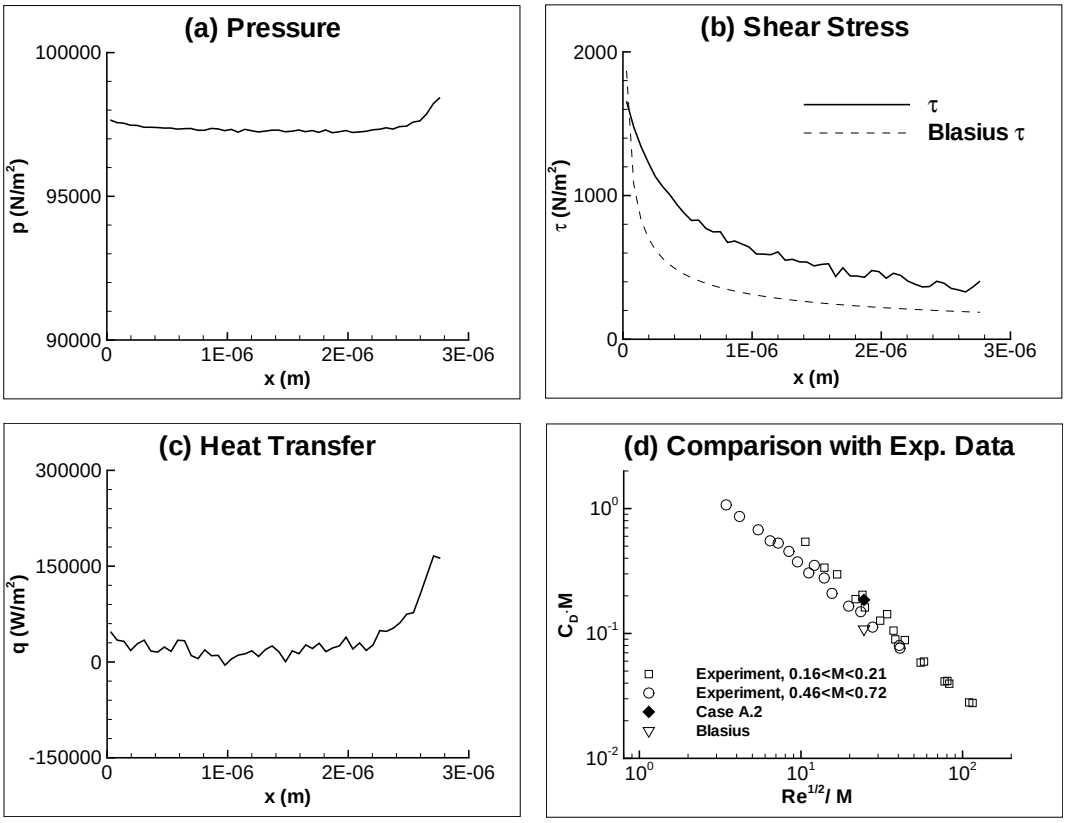

Figure 3.9: Case A.2 ; Surface properties and comparison with experimental data.

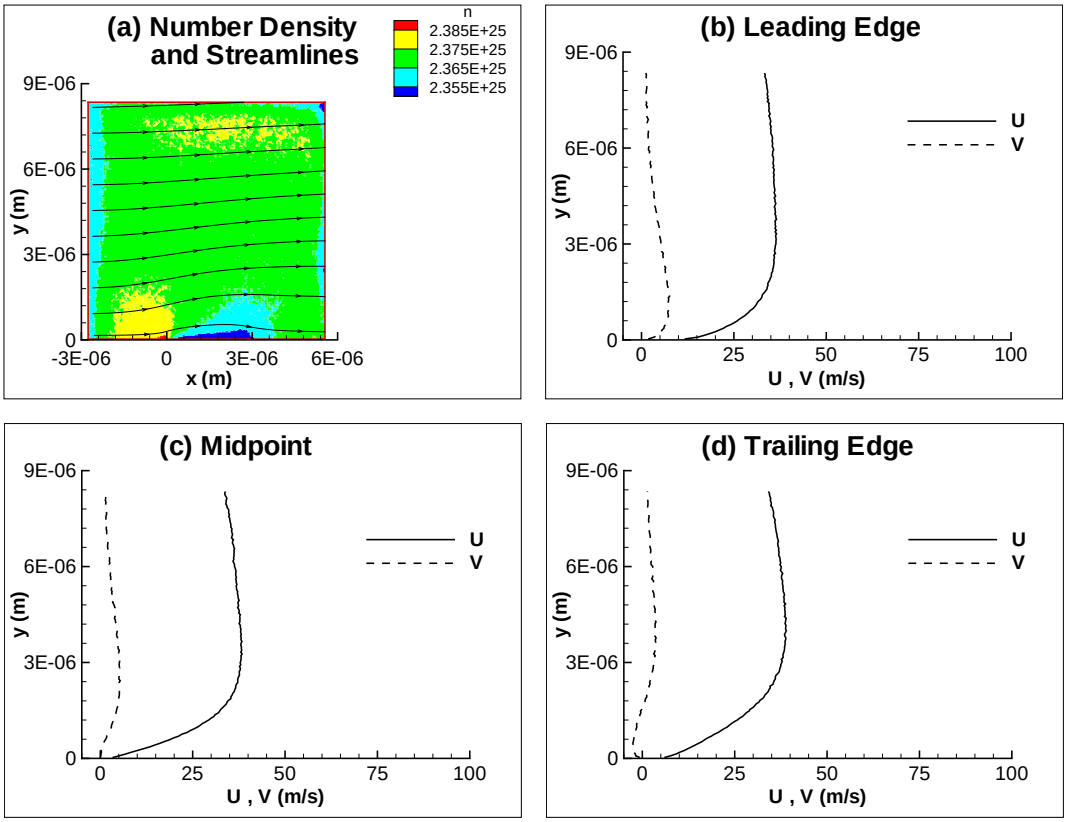

Figure 3.10: Case A.3 ; Number density contours, streamlines and velocity profiles.

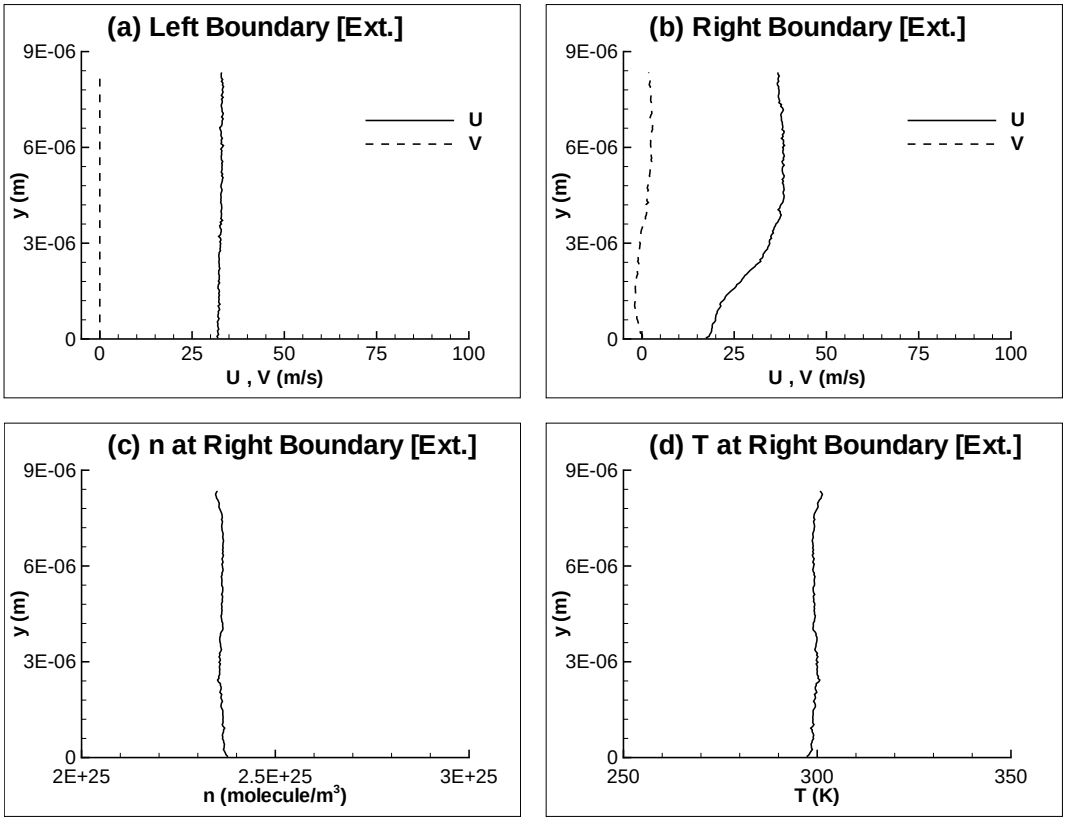

Figure 3.11: Case A.3 ; Extrapolated flowfield variables at left and right boundaries.

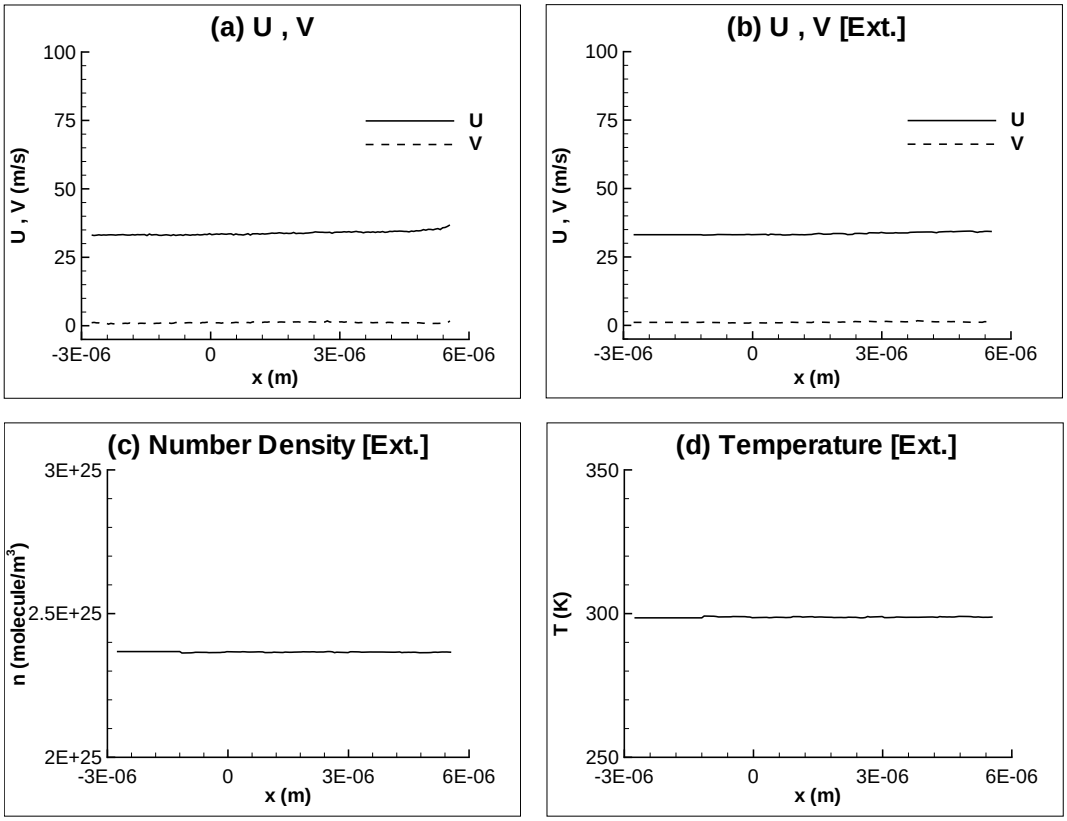

Figure 3.12: Case A.3 ; Velocities and extrapolated flowfield variables at top boundary.

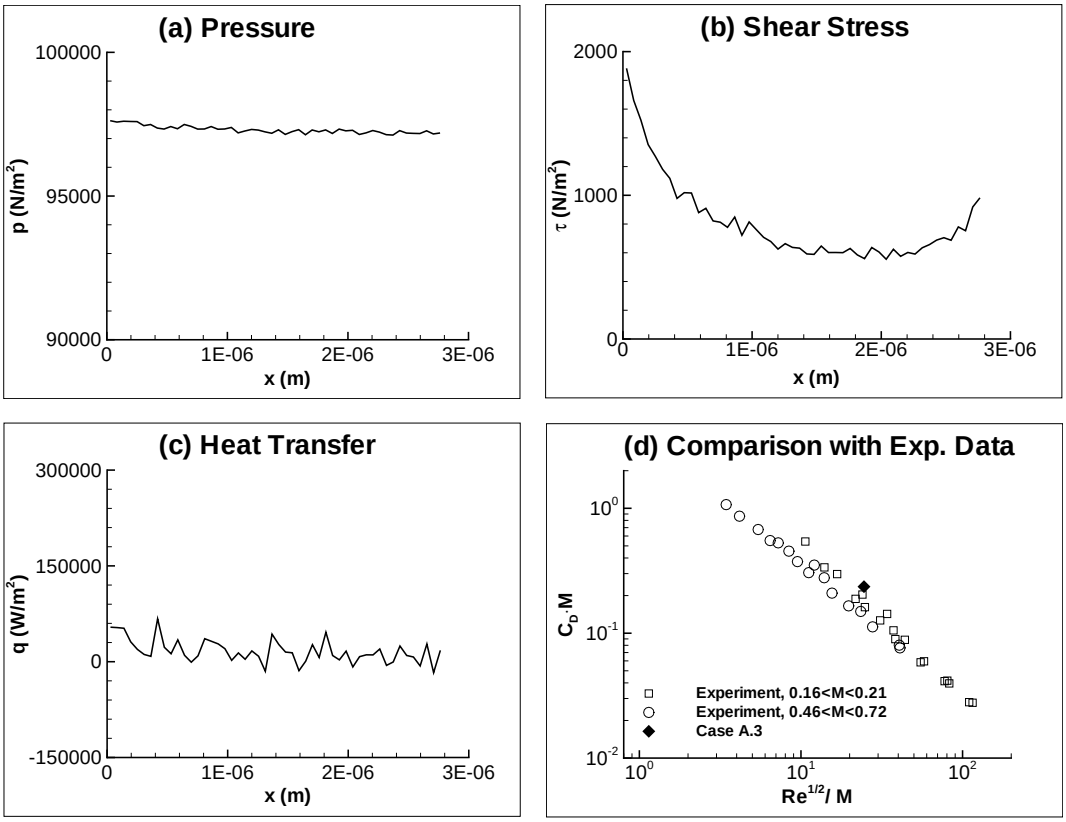

Figure 3.13: Case A.3 ; Surface properties and comparison with experimental data.

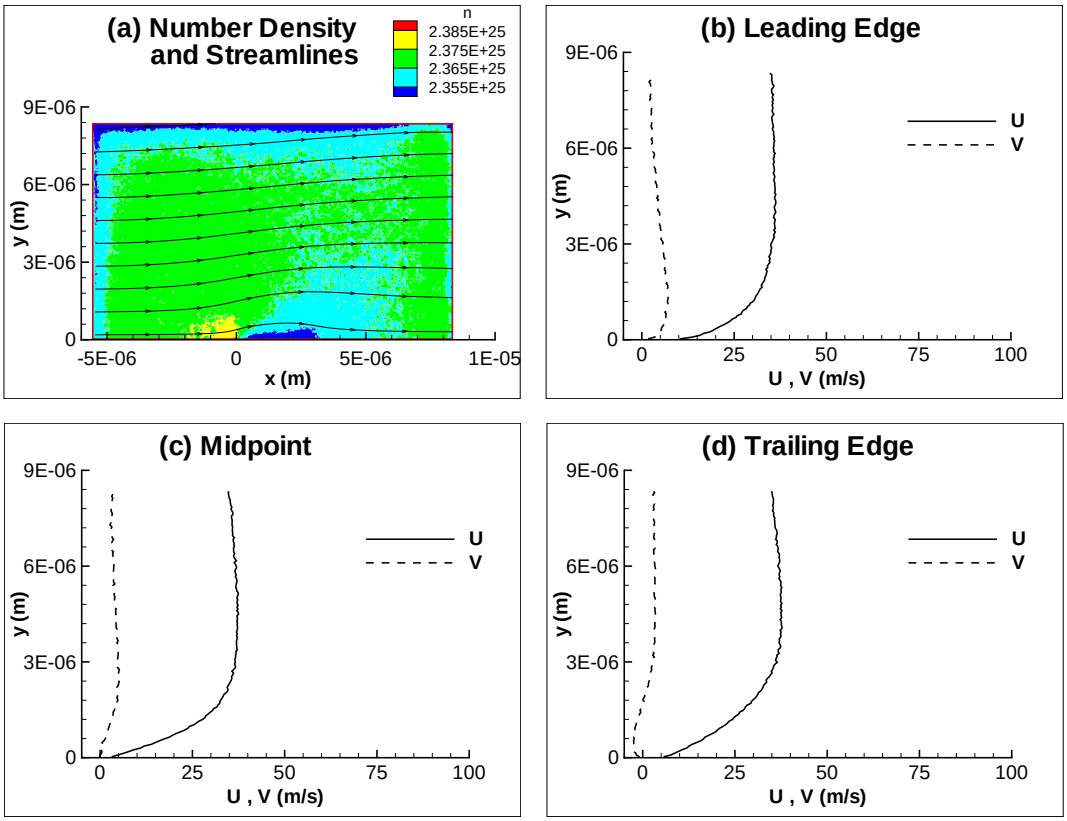

Figure 3.14: Case A.4 ; Number density contours, streamlines and velocity profiles.

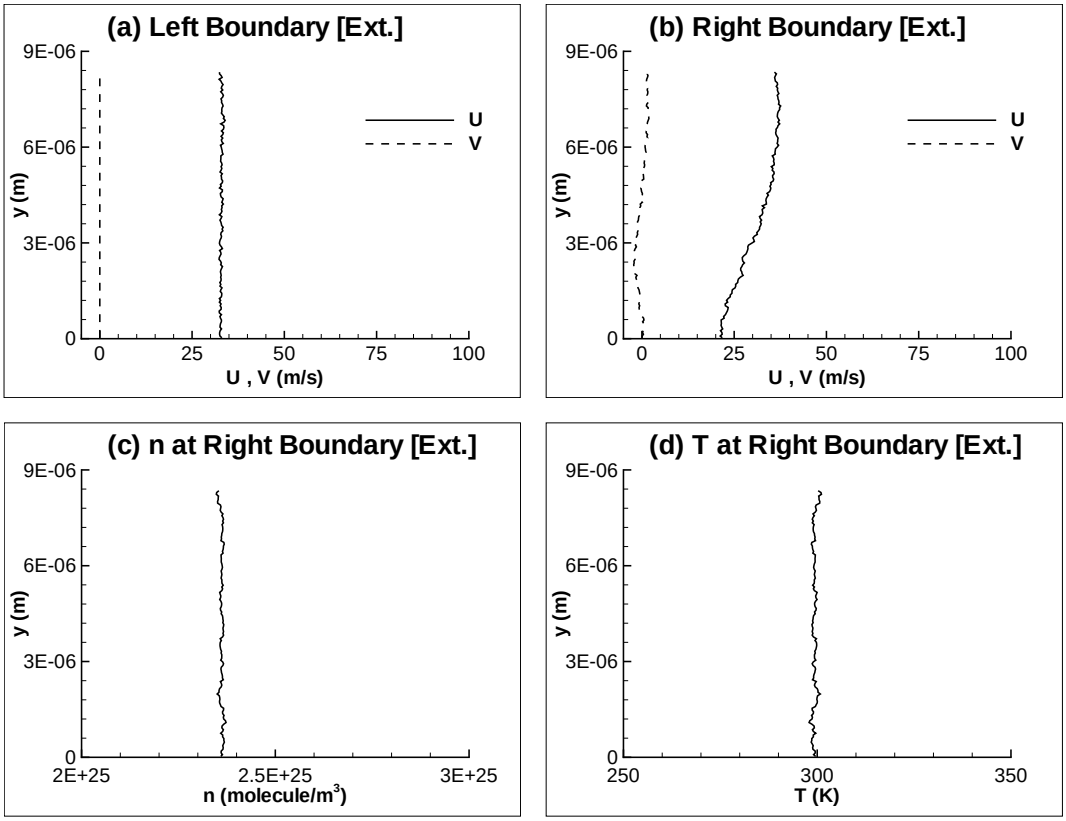

Figure 3.15: Case A.4 ; Extrapolated flowfield variables at left and right boundaries.

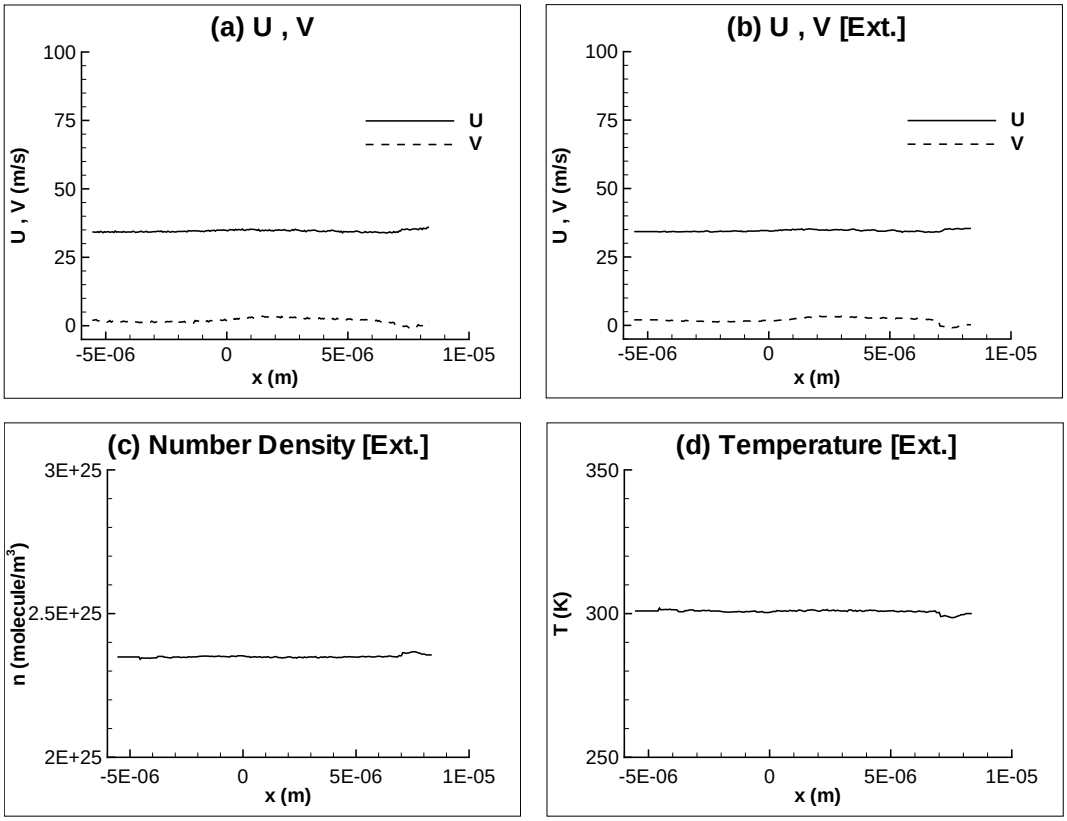

Figure 3.16: Case A.4 ; Velocities and extrapolated flowfield variables at top boundary.

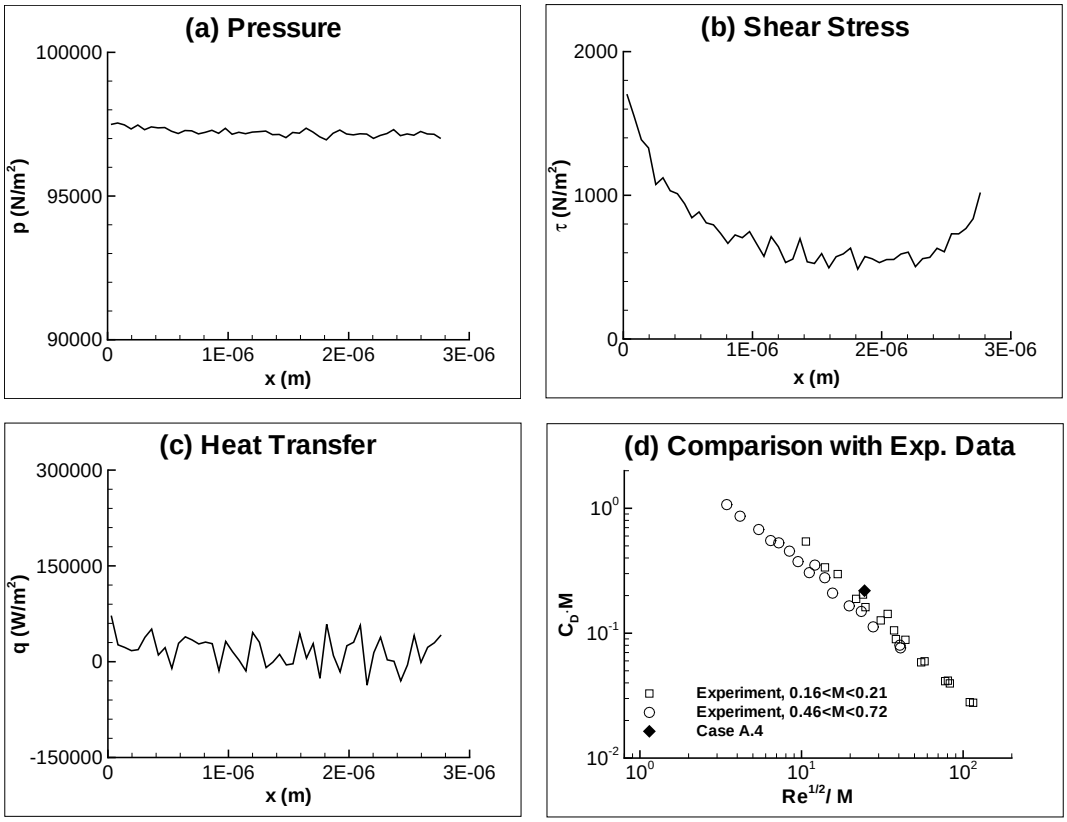

Figure 3.17: Case A.4 ; Surface properties and comparison with experimental data.

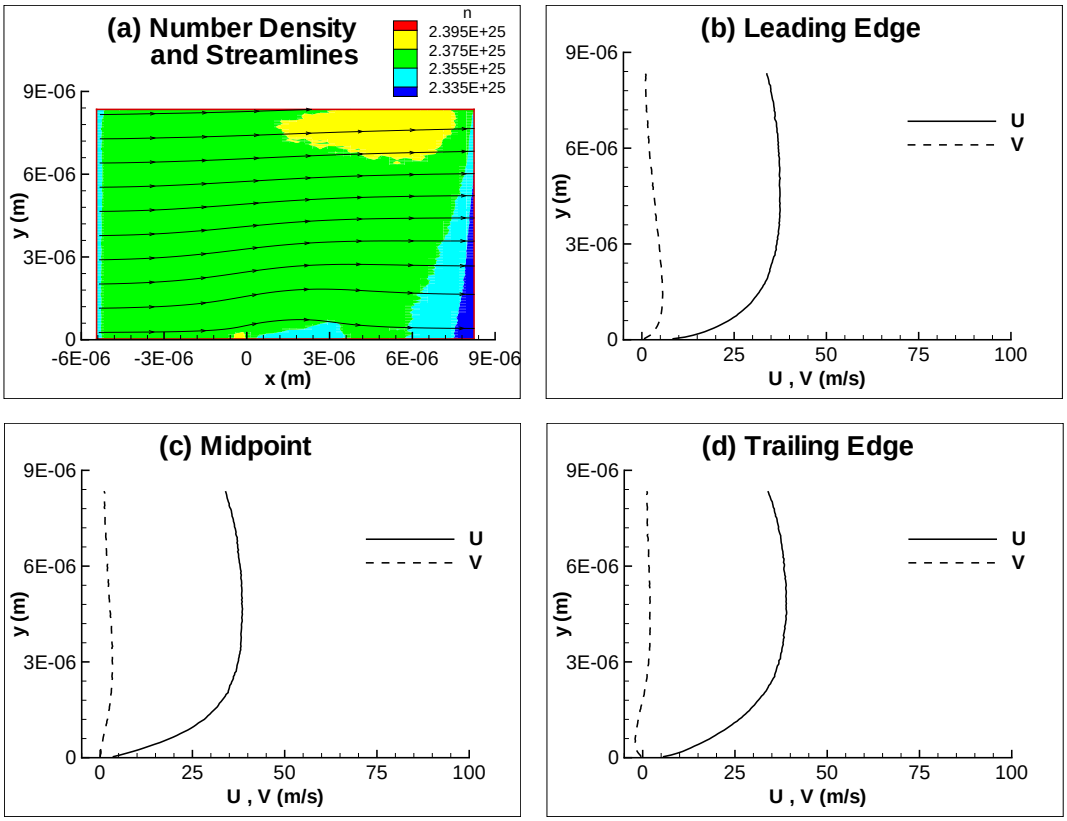

Figure 3.18: Case A.5 ; Number density contours, streamlines and velocity profiles.

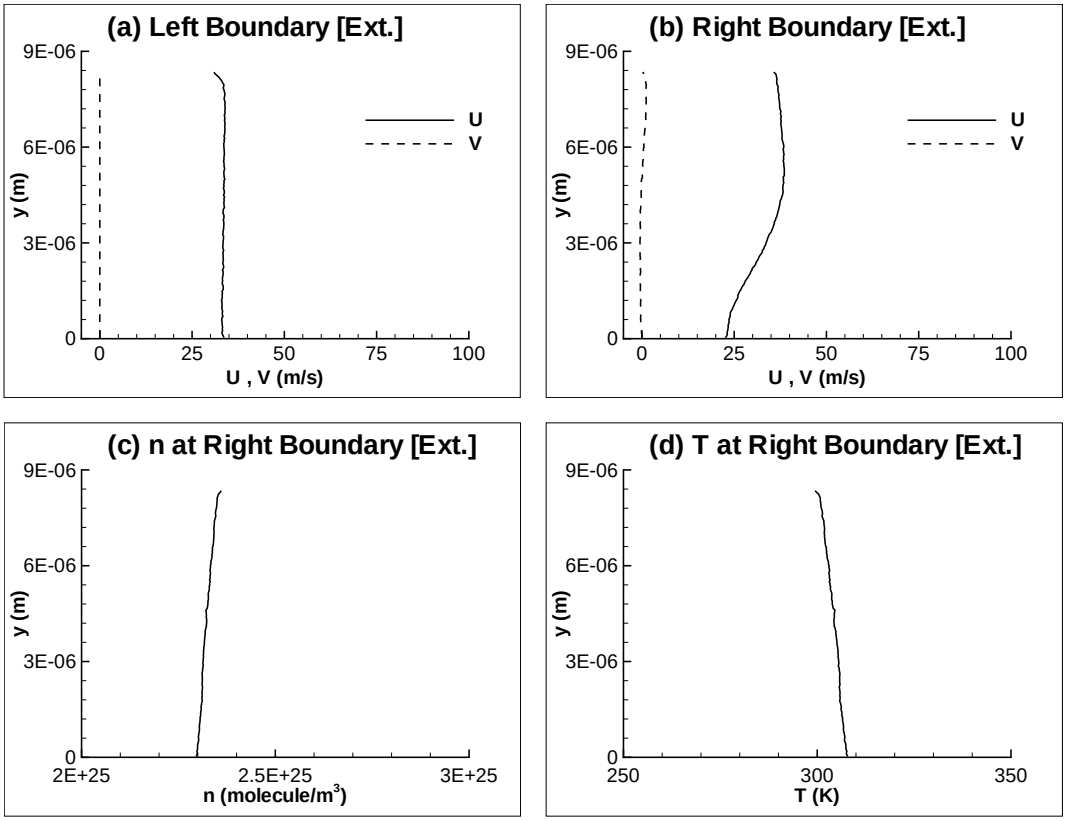

Figure 3.19: Case A.5 ; Extrapolated flowfield variables at left and right boundaries.

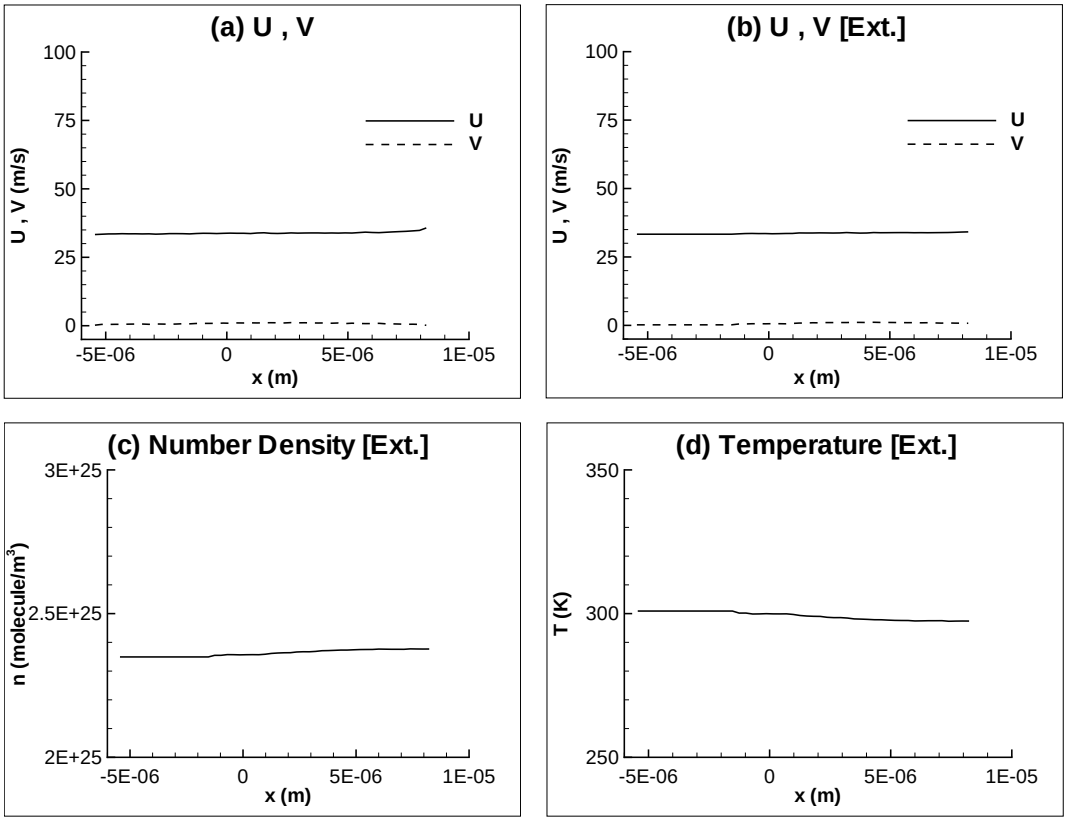

Figure 3.20: Case A.5 ; Velocities and extrapolated flowfield variables at top boundary.

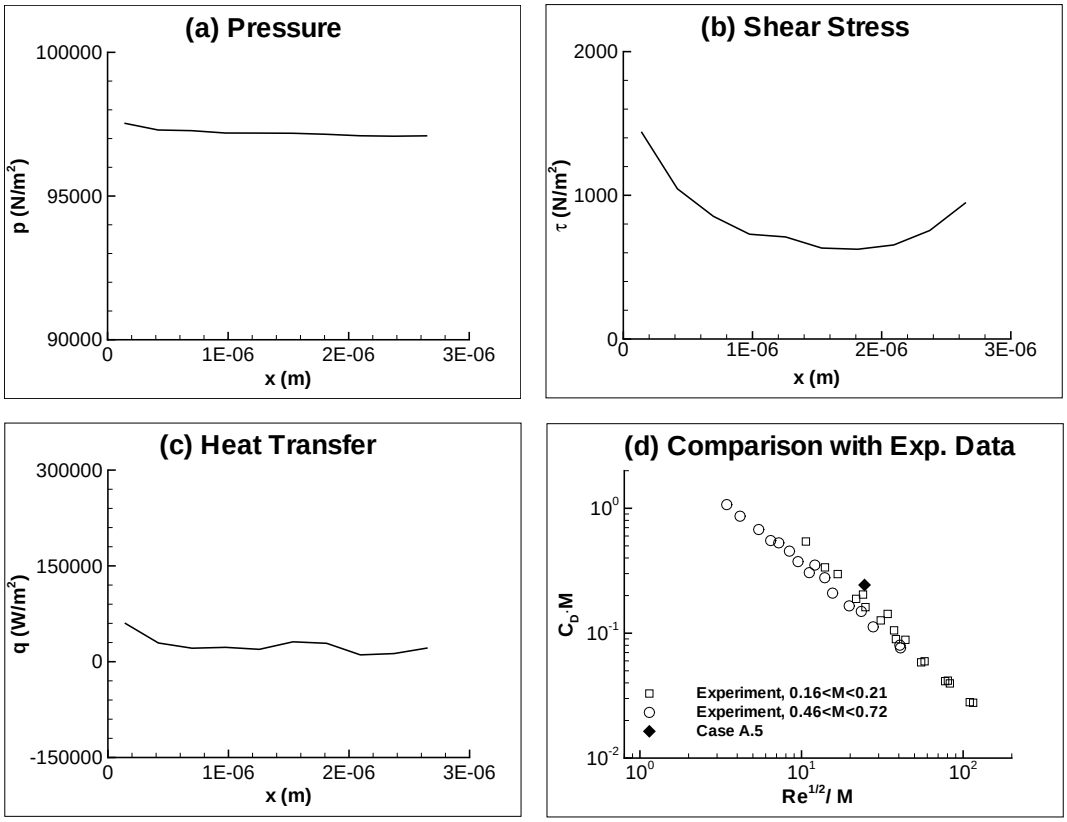

Figure 3.21: Case A.5 ; Surface properties and comparison with experimental data.

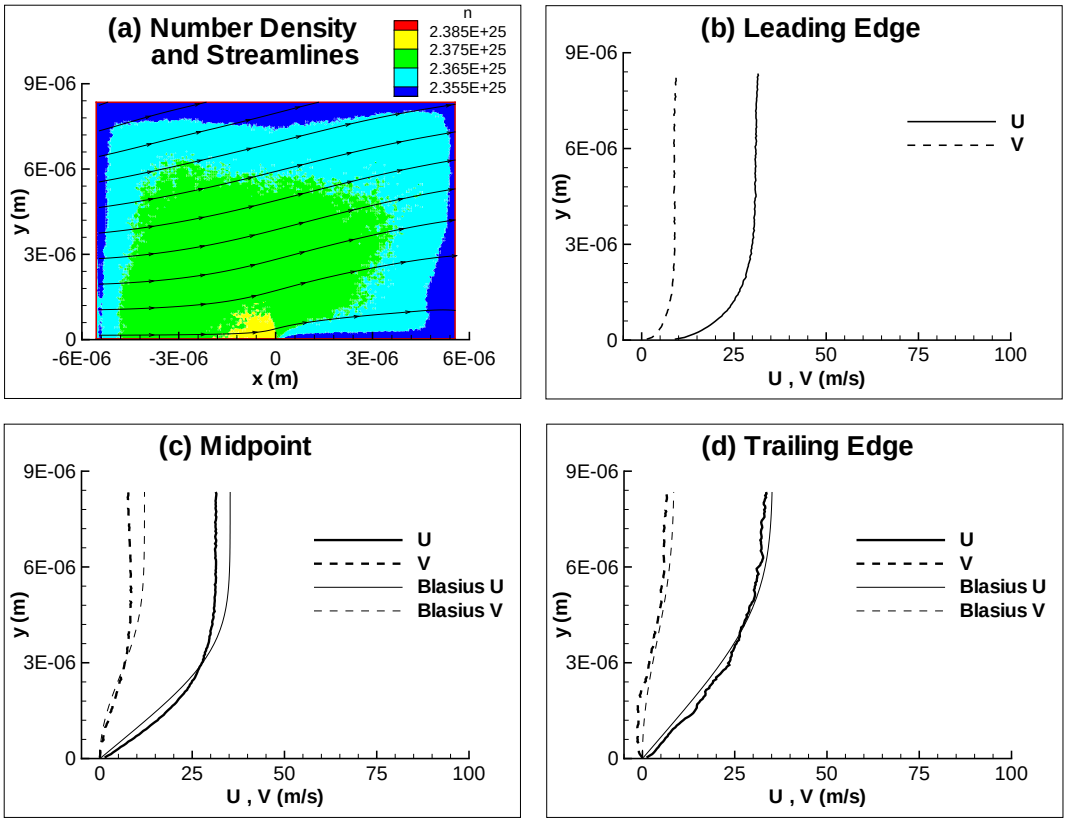

Figure 3.22: Case A.6 ; Number density contours, streamlines and velocity profiles.

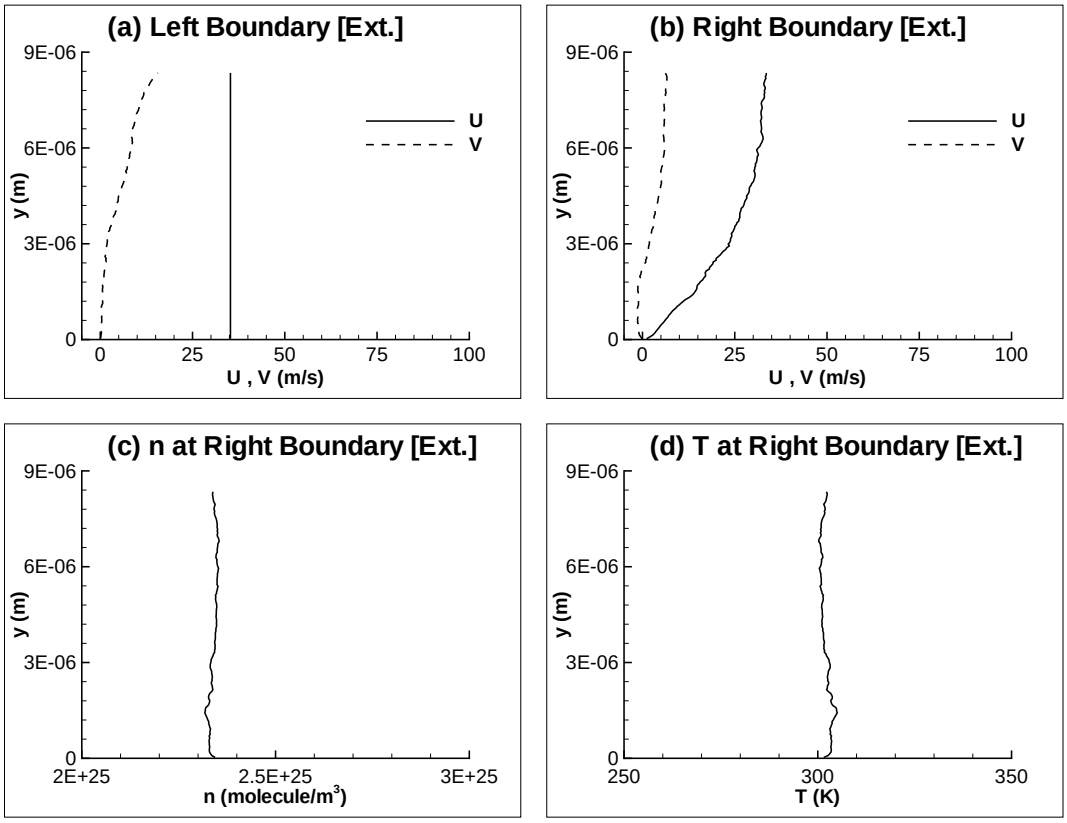

Figure 3.23: Case A.6 ; Extrapolated flowfield variables at left and right boundaries.

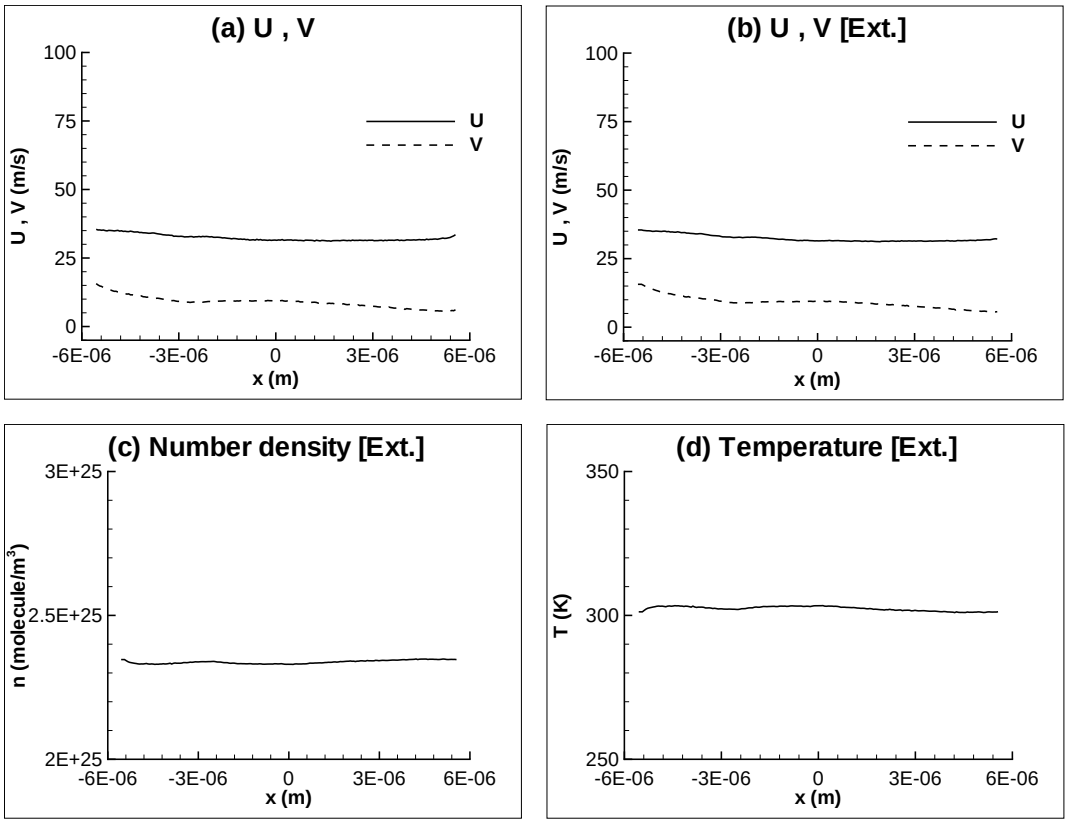

Figure 3.24: Case A.6 ; Velocities and extrapolated flowfield variables at top boundary.

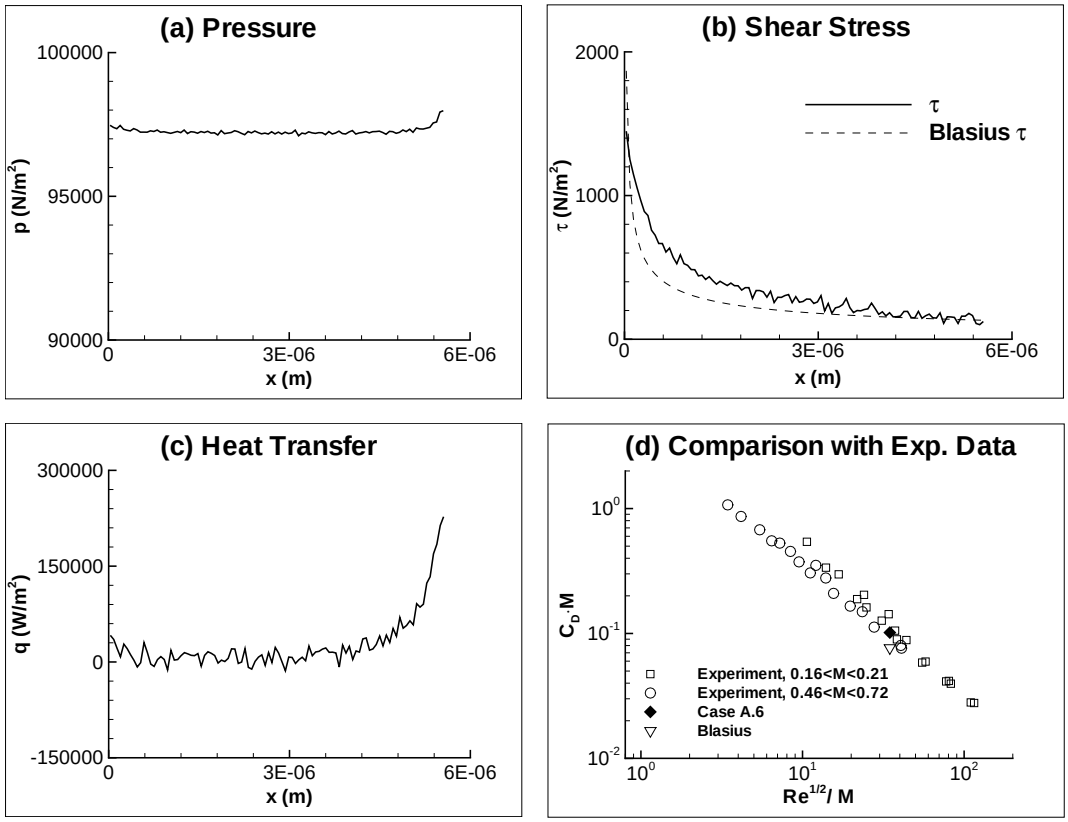

Figure 3.25: Case A.6 ; Surface properties and comparison with experimental data.

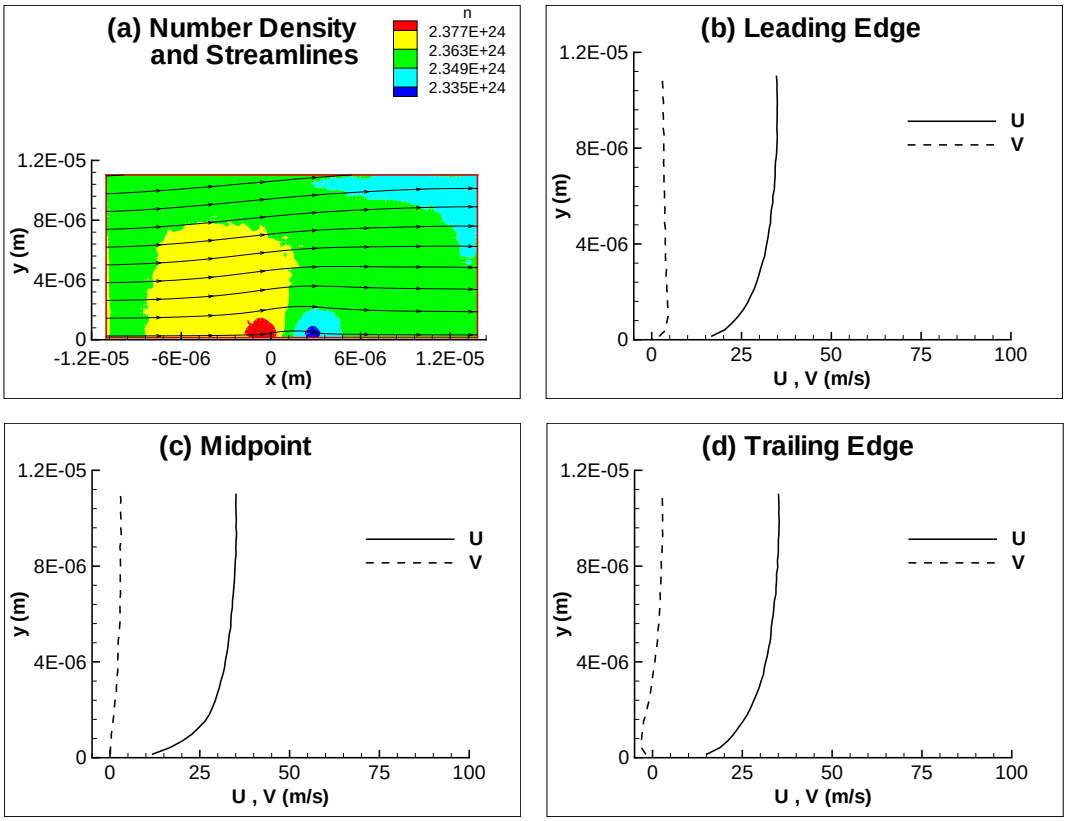

Figure 3.26: Case A.7 ; Number density contours, streamlines and velocity profiles.

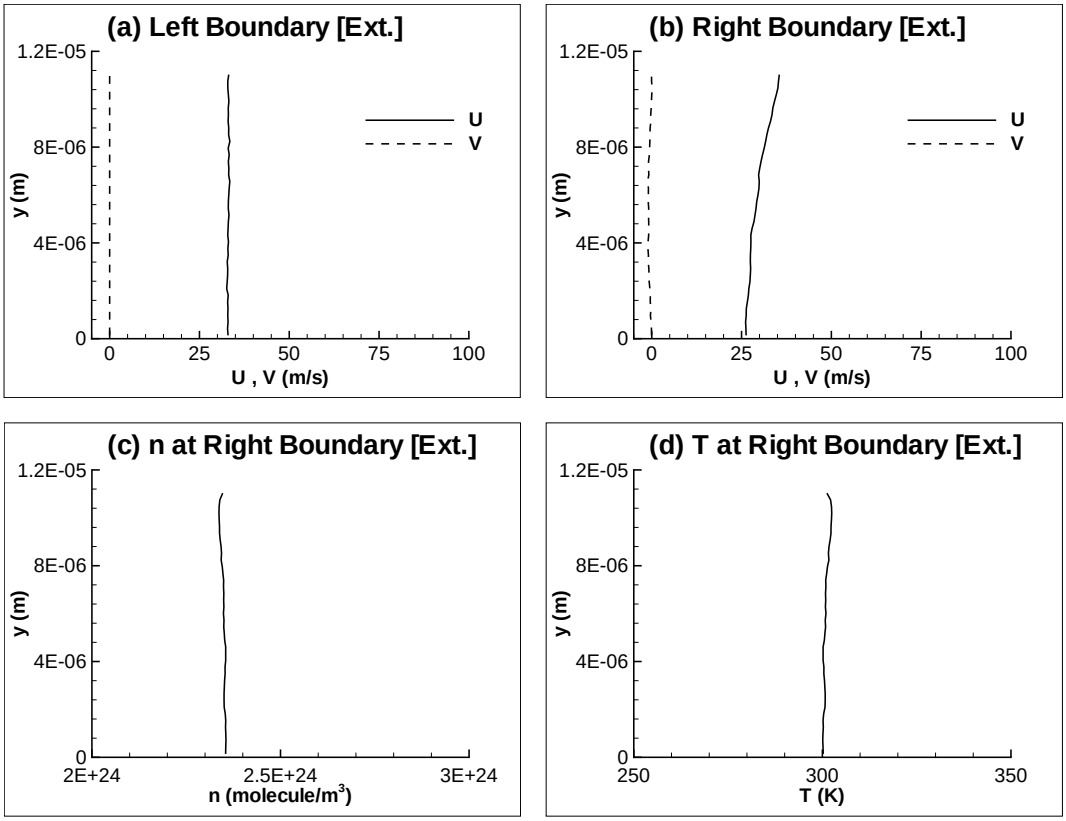

Figure 3.27: Case A.7 ; Extrapolated flowfield variables at left and right boundaries.

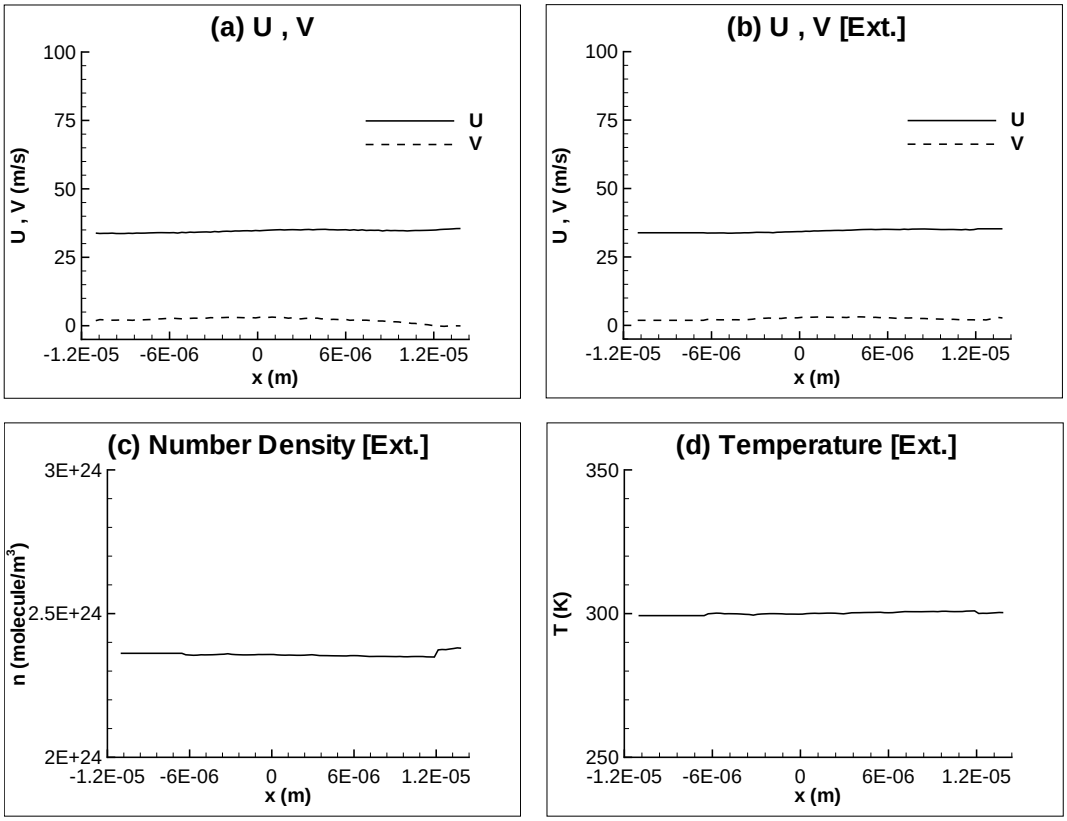

Figure 3.28: Case A.7 ; Velocities and extrapolated flowfield variables at top boundary.

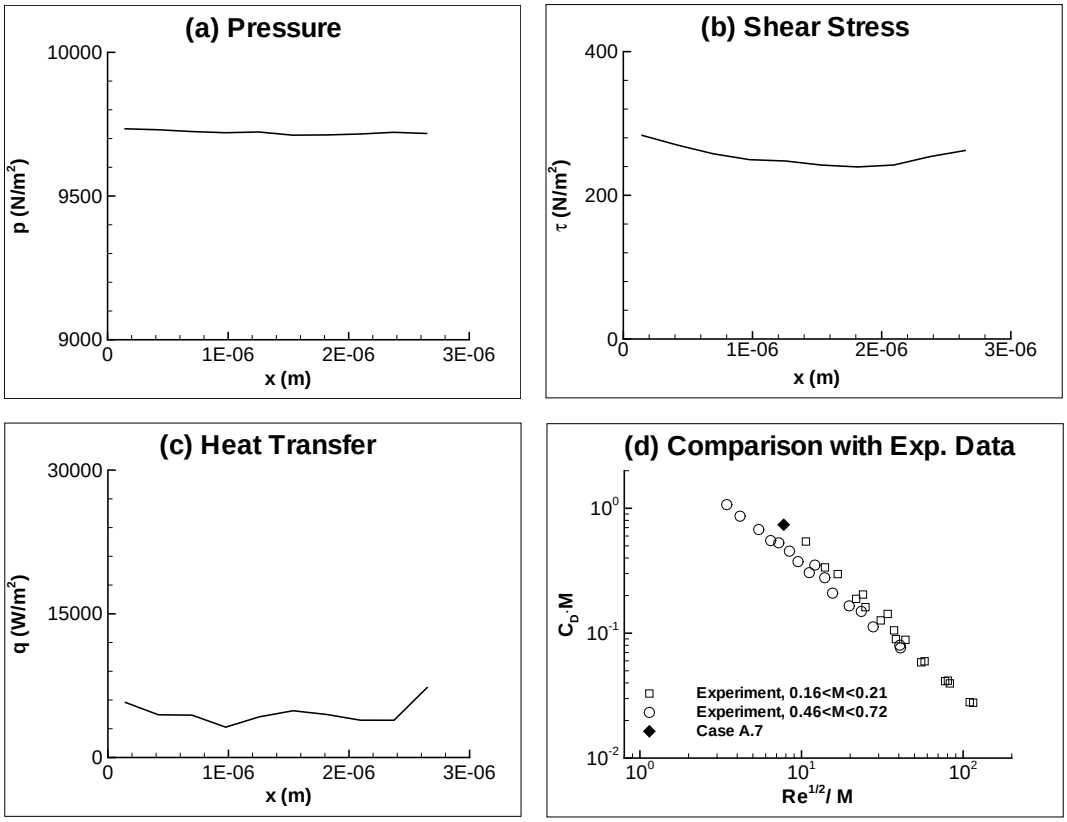

Figure 3.29: Case A.7 ; Surface properties and comparison with experimental data.

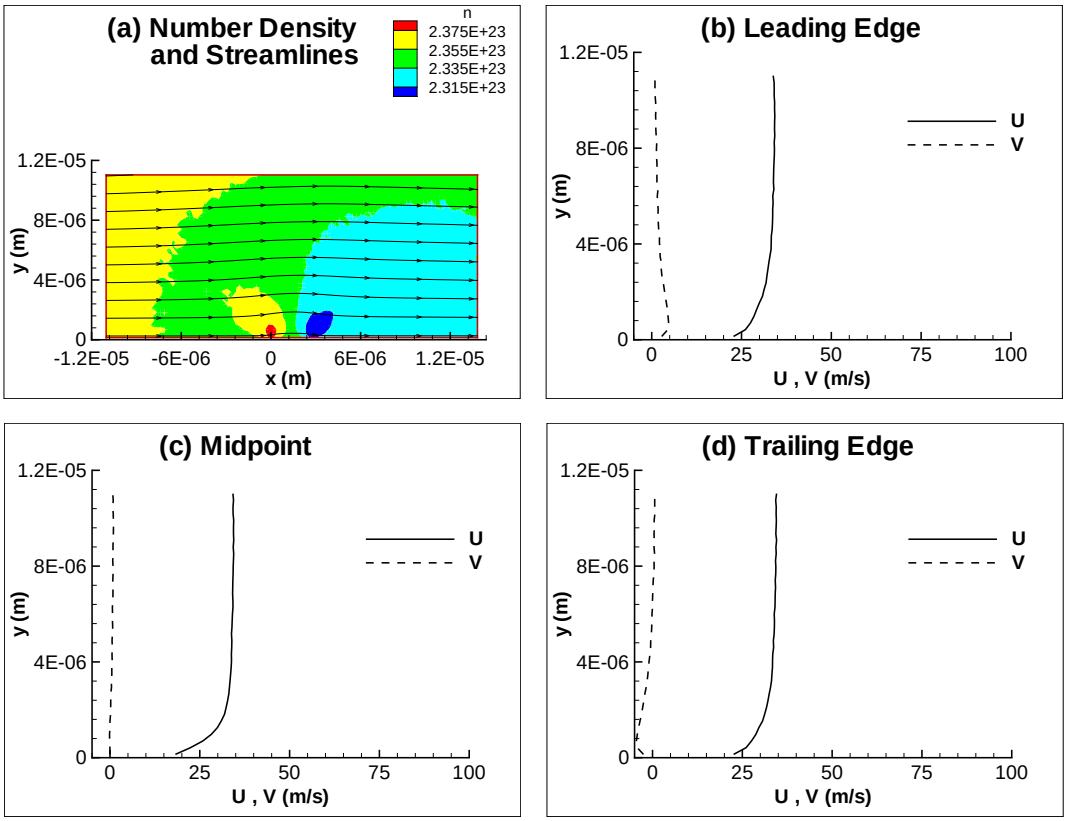

Figure 3.30: Case A.8 ; Number density contours, streamlines and velocity profiles.

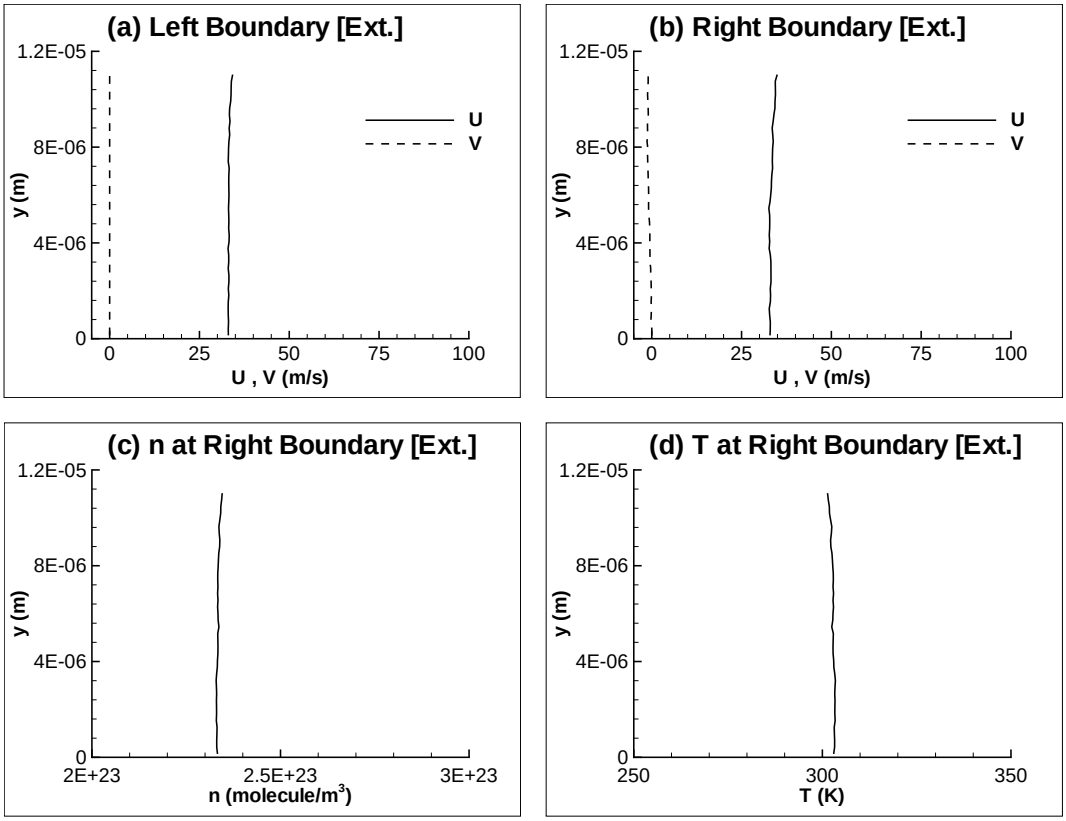

Figure 3.31: Case A.8 ; Extrapolated flowfield variables at left and right boundaries.

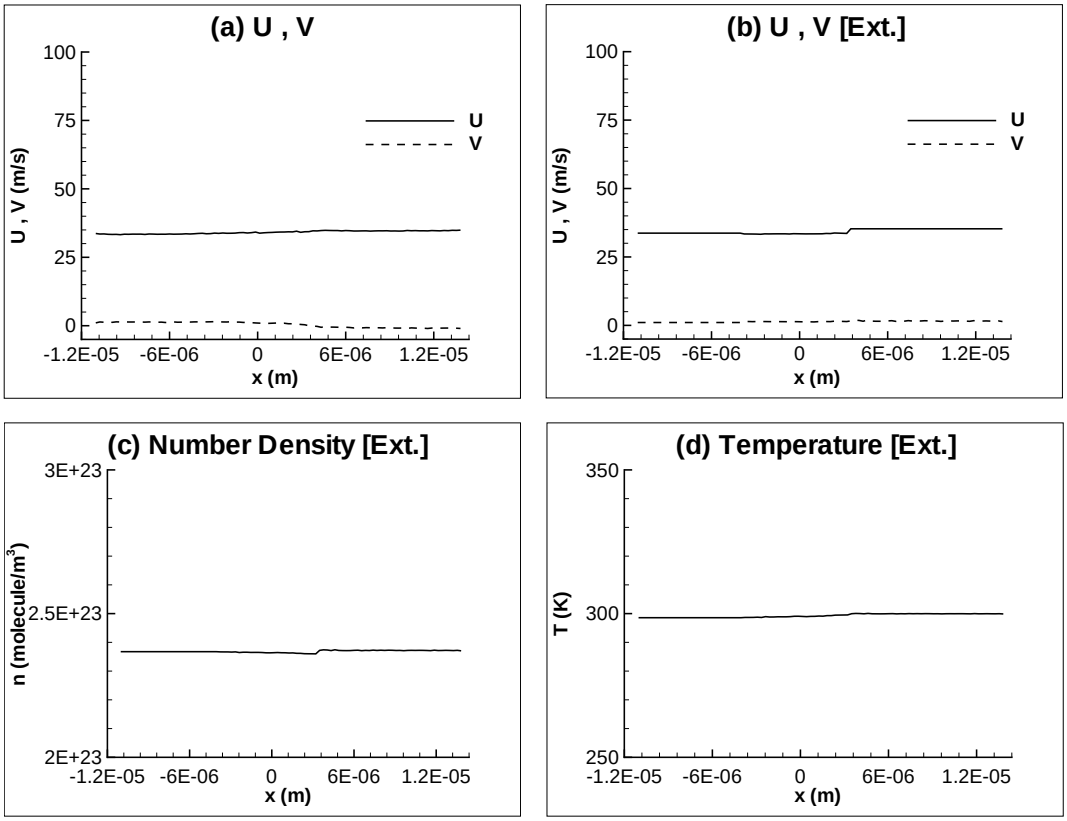

Figure 3.32: Case A.8 ; Velocities and extrapolated flowfield variables at top boundary.

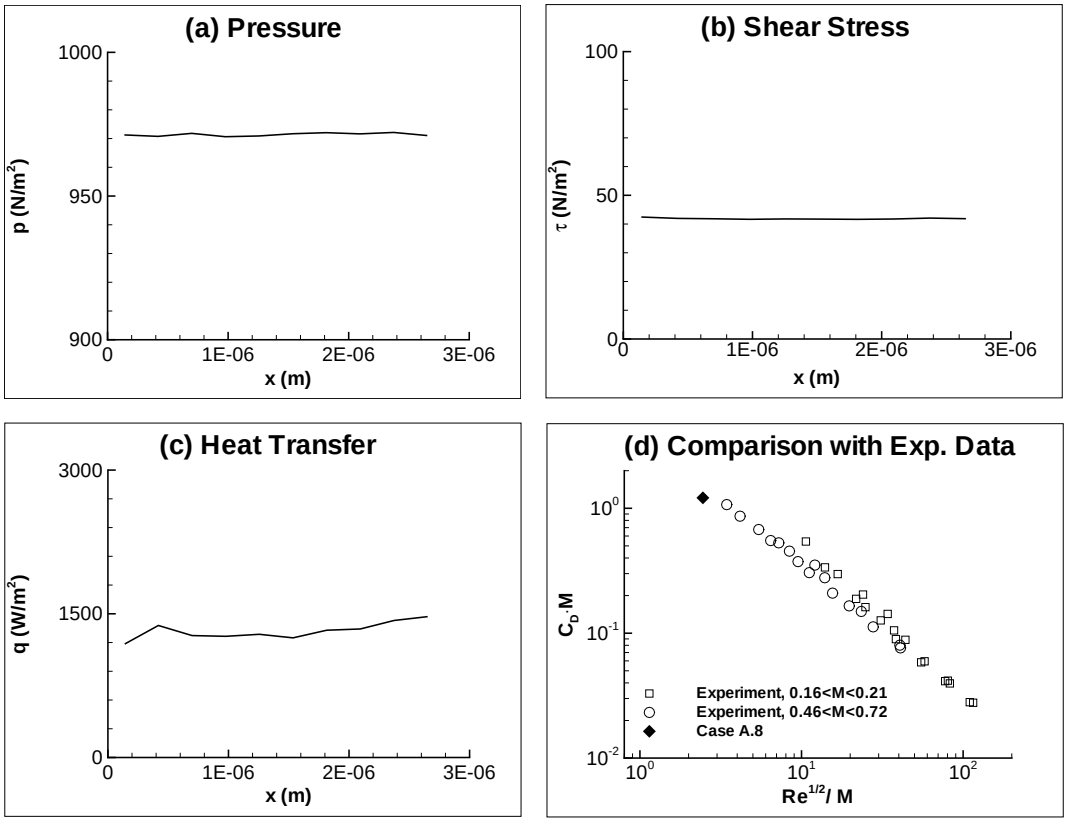

Figure 3.33: Case A.8 ; Surface properties and comparison with experimental data.

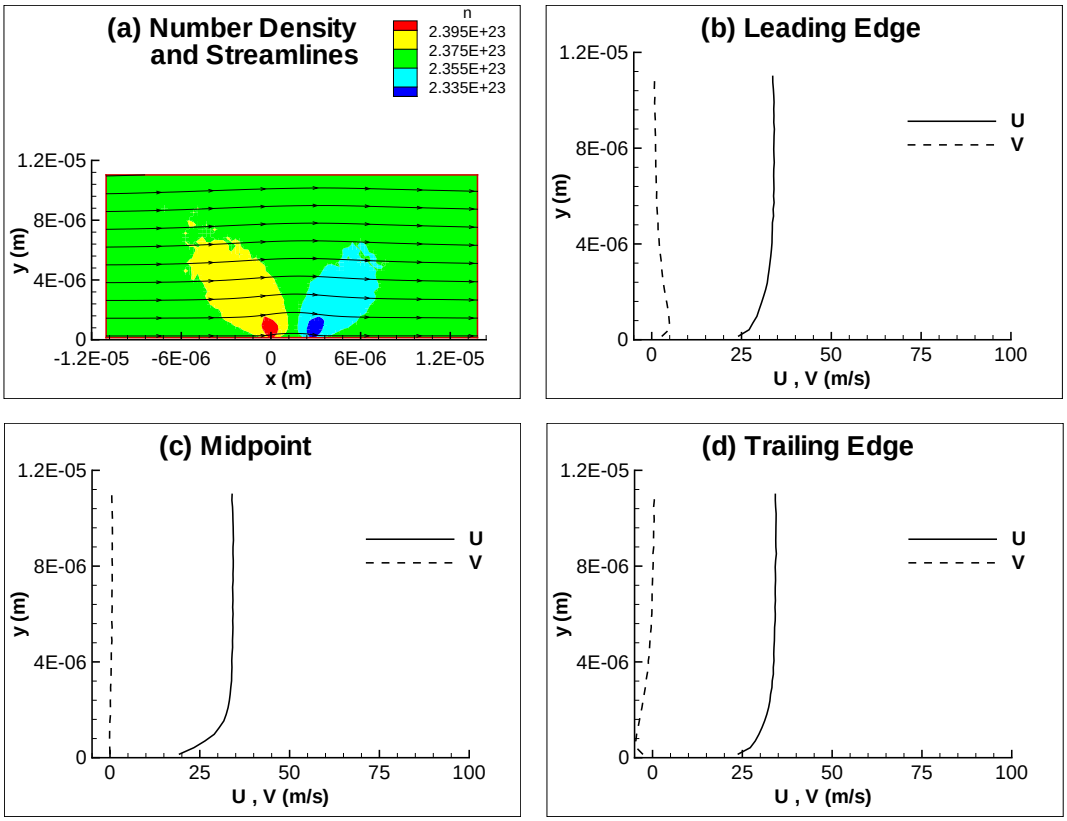

Figure 3.34: Case A.9 ; Number density contours, streamlines and velocity profiles.

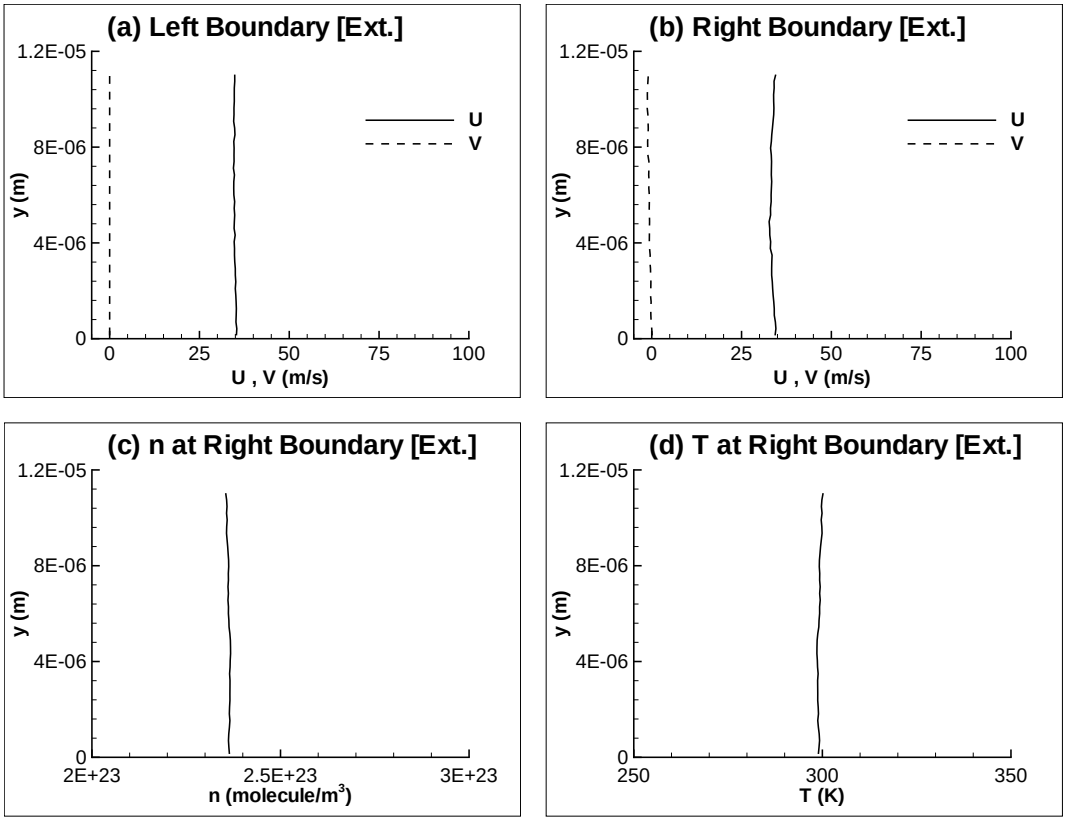

Figure 3.35: Case A.9 ; Extrapolated flowfield variables at left and right boundaries.

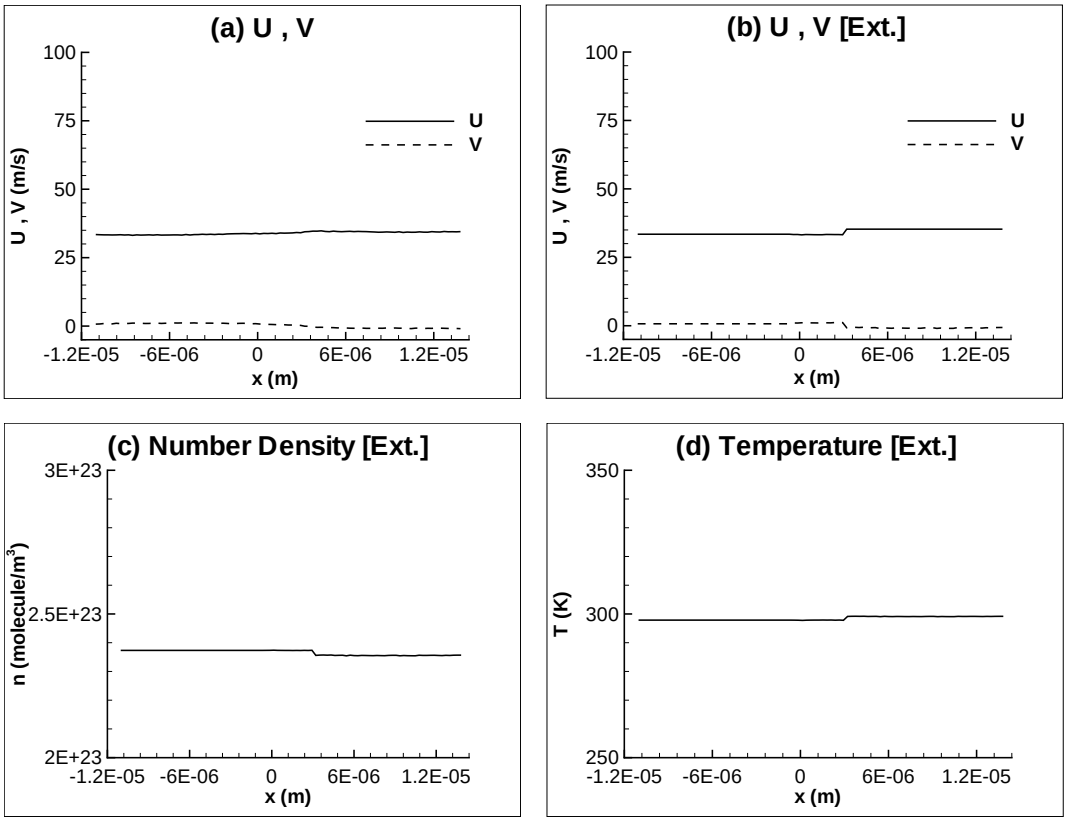

Figure 3.36: Case A.9 ; Velocities and extrapolated flowfield variables at top boundary.

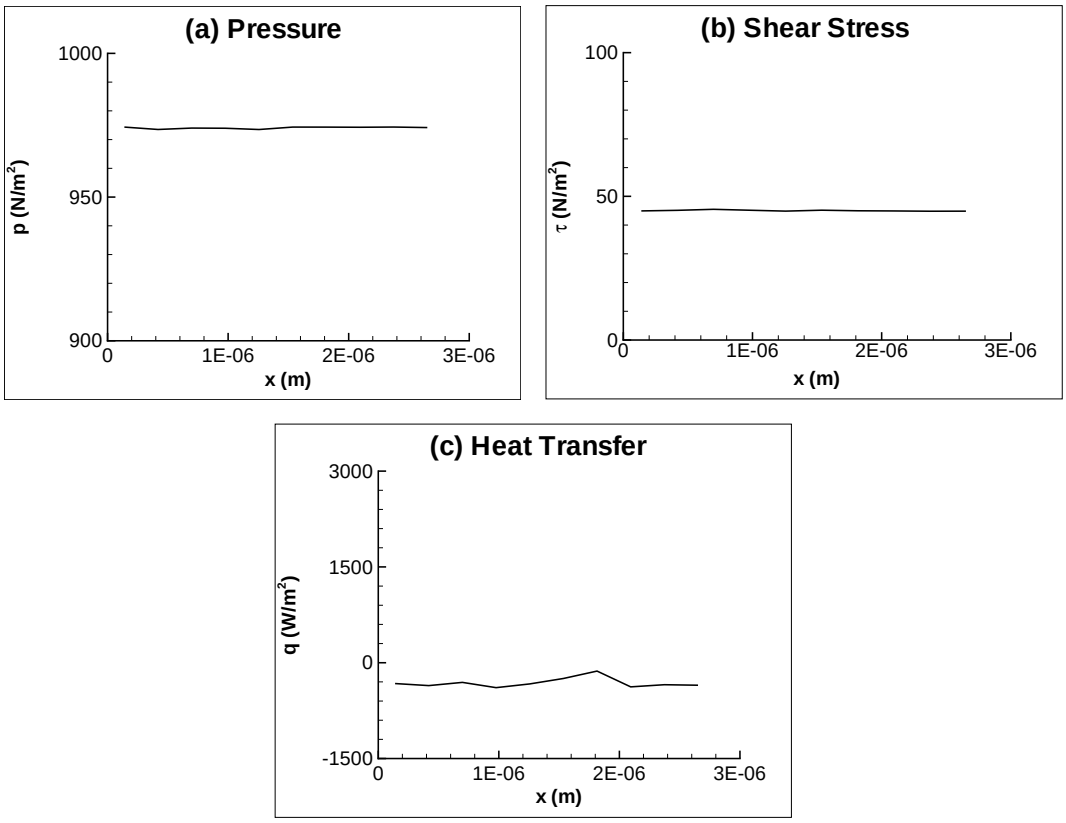

Figure 3.37: Case A.9 ; Surface properties.

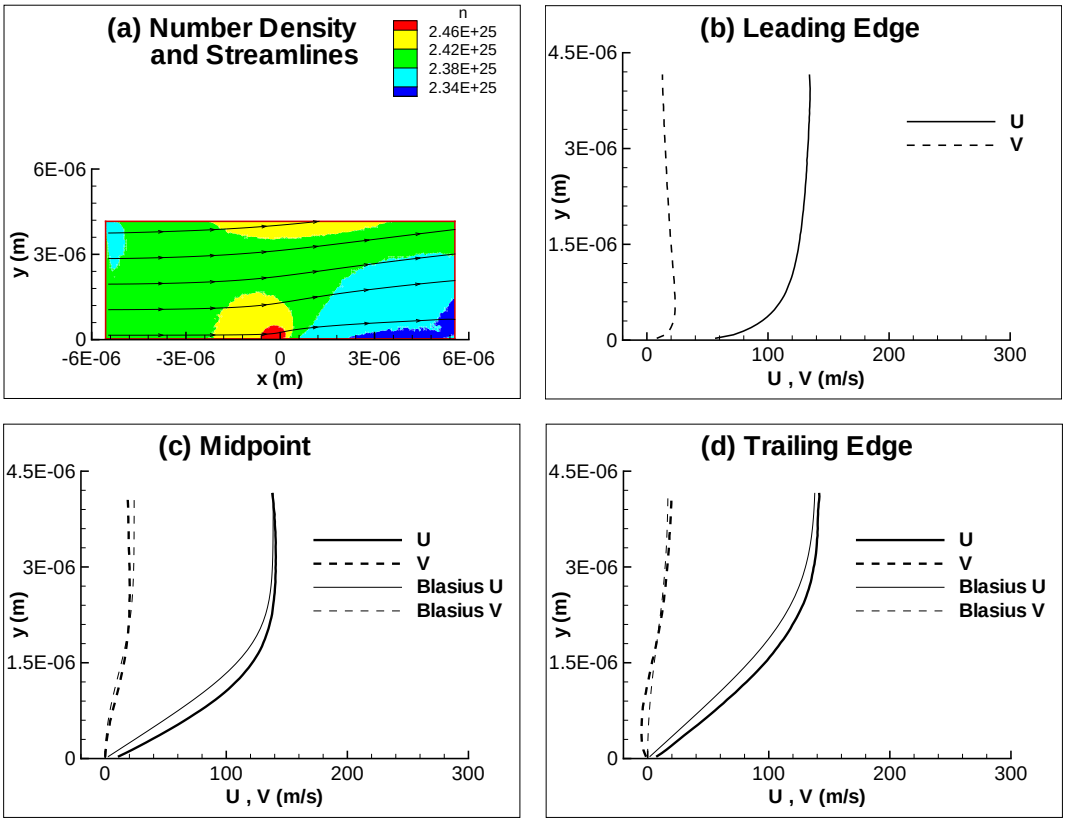

Figure 3.38: Case A.10 ; Number density contours, streamlines and velocity profiles.

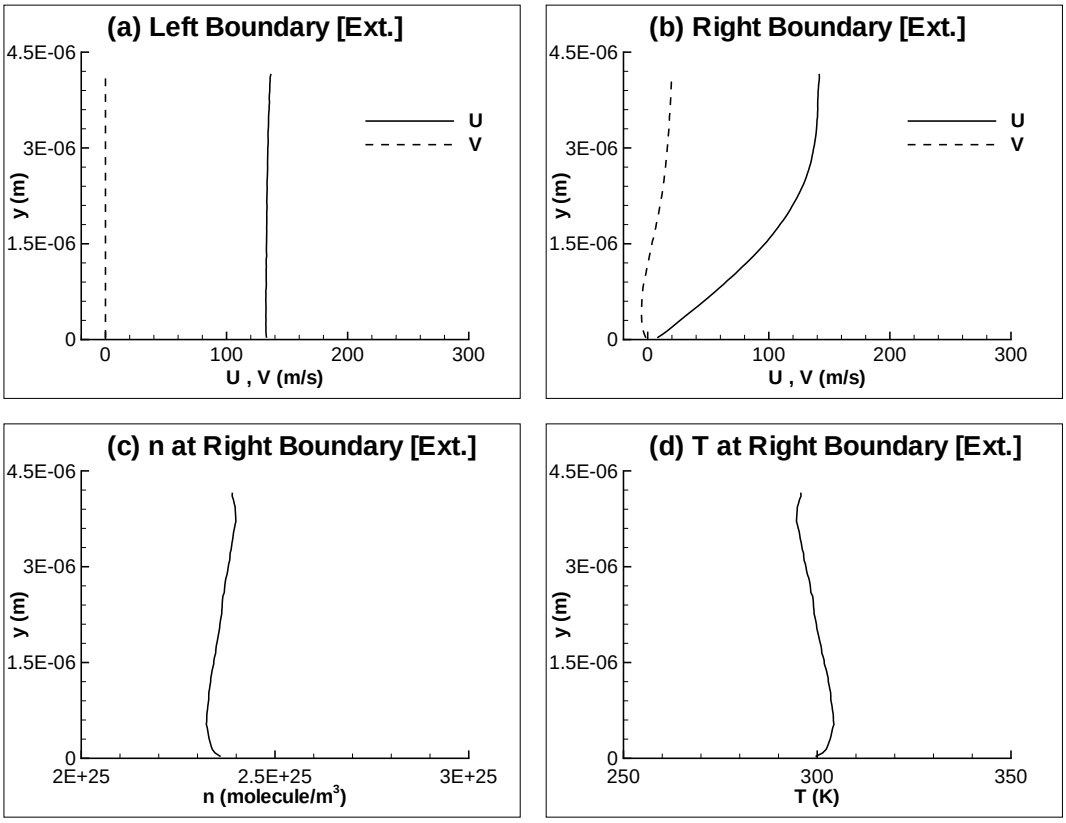

Figure 3.39: Case A.10 ; Extrapolated flowfield variables at left and right boundaries.

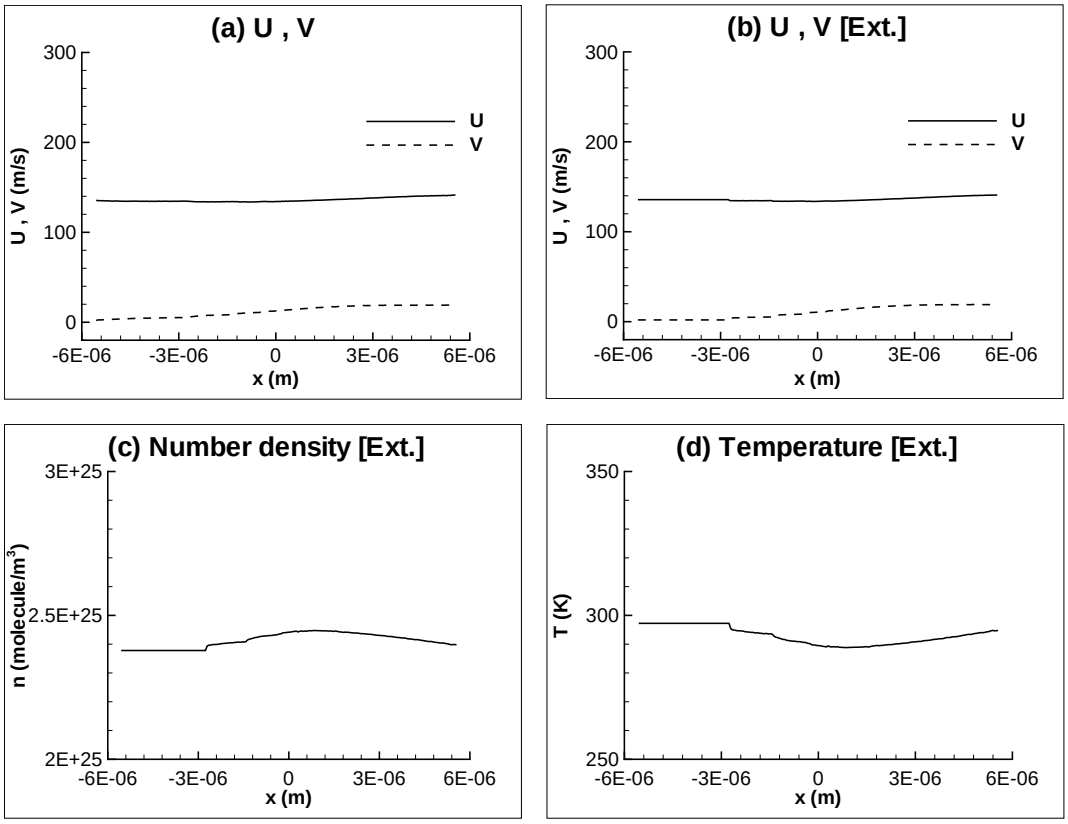

Figure 3.40: Case A.10 ; Velocities and extrapolated flowfield variables at top boundary.

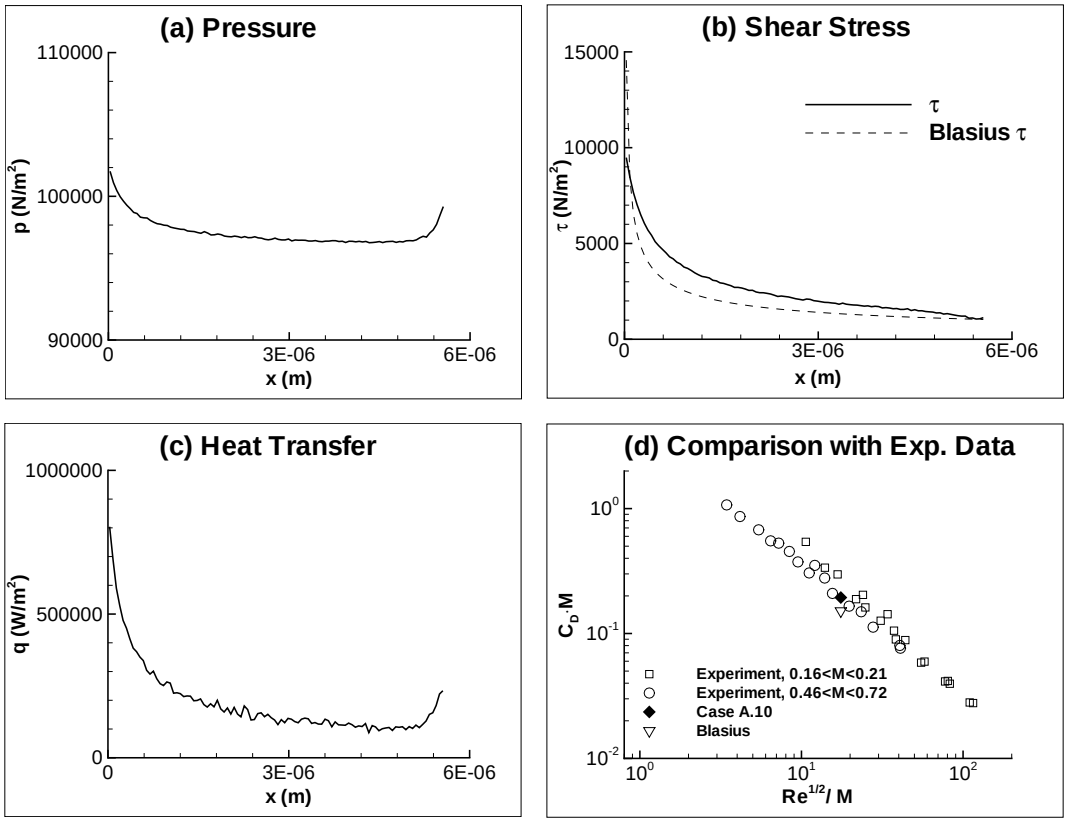

Figure 3.41: Case A.10 ; Surface properties and comparison with experimental data.

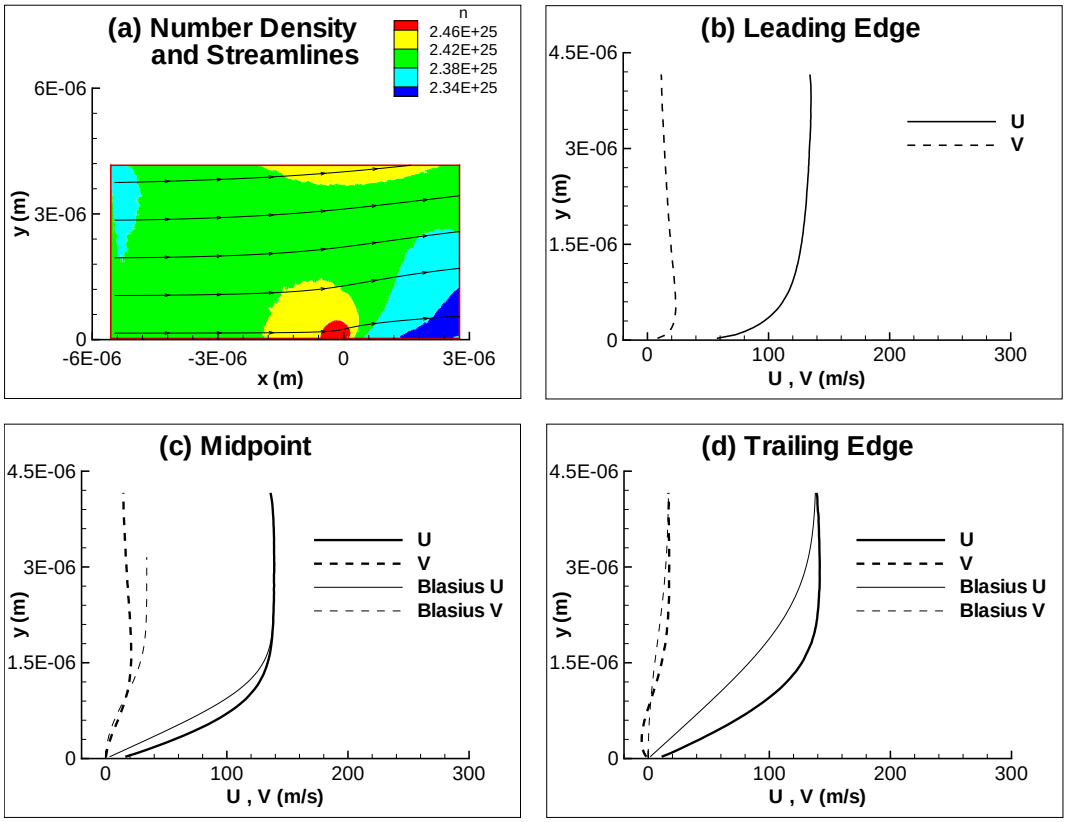

Figure 3.42: Case A.11 ; Number density contours, streamlines and velocity profiles.

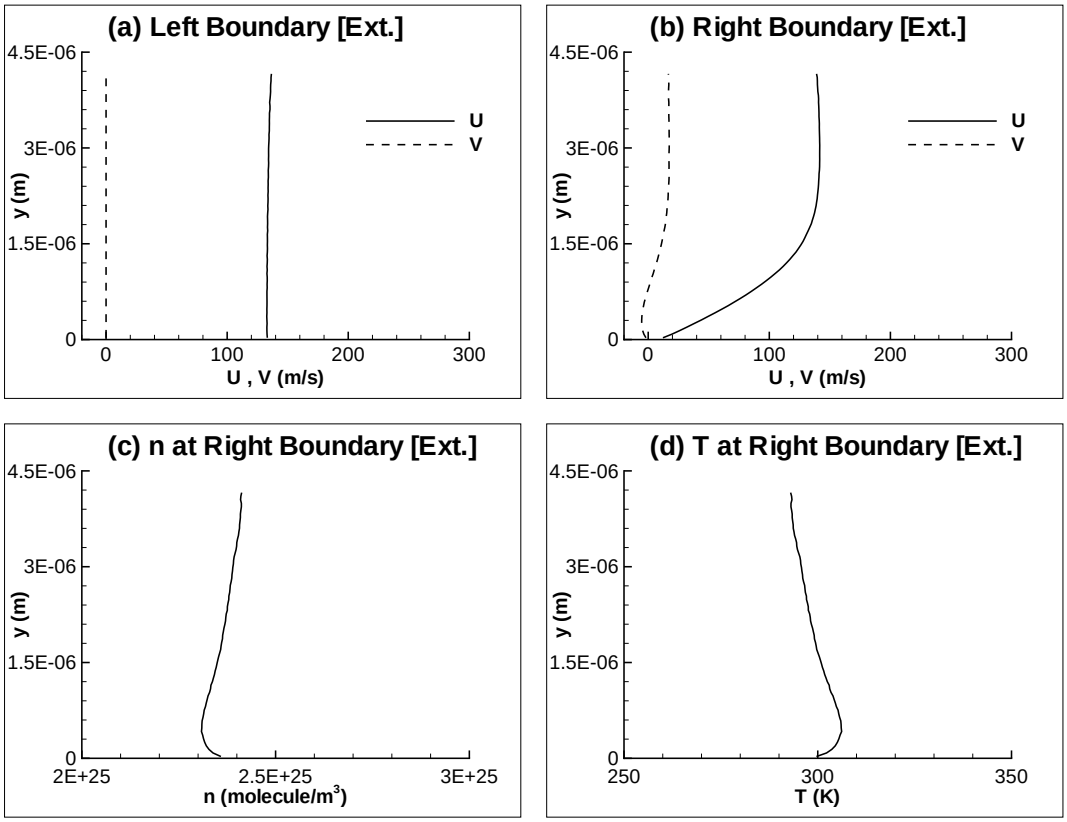

Figure 3.43: Case A.11 ; Extrapolated flowfield variables at left and right boundaries.

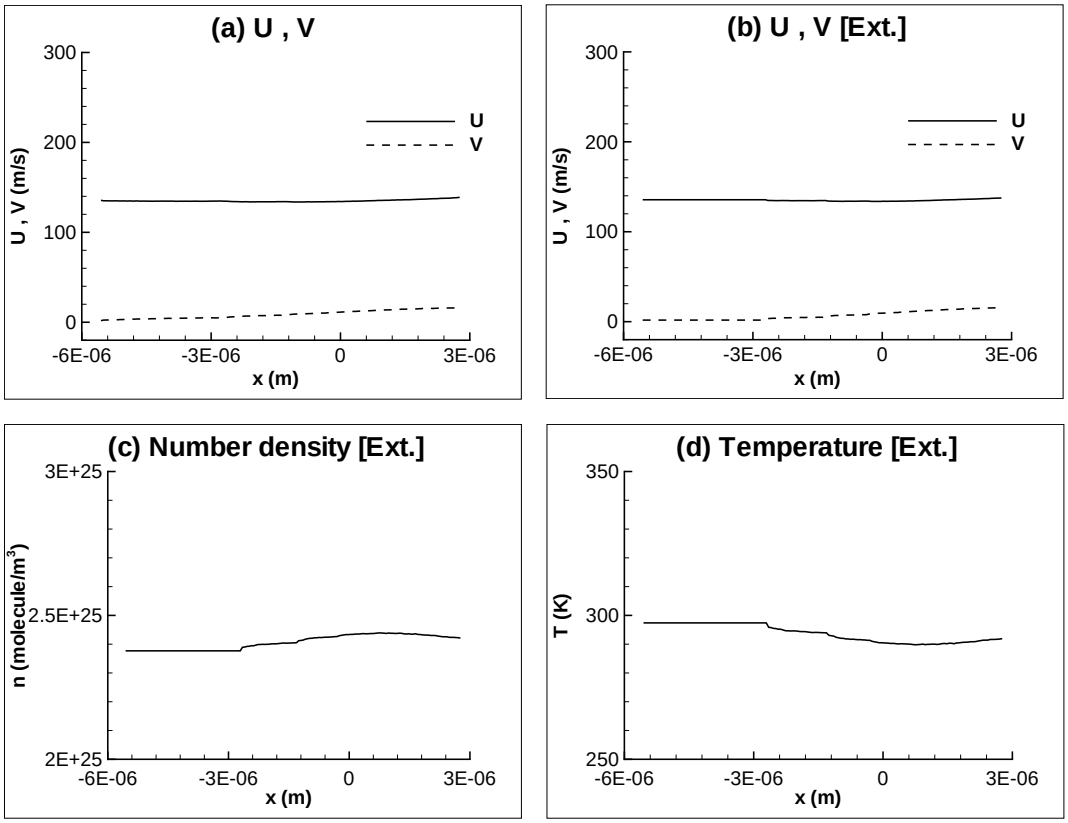

Figure 3.44: Case A.11 ; Velocities and extrapolated flowfield variables at top boundary.

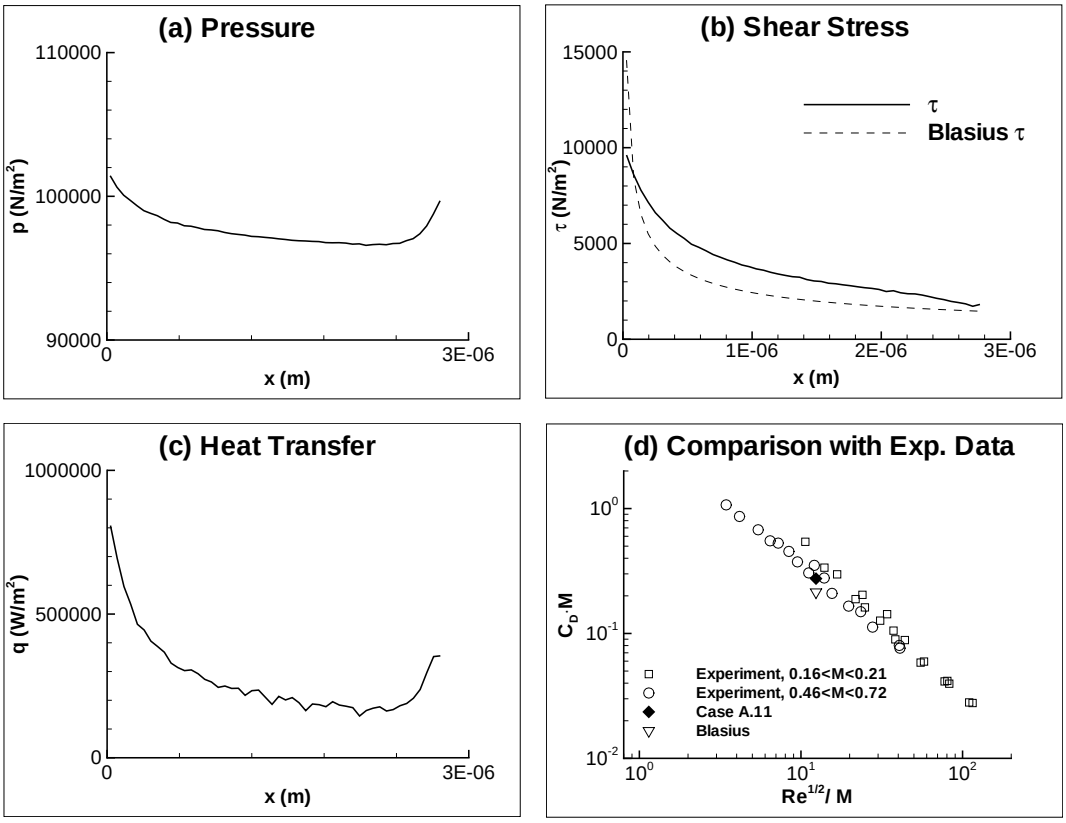

Figure 3.45: Case A.11 ; Surface properties and comparison with experimental data.

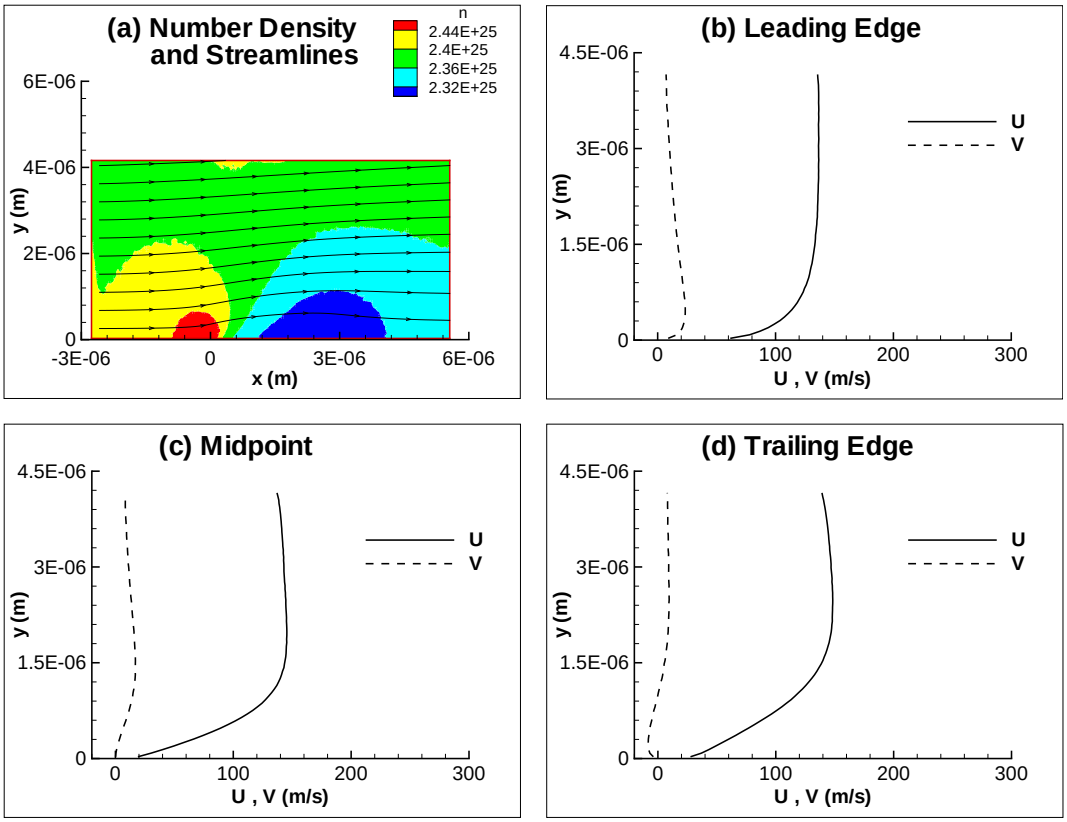

Figure 3.46: Case A.12 ; Number density contours, streamlines and velocity profiles.

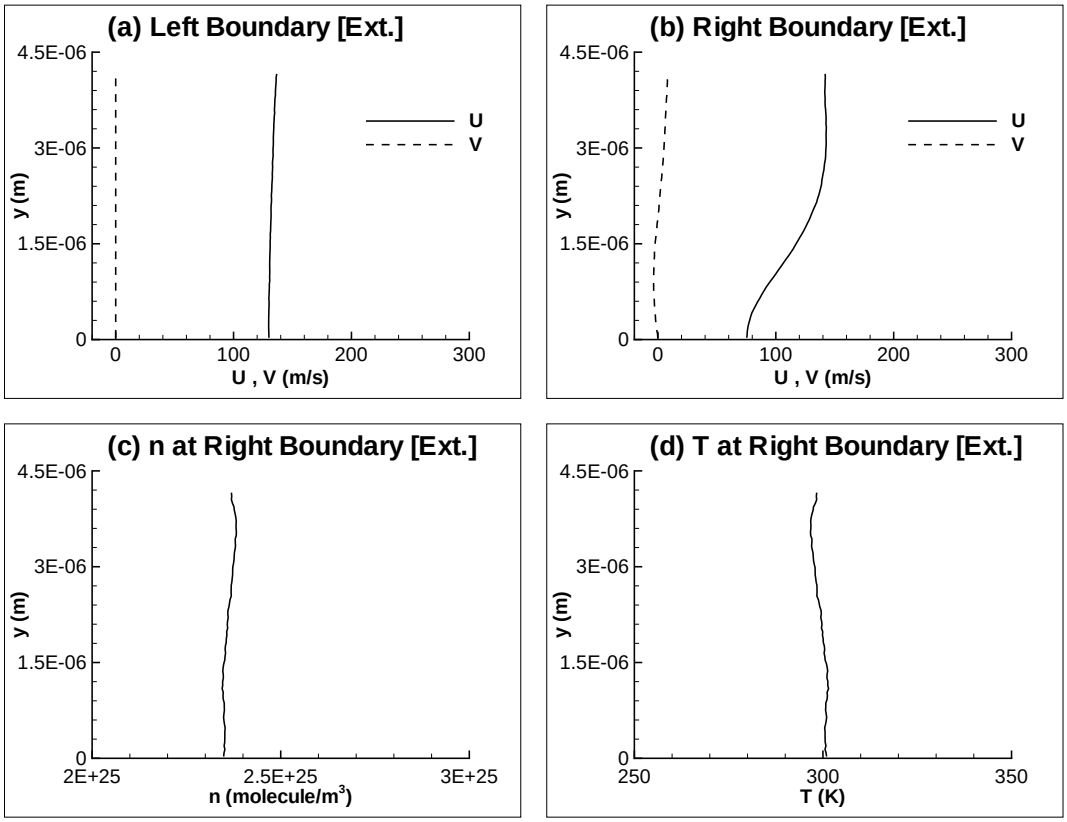

Figure 3.47: Case A.12 ; Extrapolated flowfield variables at left and right boundaries.

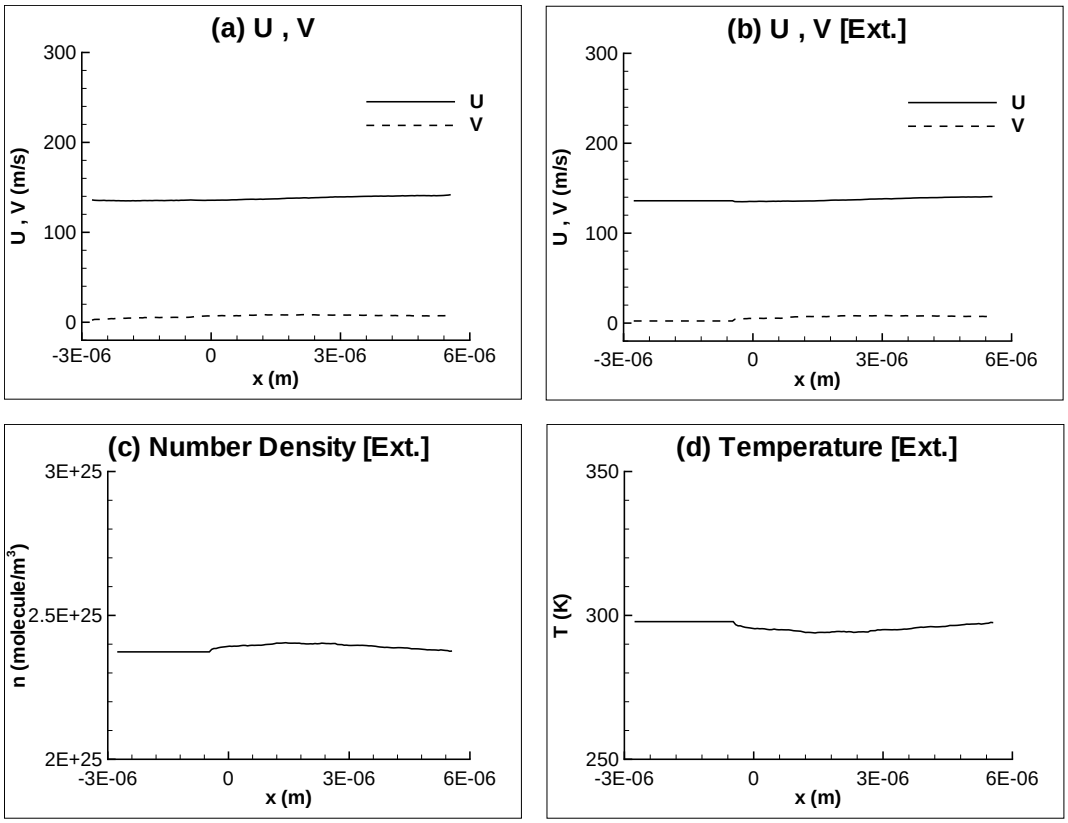

Figure 3.48: Case A.12 ; Velocities and extrapolated flowfield variables at top boundary.

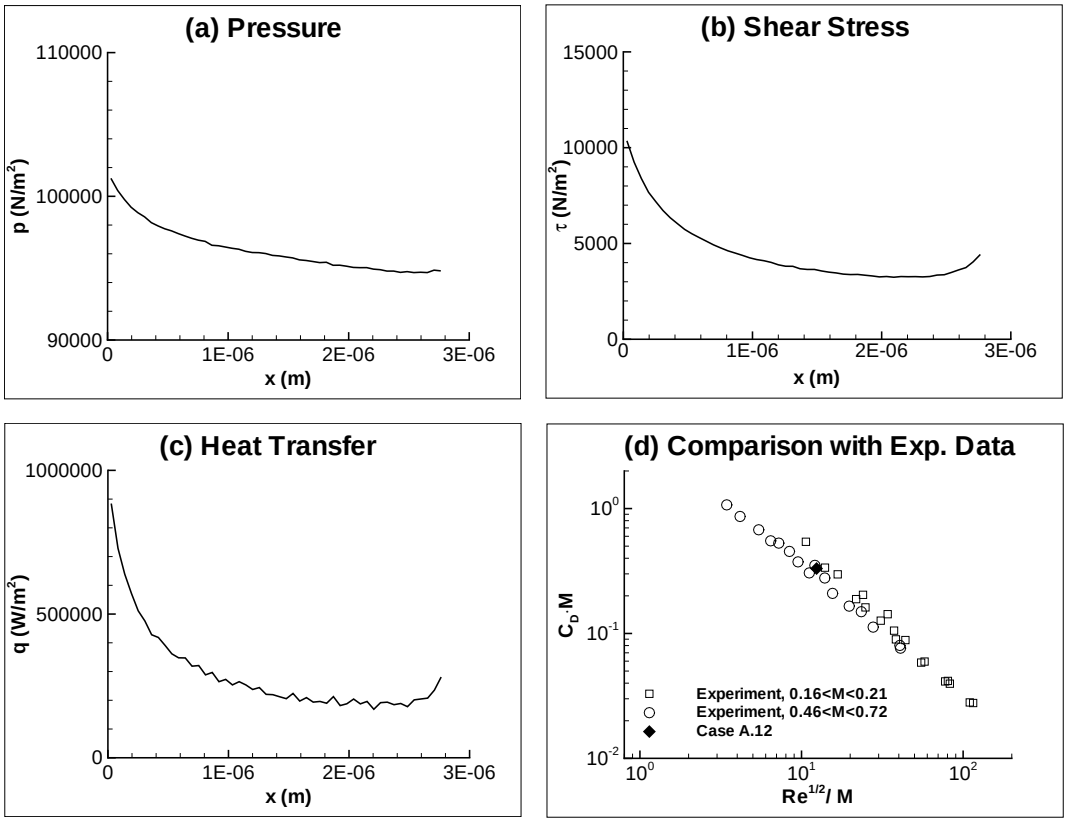

Figure 3.49: Case A.12 ; Surface properties and comparison with experimental data.

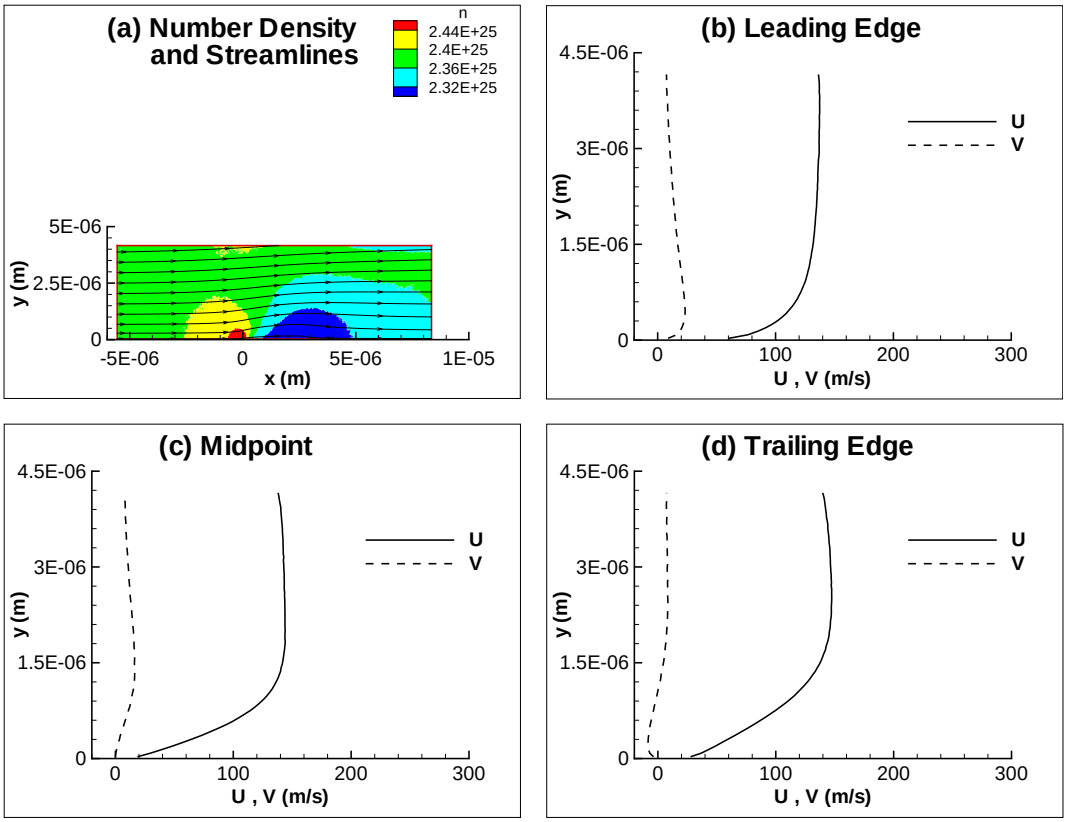

Figure 3.50: Case A.13 ; Number density contours, streamlines and velocity profiles.

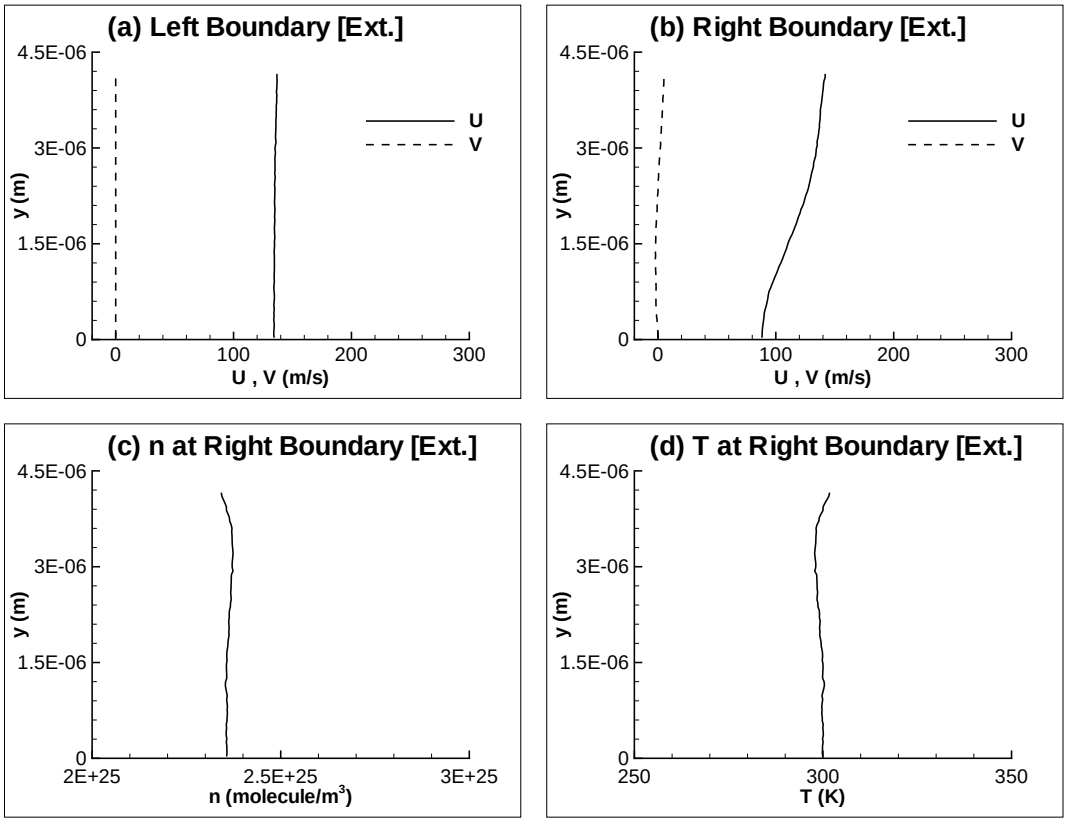

Figure 3.51: Case A.13 ; Extrapolated flowfield variables at left and right boundaries.

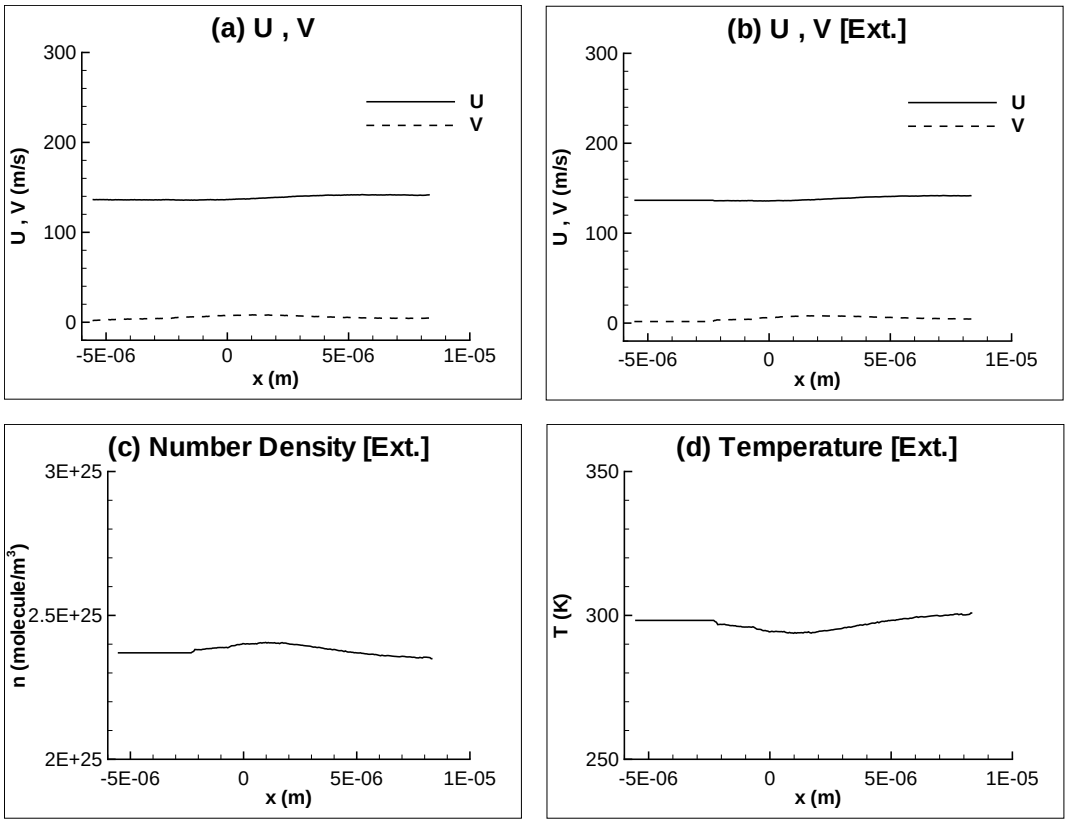

Figure 3.52: Case A.13 ; Velocities and extrapolated flowfield variables at top boundary.

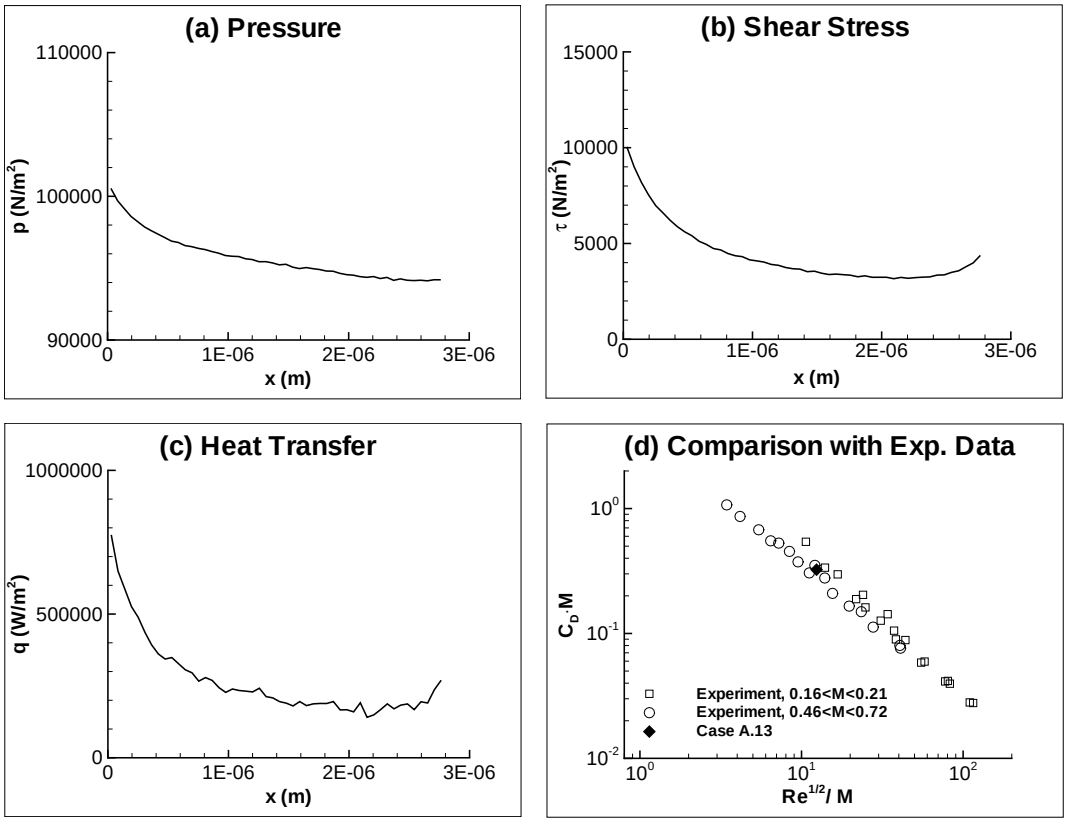

Figure 3.53: Case A.13 ; Surface properties and comparison with experimental data.

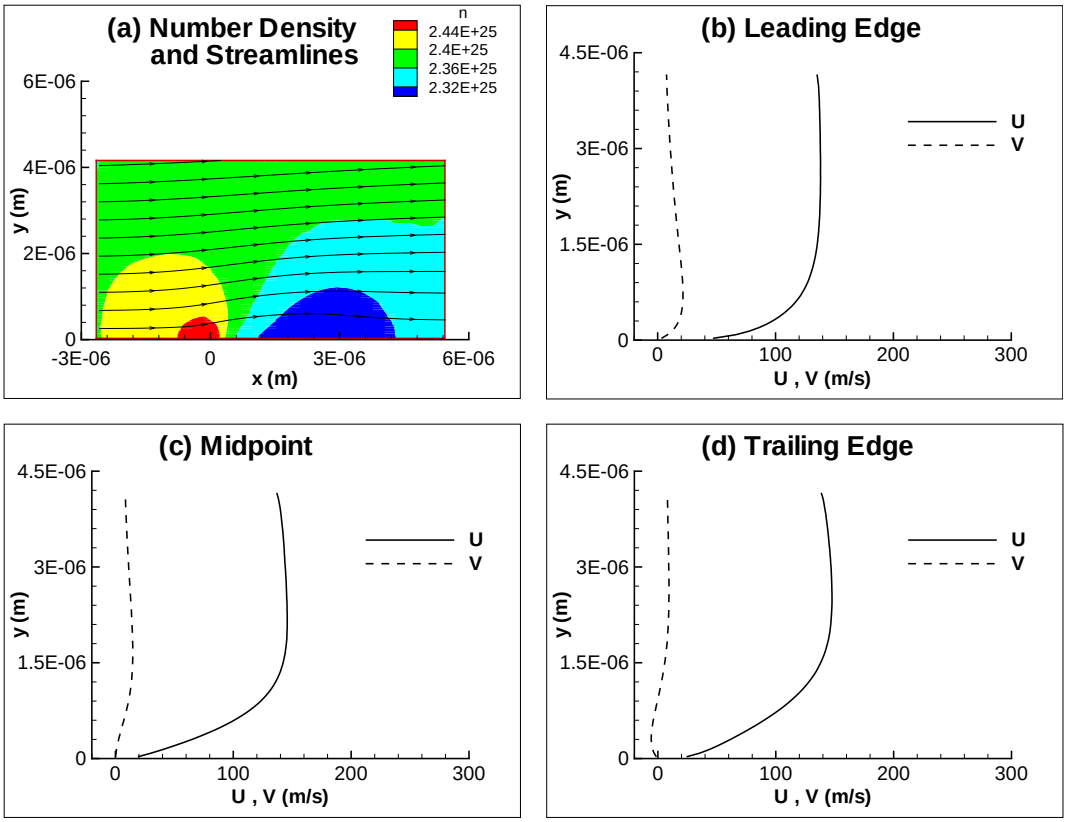

Figure 3.54: Case A.14 ; Number density contours, streamlines and velocity profiles.

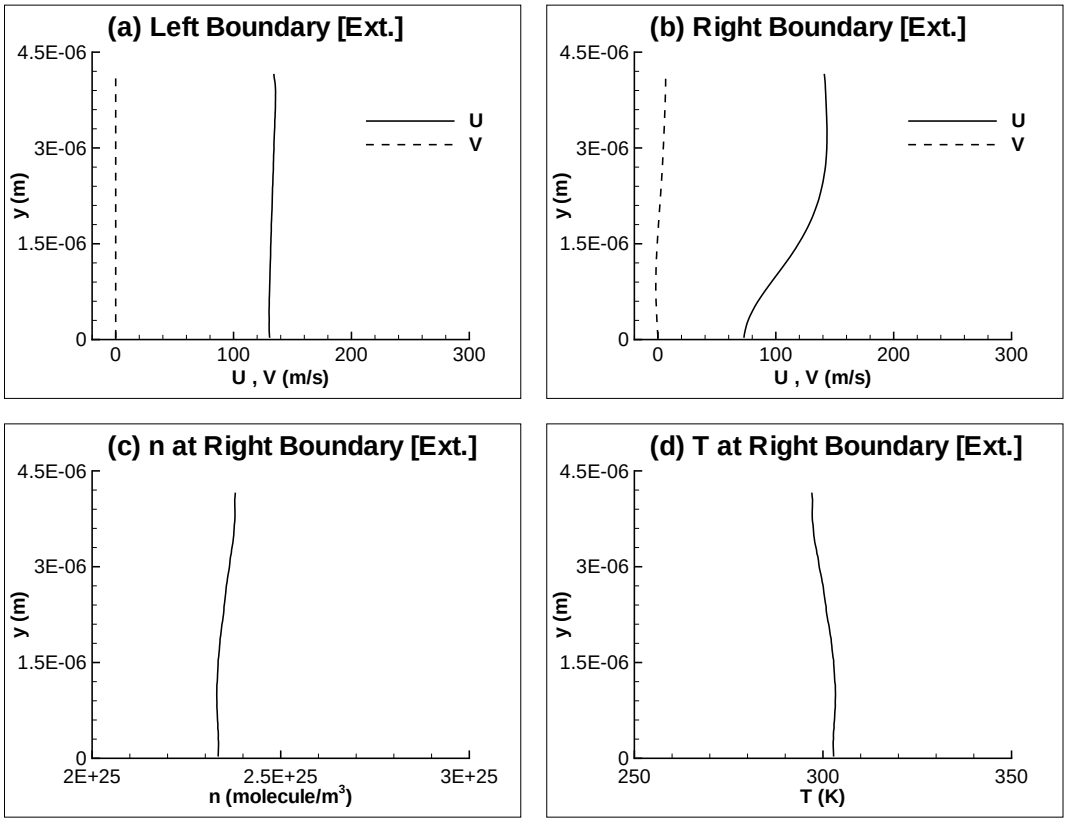

Figure 3.55: Case A.14 ; Extrapolated flowfield variables at left and right boundaries.

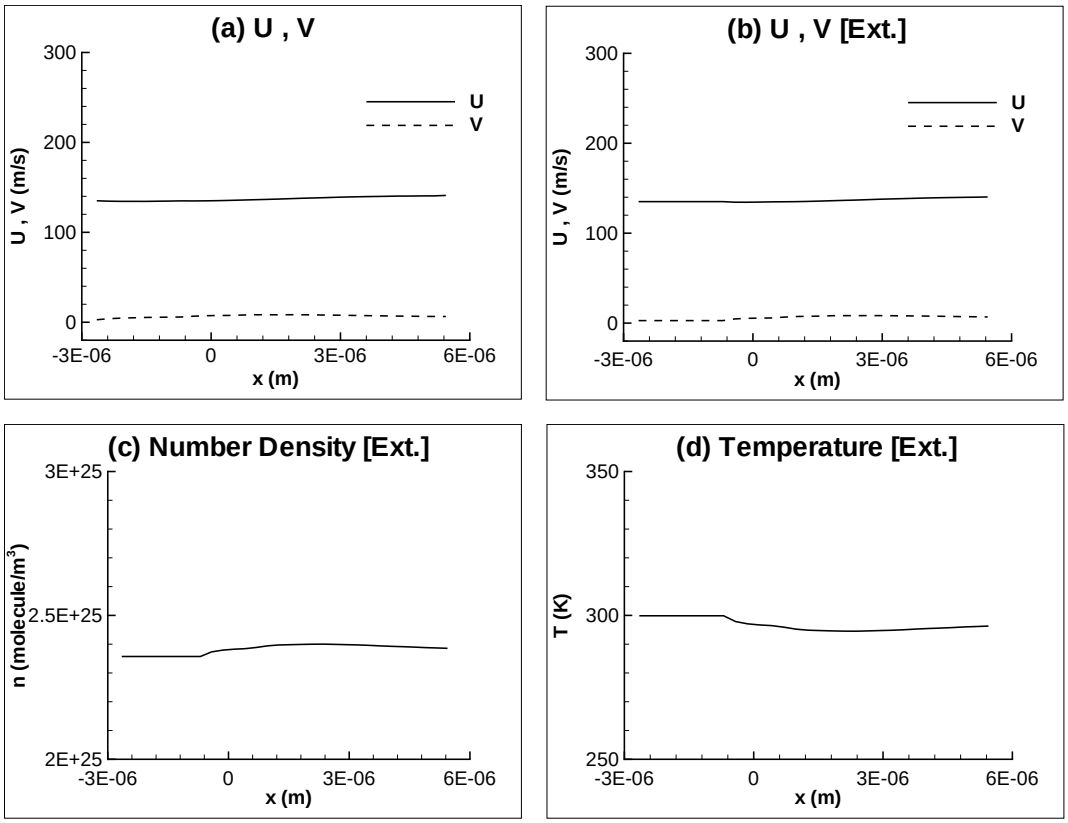

Figure 3.56: Case A.14 ; Velocities and extrapolated flowfield variables at top boundary.

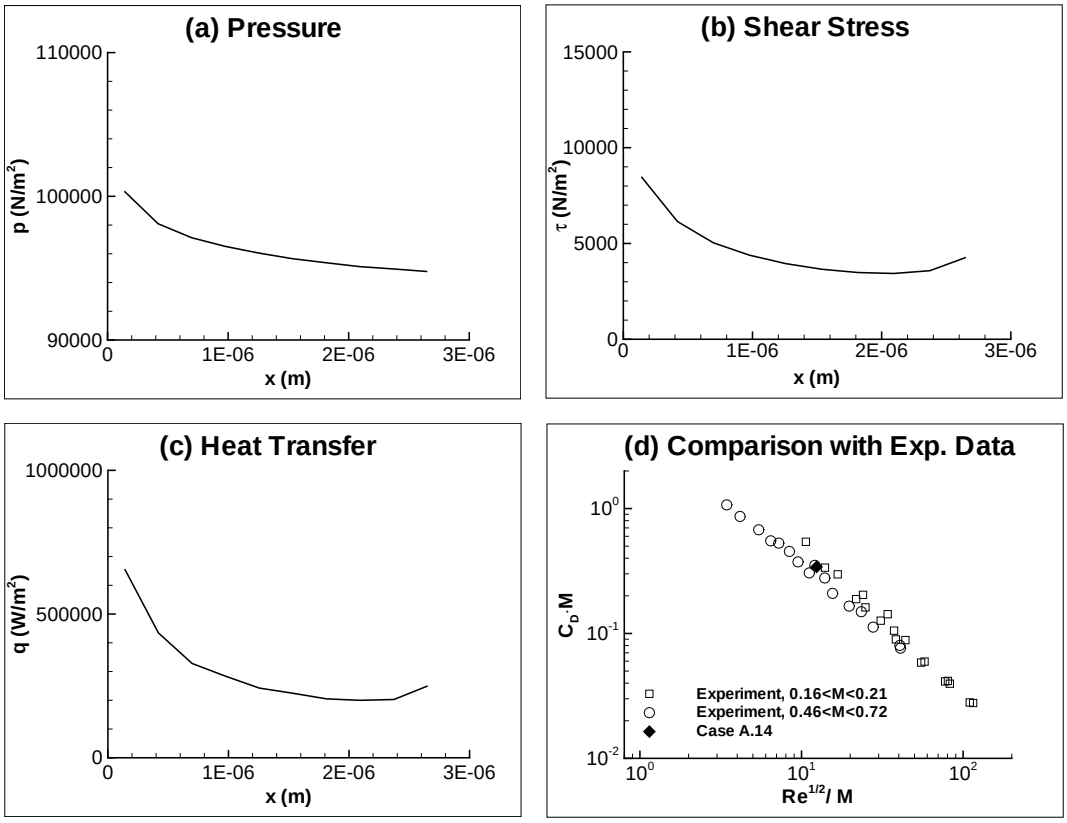

Figure 3.57: Case A.14 ; Surface properties and comparison with experimental data.

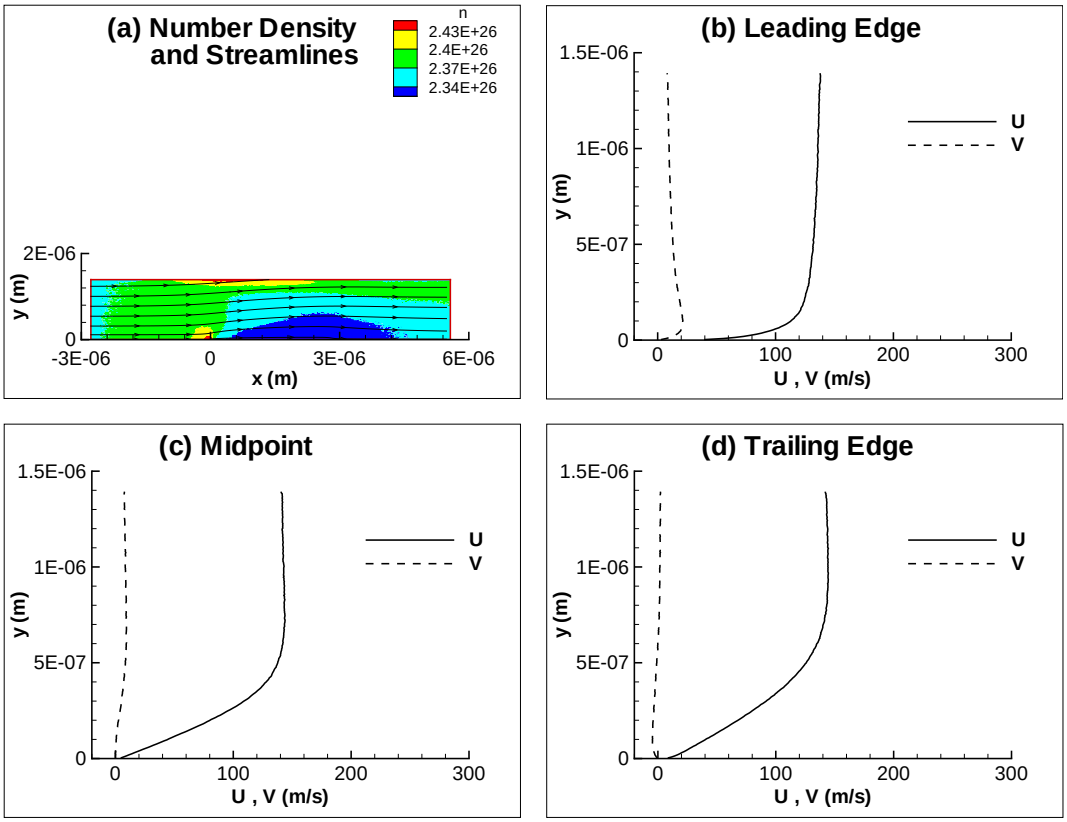

Figure 3.58: Case A.15 ; Number density contours, streamlines and velocity profiles.

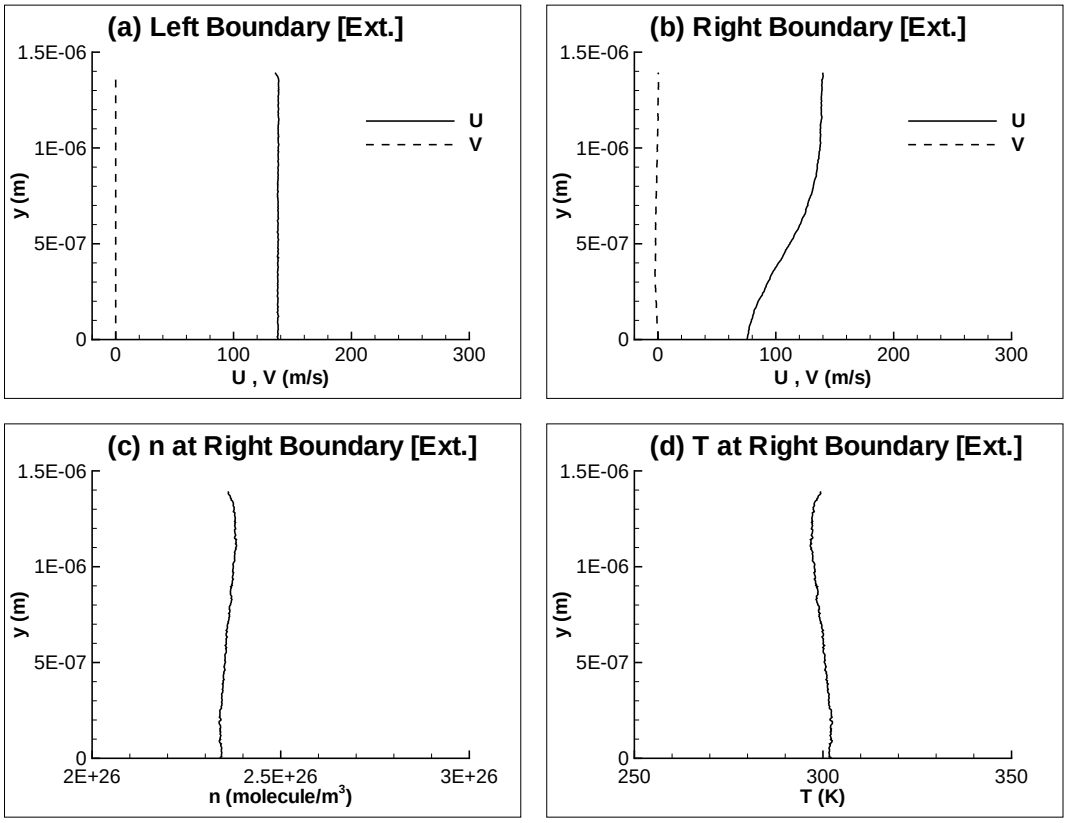

Figure 3.59: Case A.15 ; Extrapolated flowfield variables at left and right boundaries.

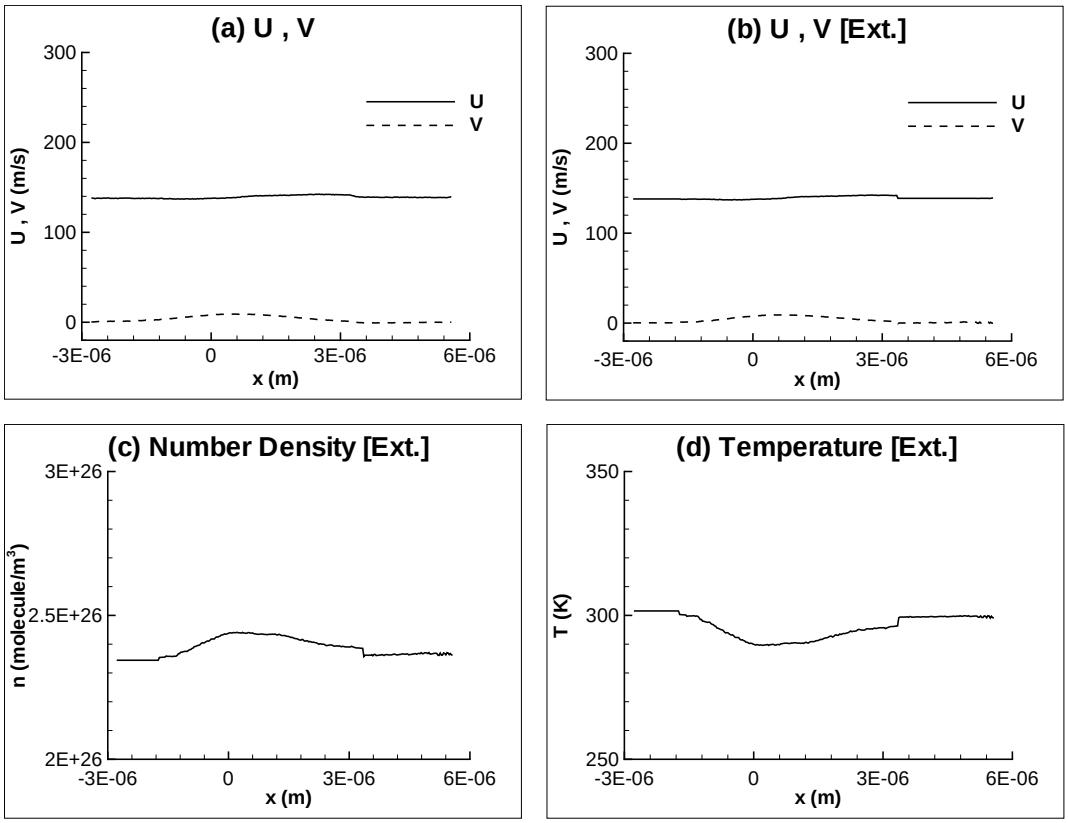

Figure 3.60: Case A.15 ; Velocities and extrapolated flowfield variables at top boundary.

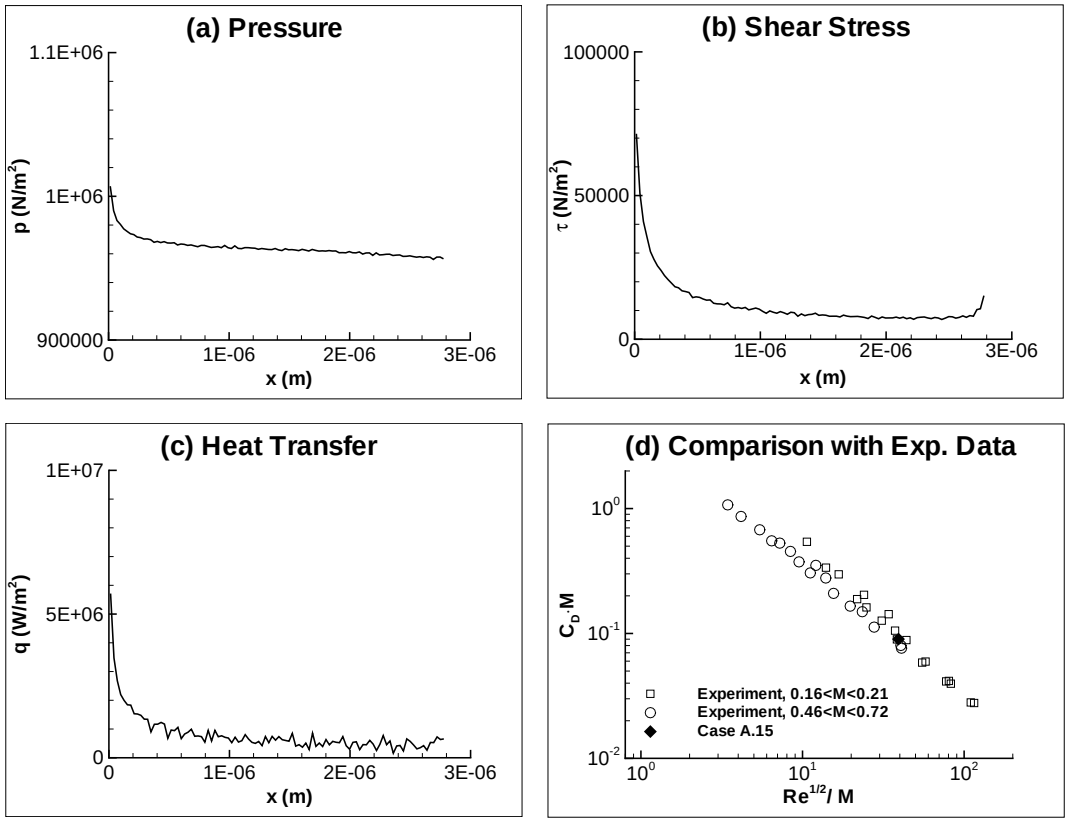

Figure 3.61: Case A.15 ; Surface properties and comparison with experimental data.

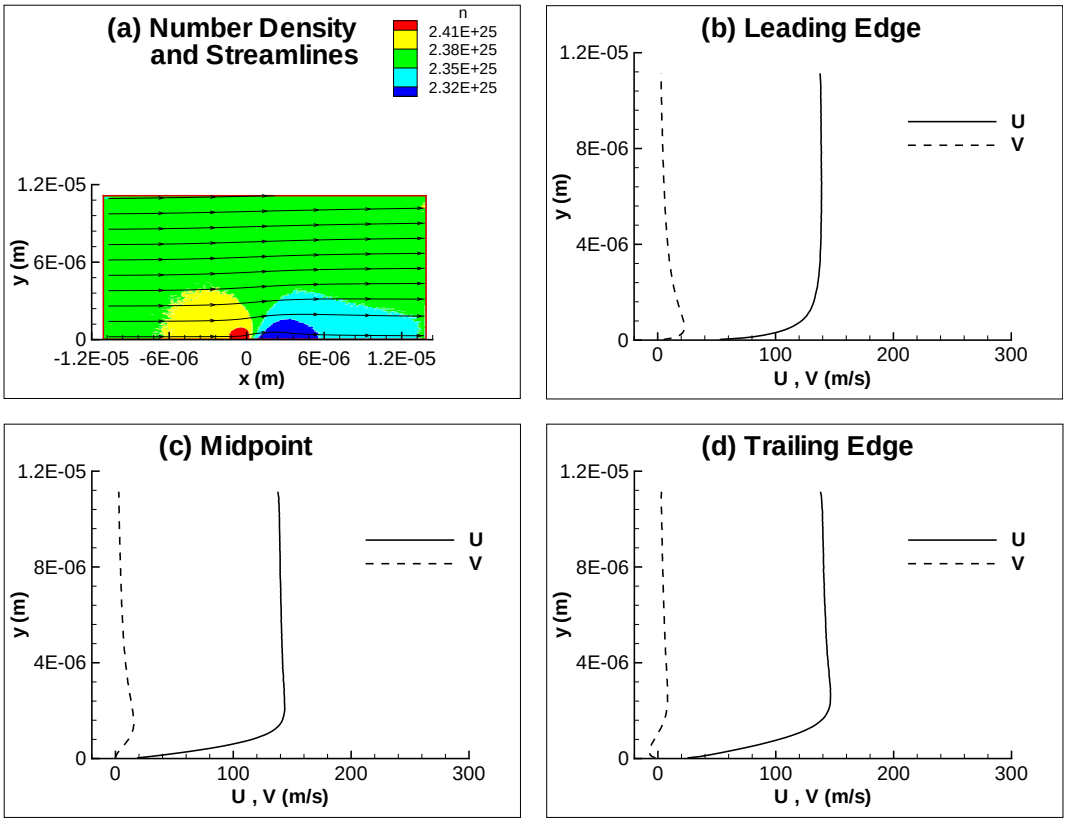

Figure 3.62: Case A.16 ; Number density contours, streamlines and velocity profiles.

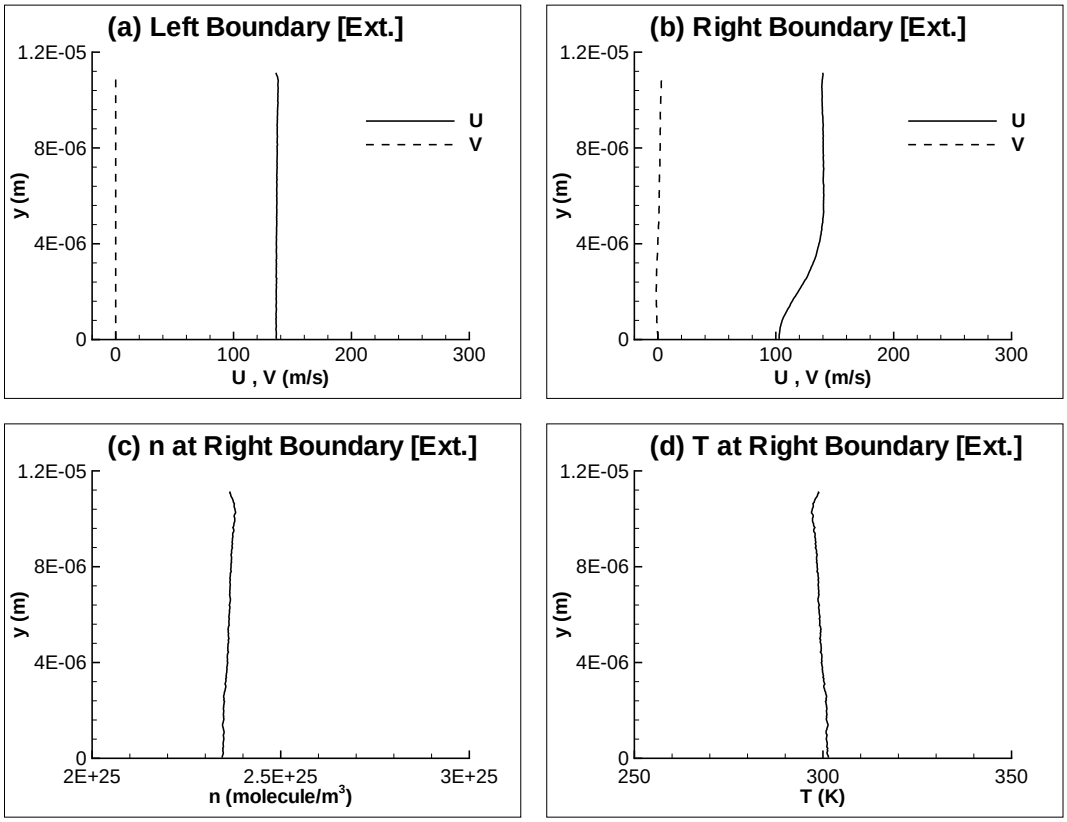

Figure 3.63: Case A.16 ; Extrapolated flowfield variables at left and right boundaries.

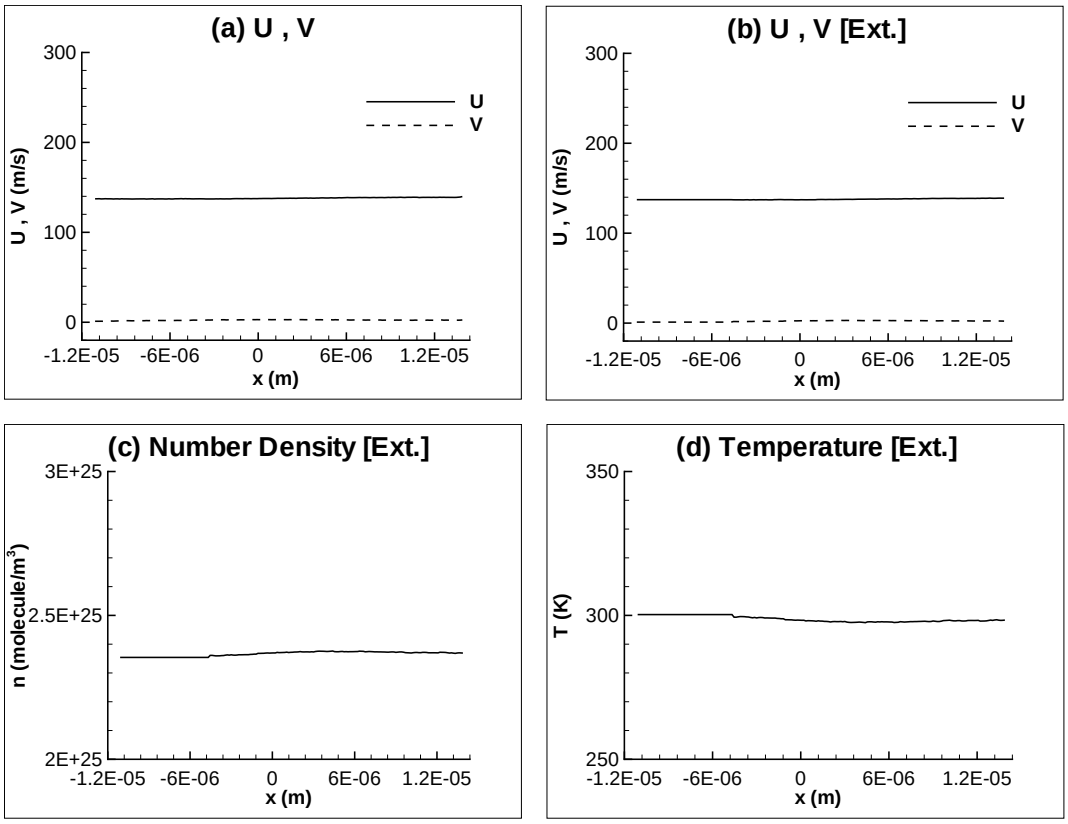

Figure 3.64: Case A.16 ; Velocities and extrapolated flowfield variables at top boundary.

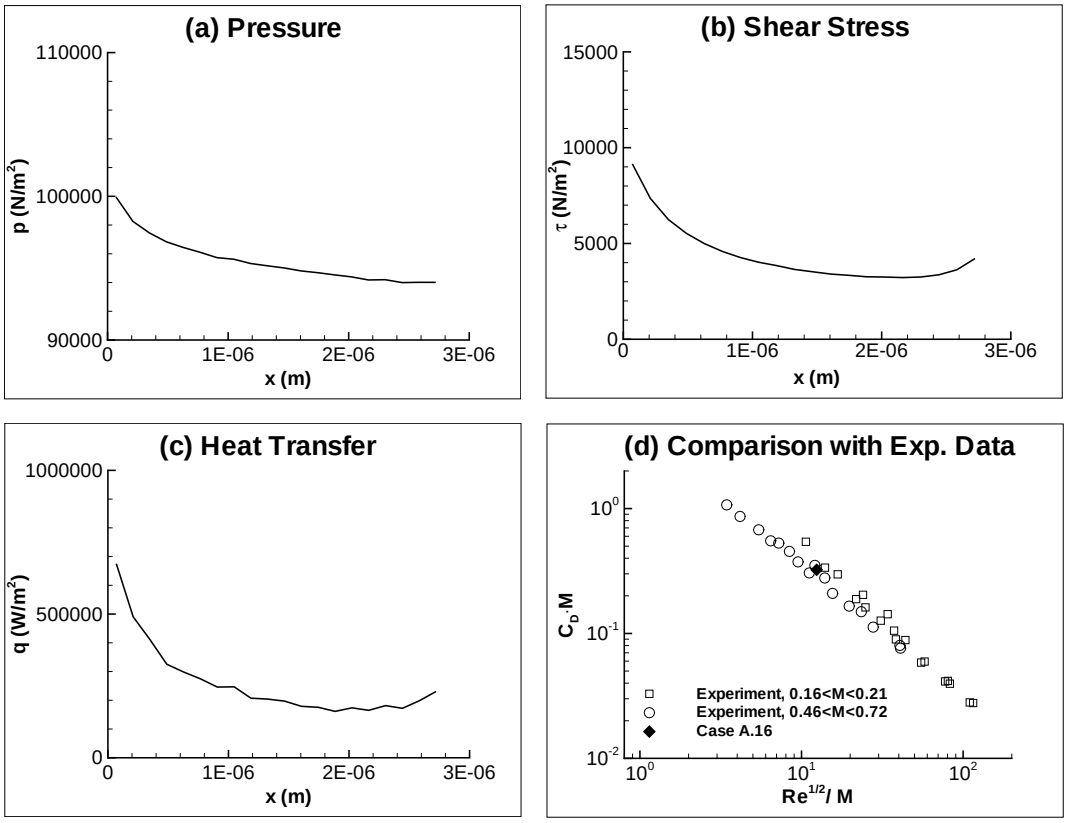

Figure 3.65: Case A.16 ; Surface properties and comparison with experimental data.

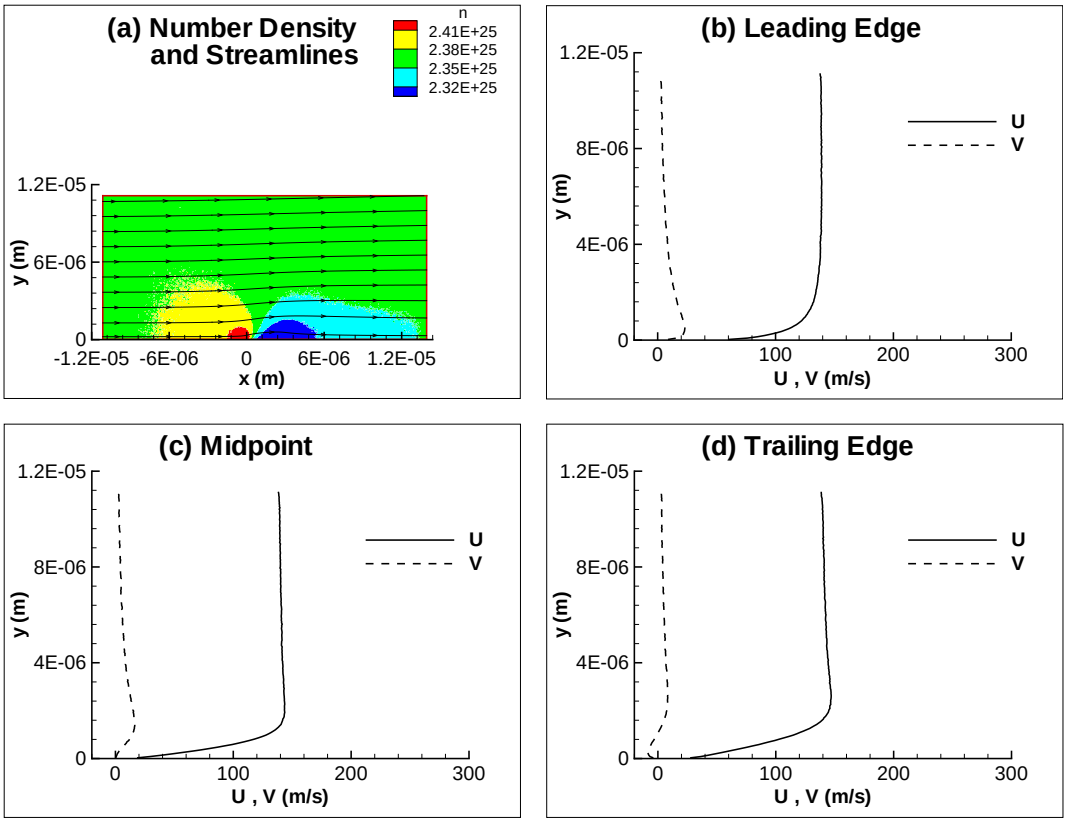

Figure 3.66: Case A.17 ; Number density contours, streamlines and velocity profiles.

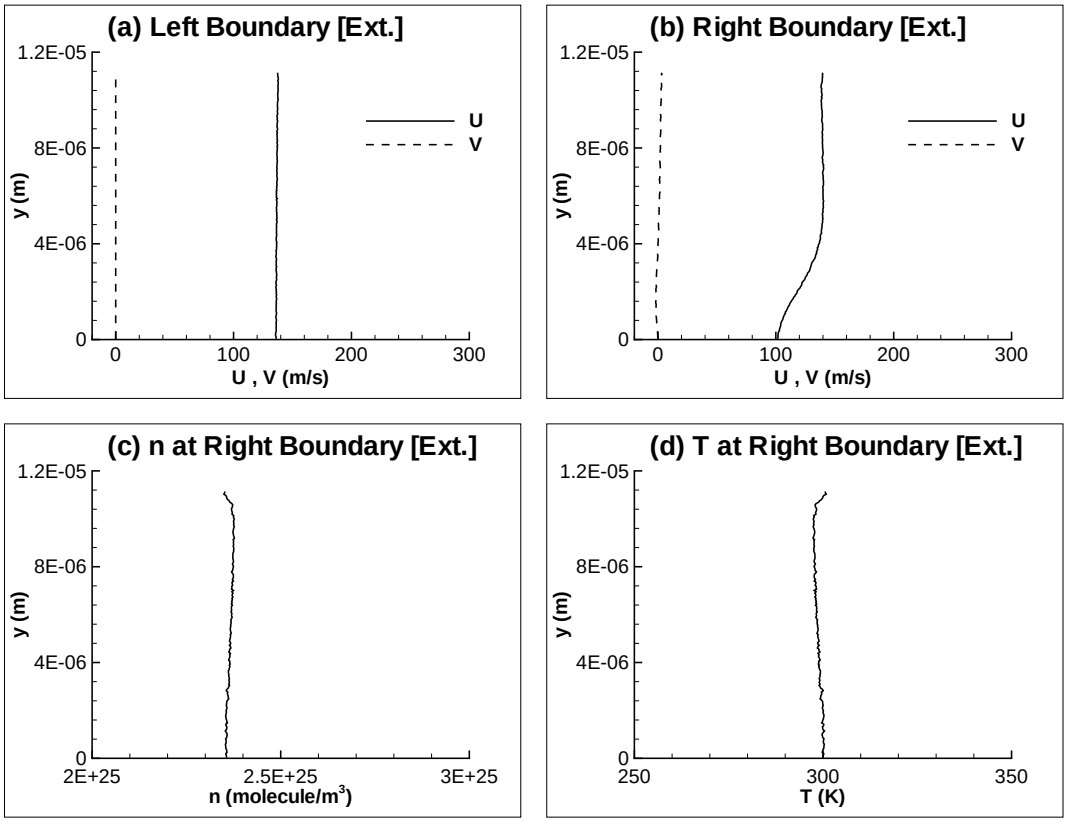

Figure 3.67: Case A.17 ; Extrapolated flowfield variables at left and right boundaries.

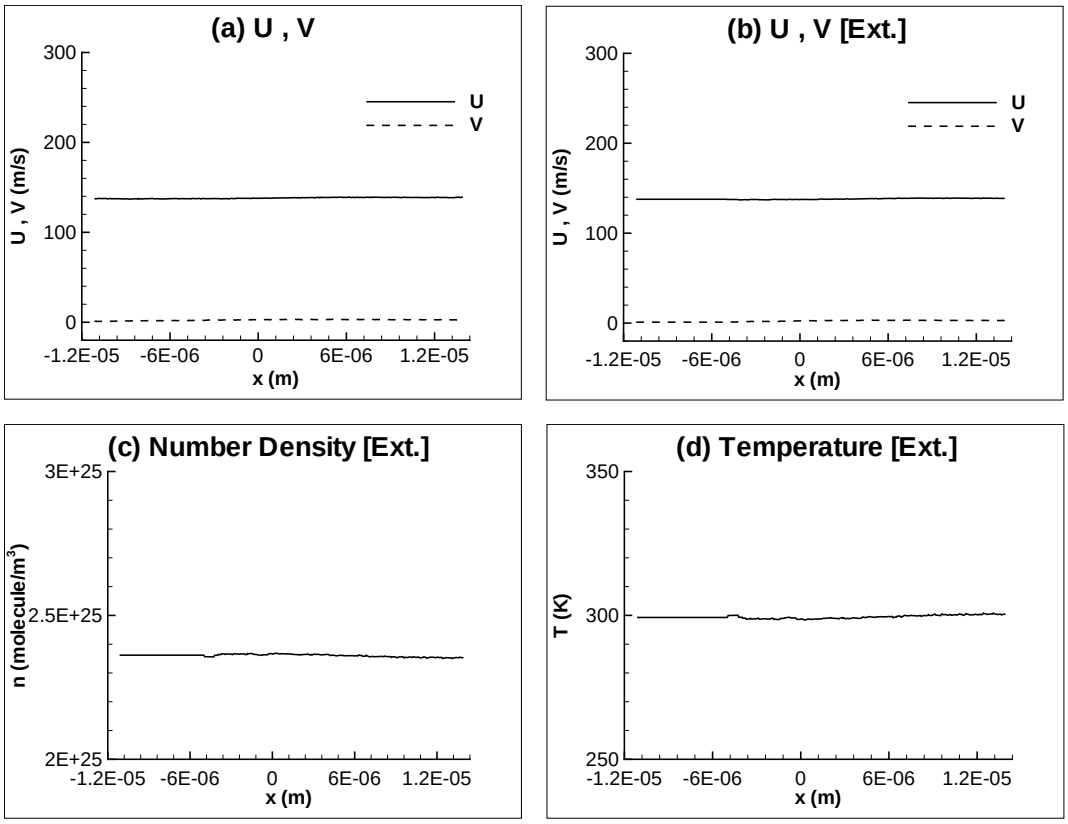

Figure 3.68: Case A.17 ; Velocities and extrapolated flowfield variables at top boundary.

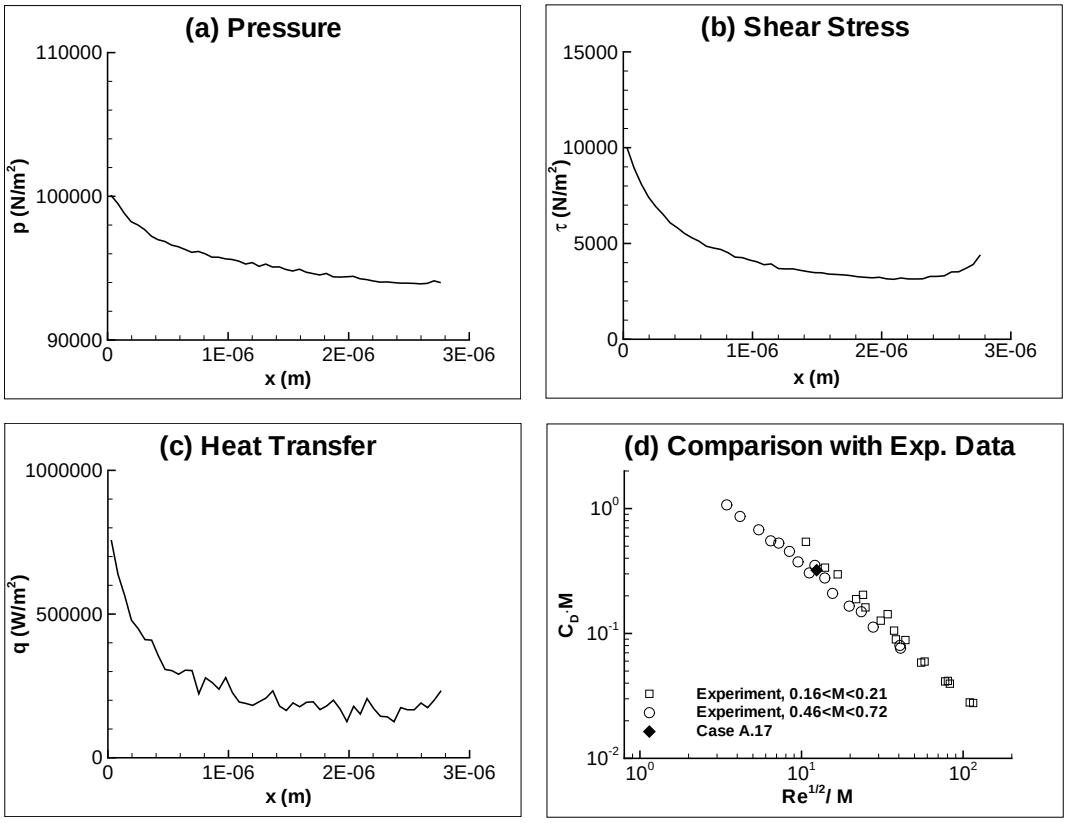

Figure 3.69: Case A.17 ; Surface properties and comparison with experimental data.

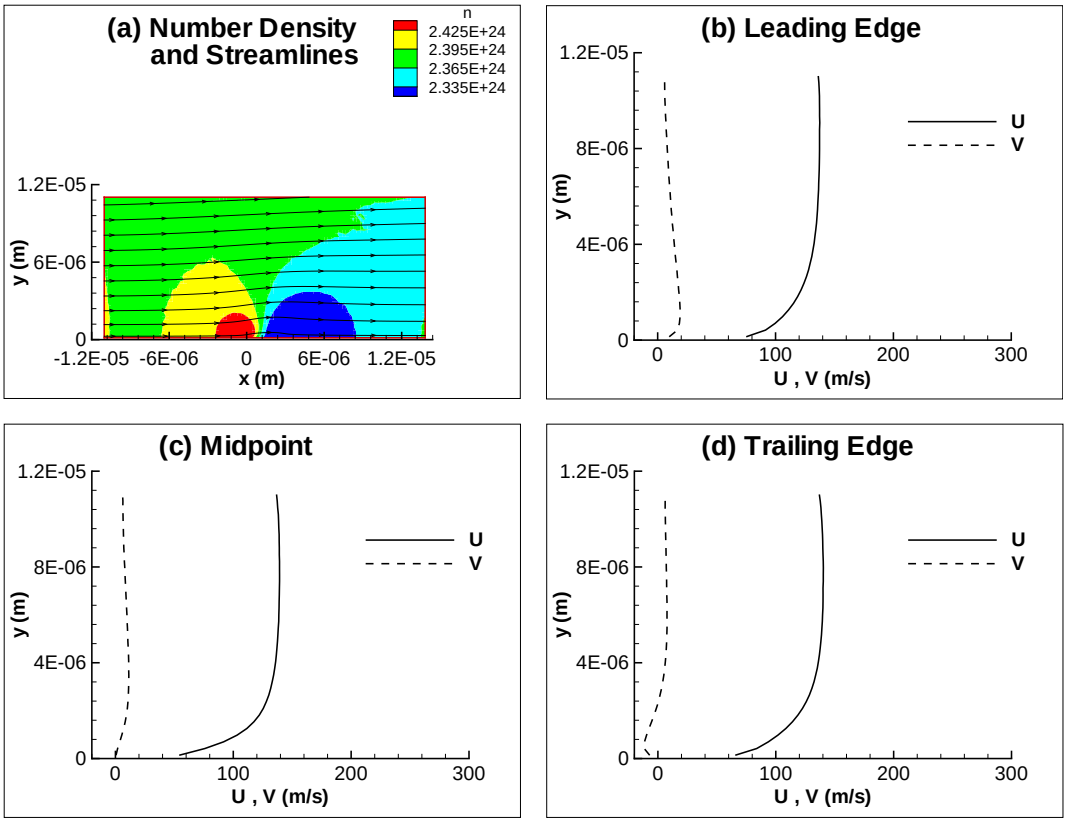

Figure 3.70: Case A.18 ; Number density contours, streamlines and velocity profiles.

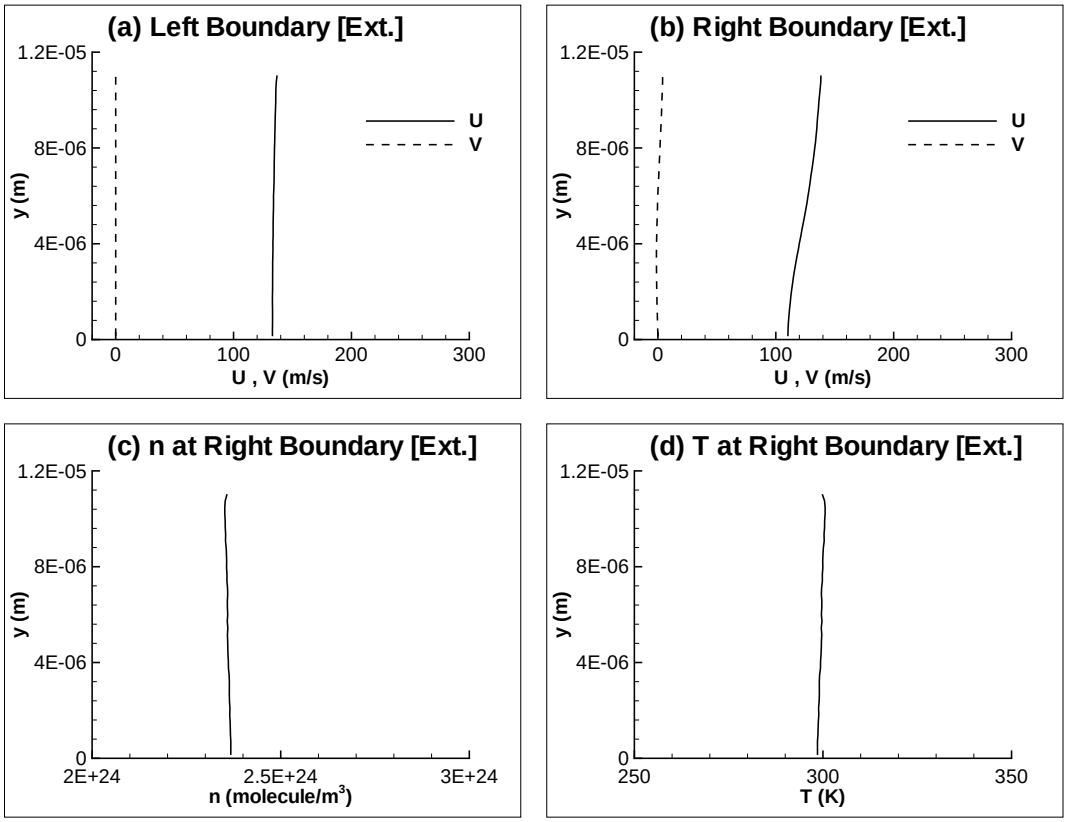

Figure 3.71: Case A.18 ; Extrapolated flowfield variables at left and right boundaries.

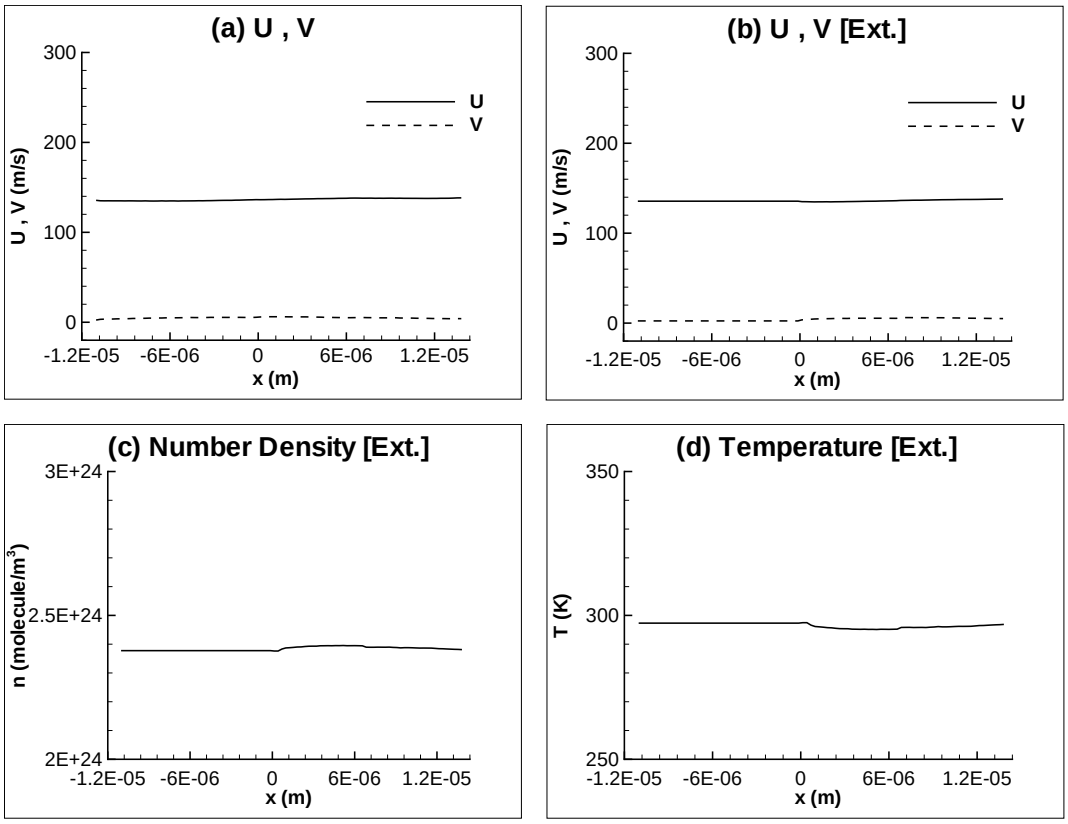

Figure 3.72: Case A.18 ; Velocities and extrapolated flowfield variables at top boundary.

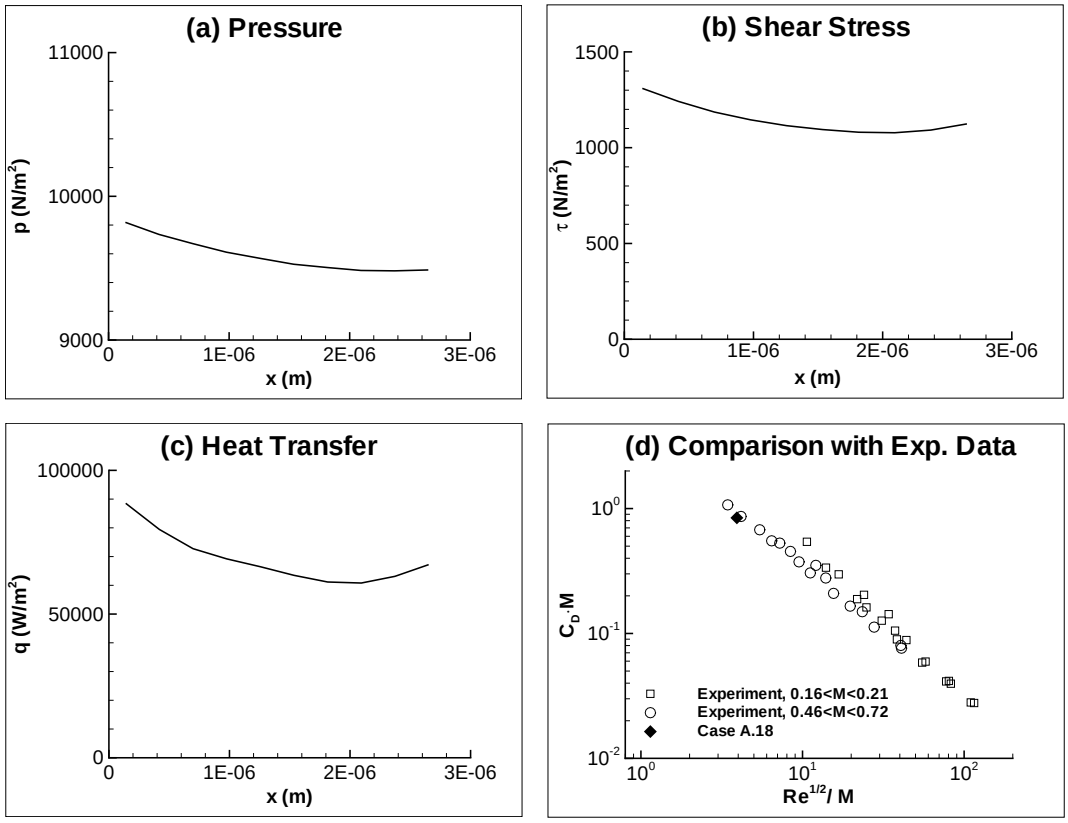

Figure 3.73: Case A.18 ; Surface properties and comparison with experimental data.

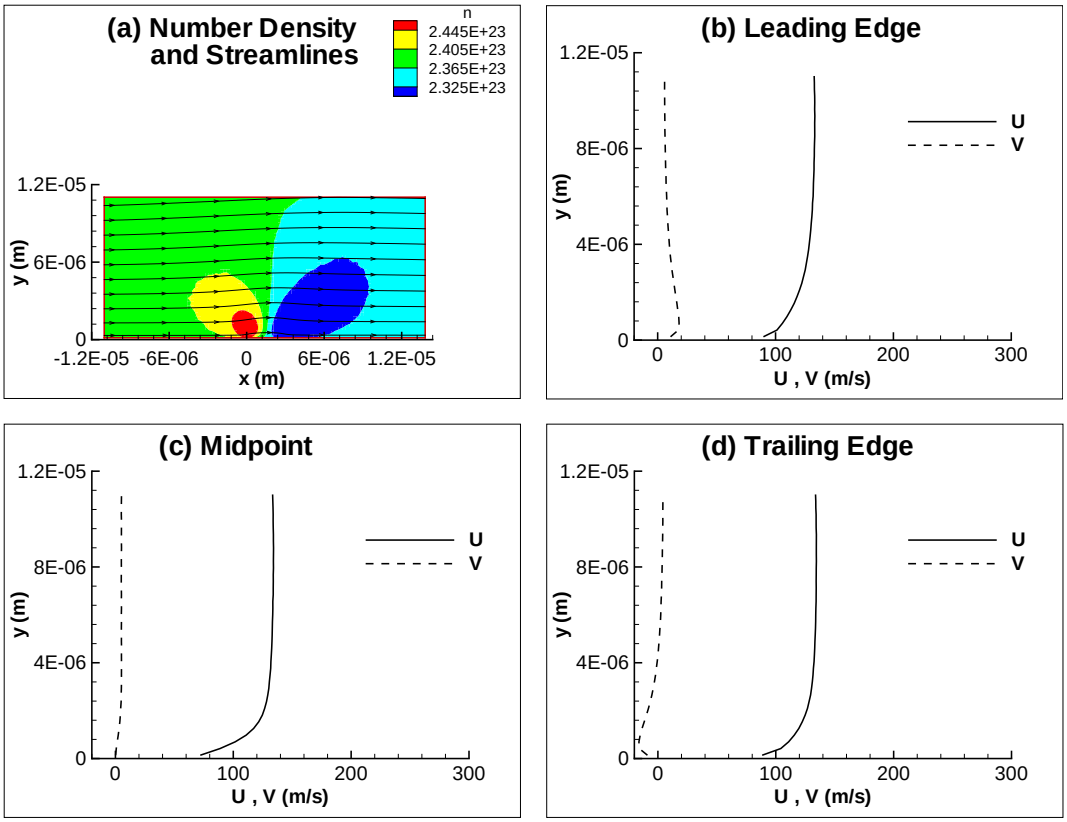

Figure 3.74: Case A.19 ; Number density contours, streamlines and velocity profiles.

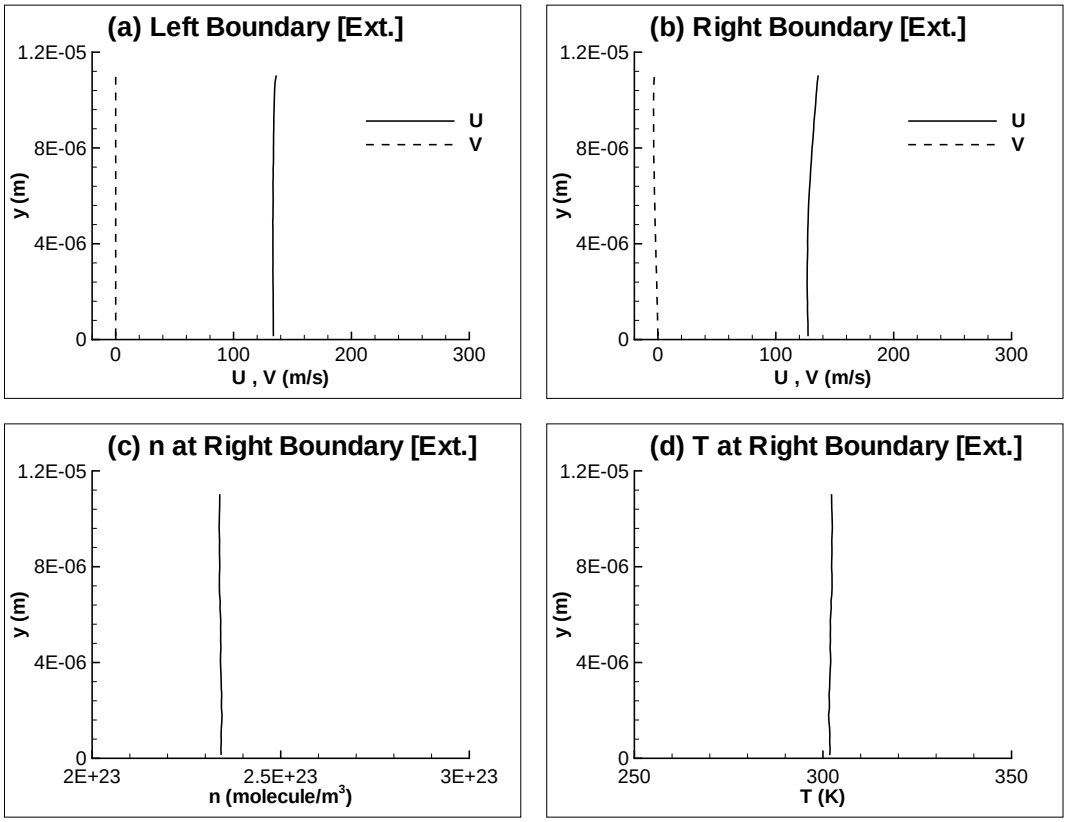

Figure 3.75: Case A.19 ; Extrapolated flowfield variables at left and right boundaries.

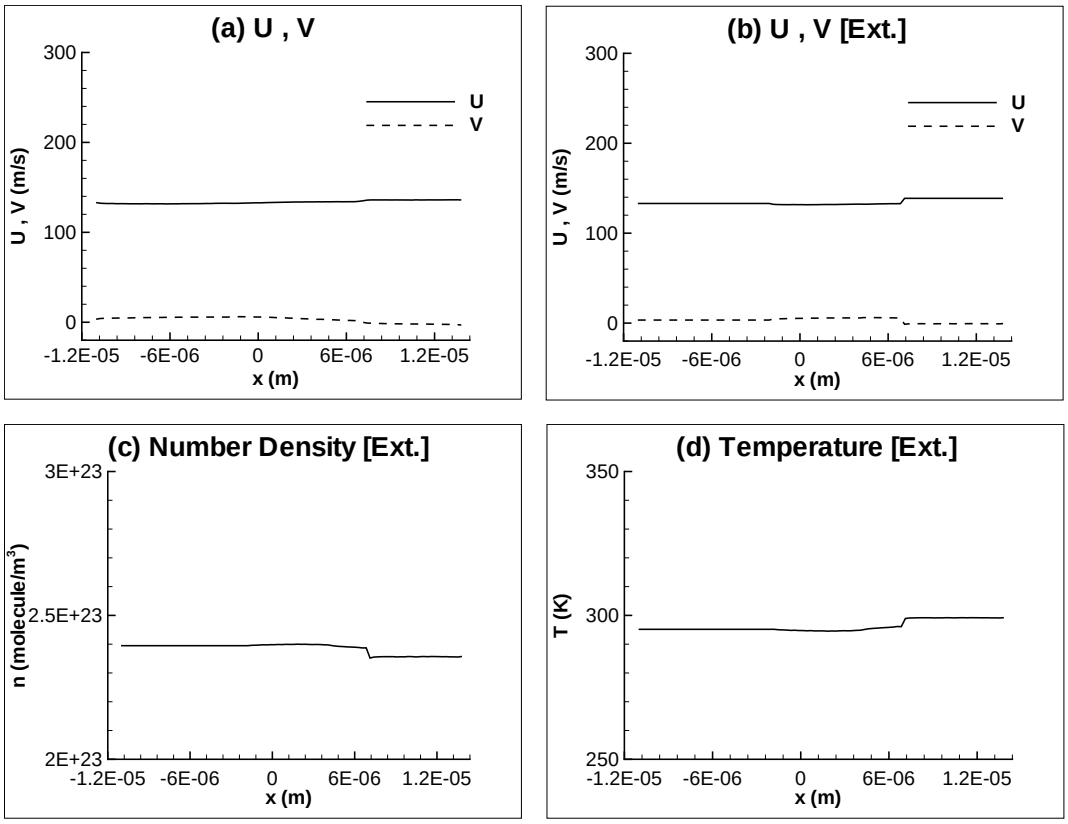

Figure 3.76: Case A.19 ; Velocities and extrapolated flowfield variables at top boundary.

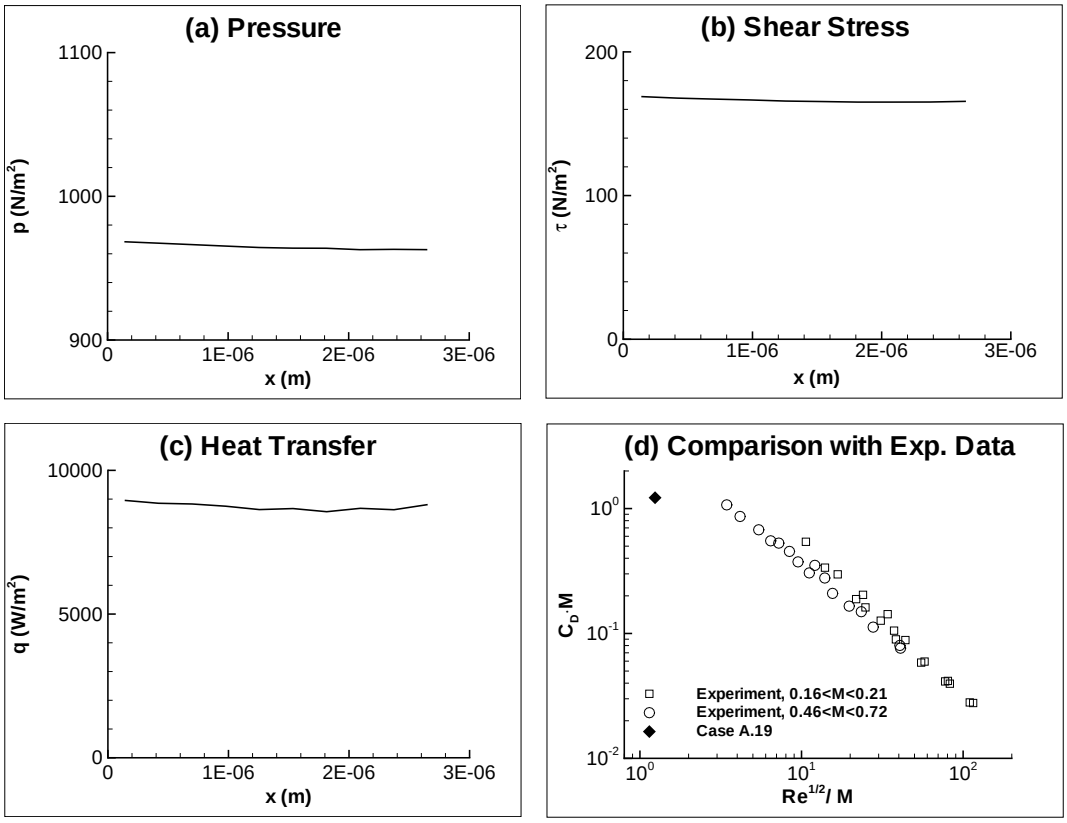

Figure 3.77: Case A.19 ; Surface properties and comparison with experimental data.

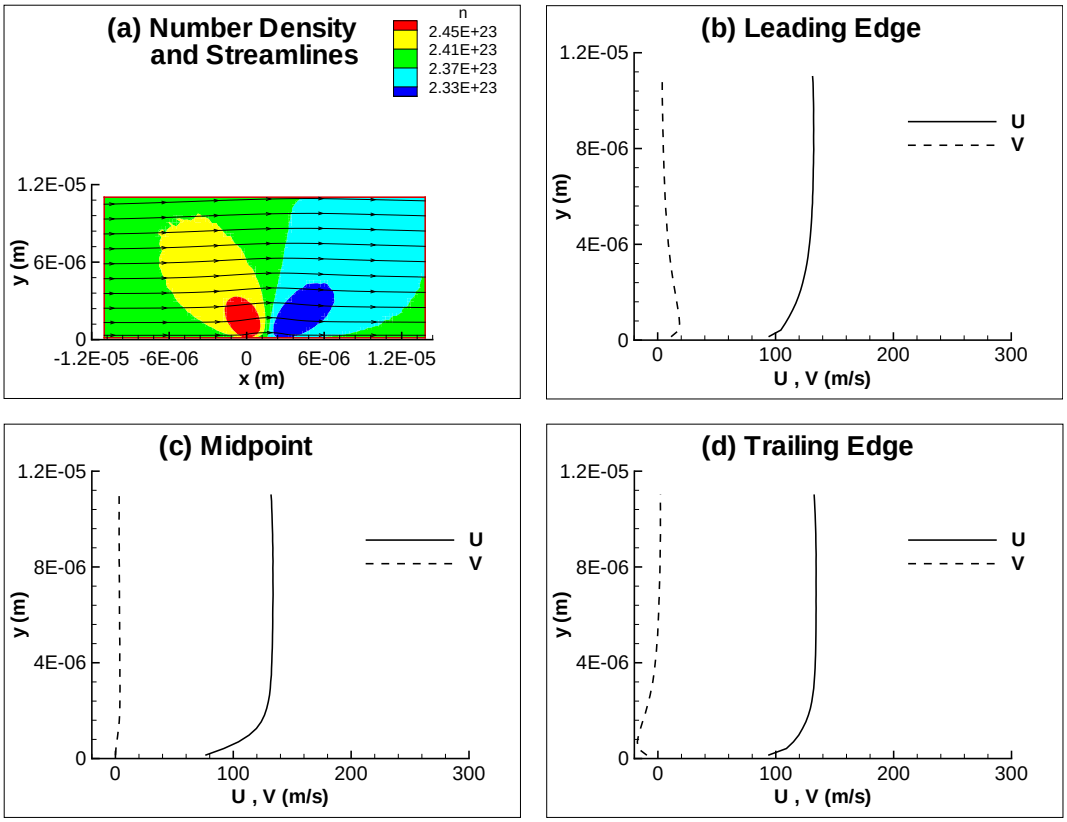

Figure 3.78: Case A.20 ; Number density contours, streamlines and velocity profiles.

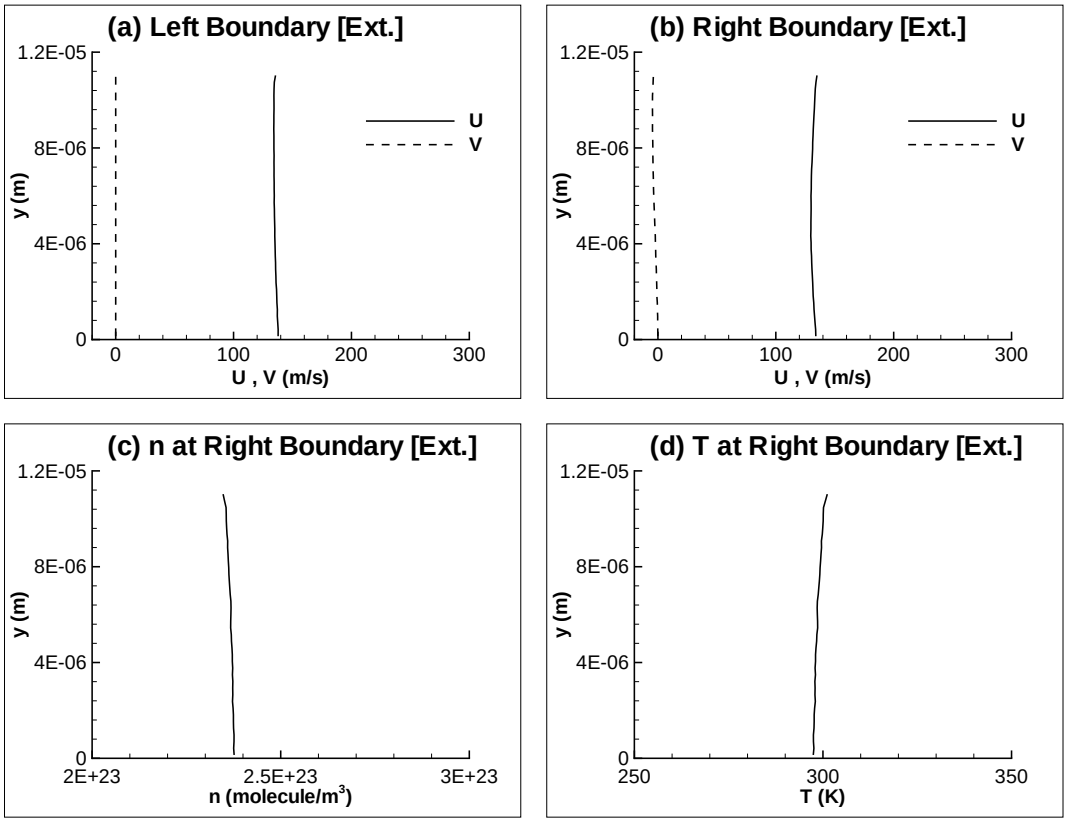

Figure 3.79: Case A.20 ; Extrapolated flowfield variables at left and right boundaries.

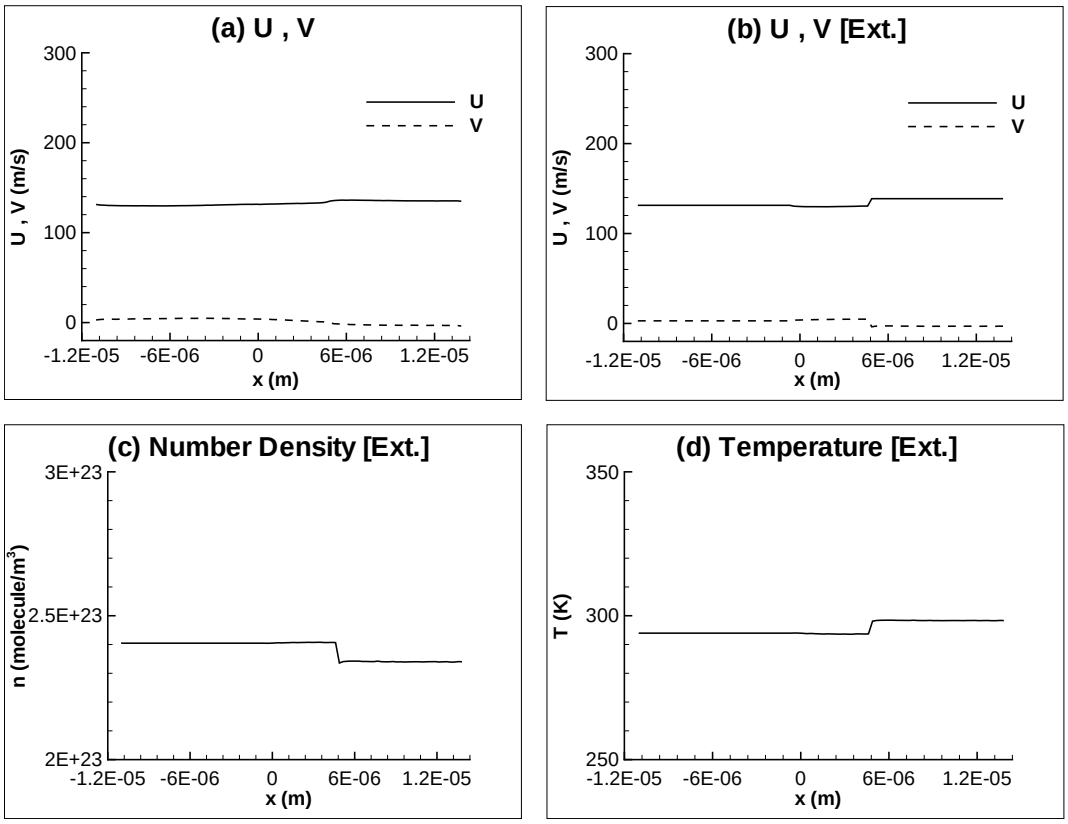

Figure 3.80: Case A.20 ; Velocities and extrapolated flowfield variables at top boundary.

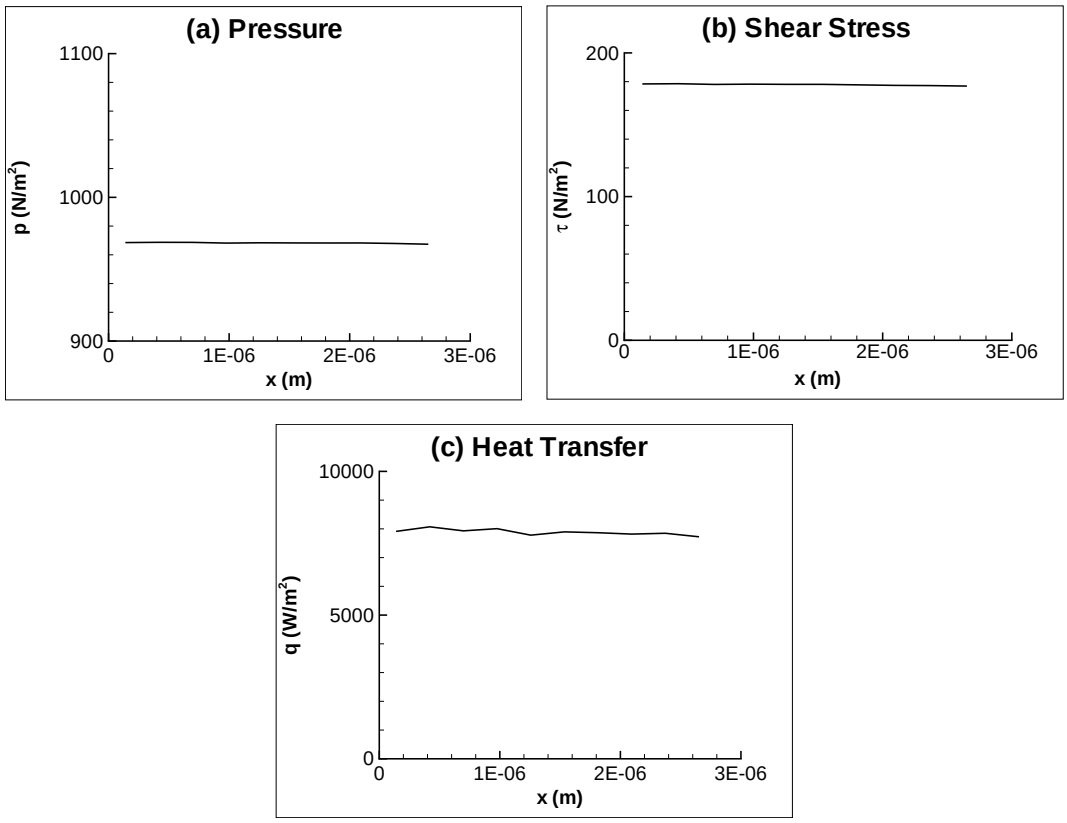

Figure 3.81: Case A.20 ; Surface properties.

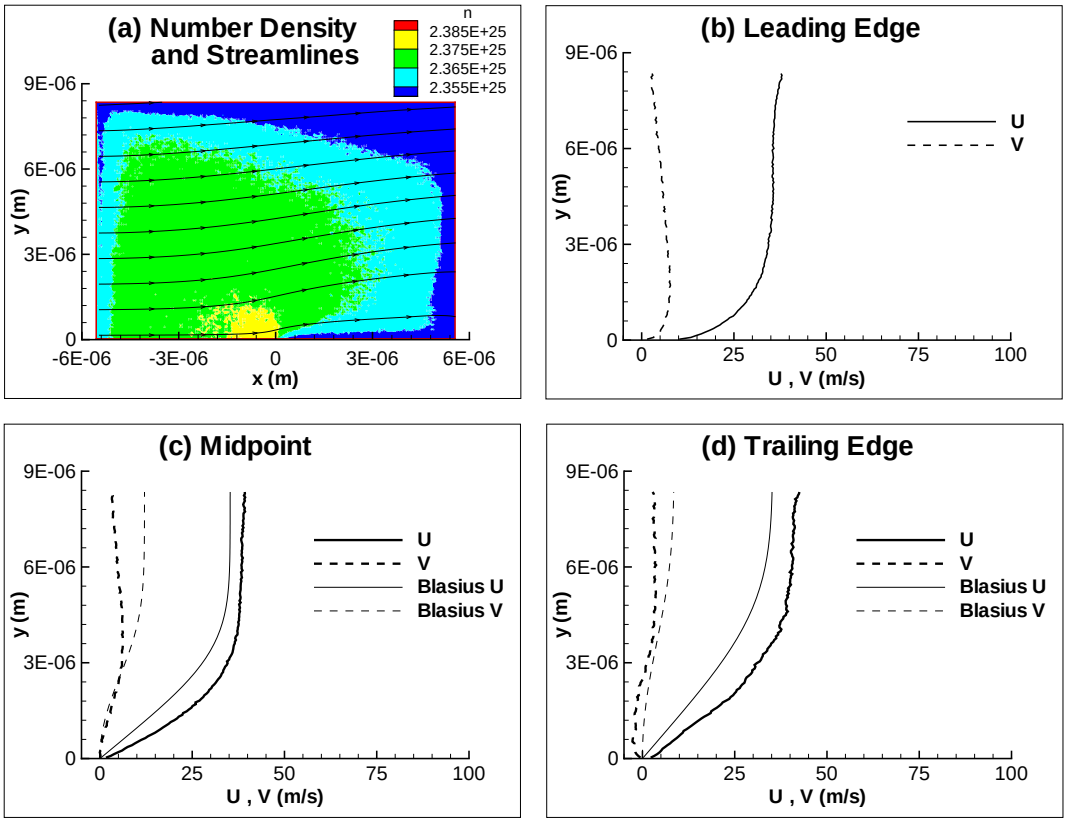

Figure 3.82: Case B.1 ; Number density contours, streamlines and velocity profiles.

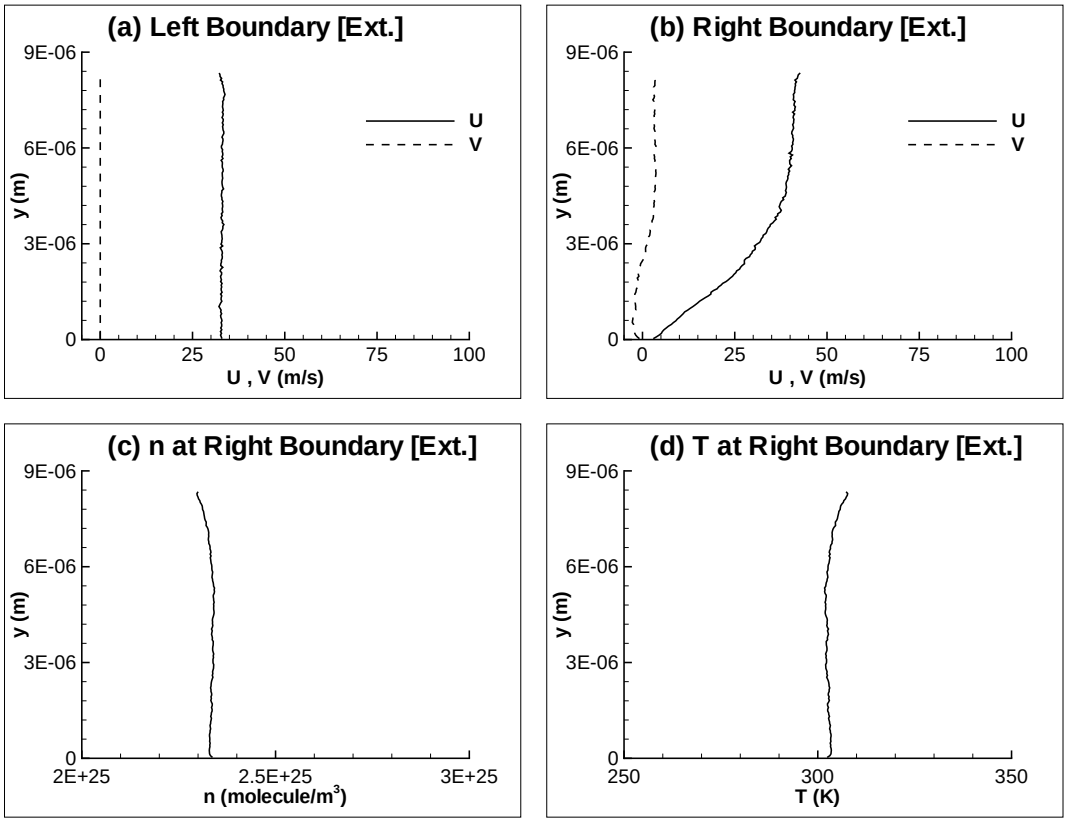

Figure 3.83: Case B.1 ; Extrapolated flowfield variables at left and right boundaries.

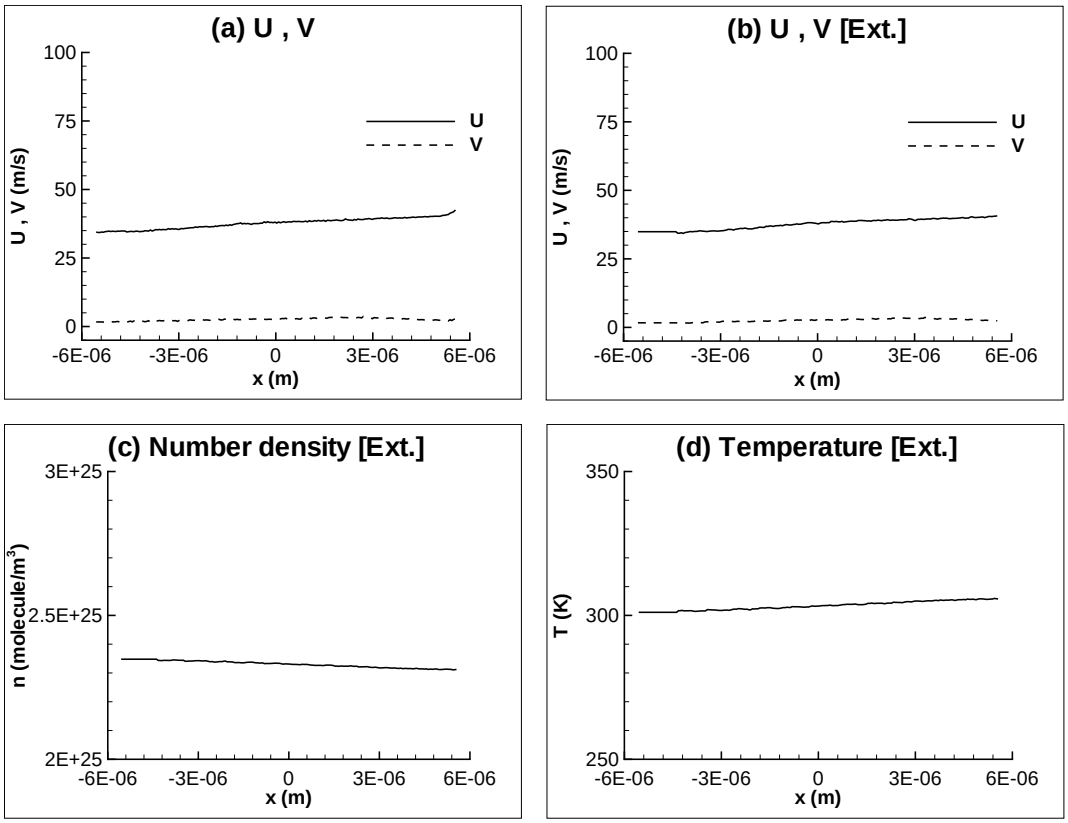

Figure 3.84: Case B.1 ; Velocities and extrapolated flowfield variables at top boundary.

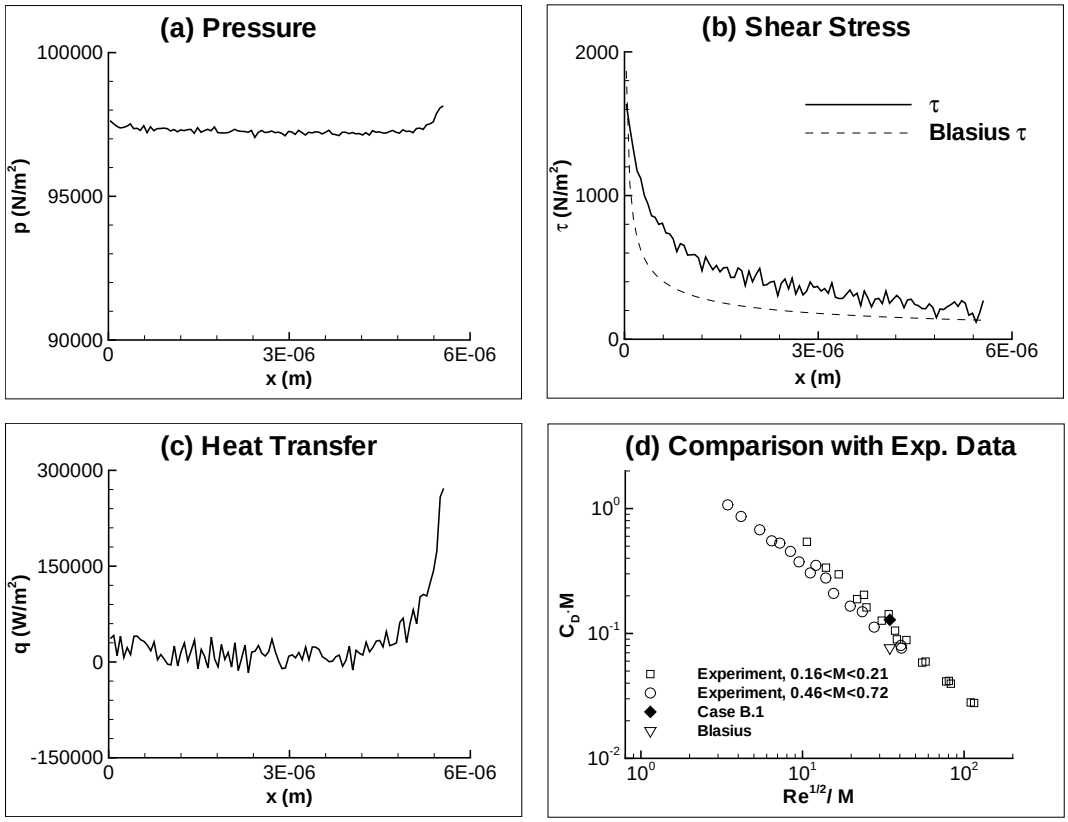

Figure 3.85: Case B.1 ; Surface properties and comparison with experimental data.

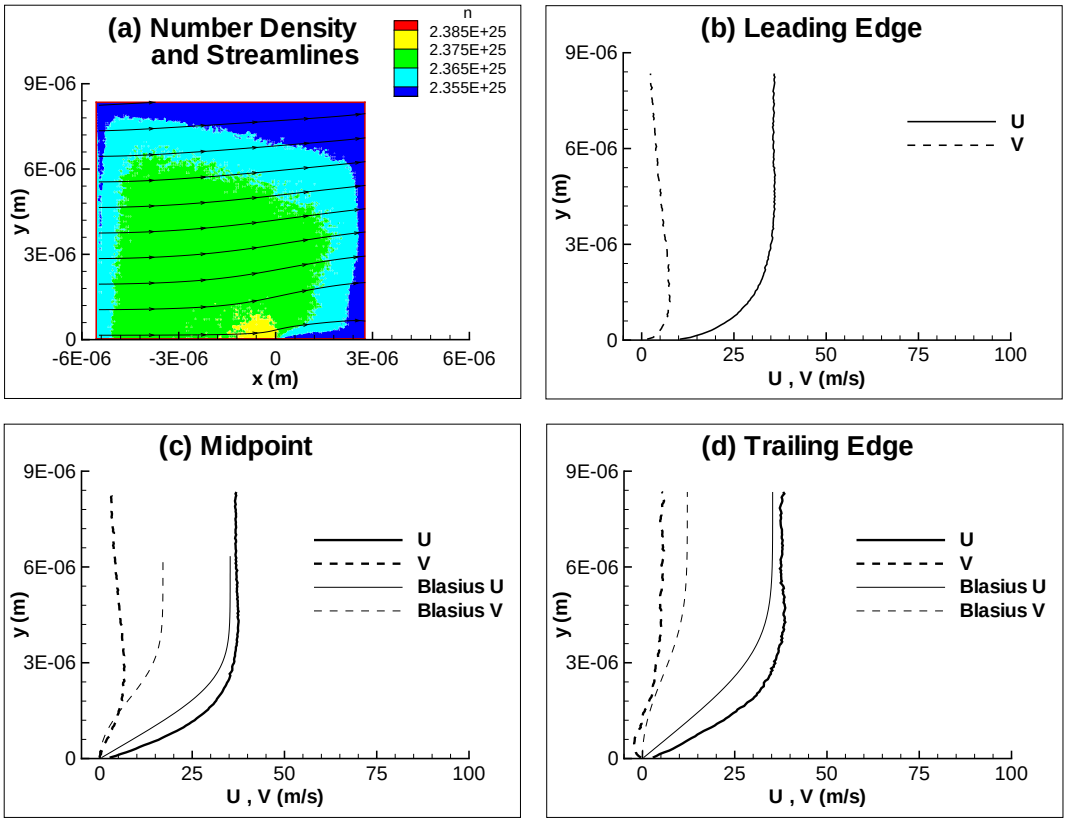

Figure 3.86: Case B.2 ; Number density contours, streamlines and velocity profiles.

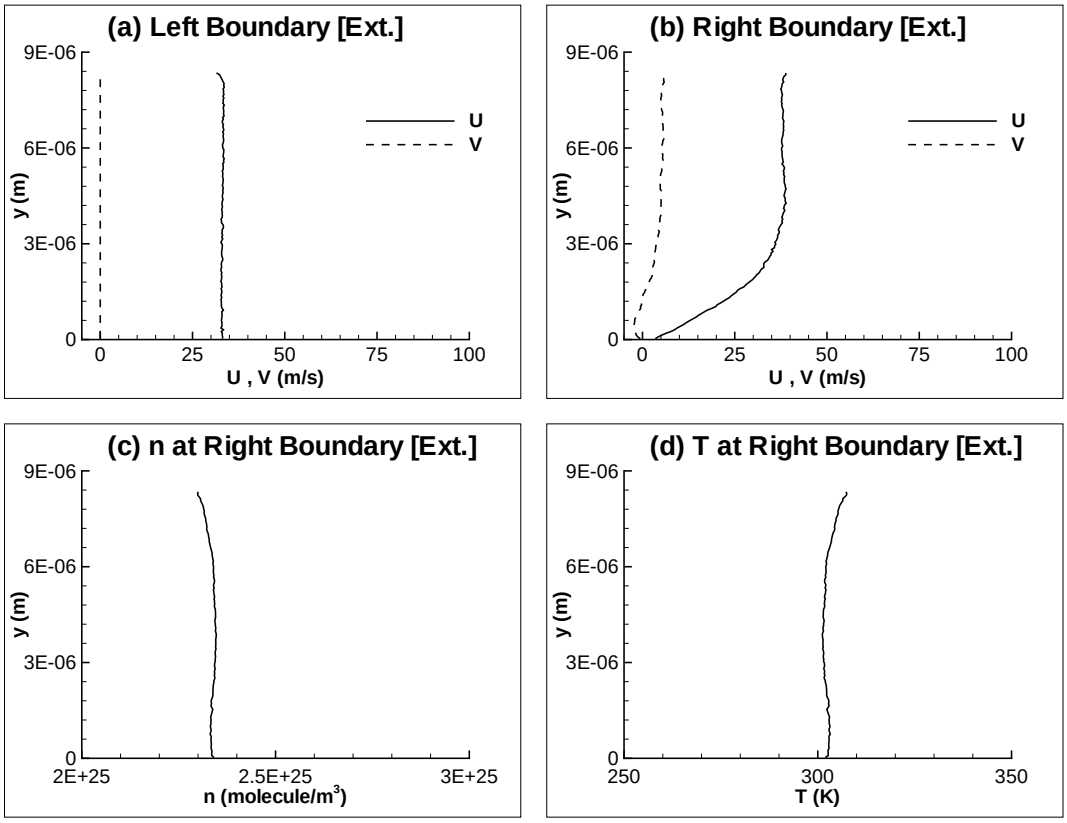

Figure 3.87: Case B.2 ; Extrapolated flowfield variables at left and right boundaries.

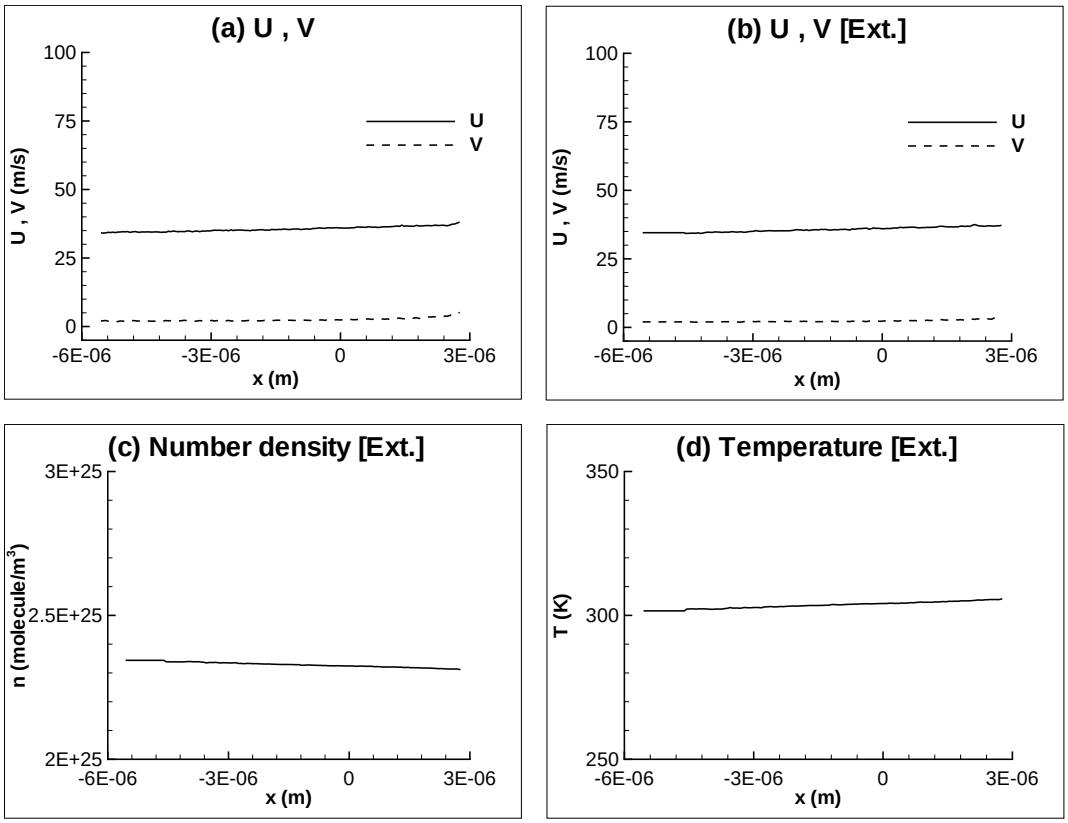

Figure 3.88: Case B.2 ; Velocities and extrapolated flowfield variables at top boundary.

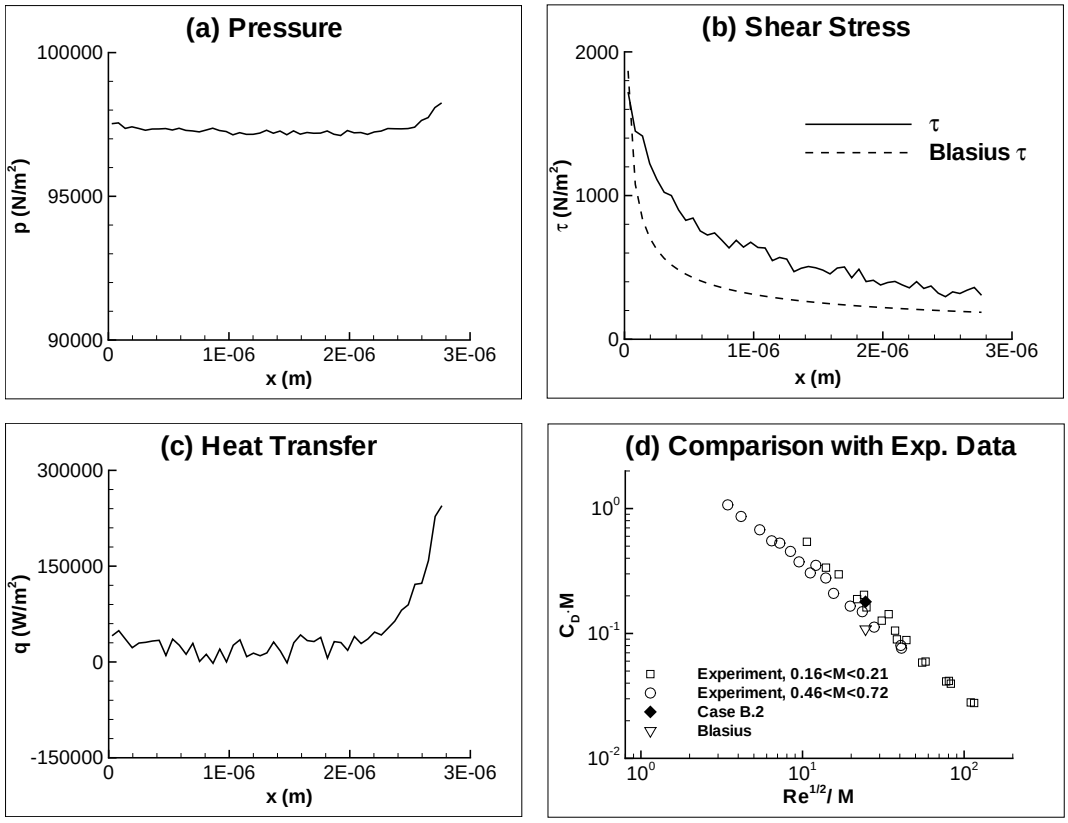

Figure 3.89: Case B.2 ; Surface properties and comparison with experimental data.

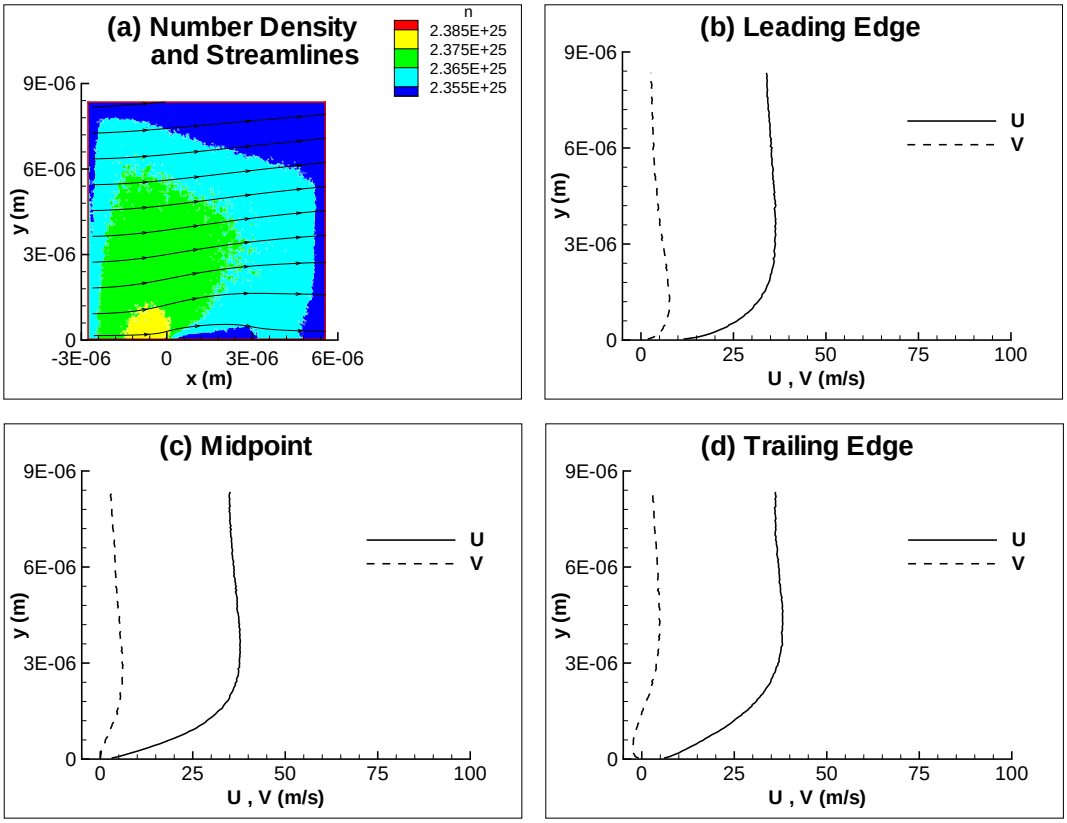

Figure 3.90: Case B.3 ; Number density contours, streamlines and velocity profiles.

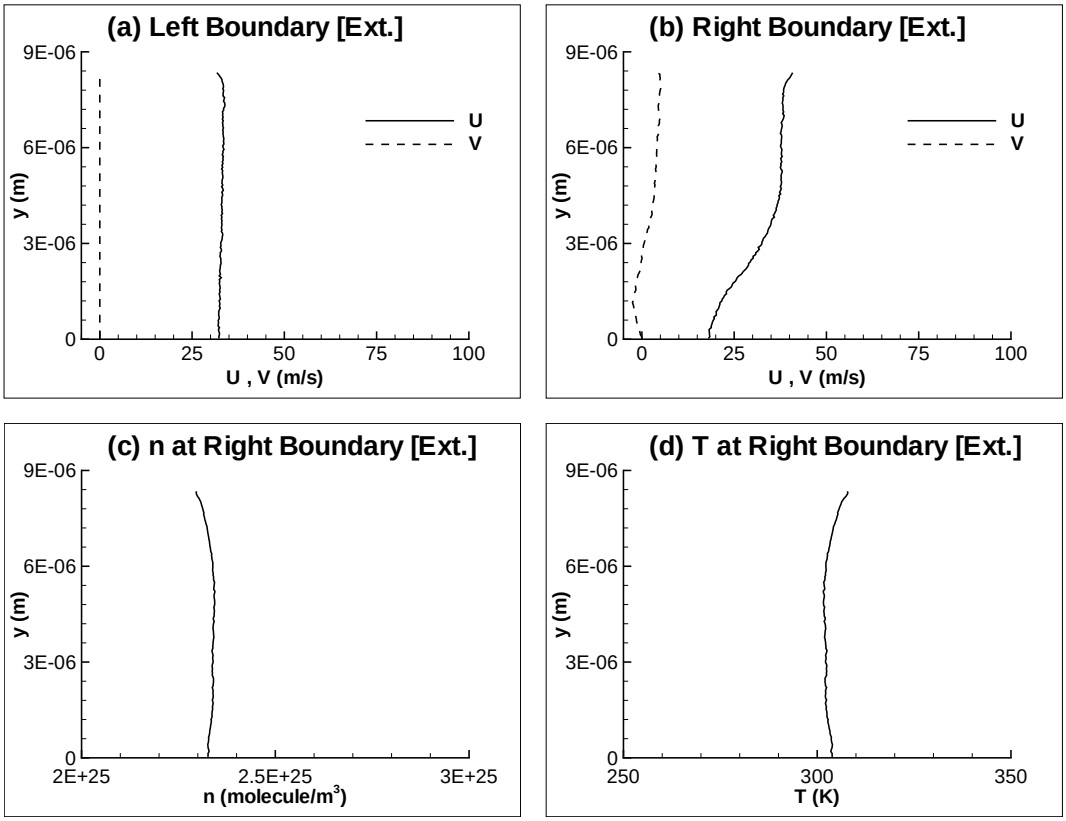

Figure 3.91: Case B.3 ; Extrapolated flowfield variables at left and right boundaries.

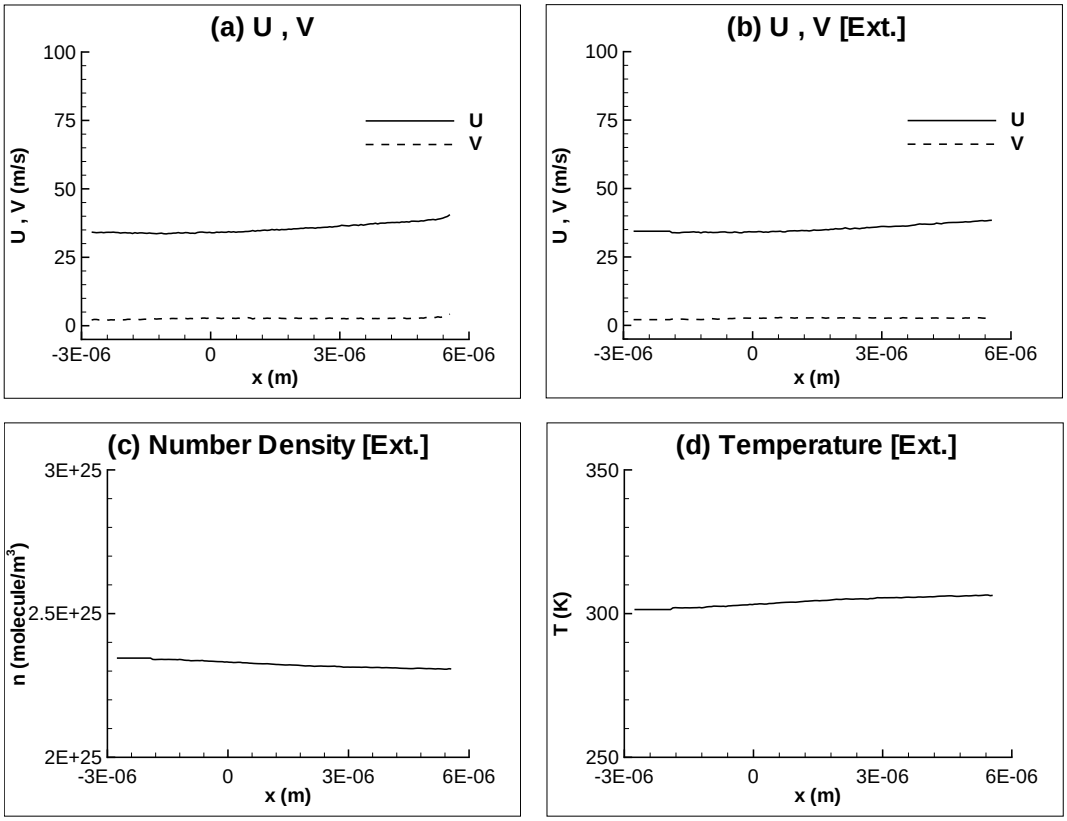

Figure 3.92: Case B.3 ; Velocities and extrapolated flowfield variables at top boundary.

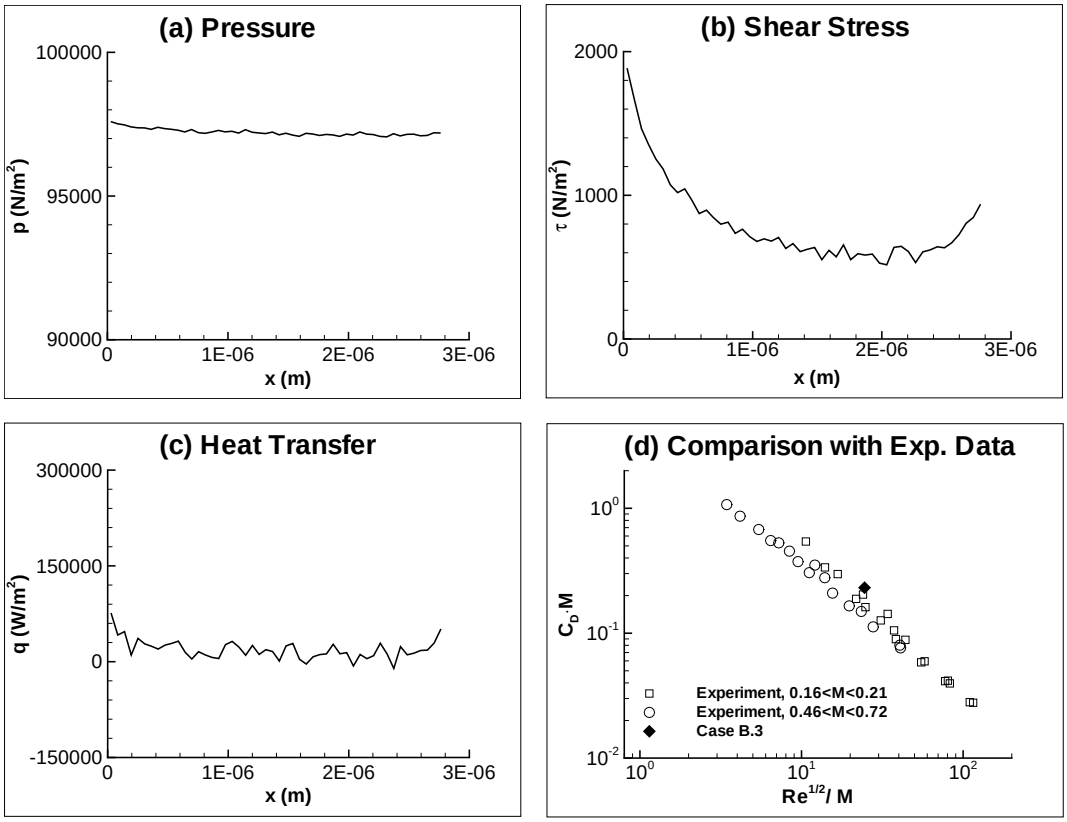

Figure 3.93: Case B.3 ; Surface properties and comparison with experimental data.

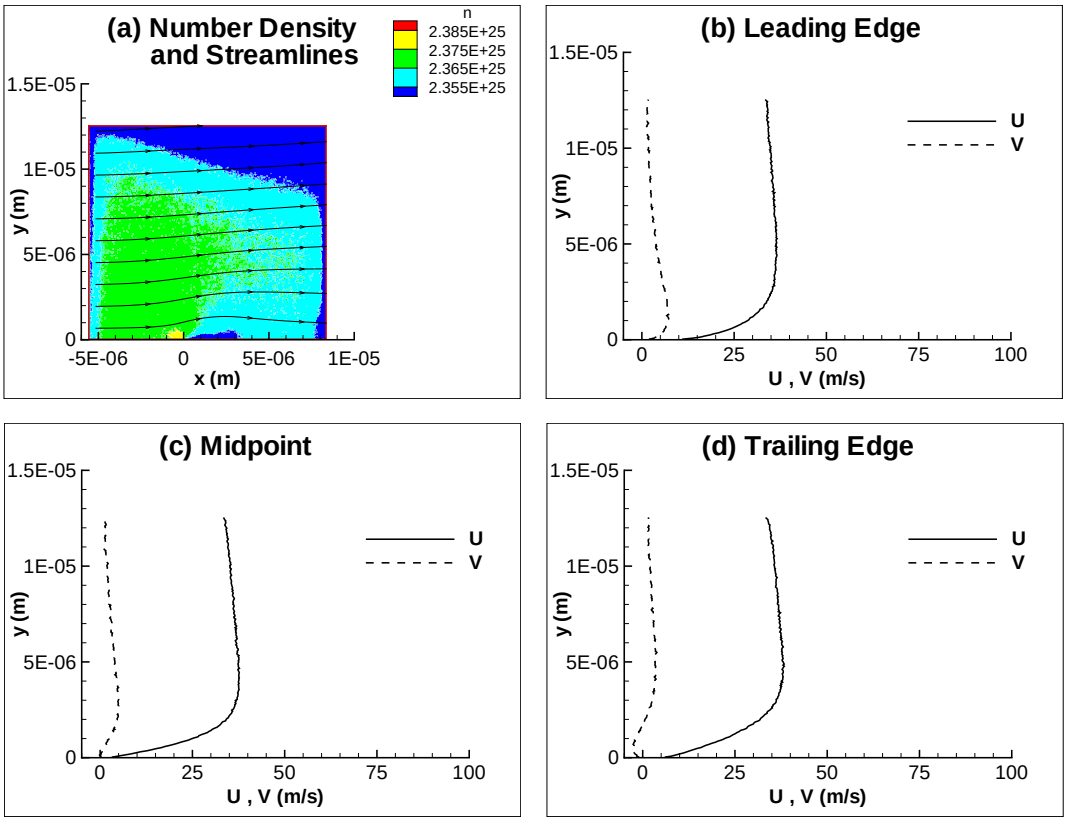

Figure 3.94: Case B.4 ; Number density contours, streamlines and velocity profiles.

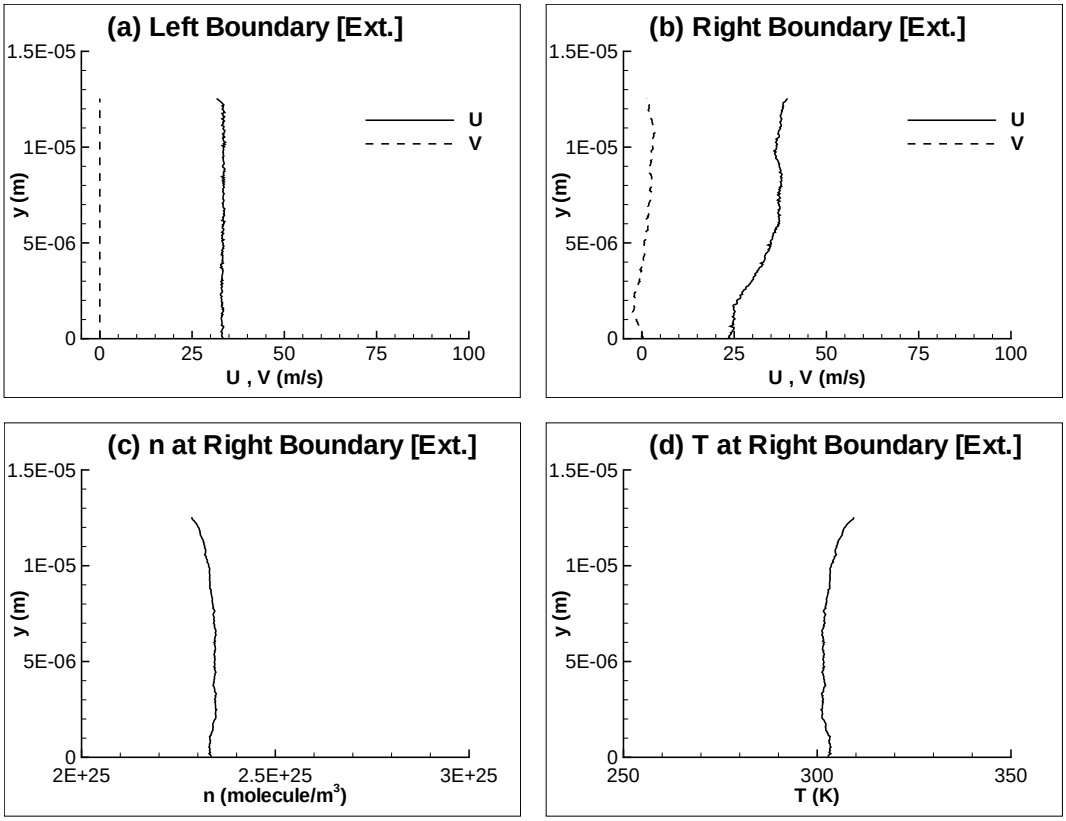

Figure 3.95: Case B.4 ; Extrapolated flowfield variables at left and right boundaries.

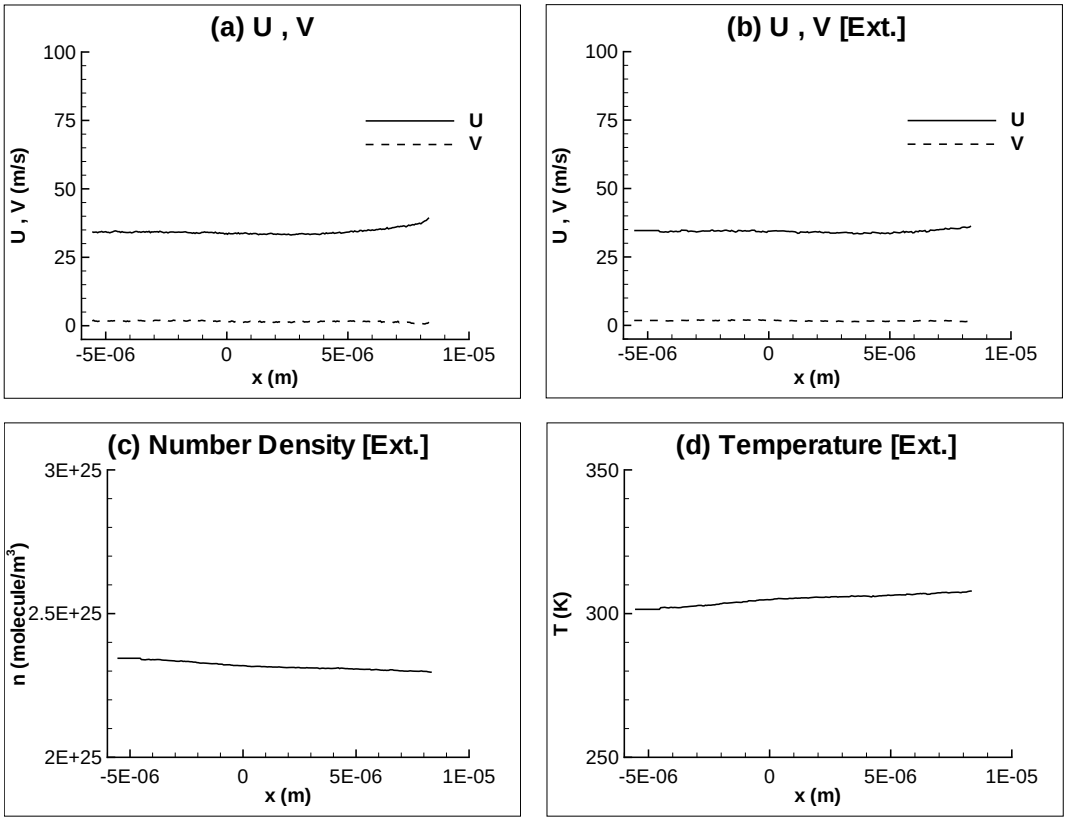

Figure 3.96: Case B.4 ; Velocities and extrapolated flowfield variables at top boundary.

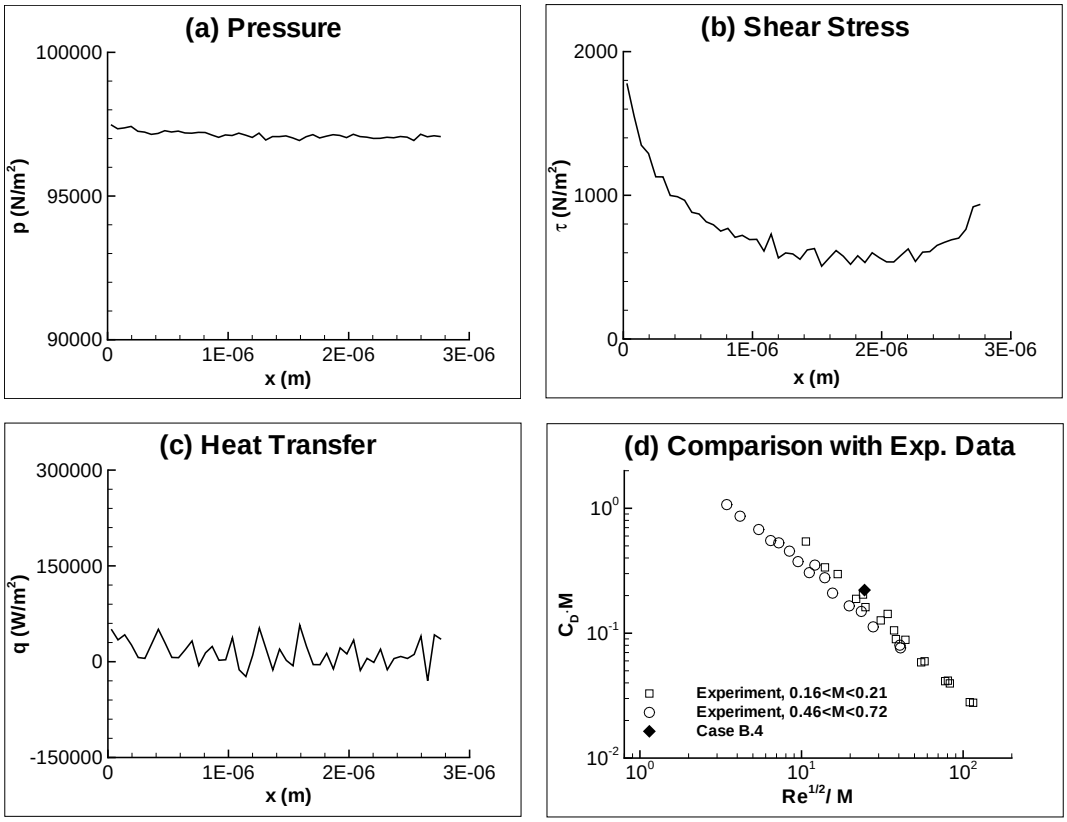

Figure 3.97: Case B.4 ; Surface properties and comparison with experimental data.

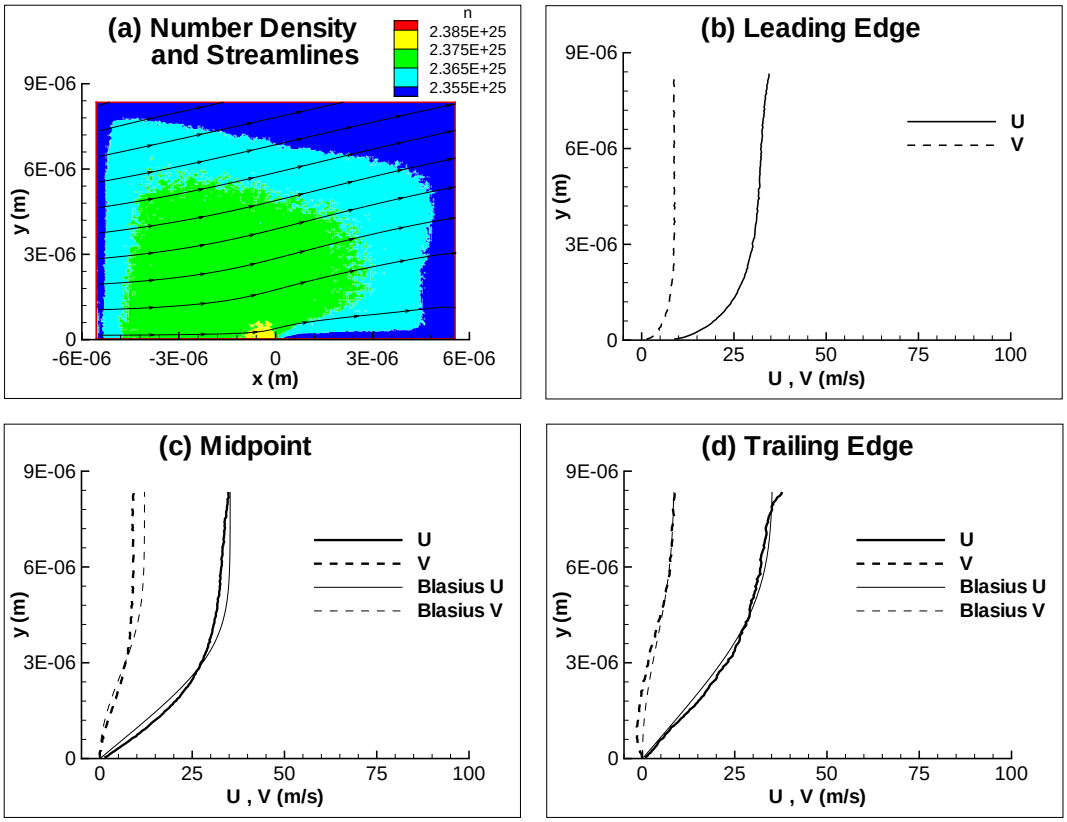

Figure 3.98: Case B.5 ; Number density contours, streamlines and velocity profiles.

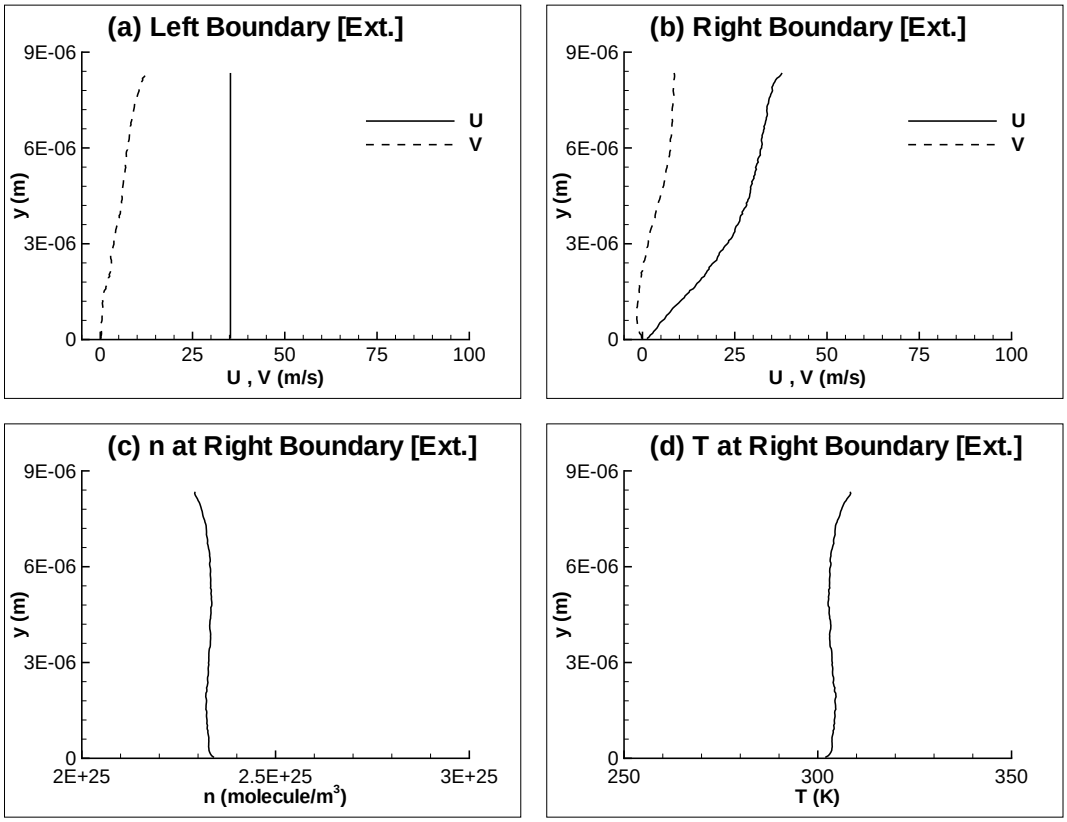

Figure 3.99: Case B.5 ; Extrapolated flowfield variables at left and right boundaries.

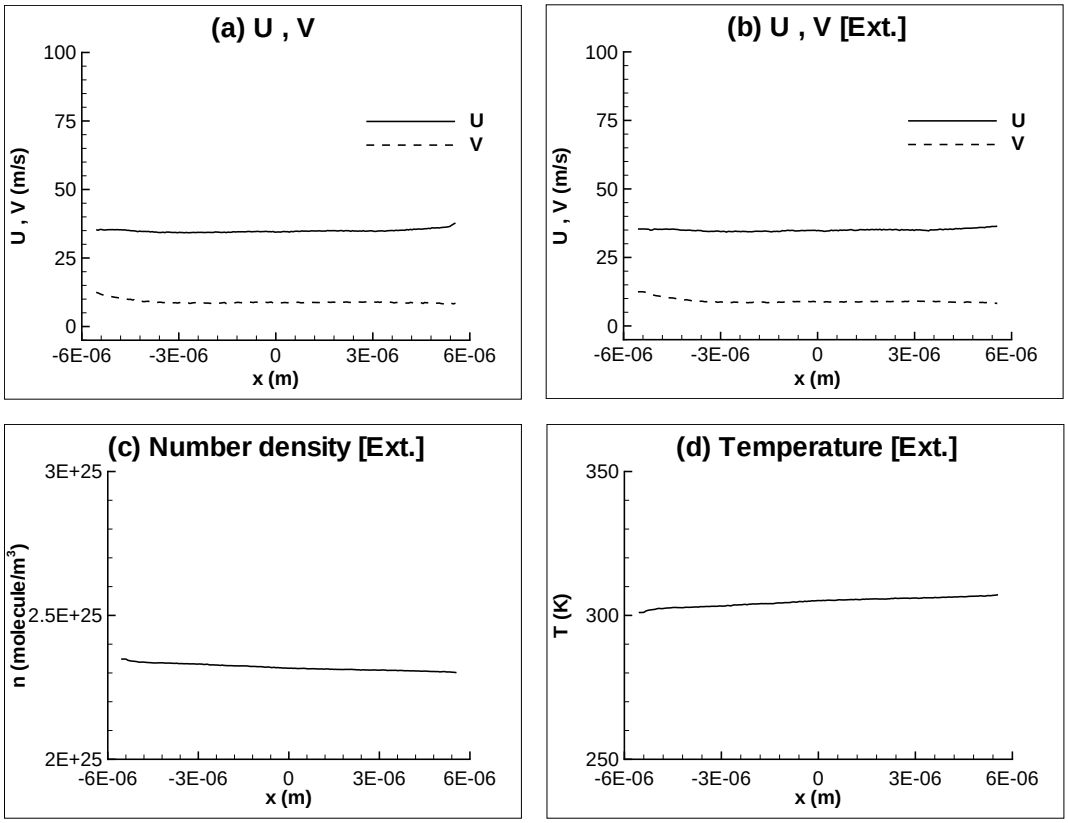

Figure 3.100: Case B.5 ; Velocities and extrapolated flowfield variables at top boundary.

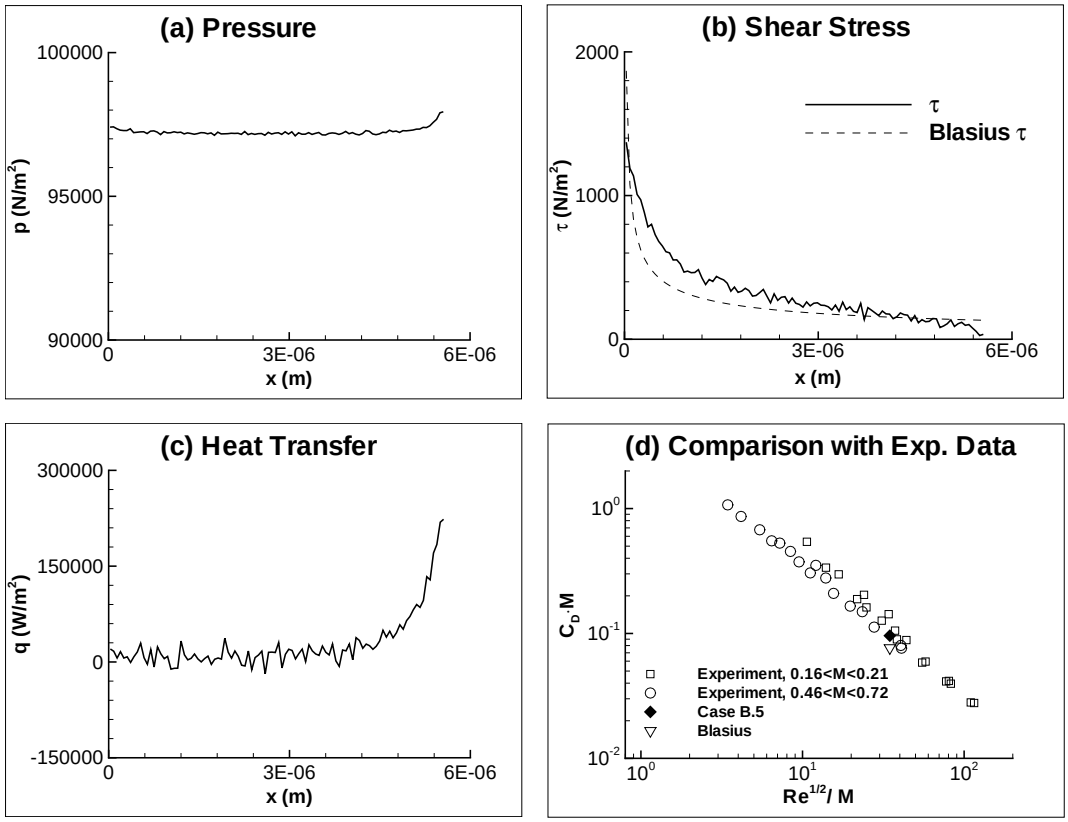

Figure 3.101: Case B.5 ; Surface properties and comparison with experimental data.

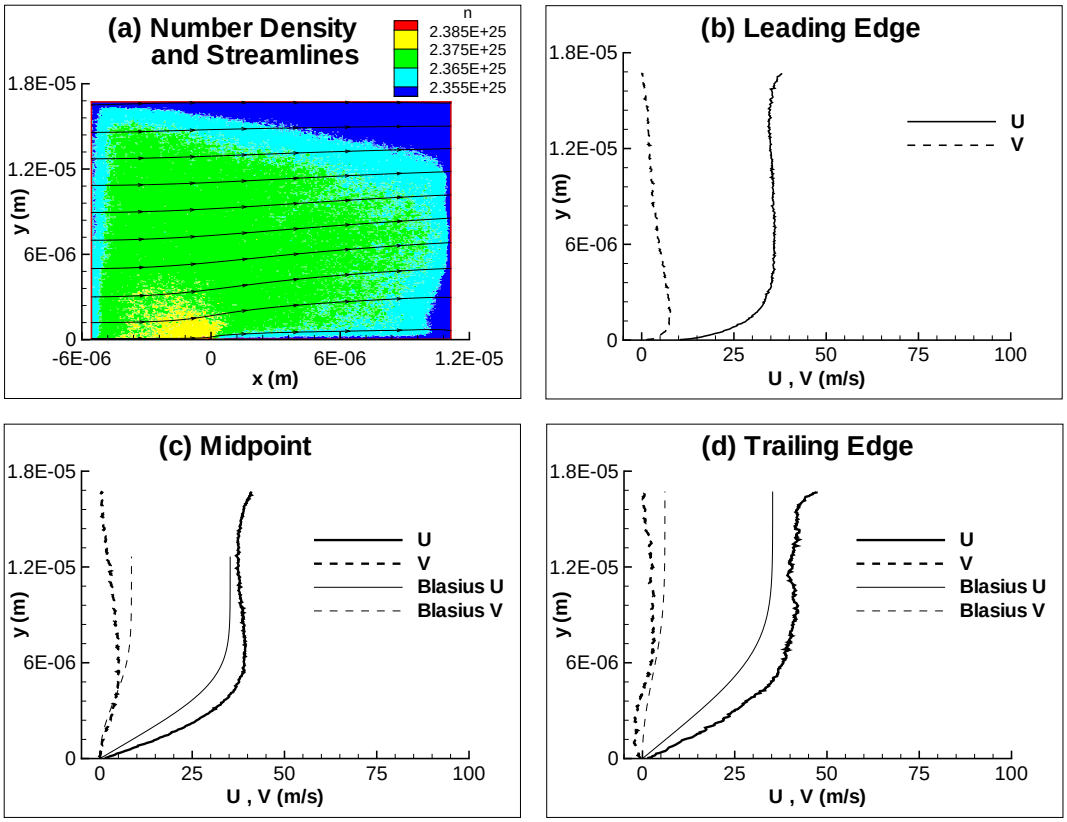

Figure 3.102: Case B.6 ; Number density contours, streamlines and velocity profiles.

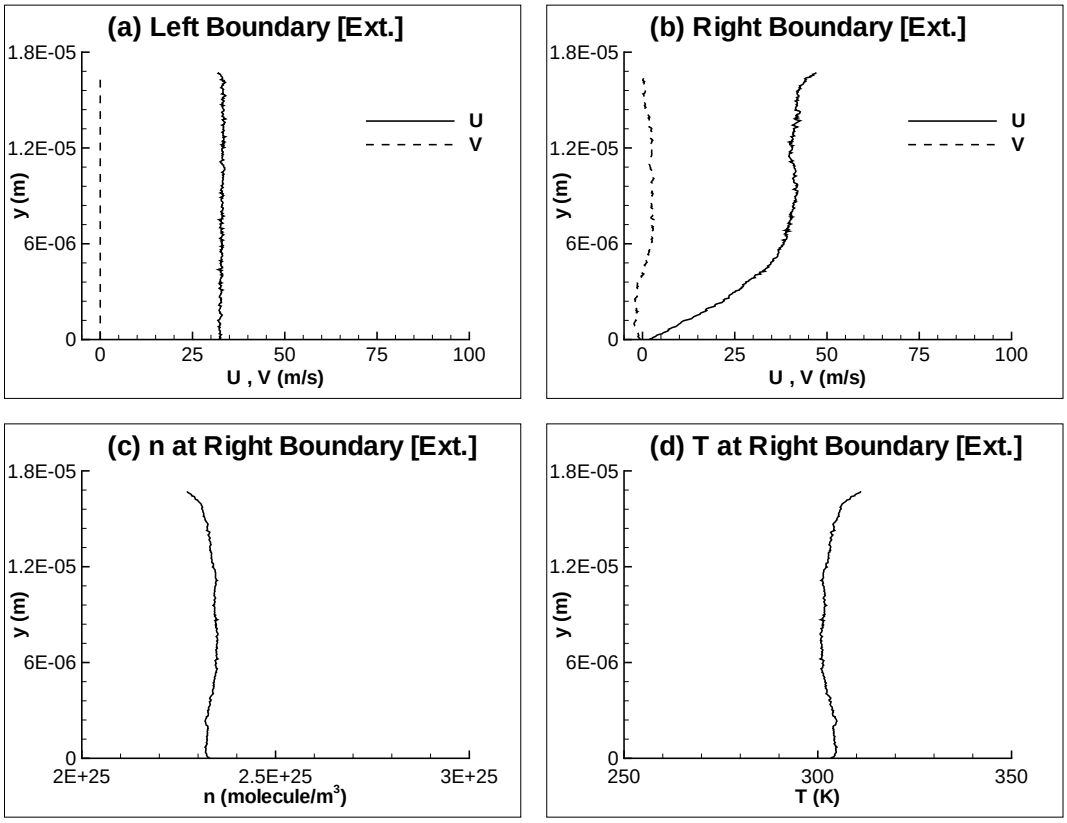

Figure 3.103: Case B.6 ; Extrapolated flowfield variables at left and right boundaries.

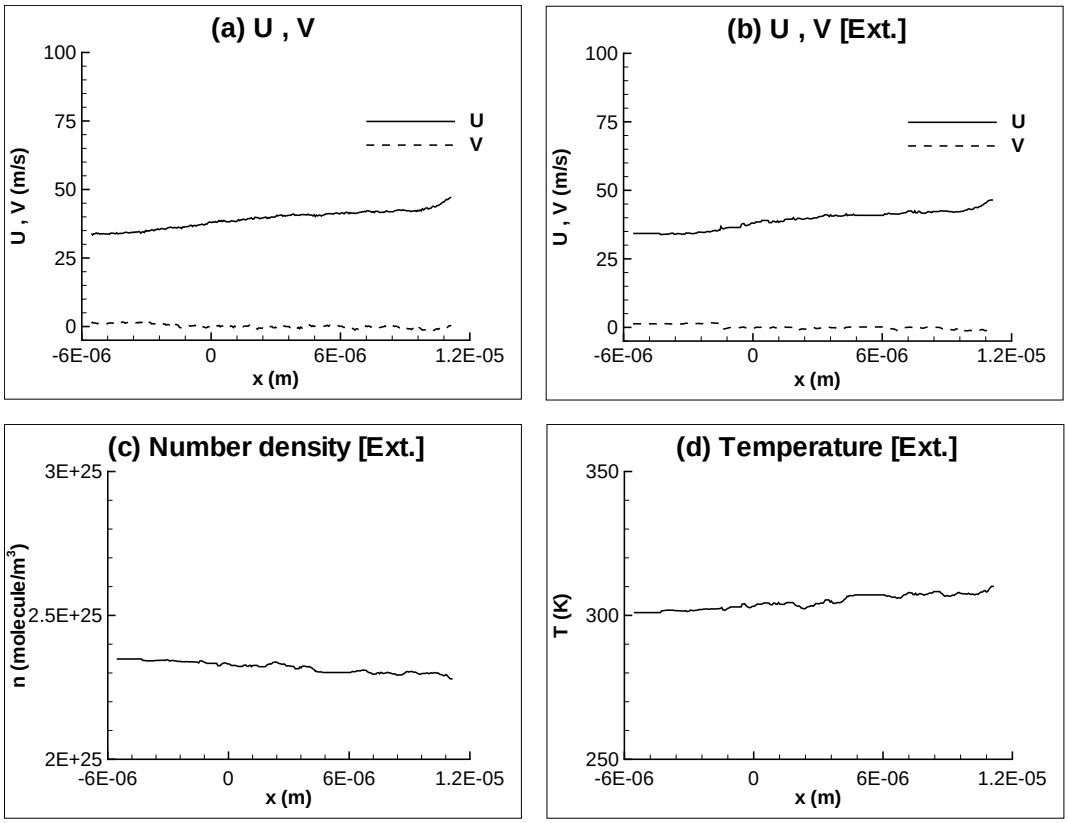

Figure 3.104: Case B.6 ; Velocities and extrapolated flowfield variables at top boundary.

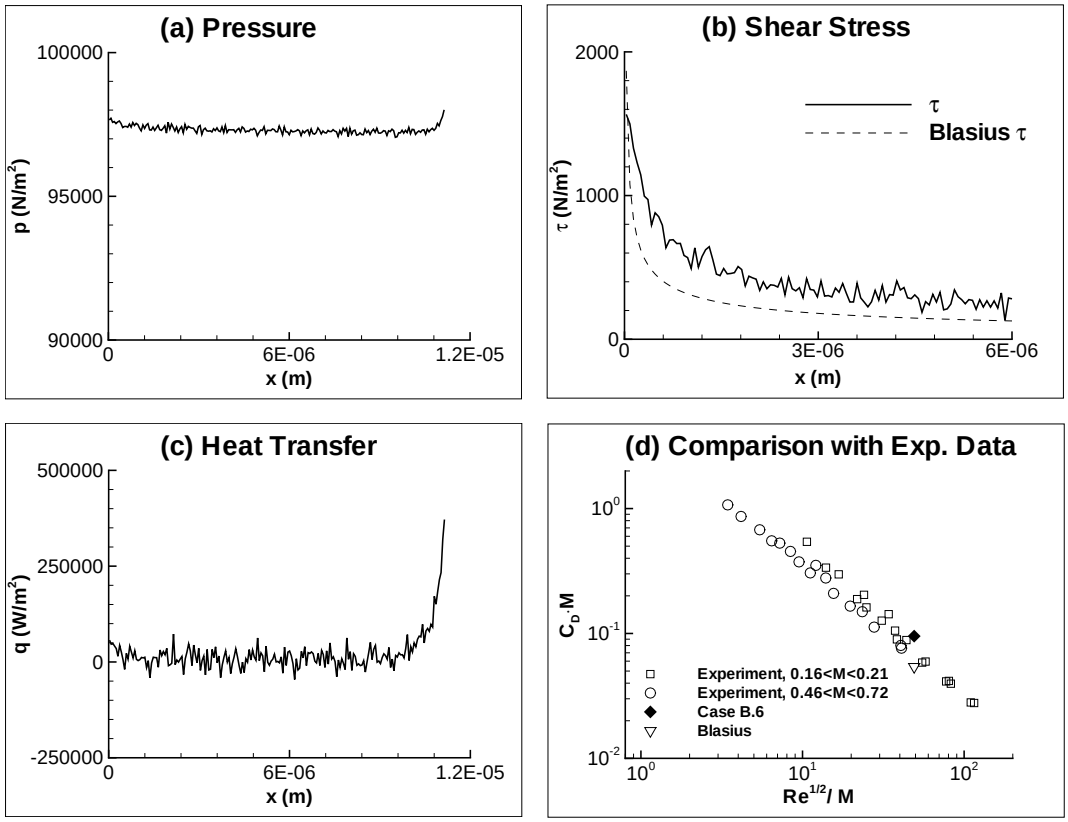

Figure 3.105: Case B.6 ; Surface properties and comparison with experimental data.

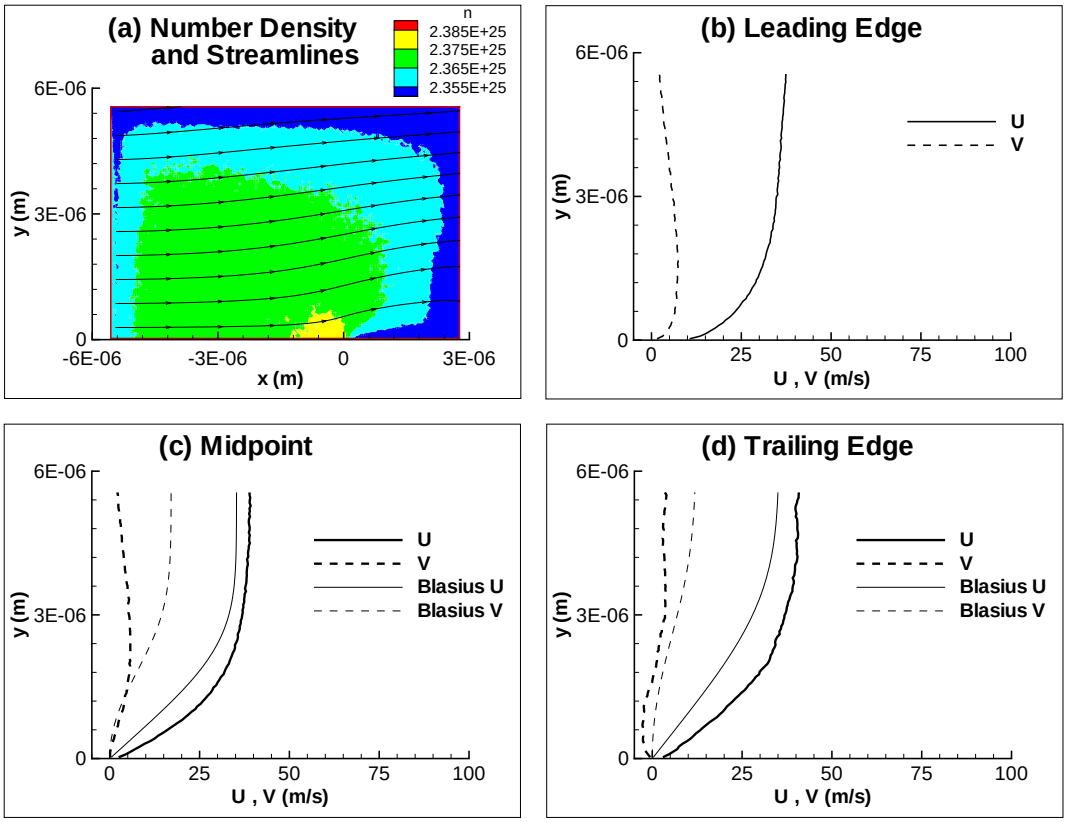

Figure 3.106: Case B.7 ; Number density contours, streamlines and velocity profiles.

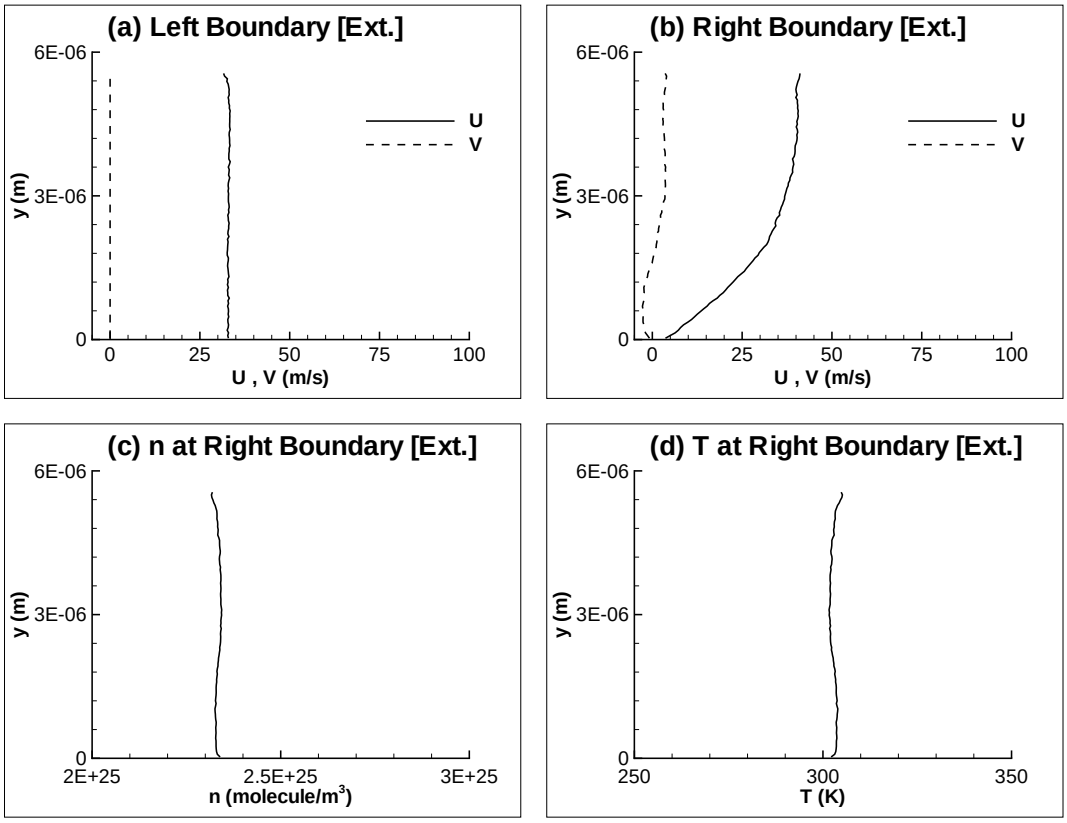

Figure 3.107: Case B.7 ; Extrapolated flowfield variables at left and right boundaries.

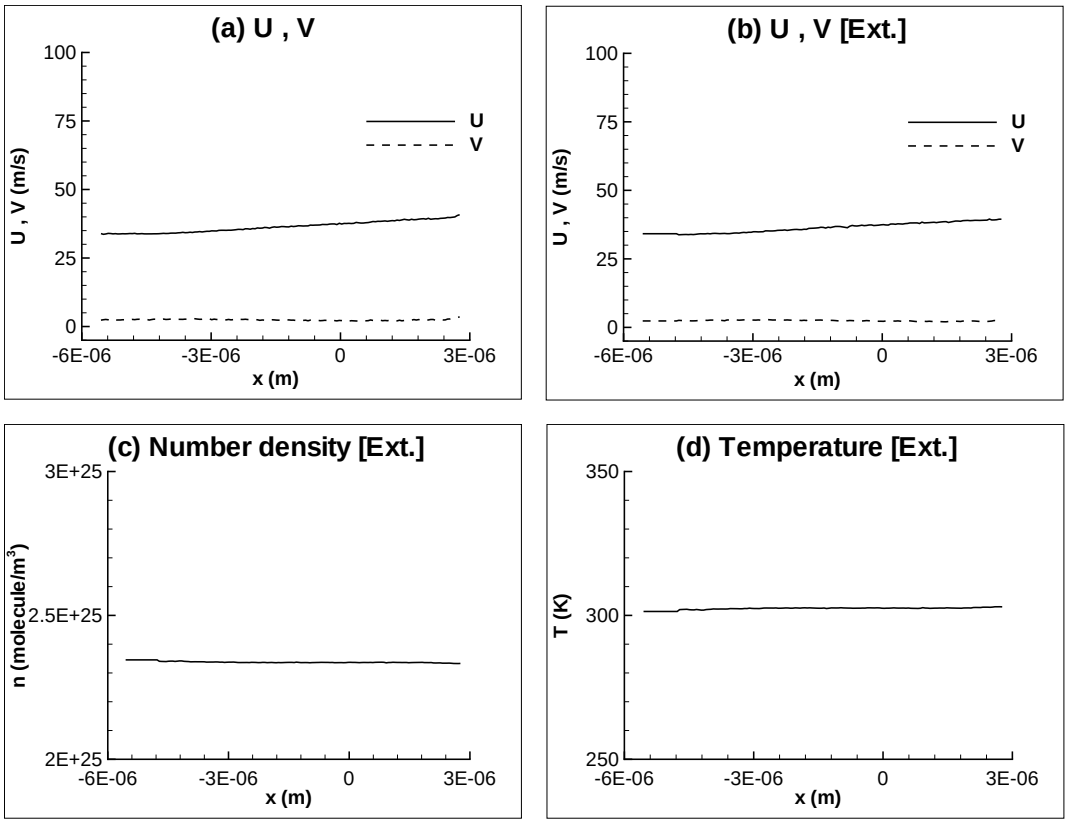

Figure 3.108: Case B.7 ; Velocities and extrapolated flowfield variables at top boundary.

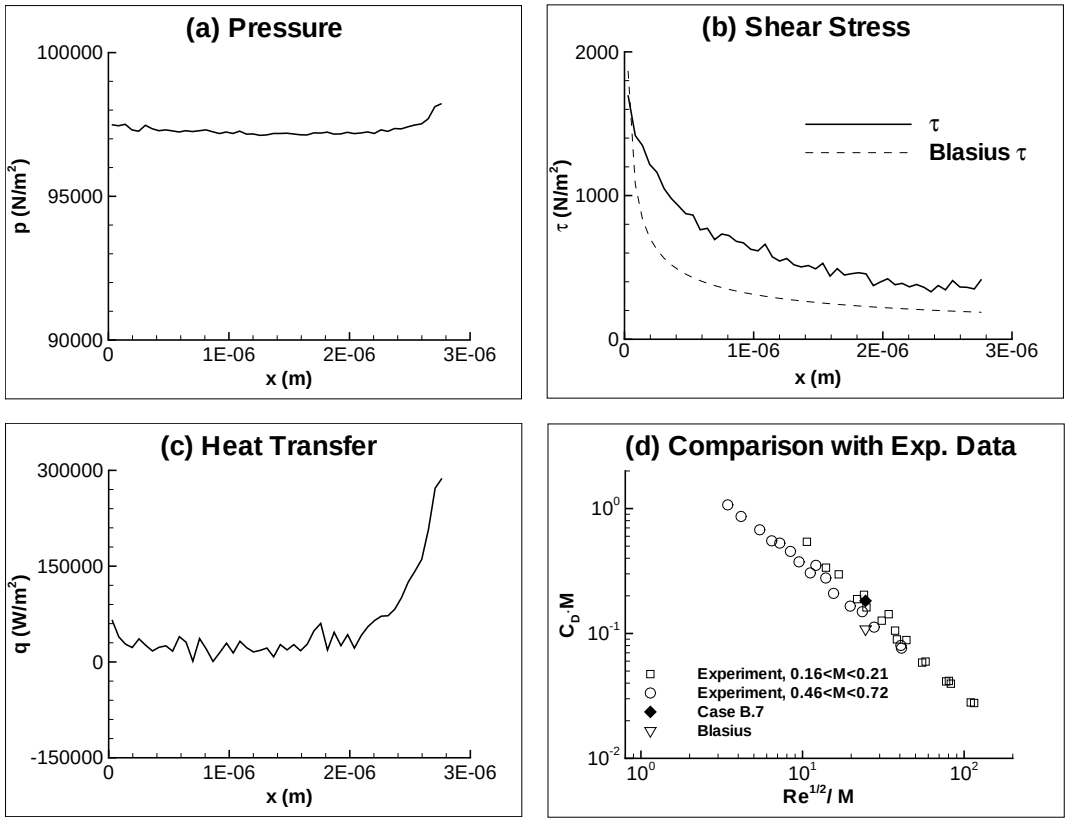

Figure 3.109: Case B.7 ; Surface properties and comparison with experimental data.

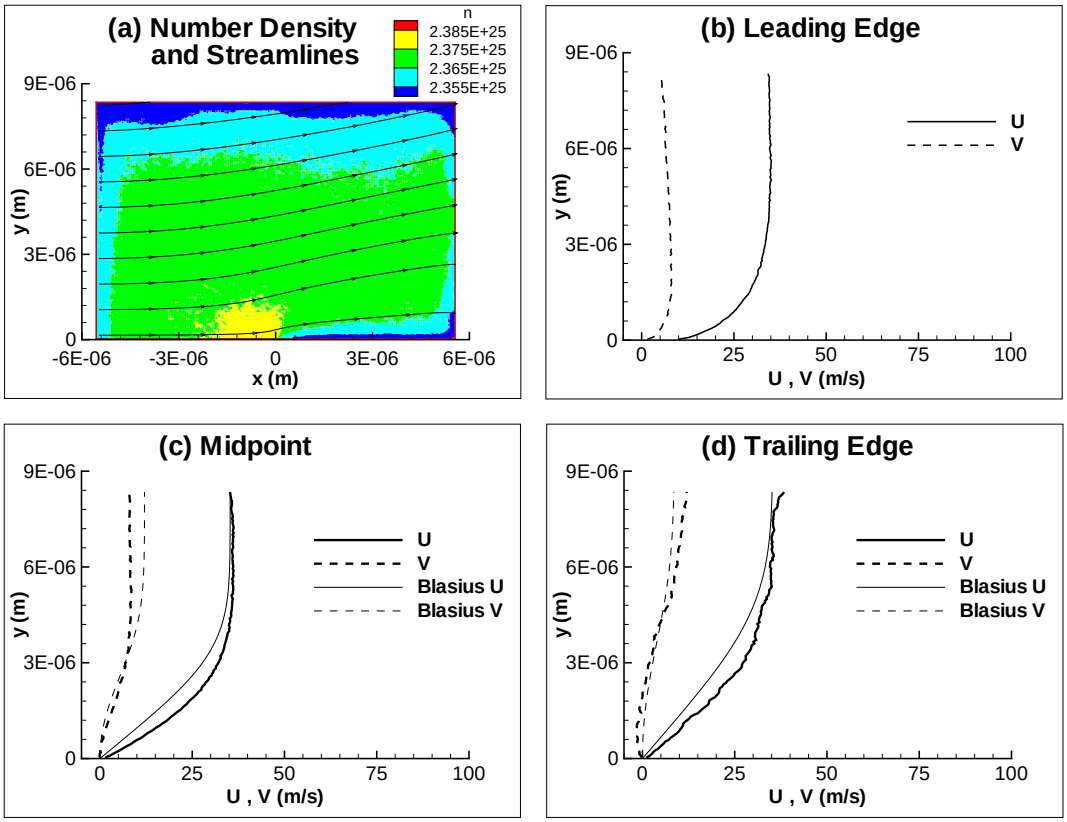

Figure 3.110: Case C.1 ; Number density contours, streamlines and velocity profiles.

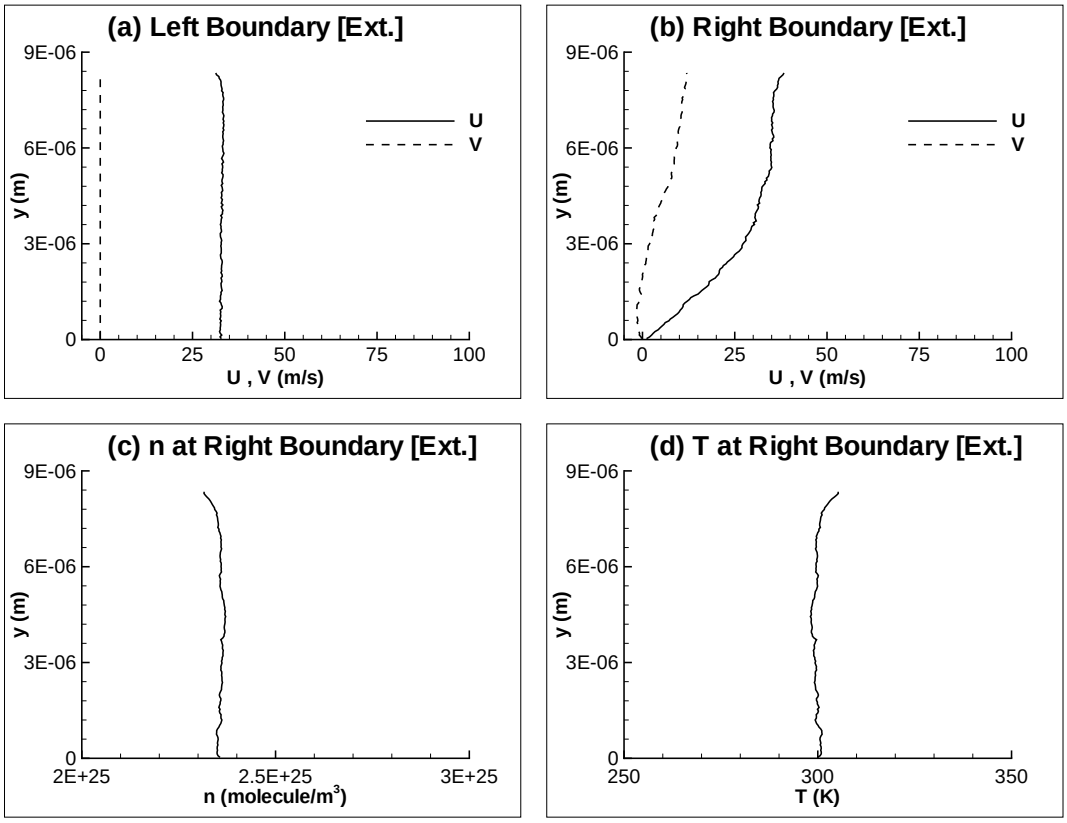

Figure 3.111: Case C.1 ; Extrapolated flowfield variables at left and right boundaries.

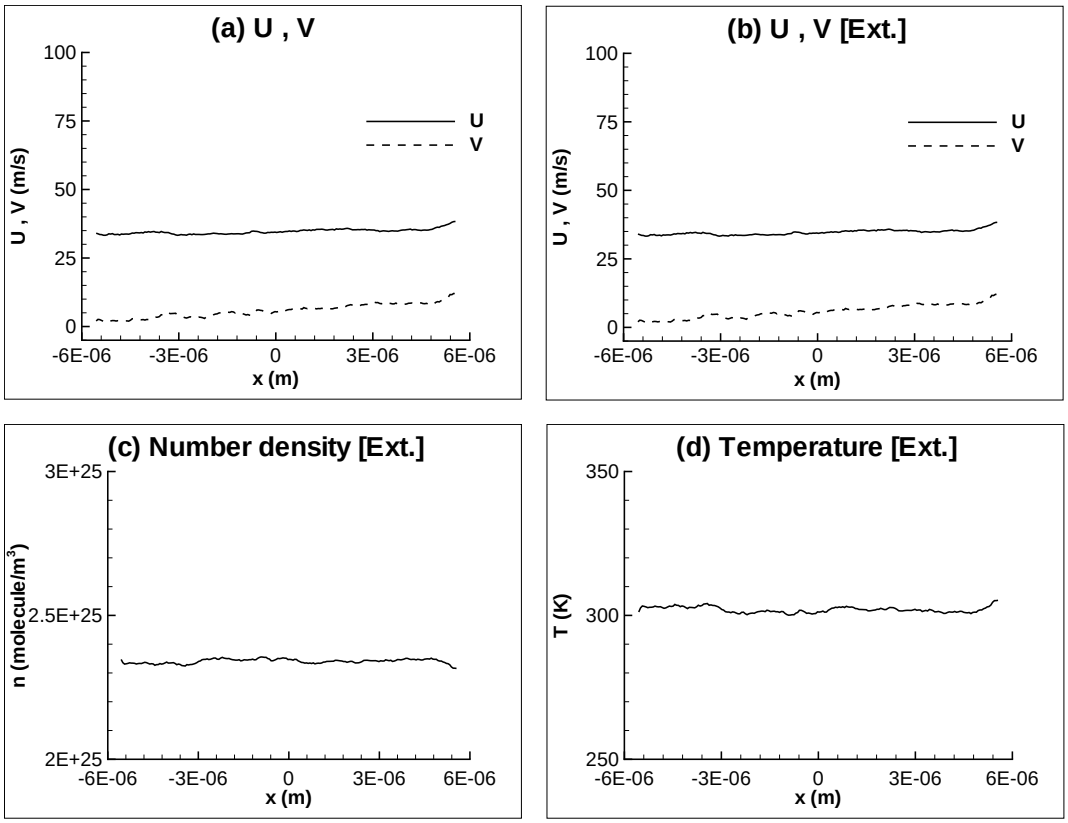

Figure 3.112: Case C.1 ; Velocities and extrapolated flowfield variables at top boundary.

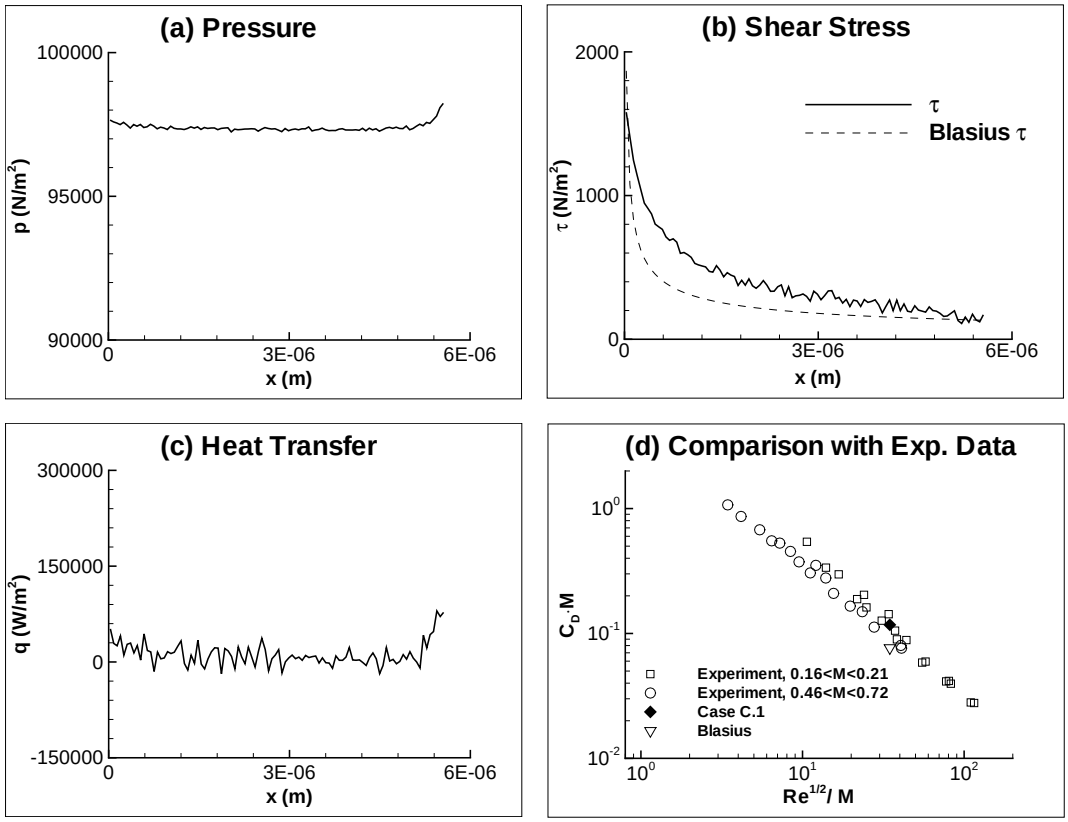

Figure 3.113: Case C.1 ; Surface properties and comparison with experimental data.

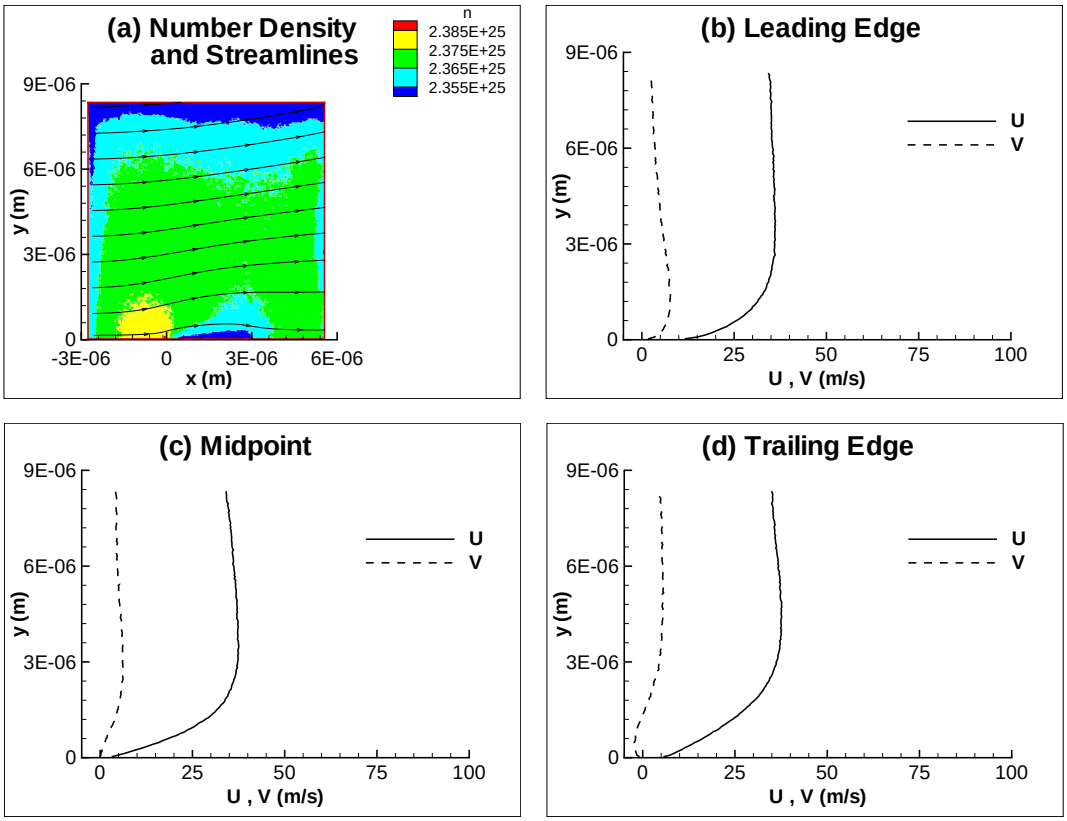

Figure 3.114: Case C.2 ; Number density contours, streamlines and velocity profiles.

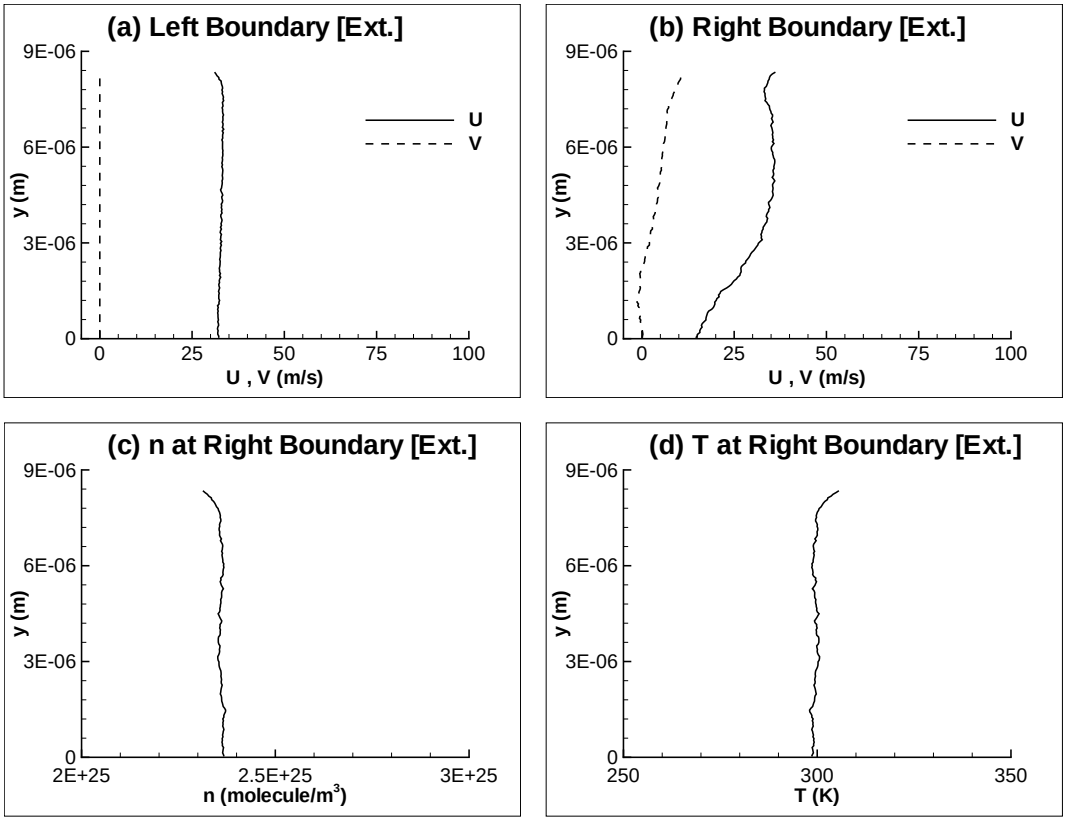

Figure 3.115: Case C.2 ; Extrapolated flowfield variables at left and right boundaries.

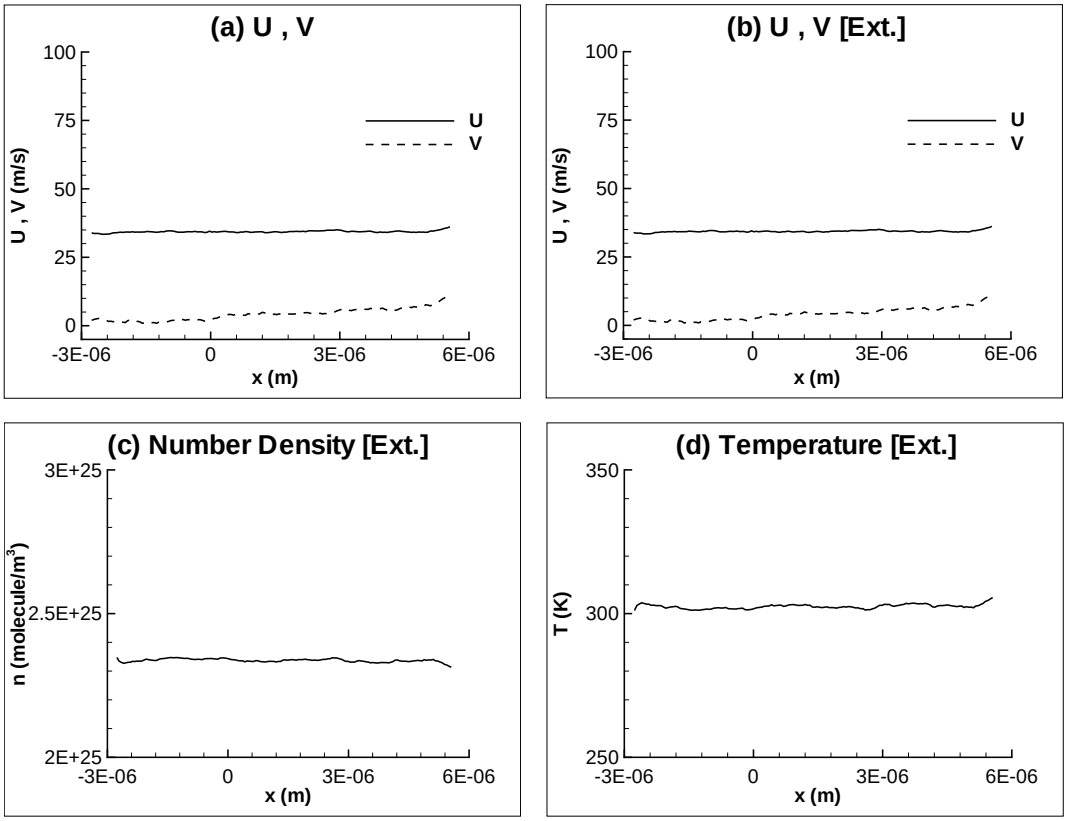

Figure 3.116: Case C.2 ; Velocities and extrapolated flowfield variables at top boundary.

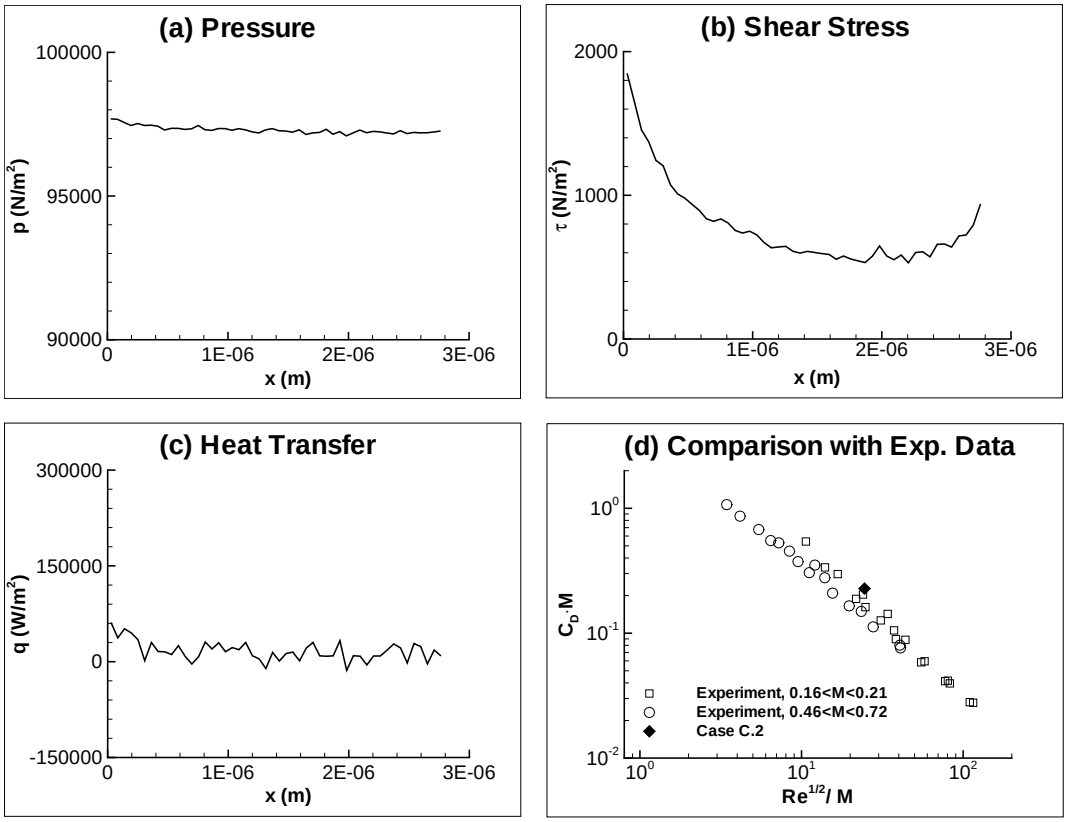

Figure 3.117: Case C.2 ; Surface properties and comparison with experimental data.

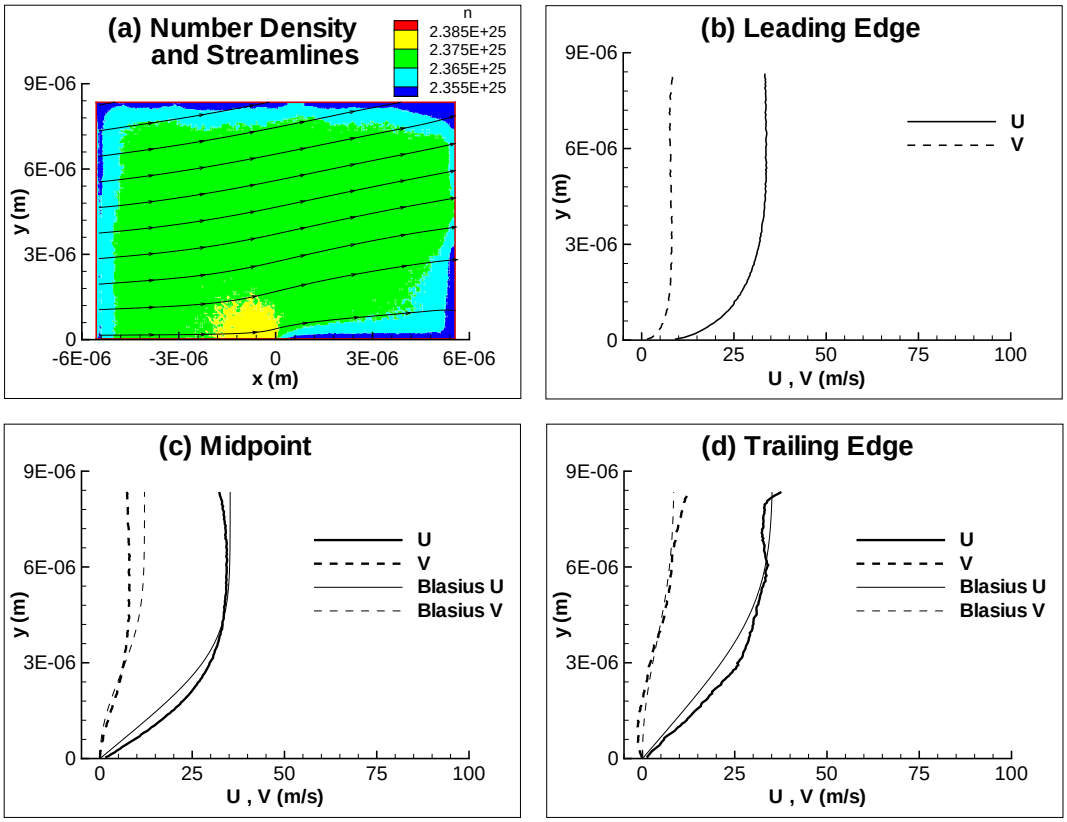

Figure 3.118: Case C.3 ; Number density contours, streamlines and velocity profiles.

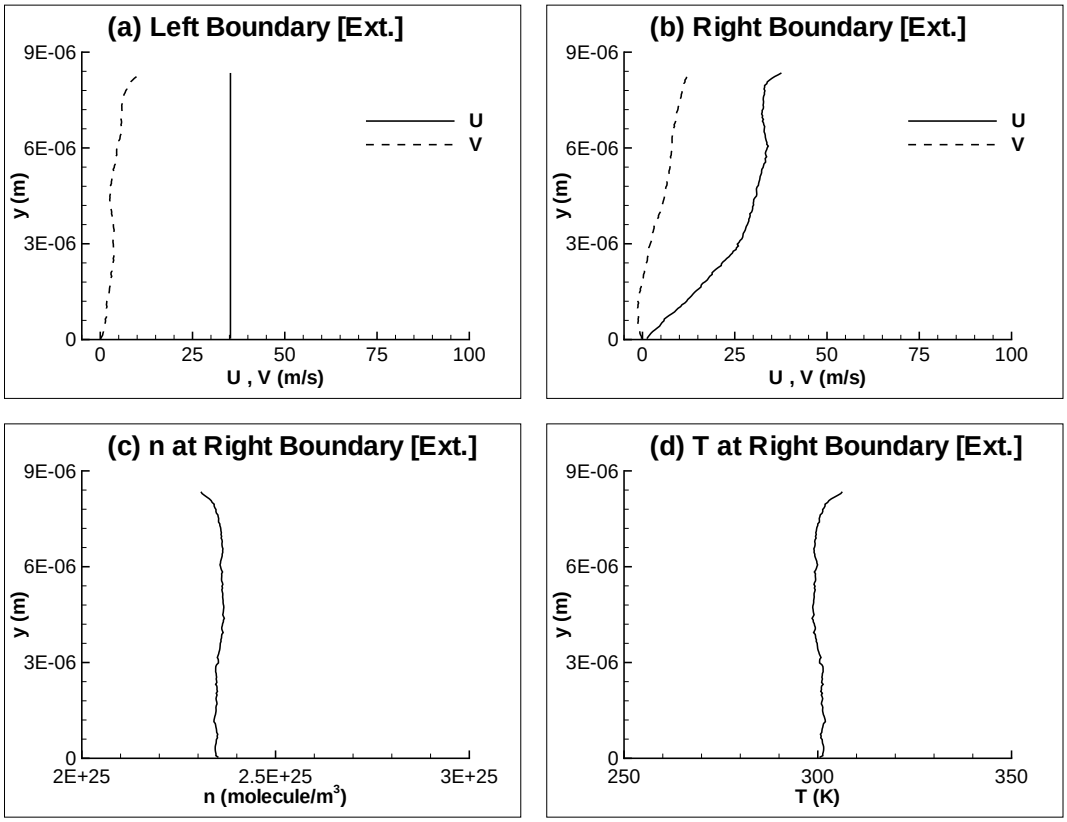

Figure 3.119: Case C.3 ; Extrapolated flowfield variables at left and right boundaries.

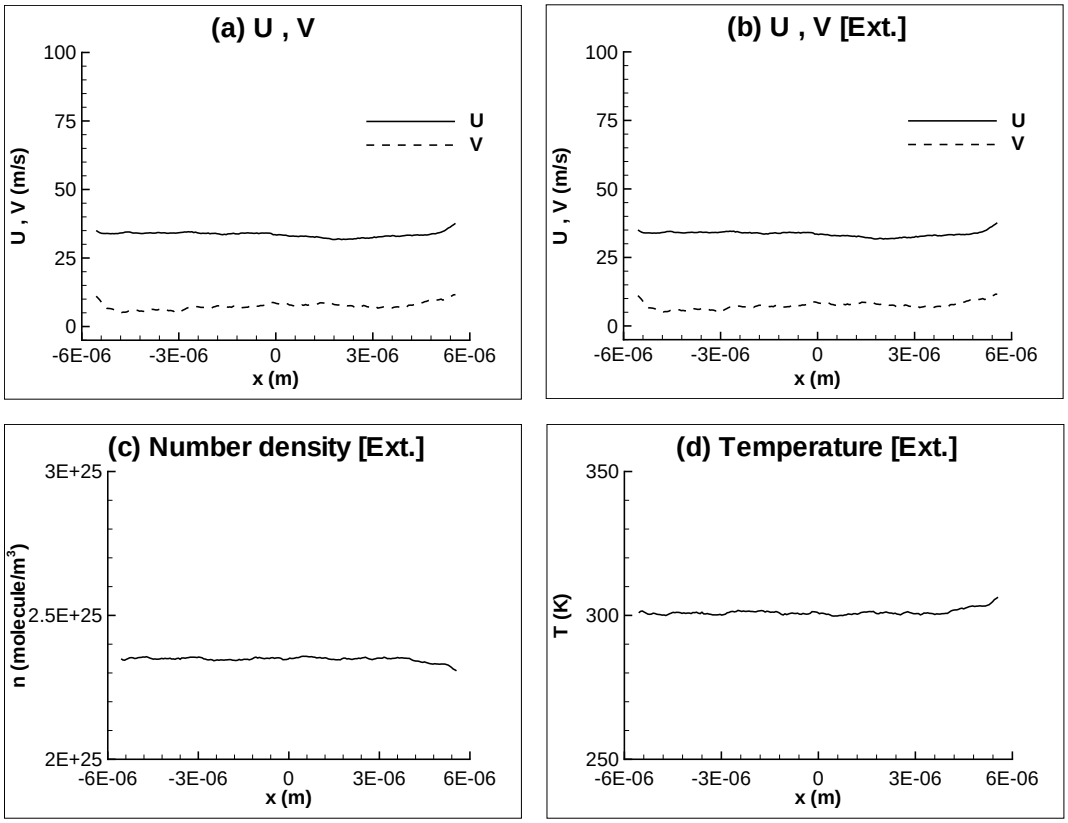

Figure 3.120: Case C.3 ; Velocities and extrapolated flowfield variables at top boundary.

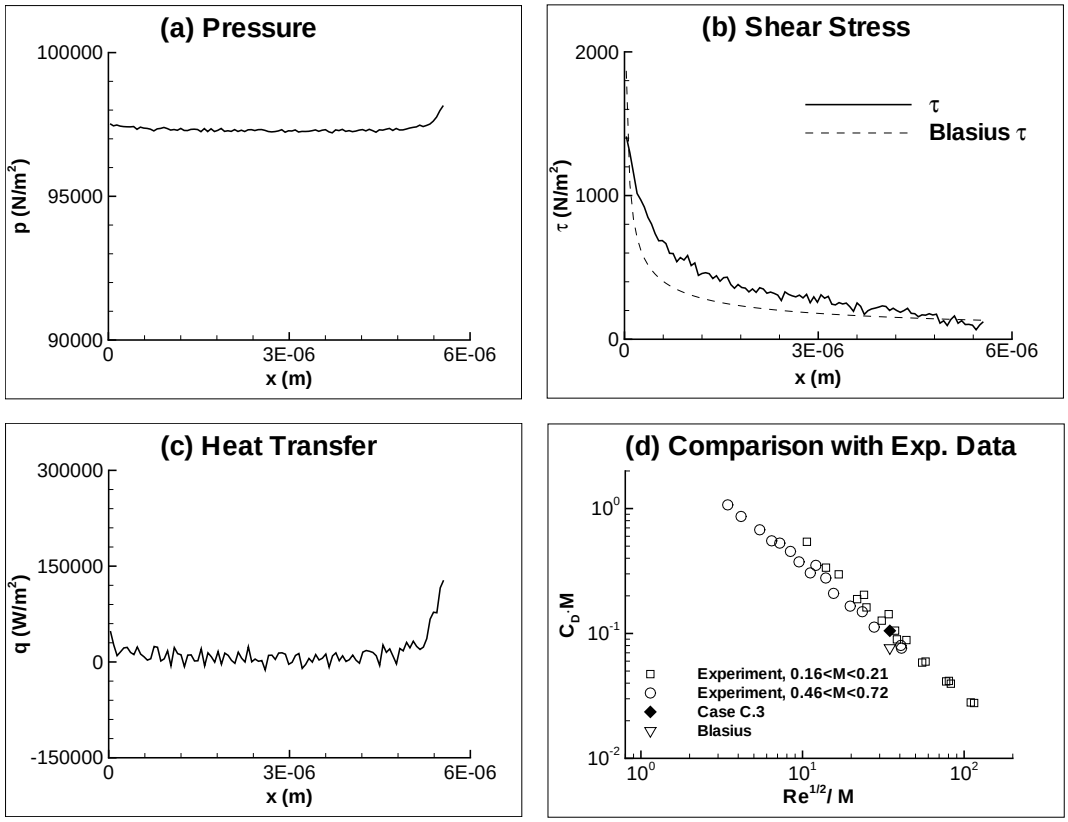

Figure 3.121: Case C.3 ; Surface properties and comparison with experimental data.

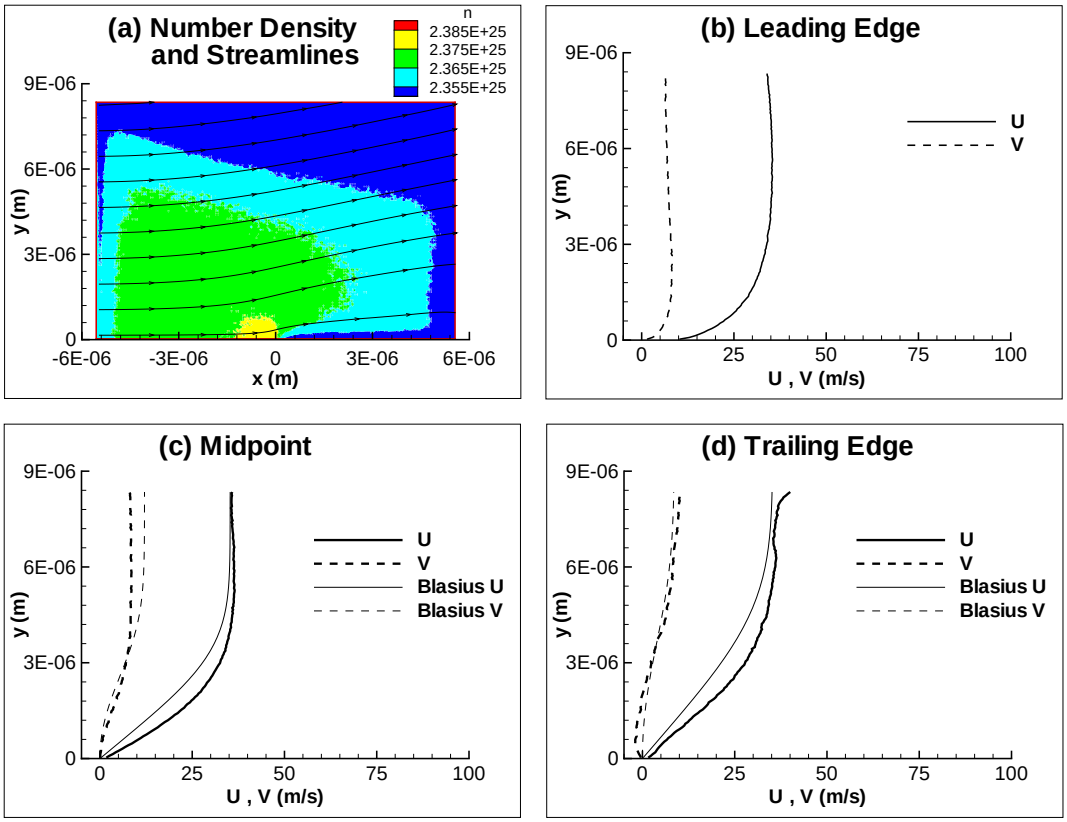

Figure 3.122: Case D.1 ; Number density contours, streamlines and velocity profiles.

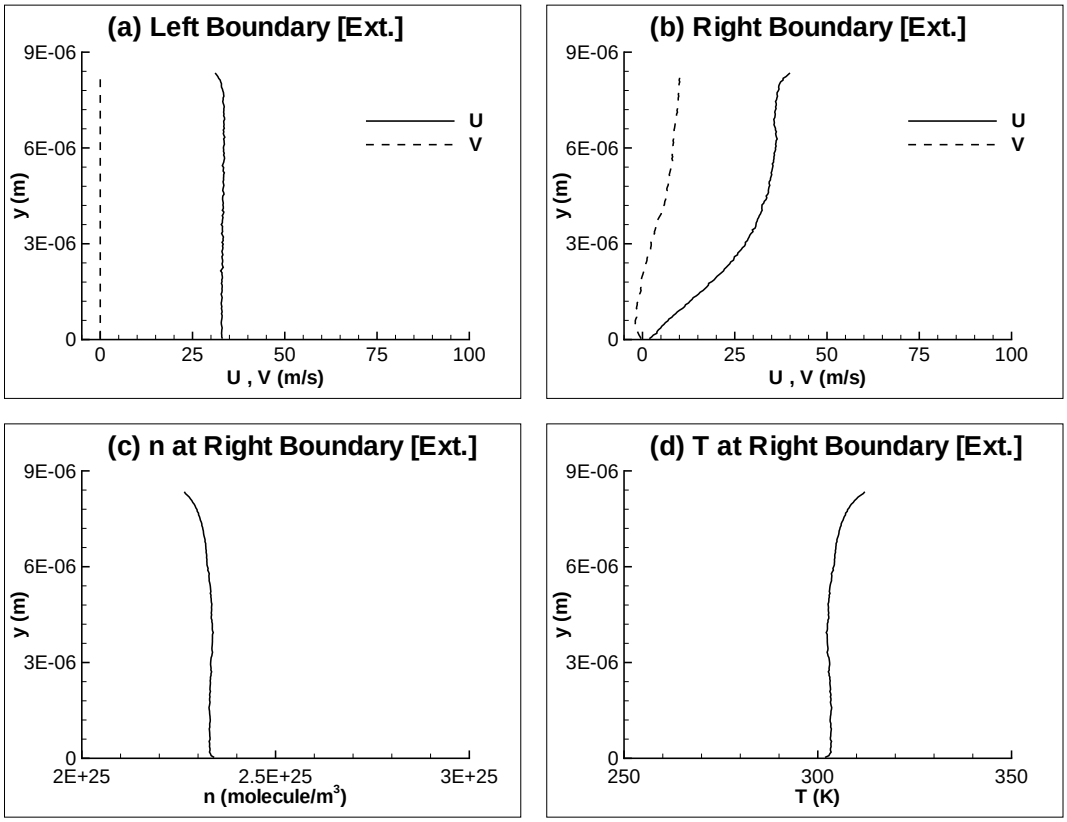

Figure 3.123: Case D.1 ; Extrapolated flowfield variables at left and right boundaries.

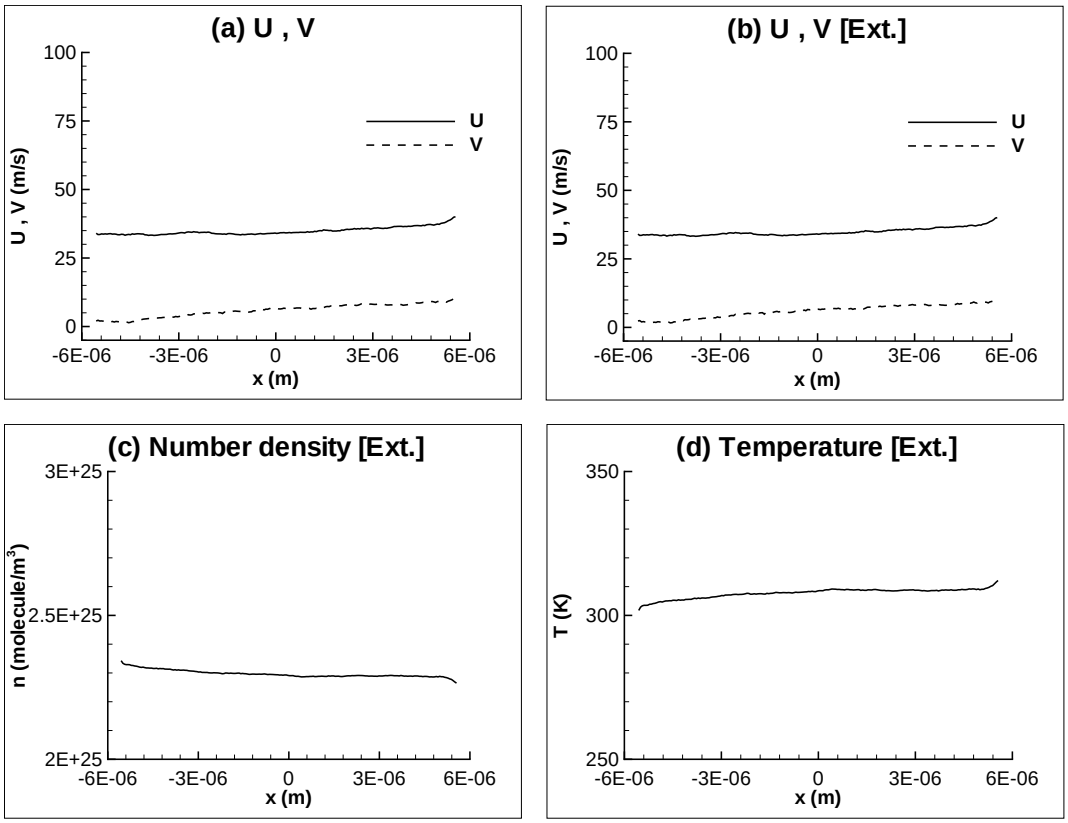

Figure 3.124: Case D.1 ; Velocities and extrapolated flowfield variables at top boundary.

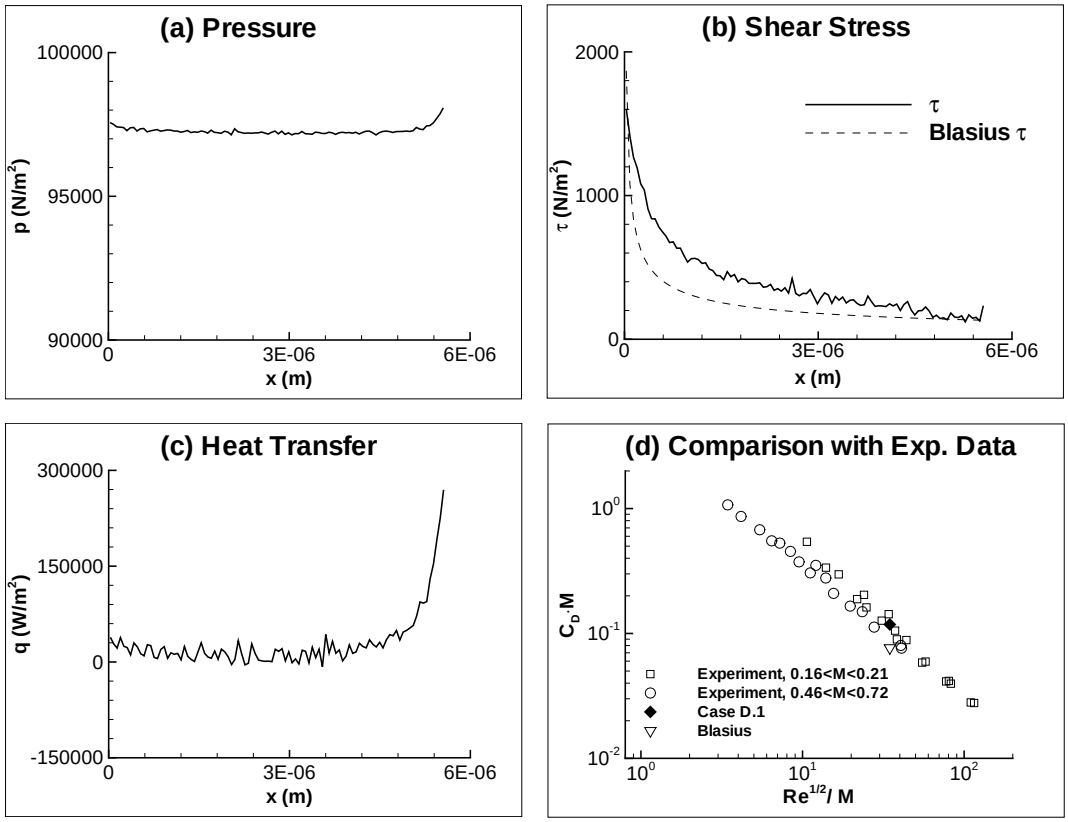

Figure 3.125: Case D.1 ; Surface properties and comparison with experimental data.

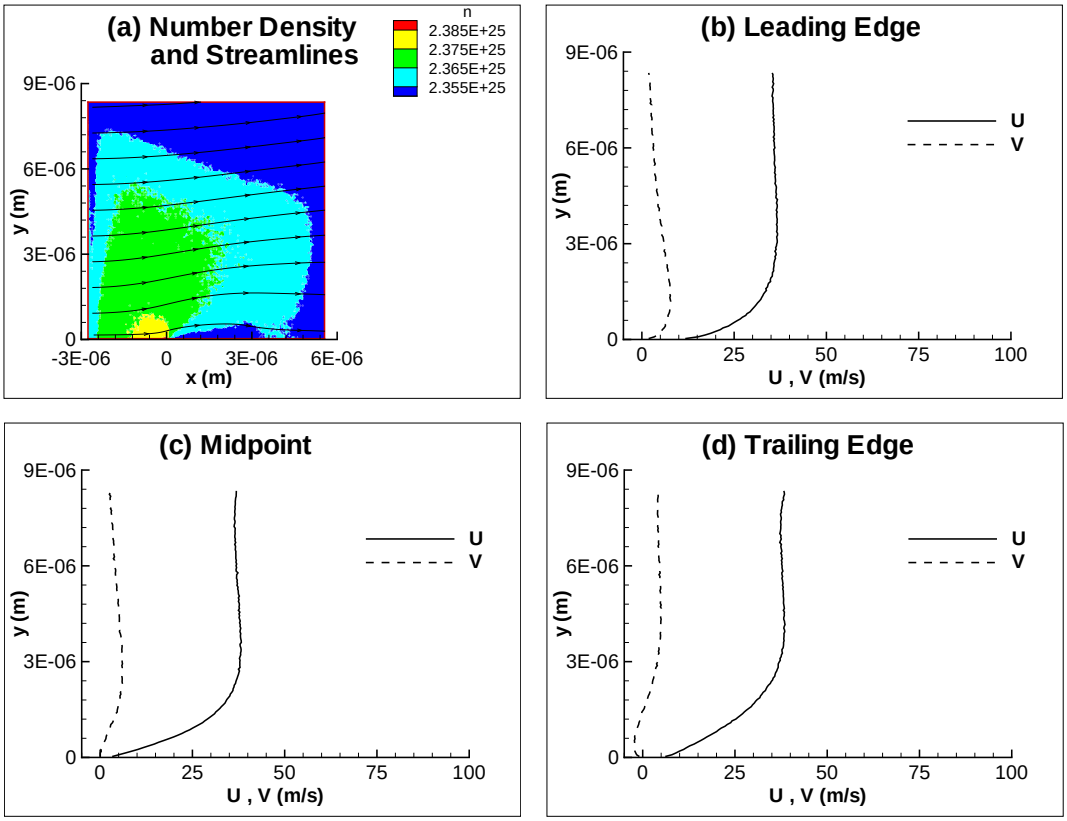

Figure 3.126: Case D.2 ; Number density contours, streamlines and velocity profiles.

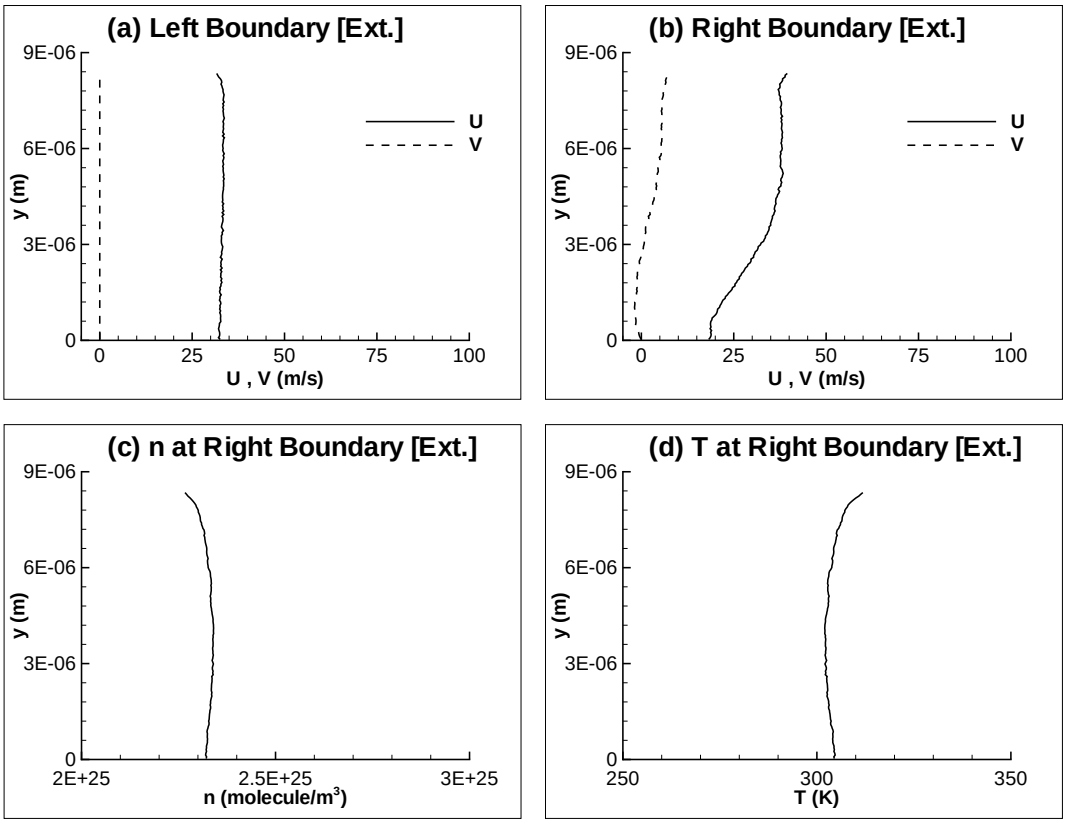

Figure 3.127: Case D.2 ; Extrapolated flowfield variables at left and right boundaries.

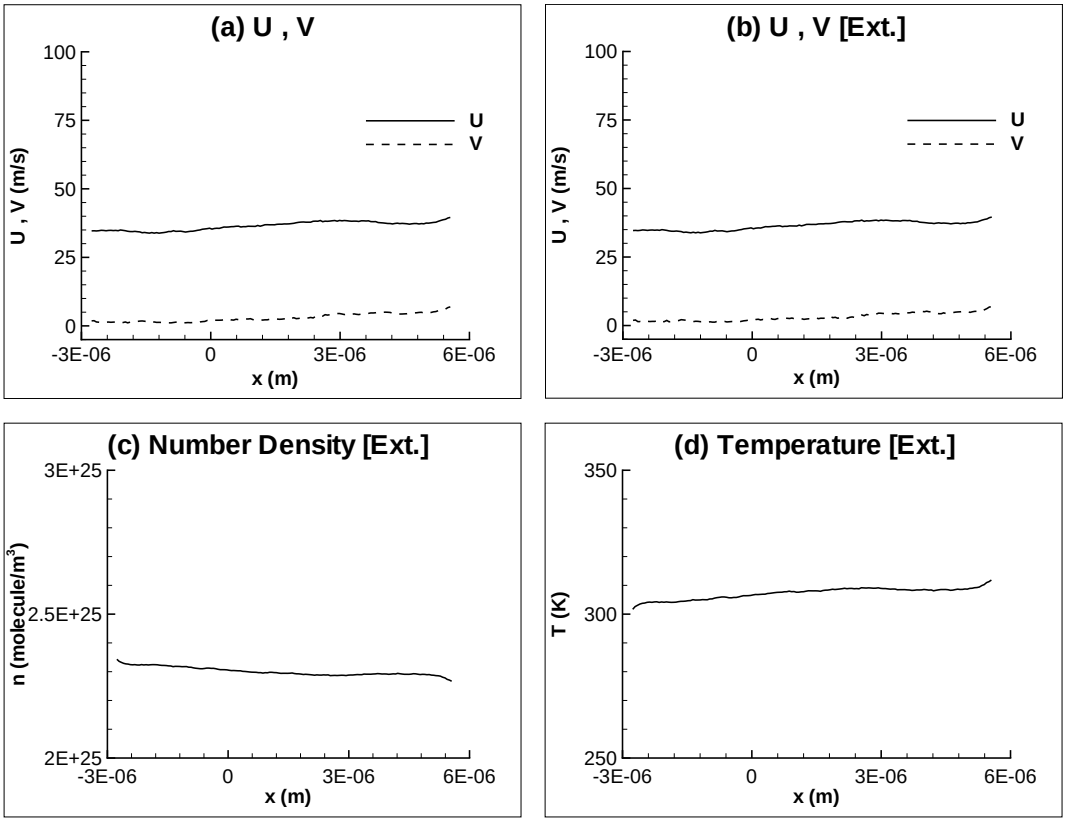

Figure 3.128: Case D.2 ; Velocities and extrapolated flowfield variables at top boundary.

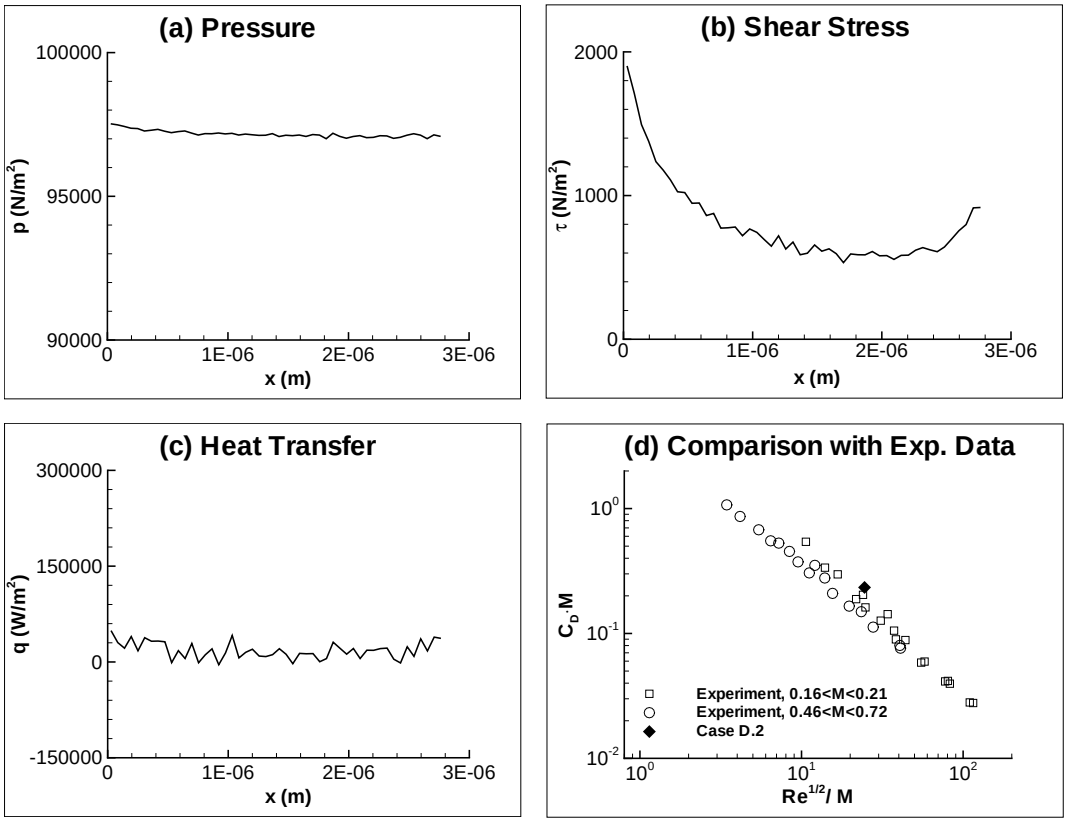

Figure 3.129: Case D.2 ; Surface properties and comparison with experimental data.

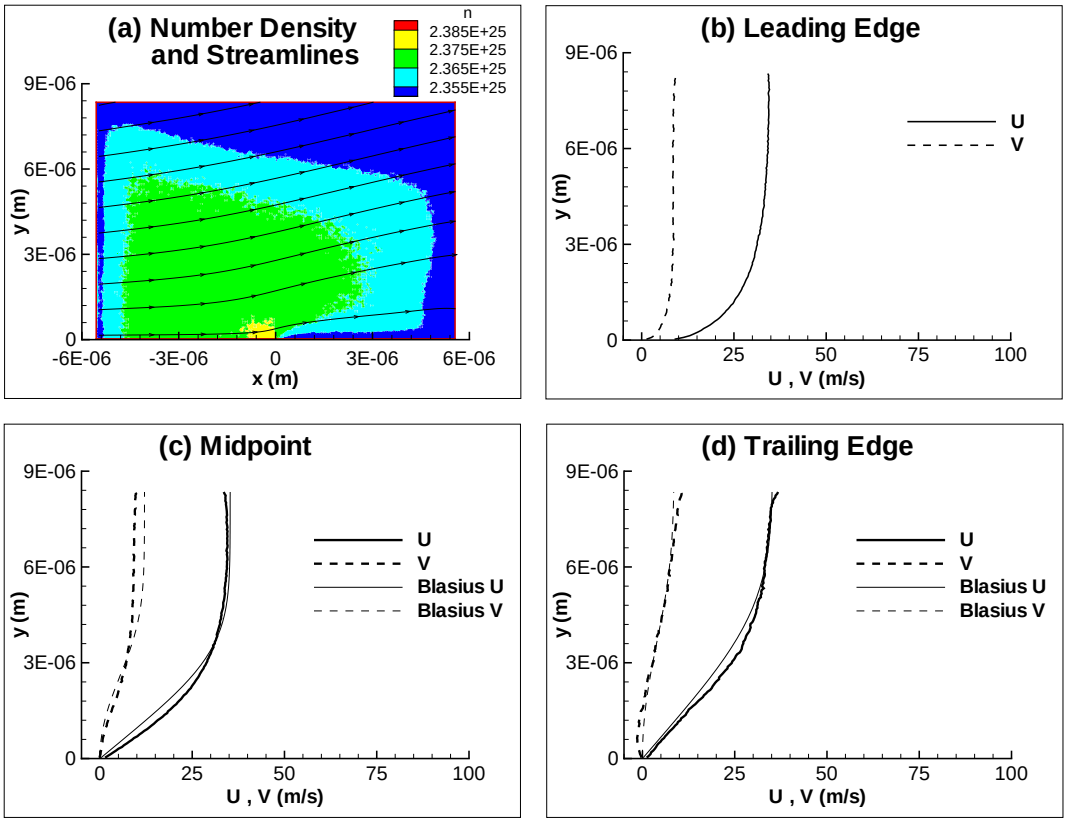

Figure 3.130: Case D.3 ; Number density contours, streamlines and velocity profiles.

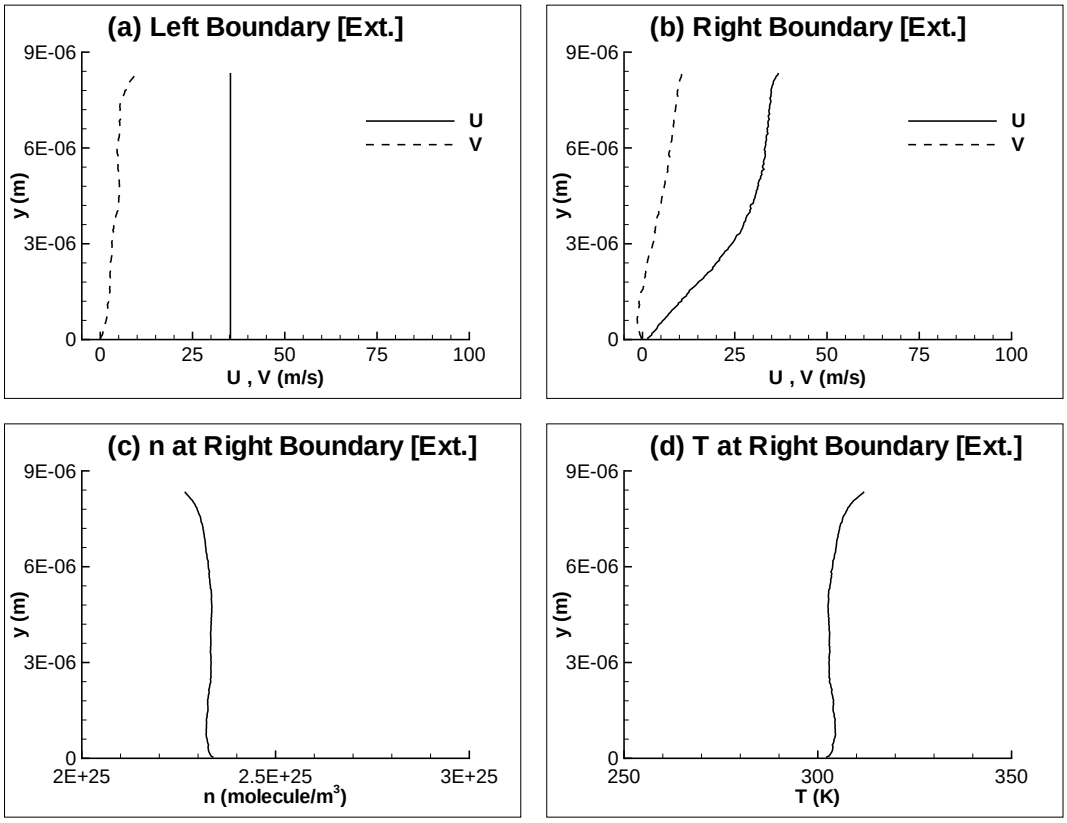

Figure 3.131: Case D.3 ; Extrapolated flowfield variables at left and right boundaries.

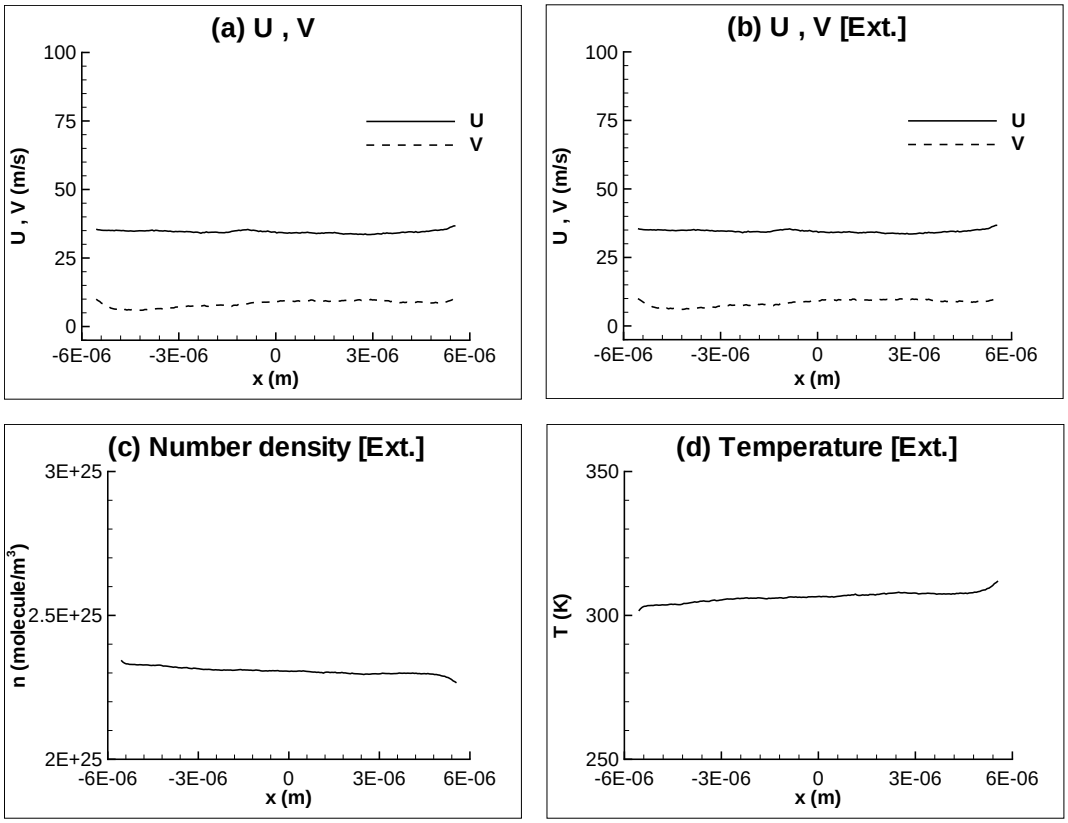

Figure 3.132: Case D.3 ; Velocities and extrapolated flowfield variables at top boundary.

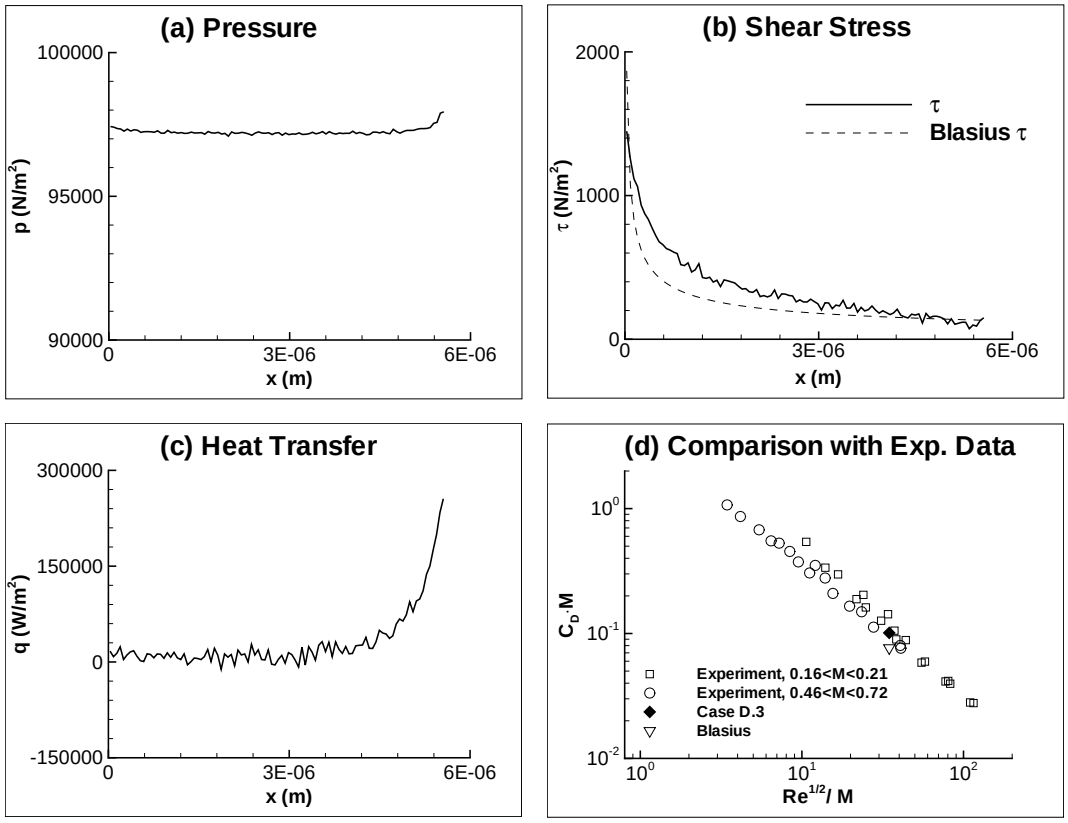

Figure 3.133: Case D.3 ; Surface properties and comparison with experimental data.

3.5 Discussions

The preliminary calculations performed in this thesis show that the results are sensitive to the boundary conditions used. However, when the boundary conditions explained in Section 3.3 are used, the results are found to be reasonably close to each other and in good agreement with the available experimental data. Figures 3.2 - 3.133 show the results of these test runs. The differences between these test run results are discussed below.

In Cases A.1 to A.20 streamline extrapolation technique is used with the Neumann boundary condition for the outflow boundaries. Cases A.1 and A.2 have the same boundary conditions and inflow parameters and the only difference between them is the plate length. (In Case A.2 half of the plate length of Case A.1 is used.) It can be seen from the figures that results are consistent. For both cases, the calculated drag coefficient is in close proximity of the experimental results.

Finite plate vs. semi-infinite plate comparisons begin with Case A.2 and Case A.3. Both cases capture the freestream values (i.e. temperature, number density, velocities) at the outflow boundaries. On the other hand, there are some differences in their surface properties (i.e. p, τ, q) near the end of plate (compare Figure 3.9 and Figure 3.13) due to the presence of the downstream region in the finite-plate configuration.

The effect of domain size is compared in Case A.3 and Case A.4. The increased upstream and downstream lengths help to produce smoother velocity profiles near the top edge. Increasing the domain size shows its effect also on the drag coefficient. Case A.4 has a slightly better calculated drag coefficient compared to Case A.3, as expected. Also, note that calculated drag coefficient for Case A.2 is in slightly better agreement with the experimental data as compared to that for Case A.4, (although one would expect the opposite because in Case A.4 the downstream is also considered).

The computational time is a very important issue in numerical simulations. In the DSMC method, the computational time is proportional to the number of molecules in the domain. Hence, to reduce the CPU time, one can try to increase the cell sizes in the directions where the flow gradients are small. This reduces the total number of cells and hence the total number of molecules in the domain. In the early part of this thesis study, an extensive sensitivity analysis has been performed on the cell sizes both in the streamwise (x) and transverse (y) directions. The results of those calculations show that the flows are more sensitive to Δy than to Δx. For instance, when $\Delta y \approx 2.5\,\lambda$ is used instead of $\Delta y \approx \lambda$, then drag coefficient shows 20% error, and the total heat transfer shows 12% error. On the other hand when $\Delta x \approx 2.5\,\lambda$ is used instead of $\Delta x \approx \lambda$, the drag coefficient shows 1% error and total heat transfer has 2% error. Consequently, in this thesis $\Delta y \approx \lambda$ is used in all calculations. Also, in most calculations $\Delta x \approx \lambda$ is taken, except in a few cases $\Delta x \approx 2.5\,\lambda$ or even $\Delta x \approx 5\,\lambda$ is used. For example, in Case A.5 $\Delta x \approx 5\lambda$ is considered. Remember that in the DSMC simulations, results improve when the cell sizes and the time steps are reduced. It is clearly seen from the comparison of Case A.4 and Case A.5 that some deviations occur for the larger cell size configuration. For example, in Case A.5 the number density distribution tends to increase by about 1% near the top-right corner of the domain. Moreover, the drag coefficient calculated in Case A.4 is a little better than that calculated in Case A.5.

The inflow boundary condition effects are examined by comparing the results of Case A.1 (Riemann boundary condition) and Case A.6 (with V extrapolation). Note that, the velocity profiles for Case A.6 happen to be nearly the same as the Blasius profiles along the plate. Also, in Case A.6 streamlines come into the domain with large positive angles that increase in the y-direction, which is not expected because the number density contours of Cases A.1 and A.6 show that at about one-half plate length upstream of the body the density rise is about 0.5%. Moreover, at the top boundary, transverse velocity V starts with a high value and decreases in the x-direction which is not realistic (although it is consistent with the Blasius solution).

Effects of rarefaction are also investigated in this research by changing the freestream number density and keeping the other freestream properties the same. In Cases A.7 and A.8 the freestream densities are reduced by factors of 10 and 100, respectively. Case A.9 is the same as Case A.8 except that intermolecular collisions are by-passed to get collisionless flow solutions. The calculated drag coefficient of Case A.9 is 1.305 and the theoretical free-molecule [1] result is 1.349. The results show that slip velocities increase with rarefaction. Also, at the top boundary, there are some cells with negative transverse velocities which indicate that the domain height needs to be increased.

In the present study, the Mach number effects are also investigated by increasing the freestream velocity and keeping the other freestream properties the same. In Cases A.10 to A.20, freestream Mach number is increased to $M = 0.4$. Keeping in mind that the boundary layer height is inversely proportional to the square root of the streamwise velocity, the domain height in Case A.10 is taken as half the value for Case A.1 ($M = 0.102$) to reduce the computational time. Comparison between Case A.1 and Case A.10 demonstrates that the increased freestream velocity results in smoother velocity profiles and better agreement with the Blasius solution. On the other hand, the extrapolated temperature and number density distributions at the outflow boundaries are nearly constant in Case A.1 whereas in Case A.10 there are some bulges. Also, note that the domain height is reduced a bit too much in Case A.10 (as it is evident from the number density contours). Nevertheless, the drag coefficient for Case A.10 is in very good agreement with experimental data. The discussions for the comparison between Cases A.10 and A.1 also hold for that between Cases A.11 and A.2 (in which the only difference is the plate length).

The effects of lengths of the upstream and downstream regions are also investigated for $M = 0.4$. In Cases A.12 and A.13, the length of the upstream and downstream regions are chosen as $L/2$ and L, respectively. The drag coefficient is a little better in Case A.13, as expected, because Case A.13 has a larger computational domain. However, both cases have some minor irregu-

larities in the temperature and number density distributions near the top edge which indicates that the domain height needs to be increased.

To check the effect of Δx, calculations are performed in Case A.14 which is the same as Case A.12 except that it has $\Delta x \approx 5\,\lambda$ instead of $\Delta x \approx \lambda$. The results of Case A.14 are a little worse than those of Case A.12, as expected. Note that, the drag coefficient for Case A.14 is only 3% worse than that for Case A.12.

The simulations presented in this thesis are in the *slip-flow*, *transition* and *free-molecular* regimes, except for Case A.15 which is in the *continuum* regime. For Case A.15, the freestream number density is increased to 2.36×10^{26} molecule/m^3. Note that this increases the CPU time requirement drastically because it implies a reduction in the mean free path by a factor of 10 as compared to Case A.12. If the domain size is kept the same and if Δx and Δy are of order mean free path, this requires an increase in the total number of cells by a factor of 10^2, and hence the total CPU time increases by a factor of 100. This is not affordable with the computer resources available for this thesis and hence in the present simulations, the computations are speeded up as follows: First of all, knowing that the boundary layer height is inversely proportional to the square root of the density, the domain height is reduced by factor of 3. Furthermore Δx is taken as $\Delta x \approx 5\,\lambda$ accepting a few percent error on the results and consequently the CPU time requirement is reduced by a factor 15. The computed drag coefficient of Case A.15 is still in very good agreement with the experimental data, and the results, in general, are satisfactory although there are some minor deviations near the top boundary which suggest that the domain height needs to be increased.

The size of the domain is definitely important for the proper simulation of this type of flows. In Cases A.16 and A.17, the domain is extended in all directions (upstream, downstream and height), and the length of the domain in these directions are 4 times the plate length. The only difference between them is that in Case A.16 $\Delta x \approx 2.5\,\lambda$ is used instead of $\Delta x \approx \lambda$. Sun and

Boyd [17] performed similar calculations on a flat plate using the "Information Preservation" technique and noticed that the results are very close if these lengths are chosen between 3.5 and 15.5 times the plate length. The computed drag coefficients of Cases A.16 and A.17 are in excellent agreement with the experimental data and C_D for Case A.17 is less than 1% different from that of Case A.16. This reinforces the argument made earlier for the use of $\Delta x \approx 2.5\,\lambda$ confidently in these simulations. The results of Cases A.16 and A.17 can also be compared with those of Cases A.12 and A.13 to see the improvement on the results as the domain size is increased.

Effects of rarefaction for $M = 0.4$ are further investigated in Cases A.18, A.19 by decreasing the freestream densities 10 and 100 times, respectively. Also, in Case A.20 collisionless flow is obtained by repeating Case A.19 without intermolecular collisions. The calculated drag coefficient of Case A.20 is 1.307 and the theoretical free-molecule [1] result is 1.349. Likewise in $M = 0.102$ counterpart cases (A.7, A.8, A.9), slip velocities increase with rarefaction, and again negative transverse velocities at the top boundary indicate the necessity to increase domain height.

Various outflow boundary conditions other than the one used in Cases A are also tested in the present research as Cases B, C, D (See Table 3.2). In Cases B.1 to B.7, streamline extrapolation technique is used (as in Cases A), however instead of Neumann boundary condition, Whitfield's characteristic formulation is adapted at the outflow boundaries. Note that the freestream conditions and the domain sizes for Cases B.1, B.2, B.3, B.4, B.5 are the same as those for Cases A.1, A.2, A.3, A.4, A.6, respectively (except the domain height in Case B.4 is a little higher than that in Case A.4). Comparisons between each corresponding couple indicate clearly that the boundary conditions used in Cases A produce a little better results than those used in Cases B. In all the results of Cases B, the number density tends to decrease as the flow approaches the top-right corner of the domain (however, this is only a few percent). In Cases B.6 and B.7, various domains with different plate lengths and domain heights are

considered for semi-infinite plate configurations, as a further investigation parallel to Cases B.1 and B.2. Again, as the domain size relative to plate length is increased, the results are improved.

In Cases A and B, streamline extrapolation technique is used for the outflow boundary conditions. Extrapolation using the nearest adjacent cell (along the outflow boundaries) is also tested in this study and are presented in Cases C and D. In Cases C, Neumann boundary condition with adjacent cell extrapolation is used; whereas in Cases D, Whitfield's characteristic formulation with adjacent cell extrapolation is considered. Note that the freestream conditions and the domain sizes for Cases C.1, C.2, C.3 and Cases D.1, D.2, D.3 are the same as those for Cases A.1, A.3, A.6, respectively. Comparing the results for the counterpart cases, it can be seen that the boundary condition used in Cases C gives a little better results than that used in Cases D, but the boundary condition in Cases A is superior to both Cases C and Cases D.

It should be pointed out that when the nearest cell extrapolation technique is used, the results near the top-right corner of the domain show some errors. This is caused by the use of the top-right corner cell properties both in the top and in the right boundary extrapolations. Considering that, these extrapolated values are used in the determination of the number of molecules and their properties entering that cell from the top and from the right, errors in the corner cell properties have less chance to diminish, and consequently, the neighboring cells are adversely affected. Note that, this problem is overcome by the use of streamline extrapolation technique in which the properties at the top and right boundaries of the corner cell are not solely extrapolated from that cell and the results are improved (e.g. compare Cases A.1 vs. C.1, B.1 vs. D.1 and A.6 vs. C.3).

Clearly, when extrapolation techniques are used for outflow boundary conditions, the validation of these techniques is necessary. First, in using extrapolation boundary conditions at the outflows, some errors near the exit boundaries are acceptable as long as the main flow in the rest of the domain is not distorted. This is achieved in the present study, and can be seen by

comparing the results of semi-infinite plate calculations for different plate lengths. For example, consistency of the results for Cases A.1, A.2 (for $M = 0.102$) and A.10, A.11 (for $M = 0.4$) can be seen from Figures 3.2 - 3.9, 3.38 - 3.45, respectively. Comparison can also be made of the surface properties for these cases. As can be seen from Figure 3.134, the shear stress distribution is almost the same up to 2.792×10^{-6} m for different plate lengths[5]. Similar behavior can be observed in pressure and heat transfer distributions. Second, the present results for collisionless finite-plate flows (Case A.9 ($M = 0.102$) and A.20 ($M = 0.4$)) are in very good agreement with the theoretical free-molecule flow results. Noting that the boundary conditions are the only factors in the determination of the free-molecule results and in the present collisionless flow simulations all the outflow boundary properties (except the external pressure) are extrapolated from the domain, confidence on the present boundary conditions is increased.

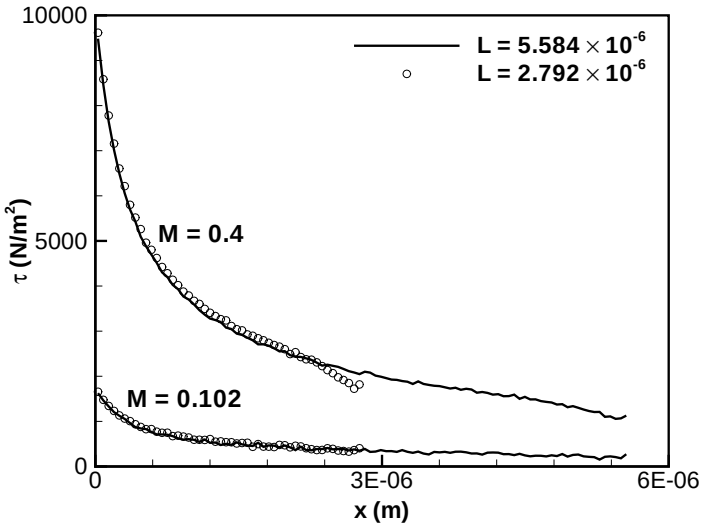

Figure 3.134: Shear stress distributions for semi-infinite plates.

Moreover, at the top boundary of the domain, the transverse velocity components are much smaller than the streamwise velocity components, and hence, the streamlines leave the domain with very small angles with respect to top boundary. Consequently, in using streamline extrap-

[5] The results near the end of the plate are a little distorted due to exit boundary condition effects.

olation at the top boundary it may be necessary to extrapolate properties from the cells quite far away from the ghost cells (see Section 2.2.3 for ghost cells). Also, during the computations, sometimes the streamlines at the top boundary may direct into the domain and the flow becomes inflow instead of outflow locally[6]. It is noteworthy that the present boundary conditions performed remarkably well under all the severe conditions mentioned above, and produced satisfactory results. It is also known that, as the domain size is increased the effects of boundary conditions decrease. In the present simulations, various domain sizes are considered and it is observed that the present boundary conditions can be confidently used even the domain size is small (approximately plate length).

The effects of rarefaction and Mach numbers can also be seen in Figures 3.135 and 3.136 in which surface pressure distributions and drag coefficients are plotted, respectively. Figure 3.135 shows that the pressure drops as the rarefaction increases, and also the uniform distribution for the pressure is distorted as the flow speed increases. Figure 3.136 depicts that the present results are in excellent agreement with the experimental data. The drag coefficients change slightly with the Mach numbers, but as the rarefaction increases the drag coefficients converge to the theoretical free-molecular value.

[6] Clearly, these problems can be avoided by choosing the alignment of the top boundary quite different from the outgoing streamlines.

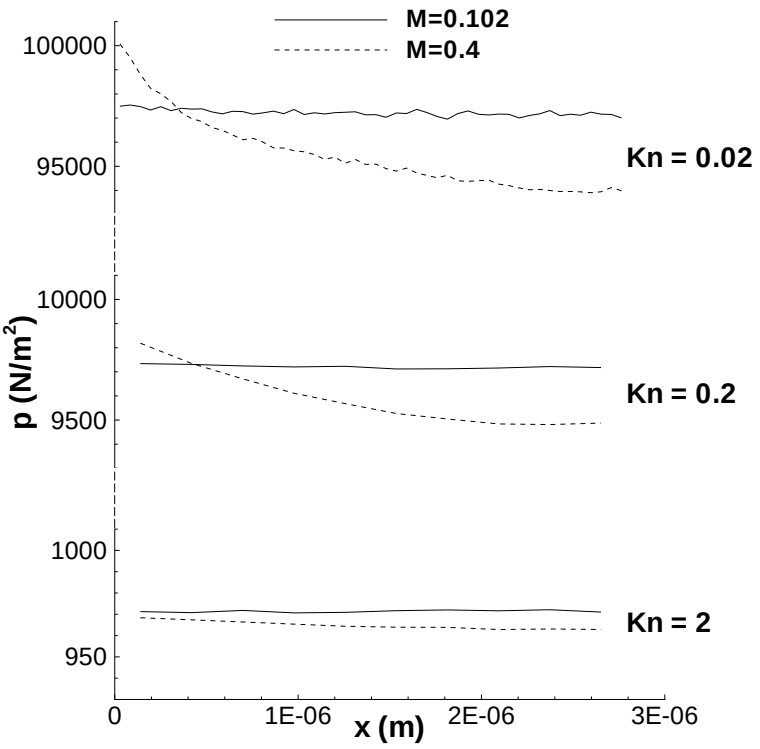

Figure 3.135: Pressure distributions for various Kn and M numbers.

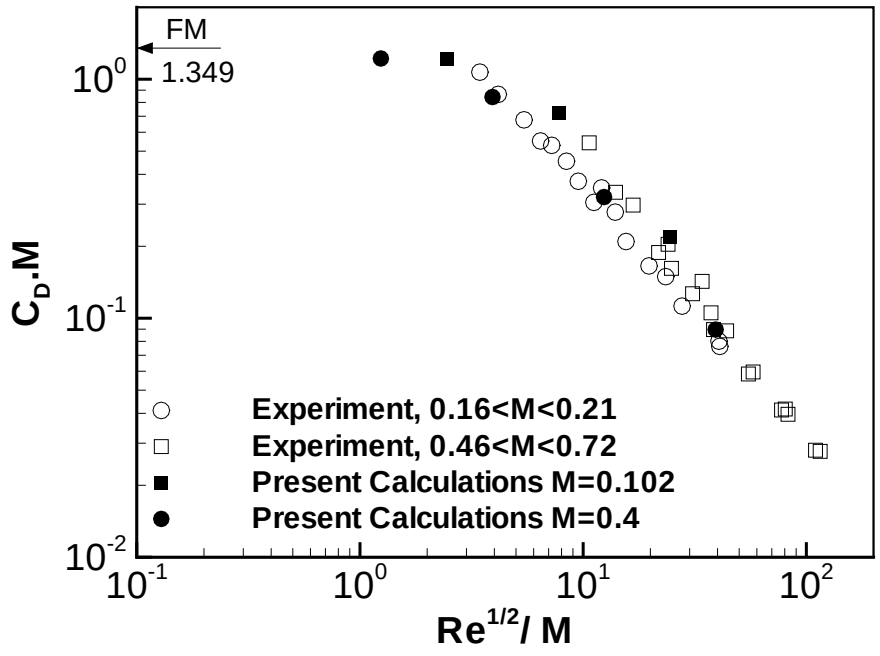

Figure 3.136: Drag coefficient for various test runs.

For the Neumann boundary condition used in this study, first order derivative and first order accurate discretization is utilized. Higher order derivatives and higher order accurate discretizations are also tested in the early stages of this investigation, however, it is found that they produce oscillations as the order of derivatives and order of accuracies increase.

The sample size has to be much larger for the subsonic rarefied flows as compared to that for supersonic flows to remove the statistical scatter on the computed results. This is evident in the present results, too. For example, although the present time-averaged results are based on approximately 10^6 samples (i.e. about 10^7 particles per cell), statistical scatter is still present on the surface heat transfer (q) and shear stress (τ) results.

Apart from these test runs, several other boundary conditions and grid structure are also tested in this study. For example, in one of the calculations, constant streamwise freestream velocity ($U = U_\infty$) is used at the top boundary instead of constant freestream pressure but the results show large deviations. Separately, nonuniform cell structure is also tested and it is observed that when large cells are used away from the body, the drag coefficient is correctly calculated but the surface heat transfer results and velocity profiles are distorted considerably.

In this study, all the calculations have been performed using an Intel XEON processor with 2.6 Ghz speed and 1 GB memory. A $Kn = 0.2$ run takes about 3.5 hours and uses %0.5 memory, and a $Kn = 0.02$ run requires 15 days and uses %8.1 memory for a sample size of 10^6.

CHAPTER 4

CONCLUSIONS

In this thesis, subsonic rarefied flows over a flat plate at constant pressure are studied using the direct simulation Monte Carlo method. An infinitely thin plate with zero angle of attack is considered. Flows with a Mach number of 0.102 and 0.4 and a Reynolds number varying between 0.063 and 246 are considered covering most of the transitional regime between the free-molecule and the continuum limits. The effects of different inflow and outflow boundary conditions are examined, and a new extrapolation technique, based on following the trajectory of a streamline, is developed. Results are obtained for a number of test runs and the drag coefficient of the plate for each case is compared with the experimental data. The outcomes of this study are listed as follows:

- In all of the cases listed in Table 3.3, the calculated drag coefficients are in very good agreement with the experimental data.
- Among the various outflow boundary conditions tested, the best results are obtained using Neumann boundary condition together with the newly developed streamline extrapolation technique (Cases A). The precision in the results decreases in the following order: Cases A, B, C and D (see Table 3.2 for the boundary conditions represented by these letters).
- One of the most important outcomes of this study is that small computational domains can be confidently used with the boundary condition of Cases A because the flow is not

distorted and the general features of the flow are correctly calculated. This helps to reduce the computational time in the simulation of dense flows.

- At the inflow boundary, two boundary conditions are considered. Riemann boundary condition is found to be more effective as compared to the other in which one of the variables, transverse velocity V, is extrapolated from the interior. It is observed that, with Riemann boundary condition, streamlines enter the domain parallel to the freestream, whereas in V extrapolation, streamlines enter the domain with large angles, which is not realistic.

- Another important observation is made on the use of cell sizes when compared to local mean free path. Results for $\Delta x \approx 2.5\,\lambda$ have less than 1-2% error when compared to those for $\Delta x \approx \lambda$. However, it is necessary to use $\Delta y \approx \lambda$ for correct results.

- The highest Reynolds number in this study is achieved in Case A.15 ($Re \cong 250$) by using $\Delta x \approx 5\,\lambda$ and by reducing the height of the domain. The computational time for this case requires maximum usage of computer resources available in this study. Noting that, the critical Reynolds number to produce turbulence on a flat plate is about 200,000, it is clear that simulation of turbulent flows on a flat plate is still far away.

- The statistical scatter in the results of $M = 0.4$ are less than that in $M = 0.102$. This is expected because as the mean flow velocities decreases, it becomes difficult to reduce the statistical scatter (associated with the DSMC technique) from the averaged results and a big sample size is required.

REFERENCES

[1] Bird, G. A., "*Molecular Gas Dynamics and Direct Simulation of Gas Flows*", Clarendon Press, Oxford, 1994.

[2] Bhatnagar, P. L., Gross, E. P., Krook, M., "*Model for Collision Processes in Gases, I. Small Amplitude Processes in Charged and Neutral One-Component Systems*", Phys. Rev. **94**, pp. 511-524.

[3] Alder, M. P., Wainwright, T. E., "*Studies in Molecular Dynamics*", J. Chem. Phys. **27**, 1957, pp. 1208-1209.

[4] Kandemir, I., Greber, I., Woo, M. J., "*Heat Conduction and Couette Flow in a Hard Sphere Gas Using a Multicell Molecular Dynamics Computational Method*", Proceedings of the 21st Int. Symp. on Rarefied Gas Dynamics, ed. by Brun, R., Campargue, R., Gatignol, R., Lengrand, J. C., Cépaduès-Éditions, Vol.2, 1999, pp. 213-220.

[5] Allen, M. P., Tildesley, D. J., "*Computer Simulation of Fluids*", Oxford University Press, 1987.

[6] Moss, J. N., Bird, G. A., "*Direct Simulation of Transitional Flow for Hypersonic Reentry Conditions*", AIAA Paper 84-0223, 1984.

[7] Scott, W. B., "*Micro Machines Hold Promise for Aerospace*", Aviation Week & Space Technology, March 1, 1993.

[8] Churchill, S. W., "*Viscous Flows: The Practical Use of the Theory*", Butterworths, Stoneham, MA, 1988.

[9] Schaaf, S. A., "*A Note on the Flat Plate Drag Coefficient*", Inst. of Engineering Research, Univ. of California, Report No. HE-150-66, Berkeley, CA, 1950.

[10] Laurmann, J. A., "*Linearized Slip Flow past a Semi-Infinite Flat Plate*", Journal of Fluid Mechanics, Vol. 11, 1961, pp. 82-96.

[11] Murray, J. D., "*Incompressible Slip Flow past a Semi-Infinite Flat Plate*", Journal of Fluid Mechanics, Vol. 22, 1965, pp. 463-469.

[12] Ilgaz, M., "*Analysis of Low-Density Internal Flows Using the Direct Simulation Monte Carlo Method*", M.S. Thesis, METU, July 2002.

[13] Nance, R. P., Hash, D. B., Hassan, H. A., "*Role of Boundary Conditions in Monte Carlo Simulation of MEMS Devices*", AIAA Paper 97-0375, 1997.

[14] Whitfield, D. L., Janus, J. M., "*Three-Dimensional Unsteady Euler Equation Solutions Using Flux Vector Splitting*", AIAA Paper 84-1552, 1984.

[15] Piekos, E. S., Breuer, K. S., "*DSMC Modeling of Micromechanical Devices*", AIAA Paper 95-2089,1995.

[16] Dogra, V. K., Moss, J. N., "*Hypersonic Rarefied Flow About Plates at Incidence*", AIAA Journal, Vol. 29, No.8, 1991.

[17] Sun, Q., Boyd, I. D., "*Drag on a Flat Plate in Low-Reynolds-Number Gas Flows*", AIAA Journal, Vol. 42, No.6, June 2004.

[18] Schaaf, S. A., Sherman, F. S., "*Skin Friction in Slip Flow*", Journal of the Aeronautical Sciences, Vol. 21, 1954, pp. 85-90.

[19] Vincenti, W. G., Kruger, C. H., "*Introduction to Physical Gas Dynamics*", John Wiley & Sons, New York, 1965.

[20] Bird, G. A., "*Monte Carlo Simulation in an Engineering Context*", Prog. Astro. Aero. 74, 1981, pp.239-255

[21] Maxwell, J.C., "*Phil. Trans. Roy. Soc. 1*", Appendix, 1879.

[22] Laney, C. B., "*Computational Gasdynamics*", Cambridge University Press, 1998.

[23] Schlichting, H., "*Boundary Layer Theory*", 7th Ed., McGraw-Hill Inc., 1979.

APPENDIX A

INTERMOLECULAR COLLISIONS

Collision process and the selection of collision pairs are based on the kinetic theory. Suppose a single molecule has a collision cross-section σ_T and the relative velocity $\mathbf{c_r}$. In the specified time interval, Δt, which is much shorter than the mean collision time, moving molecule will collide with stationary molecule if the center of the stationary molecule is in the cylinder of volume $\sigma_T\, c_r\, \Delta t$. Summing over all velocity classes gives the number of collisions of molecule per unit time (mean collision rate),

$$\nu = n\, \overline{\sigma_T\, c_r} \quad , \tag{A.1}$$

where n is the number density. The bar denotes the average value over all molecules in the sample. The total number of collisions per unit time per unit volume is

$$N_c = \frac{1}{2}\, n\, \nu = \frac{1}{2}\, n^2\, \overline{\sigma_T\, c_r} \quad . \tag{A.2}$$

Since each collision is between two molecules, one half factor is introduced.

Throughout this study, for calculating the intermolecular collisions, Bird's *"No-Time Counter (NTC)"* method [1] is applied. The probability of a collision between two molecules in a homogeneous gas is related with the production of relative speed $\mathbf{c_r}$ and collision cross-section σ_T. First of all, number of pair selections is determined for the time interval. Then one of the

collision pair is selected and the collision is computed with probability

$$\frac{\sigma_T \, c_r}{(\sigma_T \, c_r)_{max}} \quad . \tag{A.3}$$

The decision of accepting this collision pair is established using *"Acceptance-Rejection Method"* [1]. If result of the Eqn.(A.3) is greater than the generated random fraction, R_f, collision is accepted. Otherwise, process goes on until finding a collision pair.

The computational time in the NTC is proportional to the number of simulated molecules and NTC yields the exact collision rate in both simple gases and gas mixtures, under equilibrium and non-equilibrium conditions.